`

Impact of Land Use Land Cover Change on Seasonal Land Surface Temperature: Case of Ethiopia, Oromia, Adama City

Name of candidate: EYOEL MEKONNEN

A Thesis Submitted to the Department of Geomatics Engineering

School of Civil Engineering and Architecture

Presented in Partial Fulfillment of the Requirements for the degree of Master’s in Geo-Informatics

Office of Graduate Students

Adama Science and Technology University

May 2024

Adama, Ethiopia

`

Impact of Land Use Land Cover Change on Seasonal Land Surface Temperature: : Case of Ethiopia, Oromia, Adama city

EYOEL MEKONNEN

Advisor: Dejene Tesema (PHD)

A Thesis Submitted to the Department of Geomatics Engineering

School of Civil Engineering and Architecture

Presented in Partial Fulfillment of the Requirements for the degree of Master's in Geo-Informatics

Office of Graduate Students

Adama Science and Technology University

May 2024

Adama, Ethiopia

`

DECLARATION

I, Eyoel Mekonnen hereby declare that this thesis entitled "Impact of Land Use Land Cover Change on Seasonal Land Surface Temperature: Case of Ethiopia, Oromia, Adama city." is my own work and has not been submitted to any university for similar purpose. The references used in this thesis are duly recognized by proper citations.

Eyoel Mekonnnen	_______________	_______________
Name of student	Signature	Date

`

RECOMMENDATION OF ADVISORS

I, the major advisor/supervisor of this research thesis, hereby certify that I have closely advised/supervised the student while developing this thesis and read the draft thesis entitled "Impact of Land Use Land Cover Change on Seasonal Land Surface Temperature: Case of Ethiopia, Oromia, Adama city." prepared under my guidance by Eyoel Mekonnen. Therefore, I recommend the submission of the thesis to the department for further review and evaluation.

Dejene Tesema (PHD) ______________________ ______________

Major Advisor/Supervisor Signature Date

`

APPROVAL SHEET

I/we hereby certify that the recommendation and suggestion given by the thesis review committee are appropriately incorporated into the final thesis proposal entitled “Impact of Land Use Land Cover Change on Seasonal Land Surface Temperature: Case of Ethiopia, Oromia, Adama city.” by Eyoel Mekonnen.

___Dejene Tesema (PHD)______ ________________________ ______________

Major Advisor/Supervisor Signature Date

APPROVAL OF BOARD OF REVIEWERS

We, the undersigned, members of the Board of Reviewers of the thesis open defense by Eyoel Mekonnen have read and evaluated the thesis l entitled “Impact of Land Use Land Cover Change on Seasonal Land Surface Temperature: Case of Ethiopia, Oromia, Adama city.” and assessed the understanding of the candidate about the proposed research. This is, therefore, to certify that the thesis is accepted for partial fulfillment of the requirement of the degree of Master of Science in Geoinformatics.

______________________	______________________	______________________
Chairperson	Signature	Date
______________________	______________________	______________________
Reviewer 1	Signature	Date
______________________	______________________	______________________
Reviewer 2	Signature	Date

Finally approval and acceptance of the thesis is contingent upon submission of its final copy to the Office of Postgraduate Studies (OPGS) through the Department Graduate Council (DGC) and School Graduate Committee (SGC).

______________________	______________________	______________________
Department Head	Signature	Date
______________________	______________________	______________________
School Dean	Signature	Date
______________________	______________________	______________________
Office of Postgraduate Studies, Dean	Signature	Date

`

ACKNOWLEDGMENT

First and foremost, I would like to express my deepest gratitude to God for giving me the strength, knowledge, and opportunity to undertake this research and to persevere and complete it satisfactorily. Without His blessings, this achievement would not have been possible.

I am extremely grateful to my advisor, Dr. Dejene Tesema Bulti, for his invaluable advice, continuous support, and patience during my Master's study. His immense knowledge and plentiful experience have encouraged me throughout my academic research and daily life. It was a great privilege and honor to work and study under his guidance.

I also wish to express my sincere appreciation to Adama Science and Technology University, School of Civil Engineering and Architecture, and the Department of Geomatics Engineering for providing me with all the necessary facilities and support for the research. The friendly and supportive atmosphere inherent to the staff of the school and department contributed to the success of my study and made it an unforgettable experience.

I am extremely grateful to my parents and for their love, prayers, caring, and sacrifices for educating and preparing me for my future. I want to put out a special thanks to my brother Kaleb Mekonnen for being my ally and confidant during hard times. I am very much thankful to my uncle Solomon Yilma for his support and encouragement throughout this journey. I am also grateful to my colleagues and friends for their keen interest shown to complete this thesis successfully.

Lastly, I offer my regards to all of those who supported me in any respect during the completion of this project. This accomplishment would not have been possible without them. Thank you.

`

TABLE OF CONTENT

`

`

LIST OF FIGURES

`

LIST OF TABLES

`

LIST OF ACRONYMS

ABI	Advanced baseline imager
AI	Aggregation Index
ANN	Artificial Neural Network
ASTER	Advanced Space borne Thermal Emission and Reflection Radiometer
AVHRR	Advanced Very High-Resolution Radiometer
CSA	Central Statistical Agency
DEM	Digital Elevation Model
DN	Digital Number
ED	Edge Density
ERDAS	Earth Resources Data Analysis System
ETM+	Enhanced Thematic Mapper Plus
FLAASH	Fast Line-of-sight Atmospheric Analysis of Hypercubes
FRAC_MN	Mean Fractal Dimension Index
GOES-R	Geostationary Operational Environmental Satellite
JII	Interspersion and juxtaposition index
LLHM	Localized Linear Histogram Match
LP DAAC	Land Processes Distributed Active Archive Center
LSE	Land Surface emissivity
LST	Land Surface Temperature
LULC	Land-use and land-cover
MODIS	Moderate Resolution Imaging Spectroradiometer
MWA	Mono Window Algorithm
NASA	National Aeronautics and Space Administration
NDBAI	Normalized Difference Bareness Index
NDVI	Normalized difference Vegetation index
NDBI	Normalized Difference Builtup Index
NDWI	Normalized difference Water Index
NMA	National Meteorology Agency
NOAA	National Oceanic and Atmospheric Administration
OLI	Operational Land Imagery
PD	Patch Density
PV	Proportion vegetation

PLAND	Percentage of landscape
RMSE	Root-mean-square error
ROI	Region of interest
SLC	Scan Line Corrector
SLSTR	Sea and Land Surface Temperature Radiometer
STD	Standard deviation
SVM	Support Vector Machine
UHI	Urban Heat Island
USGS	United States Geological Survey

`

ABSTRACT

Rapid urbanization significantly alters land use and land cover (LULC), leading to notable changes in land surface temperature (LST) and the formation of urban heat islands (UHIs) in Adama City, Ethiopia. This study, spanning from 1991 to 2022, utilized Landsat satellite imagery and Support Vector Machine supervised classification to analyze LULC changes, showing a substantial shift from agricultural and bare lands to urban expansion. Landscape metrics indicated increased urban complexity and larger, less fragmented agricultural plots .LST data derived from thermal bands using an emissivity-corrected inverted Planck equation revealed dynamic seasonal variations. The Kiremete season saw a general decrease in mean LST across all land covers, whereas the Belge and Bega seasons an increase in LST for all LULC. These shifts highlight the sensitivity of LST to seasonal changes and urbanization. Normalized Difference Vegetation Index (NDVI) and Normalized Difference Built-up Index (NDBI) analyses were used to quantify the extent of vegetation and built-up areas. Surface Urban Heat Island Intensity (SUHII) calculations, performed through a Python-automated process, revealed a pronounced urban heat island effect in built-up areas during Kiremete, driven by the higher LSTs in these densely built environments. In contrast, the rural areas during this season maintained cooler temperatures due to soil moisture presence in bare lands and agricultural fields. However, the trends reversed during the Belge and Bega seasons. In these periods, agricultural and bare lands exhibited higher LSTs, leading to rural areas becoming hotter than urban areas. This shift resulted in a negative correlation between urban areas and LST, indicating an urban cool island effect. These findings illustrate the intricate relationship between land cover types and LST, varying by season due to differences in land cover responses to climatic conditions. Regression analysis of vegetation metrics Edge Density, Patch Density and FRAC_AM demonstrated significant cooling effects, particularly the vegetation fraction (FRAC_AM), which was consistently negatively correlated with LST. This underscores the importance of urban greenery in reducing temperature and enhancing climate resilience. The study emphasizes the urgent need for integrated urban planning and sustainable development that harmonizes growth with environmental conservation, particularly in managing urban thermal environments. These insights are critical for planners, stakeholders, and policymakers in developing strategies to mitigate the adverse effects of rising temperatures and urban expansion, highlighting the complex dynamics of SUHII across different seasons.

Keywords: Land use and land cover change, Land surface temperature, Urban heat island; Landscape metrics; Seasonal variation; Adama City; Ethiopia

CHAPTER 1. INTRODUCTION

1.1 Background of the study

More than half of the world's population lives in cities today, and this figure is anticipated to rise to 66% by 2050. (Desa, U.N., 2014). This figure shows a fluctuating rise in the number of urban residents. African and Asian developing nations, in particular, are more responsible for this rapid rise in urbanization (UN-HABITAT, 2010, 2013). Specifically, urbanization in Africa is anticipated to grow by 1.1% year from 2010 to 2015, reaching a predicted 56% urbanization rate. In the same way that Ethiopia is a country in Africa, there were 19% urban people in 2014 and 38% were projected in 2050. The UN study from 2014 states that Ethiopia's urban growth rate between 2010 and 2015 was 2.3%. (Desa, U.N., 2014). The need for and accessibility to housing, roads, transportation, energy, sani-tation, and other social facilities are all impacted by population growth. Additionally, urbanization significantly increases market inflation and real estate values. Urbanization's rapid growth has also resulted in a number of environmental issues (Bonan, 2002; Wu, 2008a, 2008b).

As a result the urban and rural landscapes are both changed by the rapid growth of the urban population. Extreme LULC change primarily affects the surface temperature of the urban and the surrounding area by replacing natural vegetation and greenery areas with impervious surfaces (concrete, asphalt, parking lots, rooftops, and building walls) (Balew & Korme, 2020; Feyisa et al., 2016; Pham et al., 2011; Gluch et al., 2006; Chaka & Oda, 2021; Zhao et al., 2016) . One of the key factors influencing the surface temperature is the albedo effect. Albedo refers to the reflectivity of a surface, which determines the amount of solar radiation that is reflected back into the atmosphere. Urban surfaces, such as concrete and asphalt, typically have lower albedo values compared to natural surfaces like vegetation. This means that urban areas absorb more solar radiation, leading to higher surface temperatures and contributing to the Urban Heat Island (UHI) effect (Taha, 1997; Akbari et al., 2001). As a result, LULC alterations alter near-surface energy by raising solar energy absorption surfaces, increasing evapotranspiration, and producing high surface heat. Because these biophysical materials have a high capacity to reflect heat back into the environment and contribute to warming the surrounding area, a hasty change in urban morphology, in particular the expansion of IS, continuously produced excessive heat and emitted to the atmosphere and increased LST. Studies demonstrate that LULC change is the major cause for the fluctuations in LST (Balew & Korme, 2020; Dissanayake et al., 2019; Liu et al., 2015a; Priyankara et al., 2019 ; Ranagalage et al., 2018a, b, 2019a; Rousta et al., 2018; Simwanda & Murayama, 2018; Simwanda et al., 2019; Chaka & Oda, 2021) Impervious surfaces in metropolitan areas will also absorb and store more solar radiation and heat while also preventing long-wave sky radiation loss (Oke, 1988; RIZWAN et al., 2008), resulting in the phenomena known as the Urban Heat Island (UHI) effect, in which air and land surface temperatures (LST) in urban areas are higher than in adjacent rural areas. Urban heat islands are caused by a variety of urban features, including buildings, concrete, asphalt, and industrial activities (Dousset & Gourmelon, 2003;L. Liu & Zhang, 2011). Most of the earth's surface has already been altered, according to several earlier studies, with the exception of those regions that are remote or difficult to access.

1.2 Statement of the Problem

Land-use and land-cover (LULC) changes caused by fast urban expansion generate variations in land surface temperature (LST) which can substantially alter the quality of the environment. In an urban setting, high temperatures or heat waves may have an impact on both the environment and people's health. As the surface air warms, the air quality deteriorates. Heat waves can have a negative impact such as increased energy demand, higher air pollution and greenhouse gas emissions, deteriorated human health and comfort, and poor water quality. Rising Surface Temperature can also have a significant impact on increment of Albedo values as they contribute to higher LST and UHI formations.

As a Result The environmental impact of urbanization-induced LULC alterations has been the principal focus of a corpus of Research studies in recent decades .The ecology of both urban and rural areas is changing as natural vegetation and green areas are replaced by impermeable surfaces, and the composition and geometry of land cover is changing as a result of urban growth, which has also been connected to a rise in the temperature of the earth’s surface in urban areas. Studies conducted in a few urban areas of Ethiopia have observed the relationship and characteristics of Land surface Temperature with respect to LULC classes (Chaka & Oda, 2021; Nega et al., 2019), Land scape structure and its relationship with Land surface Temperature (Terfa et al., 2020), spatiotemporal pattern of Land surface Temperature (Asfaw, 2017; Moisa et al., 2022; Tafesse & Suryabhagavan, 2019), Behavior of land surface temperatures along the urban-rural gradient (Balew & Semaw, 2022; Dissanayake et al ., 2019) and Relationship between LST and well-known indices like NDVI and NDBI that had a more significant effect on the temperature of the land (Warkaye et al., 2018; Tafesse & Suryabhagavan, 2019) have undergone analysis. These investigations, however, mainly focused on the situation during the dry season; little effort has been made to investigate seasonal fluctuations in the link between urbanized-induced LULC changes and land surface temperature. This resulted in a limited understanding of how geographical and temporal environmental elements interact to influence the creation of UHIs, particularly in Adama City.

As adama City, a fast expanding regional center in the Great Rift Valley distinguished by its hot climate .It must meet the cooling requirements of urban growth, and the impacts of the various seasons as they are very diverse. By addressing this issue, planners and stakeholders will be able to create evidence-based planning, building, and management solutions to handle the problems associated with a changing urban thermal environment. It is also useful for agriculturalists and crop breeders to understand the impact of rising land surface temperatures on different seasons, particularly the winter season, as this poses a serious danger to winter agricultural productivity. Additionally, it deepens our understanding of the phenomenon and influences our future policy goals.

1.3 General Objective

To analyze the impacts of land use and land cover changes on the spatiotemporal and seasonal variations of land surface temperature of Adama city from 1991 to 2022.

1.4 Specific Objectives

The specific objectives of this proposal is to:

- To assess the spatiotemporal dynamics of land use and land cover changes in Adama City from 1991 to 2022.
- To determine the temporal trends and seasonal variations of land surface temperature in Adama City over the study period using satellite-derived data.
- To investigate the relationships between changes in land use/land cover and variations in land surface temperature in Adama City.
- To evaluate the implications of land use/land cover dynamics on the formation of urban heat islands and the development of heat-related urban microclimates in Adama City.
- To analyze the link between land surface temperature (LST) and the spatial pattern of vegetation of the study area.

1.5 Research Questions

1. What are the spatiotemporal dynamics of land use and land cover changes in Adama city from 1991 to 2022, as determined by remote sensing and GIS techniques?
2. How do the temporal trends and seasonal variations of land surface temperature in Adama City evolve over the study period (1991 – 2022), as observed from satellite-derived data?
3. What are the relationships between changes in land use/land cover and variations in land surface temperature in Adama City?
4. What are the implications of land use/land cover dynamics on the formation of urban heat islands and the development of heat-related urban microclimates in Adama City?
5. How did the spatial arrangement vegetation impact the temperature of the land in Adama City?

1.6 Scope of the study

The Geographic emphasis of this study will be the Oromia Regional State's Adama city Administrative Boundary. The contextual Scope, on the other hand will investigate how LULC composition and configuration patterns have evolved over the study period (1991 to 2022), and will examine the impact of land use land cover change on multitemporal and seasonal LST profile or urban and rural area of Adama city , assess the impact of vegetation land cover configuration and built-up dynamics on Land surface temperature in, will give an insight between the relationship of Land use Land cover classes and Land surface temperature and the effect of SUHII on LST and Land Use Land Cover.

1.7 Significance of the study

Adama City is a regional center in the Great Rift Valley that is expanding quickly and is renowned for its hot climate. It is necessary to address the cooling requirements of urban growth as well as the diverse effects of the numerous seasons. By addressing this problem, planners and stakeholders will be able to create evidence-based planning, building, and management solutions to deal with the problems caused by a changing urban thermal environment. For agriculturalists and crop breeders in particular, understanding how rising land surface temperatures affect various seasons—particularly the winter season, when they pose a serious danger to agricultural productivity—is beneficial. Additionally, it helps us better understand the issue and refines our goals for future legislation.

CHAPTER 2. LITERATURE REVIEW

2.1 Urbanization

Urbanization is defined as "the progressive increase in the number of people living in urban areas" and "the methods in which each culture adjusts to the change." the method by which a community transitions from a country to an urban way of existence (NLM, 2014). By 2050, it is anticipated that 64% of Africa and Asia and 86% of the developed world would have urbanized populations (The Economist, 2012). Notably, the United Nations has also recently predicted that cities will absorb almost all of the increase in the world population between 2017 and 2030, or around 1.1 billion new urban residents over the next 13 years. (Barney, 2015)

According to a recent report by the Organization for Economic Co-operation and Development, Africa's rate of urbanization and urban population growth has significantly varied across the entire continent as well as within its various regions (OECD, 2020). According to the research (OECD, 2020), Africa is one of the world's least urbanized areas, and its urbanization rate will continue to be among the fastest in the coming years. In fact, only 27 million people lived in Africa's cities in 1950, compared to the region's current urban population of 567 million. Notably, the (OECD) report asserts that high population growth and the reclassification of rural settlements have been the main drivers of Africa's rapid urbanization since 1990. It also predicts that between now and 2050, Africa's population will double, with urban areas absorbing two-thirds of the increase.

2.1.1 Urbanization in Ethiopia

Ethiopia's urbanization has been increasing at a rate of 4.5%, higher than the 4% of Sub-Saharan Africa, and is projected to increase at a rate of 5.4% (World Bank Group, 2015). Urban population grew by 414% between 1984 and 2021, from 4.45 million to 22.88 million. In 2018, natural growth (40%), migration from rural to urban (33%), and reclassification of rural settlements (24%) were the key forces behind the rapid urbanization expansion.(Mezgebo, n.d.)

There are already 159 cities with a population of more over 20,000 people, up from 85 in 2007; by 2037, there are projected to be over 440. Rapid urbanization and structural change have occurred simultaneously in Ethiopia. Over 69% of the workforce is still employed in agriculture, making it the major sector (Mezgebo, 2021) The low level of employment in industry (approximately 10%) demonstrates that urbanization is likely tied to the rise of consuming cities and has little positive externalities in terms of job creation and productive investments, notwithstanding its falling contribution to Gross domestic product (GDP).

2.2 Land use Land cover change

Land cover modifications involve changing the circumstances within a category as well as changing the type of land cover. While land-use change happens when experts conclude that a transition to a different category of land use is desirable (Mezgebo, n.d.; Patel et al., 2019) Over the past few decades, the understanding of land-use/land-cover change has progressed from simplification to realism and complexity. Early studies focused mostly on the physical side of the change, but later research agendas focused on global environmental change. Because of the alteration in land use and cover, scientists discovered that land surface processes affect climate. It was established in the mid-1970s that land cover change impacts surface albedo and thus surface atmosphere energy exchanges, which has an effect on regional climate ((Otterman, 1974); (Charney et al., 1977); (Sagan et al., 1979). Additional effects of changing land use and cover on ecosystems, products, and services were discovered. Impacts on biotic diversity globally (Sala et al., 2001), soil degradation (Stanley et al., 2015), and the capacity of biological systems to meet human requirements are the main causes for concern (Vitousek et al., 1997)

Human populations and land usage have changed the vast majority of the terrestrial biosphere into anthropogenic biomes. A number of novel ecological patterns and processes have emerged as a result of this transition, which has been significant for more than 8000 years (Ellis, 2011). Researchers from a wide range of disciplines, from those who advocate modeling spatiotemporal patterns of land conversion to those who attempt to understand the causes, impacts, and consequences, have recently been more interested in topics related to LULC transformation. Changes in the land cover have an impact on land use, and the reverse is also true. However, a change in either is not always the effect of the other. The degradation of the land is not always implied by changes in land cover due to land use. Land cover changes, however, are a result of numerous shifting land use patterns that are motivated by numerous socioeconomic factors. These modifications have an impact on processes such as biodiversity, water and radiation budgets, and others that affect the climate and biosphere (Riebsame et al., 1994)

Recent shifts in land use have been characterized by agricultural land losses. East Africa, like the rest of the world, is not exempt from these changes in land use and cover. In particular, very quick changes are evident in Ethiopia (Regasa et al., 2021) as a result of population pressure, resettlement initiatives, climate change, and other man- and nature-induced driving forces. The primary causes of the Ethiopian landscape's decline in natural status, as in other nations, are anthropogenic activity. (Regasa et al., 2021) Ethiopian lands underwent a transformation from natural to agricultural land use, waterbody, commercial agriculture, and built-up/settlement over the last ten years. Some areas of the forest land, pasture land, swamp/wetland, shrubland, rangeland, and bare/rock out cropland cover classes were converted to other LULC class types, owing to rising anthropogenic pressure.

The study by (Abdul Athick & Shankar, 2019) in the Adama woreda revealed an intriguing aspect: construction build up, dense vegetation, and sparse vegetation all increased in area by roughly 160%, 30%, and 78%, respectively, at the expense of barren land, which decreased by 8.5%. Water bodies, however, did not experience much change.

One land use change may have an impact on another. The majority of land use change ecological effects are interacting under various land use modifications. For instance, deforestation has impacted freshwater quality and changed the energy balance of the planet, which has resulted in the siltation of A challenge to a better understanding of the land use change issue is global warming, which results from the interaction of various land uses along their change trajectories. The human environmental sciences face a research challenge related to changes in the land and ecosystems and their effects on sustainability and global environmental change

2.3 Supervised Image classification

Supervised image classification is a classification technique in which the user chooses representative sample pixels from an image and instructs the image processing software to use these training sites as models for classifying the rest of the pixels in the image. It is commonly known that choosing an appropriate classifier is crucial for increasing classification accuracy (Lu & Weng, 2007) Several supervised classification classifiers and algorithms, including the parallelepiped, minimum distance, maximum likelihood, non-parametric classifiers, and machine learning techniques like the support vector machine,

`

decision tree method, and artificial neural networks, have been developed over the past few decades.

Parallelepiped classifiers algorithm

To determine if a particular pixel belongs to the designated class or not, a standard threshold is provided. The parallelepiped is based on the threshold of the standard deviation from the mean of each class (a class limit dimension). The pixels are categorised if the threshold range falls between the defined low and high. Unclassified areas are those that do not fall inside the given threshold range.

This supervised classifier is fairly straightforward. Here, based on maximum and minimum pixel values, two image bands are employed to estimate the training area of the pixels in each band. Although the parallelepiped classification method is the most precise, it is not the most popular. Additionally, training pixels may overlap, leaving many pixels unlabeled. The candidate pixel's data values are contrasted with the upper and lower bounds. (Perumal & Bhaskaran, 2010)

Minimum distance classifiers algorithm

It is based on the minimal distance decision rule, which determines the spectral separation between the mean vector for each sample and the measurement vector for the candidate pixel. The candidate pixel is then assigned to the class with the shortest spectral distance. (Perumal & Bhaskaran , 2010)

As a distinctive prototype, classes that are near one another are grouped. It is used to determine each class's mean vector and assign each pixel to the nearest group.

Maximum Likelihood classifiers algorithm

The vector of a class with the highest probability is assigned among all the probabilities of vectors allotted to various classes. Based on the user-provided threshold value, the pixels are assigned to each class. The pixels are unclassified if the class probability value is less than the user-set threshold value (Ahmad et al., 2012). It is a parametric approach in decision making where the model parameters need to be estimated before they are applied for classification

MLC is a process for determination of known class distribution as the maximum for a given statistic (Scott & Symons, 1971). This method has been used most widely and frequently in remote sensing where a pixel is assigned to the corresponding class with the maximum likelihood. If there has been m predefined classes, in that case the class posteriori probability is expressed

This Classification use the training data by estimating the means and variances of the classes, which are then utilized to estimate probabilities while also taking into account the variety of brightness values in each class. This classifier is Based on Bayesian probability theory. When accurate training data is made available, it is one of the most effective classification methods and algorithms. (Perumal & Bhaskaran, 2010)

The measurement vector with the highest likelihood of belonging to a certain class is given that classification. The MLC has an advantage over other known parametric classifiers in that it considers the variance-covariance within class distributions, and it outperforms them for normally distributed data (Erdas, 1999). However, the outcomes might not be adequate for data with a non-normal distribution.(Otukei & Blaschke, 2010)

Spectral Angle Mapper

An n-dimensional angle is used by the Spectral Angle Mapper, a physically based spectral classification, to match pixels to reference spectra. By calculating the angle between the spectra and treating them as vectors in a space with dimensionality equal to the number of bands, this technique calculates the degree of spectral similarity between two spectra. (Perumal & Bhaskaran, 2010)

Decision Tree classifiers algorithm

A decision tree classifier is a non-parametric classifier, meaning that no previous statistical assumptions about the distribution of the data are necessary. However, the decision tree's fundamental structure consists of a root node, a number of internal nodes, and then a set of terminal nodes. Recursively, the input is dispersed along the decision tree in accordance with the established classification scheme. Each node needs to have a decision rule, which may be achieved using a splitting test.(Otukei & Blaschke, 2010)

There are no complex design or training requirements for this method. Although computational efficiency is strong, it necessitates sophisticated calculations, and accuracy may entirely depend on feature design and selection.

`

Support Vector Machines classifiers algorithm

This classification is applied for a complex dataset where the input numeric attributes are normalized and pre-processed before classifying. It is a non-parametric statistical learning method (Ustuner et al., 2015). Various kernel types such as, linear, polynomial, sigmoid, radial basis function can be set.SVM is a nonparametric approach, where the theoretic background is supervised machine learning

This classification involves consideration of the training and testing sets from separate data. Each training set has separate target value and several attributes. Main function of the SVM is to predicts the target values of the given test data.The original goal of SVM, a non-parametric supervised machine learning technique, was to address binary classification issues [41(Implementation of Machine-Learning Classification in Remote Sensing: An Applied Review | Semantic Scholar, n.d.), (Huang et al., 2002)]. Based on the idea of structural risk minimization (SRM), it optimizes and isolates the hyper-plane and the data points closest to the hyper-spectral plane's angle mapper (SAM). It uses a hyper-spectral plane to divide data points into several classes. The vectors used in this technique guarantee that the margin's width will be maximized [(Bouaziz et al., 2017)]. Multiple continuous and categorical variables, as well as linear and non-linear samples with varying levels of class membership, can all be supported by SVM. Support vectors are the training samples or bordering samples that define the SVM's hyper-plane or margin [(Shih et al., 2019)].

Artificial Neural Network classifiers algorithm

In order to apply meaningful labels to images, algorithms using an artificial neural network method imitate the learning process used by humans. ANN mimics a select few mental processes (Mahmon & Ya'Acob, 2014) It consists of a series of layers, each of which contains a group of neurons, connected by weighted connections between the layers above and below. The network structure has a significant impact on the artificial neural network's accuracy and performance (Kaur & Jyoti, 2014) ANN networks are a self-adaptive and data-driven approach. The processing speed is fast and can accommodate erratic input. However, ANN training takes time, and selecting the right network design can be challenging.

WHY SVM IS BETTER

Results obtained from analysis of the hyperspectral data suggest that classification accuracy using SVM increases almost continuously as a function of the number of features, with the size of the training data set held constant, whereas the overall classification accuracies produced by the ML, DT and NN classifiers decline slightly once the number of bands exceeds 50 or so. Thus, suggesting that the Hughes phenomenon' (Hughes, 1968) of decreasing classifier performance as the dimensionality of the feature space increases beyond a threshold is not supported by the experiments using the support vector classifiers.

Further, the training time taken by support vector classifier is 0.30 minutes in comparison of 58 minutes by the NN classifier on a dual processor sun machine. Results suggest that support vector classifier performance is statistically significant in comparison with NN and ML classifiers. To study the behavior of support vector classifier with DAIS Hyperspectral data a total of sixty five features (bands) was used, a total of 65 features (spectral bands) were available, as seven features with severe striping were discarded, as explained above. The initial number of features used was five, and the experiment was repeated with 10, 15, 65 features, giving a total of 13 experiments. The study suggests that, in comparison to the other classifiers, the performance of the support vector classifier is quite good with small training data set irrespective of the number of features used.

Methods	Assumptions	Advantages	Limitations and Disadvantages
Parallelepiped classifiers algorithm	Minimum and Maximum value of pixel for the selection of training area	Very precise and straight forward	training pixels may overlap and leave unlabeled pixels
Minimum distance classifiers algorithm	Minimum distance rule to separate spectral difference	fast in execution, computation time is minimum as it depends mainly on the training dataset and all pixels will be classified	Prone to errors resulting in misclassification of pixels as it will classify a pixel. Spectral distance is calculated for all values of a class mean; the unclassified pixel is assigned to the class with the lowest spectral distance resulting in classification of all pixels.
Maximum Likelihood classifiers algorithm	estimating the means and variances of the classes, which are then utilized to estimate probabilities Based on Bayesian probability theory	considers the variance-covariance within class distributions, and it outperforms other classifications them for normally distributed data	outcomes might not be adequate for data with a non-normal distribution
Spectral Angle Mapper	match pixels to reference spectra and calculates the degree of spectral similarity between two spectra		
Decision Tree classifiers algorithm	Consists of a root node, a number of internal nodes, and then a set of terminal nodes. Recursively, the input is dispersed	no complex design or training requirements and efficient	Accuracy may depend on feature design and selection.

`

	along the decision tree in accordance with the established classification scheme		
Support Vector Machines classifiers algorithm	Optimizes isolates the hyper-plane and the data points closest to the hyper-spectral plane's angle mapper (SAM). It uses a hyper-spectral plane to divide data points into several classes.	applied for a complex dataset and used for mixed data computational complexity is reduced also can be used with small training datasets	dependent on user-defined parameters
Artificial Neural Network classifier algorithm	imitate the learning process used by humans	processing speed is fast and can accommodate erratic input	ANN training takes time, and selecting the right network design can be challenging.

Table 2.1 Classification Methods, assumptions, Advantages and Disadvantages of LULC

2.4 Retrieving Land surface Temperature

Inversion of Planck Function.

The Planck function is used to calculate the thermal radiation's intensity. It is a function that displays how much thermal electromagnetic radiation a blackbody can produce at a given temperature while in thermal equilibrium. Through the inversion of the Planck function, the LST of an area may be calculated if the LSE of the area is known. The ground surface is regarded as a black body, or an entity with an emissivity of 1, when calculating the brightness temperature measured by a sensor in space. The emissivity correction of brightness temperature is made possible by the Planck function. LST has been estimated using the Planck function.(Ndossi & Avdan, 2016)

The results show that the Planck function can produce the best results in comparison to the other algorithms, while the SWA algorithm has a moderate accuracy and the SCA algorithm has the lowest accuracy.(Ndossi & Avdan, 2016)

Radiative transfer equation

Radiative transfer calculations are used to determine how electromagnetic waves from the sun travel through the atmosphere to the Earth's surface as well as how scattered light and radiation from the earth's surface and atmosphere go into space. This radiative transfer equation allows for the conversion of satellite-measured radiation intensity into data about the Earth's surface and atmosphere.(*Remote Sensing and Radiative Transfer – JAXA Earth-Graphy / Space Technology Directorate I*, n.d.)

The RTE is a direct technique for retrieving LSTs that uses a single TIR band. Also referred to as the atmospheric correction method, this technique works on the idea of obtaining the intensity of the surface thermal radiation by subtracting the atmospheric influence from the total amount of thermal radiation detected by the satellite sensors, then converting it to the corresponding LST.

Difficulties and problems in the retrieval of LST from space measurements included measurements in TIR region are highly correlated resulting in instrumental noise and errors in atmospheric corrections, difficulty in implementing atmospheric corrections. (Z. L. Li et al., 2013)

`

Mono window algorithm

The mono-window approach described by Qin et al. [16] requires three important factors for LST extraction from Landsat TM/ETM+ TIR band data: ground emissivity, atmospheric transmittance, and effective mean atmospheric temperature. Qin et al. [16] described how to calculate atmospheric transmittance by simulating atmospheric conditions using the LOWTRAN 7 program. Qin et al. proposed the Mono-Window Algorithm (MWA) based on the radiative transfer equation for the Landsat TM band 6 data, which can avoid real-time dependence data. The method requires three main parameters, i.e., emissivity, atmospheric transmittance, and effective mean atmospheric temperature.

Single channel Algorithm

The single-channel (SC) algorithm was developed by Jimenez-Munoz and Sobrino it has been widely used to retrieve land surface temperature from Landsat series data for its simplicity and requirement of only one thermal infrared channel. It uses estimated atmospheric parameters (or atmospheric functions, i.e., combination of atmospheric parameters) to correct the atmospheric effect in a single channel toward retrieving LST (Cristóbal et al., 2009; Jimenez-Munoz et al., 2009; Jiménez-Munoz & Sobrino, 2003; Qin et al., 2010) the final retrieval error due to effective mean atmospheric temperature can be reduced because it requires few real-time atmospheric parameters and only the LSE and the atmospheric water vapor contents.

The model emissivity method (Hook et al., 1992), also known as the single TIR channel method, utilizes the radiance measured by the satellite sensor in a single channel selected within an atmospheric window and corrects the radiance for residual atmospheric attenuation and emission using atmospheric transmittance/radiance code, which requires input data on the atmospheric profiles. Then, by flipping the RTE, LST is extracted from the brightness observed in this channel provided that the LSE is well known or estimated in advance.

Accurate determination of the LST using this method requires high-quality atmospheric transmittance/radiance coding to estimate the atmospheric quantities involved in adequate knowledge of the channel LSE, an accurate atmospheric profile, and proper consideration of topographic impacts (Sobrino et al., 2004b).

The radiative transfer model (RTM) employed in the code, as well as the errors in the atmospheric molecular absorption coefficients and aerosol absorption/scattering

`

coefficients, are typically the main factors limiting the accuracy of atmospheric transmittance/radiance codes (Wan, 1999).

Split-Window Algorithm

A linear SW algorithm can be built by using differential absorption in two adjacent TIR channels I j in the 10-12.5 m range to linearize the RTE with regard to temperature or wavelength. The two brightness temperatures Ti and Tj recorded in the two TIR channels are combined simply linearly in this technique to represent the LST (McMillin, 1975). Rozenstein et al., (2014) and Qin et al., (2001) improved the SWA based on the work of previous scholars. SWA was developed to enabling the extraction of LST from instruments that are equipped with more than one TIR channel. The algorithm takes advantage of the differences in absorption between two thermal infrared channels in the atmospheric window between 10.5 and 12.5 µm. (Weng et al., 2019). Many SWA equations have been derived by numerous researchers for LST estimation (BECKER & LI, 1990; Price, 1984).

It should be noted that the accuracy of this LST retrieval method depends on the appropriate selection of the coefficients ak, which are beforehand determined either by empirically comparing the satellite data with in situ LST measurements or by regressing the simulated satellite data with a set of atmospheres and surface parameters. A representative in situ LST at satellite pixel scale (a few km2) that is also synced with the satellite's observations over a diverse range of surface types and atmospheric conditions is extremely challenging to acquire.(Z. L. Li et al., 2013)

With an exception of the way these algorithms calculate their parameters, they operate in the same manner (Jin et al., 2015) With the exception of the Split Window Algorithm, all of the aforementioned LST inversion techniques are used to estimate land surface temperature for Landsat sensors that have one or more thermal infrared bands, while SWA is only applicable to Landsat 8 and 9 due to its requirement of at least two thermal infrared bands.(Z. L. Li et al., 2013)

Multi-angle method

Similar to the rationale behind the SW approach, the multi-angle method is based on differential air absorption caused by variable route lengths when the same object is observed in a particular channel from several viewing angles. (Chédin et al., 1982; Li et al., 2001; Prata, 1993, 1994a,b; Sobrino et al., 1996, 2004c). This technique was primarily created based on the Along Track Scanning Radiometer (ATSR) onboard the first European Remote Sensing Satellite, which was the first sensor to operate in biangular mode (ERS-1). Within around 2 minutes, ATSR may complete a dual-angle observation of the same area of the Earth's surface. The forward view has a zenithal angle between 52° and 55°, whereas the nadir has a zenithal angle between 0° and 21.6°. Prata (1993, 1994a) developed a dual-angle approach to extract the SST and the LST from ATSR data under the supposition that the LST and SST are independent on the VZA and that the atmosphere is horizontally homogeneous and stable across the observation duration. Later, Sobrino et al. (1996) introduced an enhanced dual-angle algorithm that takes into account both the emissivity at the forward view and the emissivity at the nadir.

Although the multi-angle (dual-angle) approach performs better than the SW technique, there are a number of practical issues with using the dual-angle algorithm with satellite data (Sobrino & Jiménez-Muoz, 2005). Because the angular behavior of natural surfaces like soils and rocks is poorly understood at scales of satellite's spatial resolution, the angular dependence of the emissivity is a crucial phenomenon in the multi-angle technique (Sobrino & Cuenca, 1999)

`

Methods	Assumptions	Advantages	Limitations and Disadvantages
Inverted plank equation	ground surface is regarded as a black body, or and LST determined by inverting plank equation	Simplicity and great for the general representation of LST	Determing surface emissivity for each and every surface is difficult
Radiative transfer equation	obtaining the intensity of the surface thermal radiation by subtracting the atmospheric influence from the total amount of thermal radiation detected by the satellite sensors,	Simplicity and a direct technique for retrieving LSTs that uses a single TIR band	measurements in TIR region are highly correlated resulting in instrumental noise and errors in atmospheric corrections,
Mono window algorithm	Uses emissivity, atmospheric transmittance, and effective mean atmospheric temperature. To determine LST	avoid real-time dependence data	1) Require a priori knowledge of the pixel emissivity in the TIR channel 2) Require accurate atmospheric profiles and a good RTM to estimate atmospheric quantities
Single channel Algorithm	radiance measured by the satellite sensor in a single channel within a selected atmospheric window	1) Simplicity 2) Applicable to sensors with only one TIR channel	) The uncertainty of atmospheric profiles may have strong effects on the accuracy of LST retrieval. 4) Forward calculations of atmospheric quantities using an RTM are time-consuming 5) Use of empirical relationships provides poor results at high atmospheric water vapor contents

`

Split-Window Algorithm	using differential absorption in two adjacent TIR channels to determine Land surface Temperature	the differences in absorption between two thermal infrared channels in the atmospheric window	Only applicable for satellite data with two thermal bands available
Multi-angle method	differential air absorption caused by variable route lengths when the same object is observed in a particular channel from several viewing angles	Simplicity and high efficiency 2) Accurate atmospheric profiles are not required 3) LST retrieval accuracy is insensitive to the uncertainties in the optical properties of the atmospheric absorbents	1) Require a priori knowledge of the angular variation of the emissivity at satellite pixel scale 2) Require a significant difference in the slant path-lengths 3) Require accurate geometric registration 4) Applicable only to the homogeneous surfaces.

Table 2.2 LST retrieval Methods, Assumptions, Advantages and Disadvantages

2.5 Urban Rural Gradient Analysis

The use of urban-rural gradient analysis to illustrate the spatial distribution and variation of SUHI along urban-rural zones is a highly important method.(Balew & Semaw, 2022). There are two primary methods for performing urban-rural gradient analysis(1) Directional transects connecting the city's urban core to its rural regions (Zhang et al., 2004; Zhou & Wang, 2011) and2) Concentric rings around the city, with conventional distance intervals extending to its outskirts. (Balew & Korme, 2020; Estoque et al., 2017; Simwanda et al., 2019; Zhou & Wang, 2011). However, cities with a single-core urban growth pattern benefit more from the concentric ring urban-rural gradient analysis technique. (Estoque et al., 2017; Ranagalage et al., 2017; Simwanda et al., 2019).

2.6 Grid Based Analysis

In order to define the association between IS, CL, FL, VC, and GL density with mean LST, 210 m x 210 m grids (a window of 7 x 7 pixels) were used. According to Dissanayake et al. (2019a, b), Estoque et al. (2017), and Ranagalage et al. (2018b, 2019b), this grid size produces superior density findings and has a strong correlation with mean LST.

2.7 Landscape Metrics

The landscape metrics are quantitative indexes created to describe and evaluate the patterns of the landscape in a particular geographic area. They are also known as landscape indices, spatial indices, and spatial metrics.(Bulti, 2022). Although the term "landscape metrics" has traditionally been used to describe metrics for quantifying patterns in categorical maps (Mcgarigal K. FRAGSTATS HELP. 2015.). In recent decades, the application of these indices has provided a new means of defining the spatial heterogeneity of urbanized land and urban morphological traits.(Bulti, n.d.). Patches are used as the primary building component in the computation of landscape indices. A patch is a geographically homogeneous area with recurring themes that is unique from its surroundings.

The most often used indices in quantifying urban expansion patterns in urban studies are broken down into three categories based on the possibility for metric computations at patch-level, class-level, and landscape-levels.(Bulti, 2022.)

Patch Level Indices - Patch level indices are generated for each patch to indicate its spatial properties and context. The average patch characteristics across all patches in a class or landscape are only one example of the many landscape metrics that are typically computed using these indices. Patch area (PA) and Perimeter (PERIM) are one of the most useful characteristics of a given patch. However, calculated values of each patch have minimal significance in terms of interpretation and are very important as serving as a basis for the computation other various landscape metrics such as average patch characteristics over all patches in a class or landscape.(Bulti, 2022.)

Class Level Indices - The class level indices rely on data from patches with the same land-use type. By separately calculating the number and geographical layout of each patch type, class indices provide a way to gauge how fragmented the landscape is of each patch type. The most popular class level indices in urban studies include the number of patches, mean patch size, largest path index, landscape shape index, area weighted mean patch fractal dimension, and patch cohesion index.(Bulti, 2022.).

Landscape Level Indices – The landscape indices incorporate all of the patches of all class in the given landscape. Landscape metrics can be divided into two main categories: those that quantify the composition of the map without using spatial attributes and those that measure the spatial arrangement of the map using spatial information.(Gustafson, 1998; McGarigal & Marks, 1995). Indicators like Patch Density (PD), Edge Density, and Mean Euclidean Distance Neighbor are often utilized at the landscape level in urban studies.(Bulti, 2022.)

Landscape metrics are also classified by landscape pattern aspect. This include Area and Edge metrics, Shape metrics, core area metrics, aggregation metrics and Diversity metrics.

Area and Edge Metrics - handle patch size and the amount of edge these patches produce. This metrics are useful in describing the complexity and aggregation or fragmentation of patches and can be a useful metrics in determining configuration of patches.

Shape metrics – This metrics describe the patch shape complexity and degree of irregularity of patches. Combined with other types of metrics determinants they can give a strong indication of the type of distribution and configuration of patches at different levels such as at single patch (e.g. fractal dimension or shape index) or at a landscape level (e.g. Landscape shape index or area weighted mean patch fractal dimension)

2.8 Land Surface Emissivity Detection Methods

Day/night temperature-independent spectral-indices (TISI) based method

Becker and Li (Becker & Li, 1990), and Li and Becker (Becker & Li, 1990) first proposed a TISI-based method assuming that the TISIij (i is the MIR channel and j is the TIR channel) in the daytime without the contribution of solar illumination is the same as the TISIij in the night-time, , Li and

Becker (1993) and (Z. Li et al., 2000) further developed a day/night TISI-based method to first extract the bidirectional reflectivity in MIR channel i by eliminating the emitted radiance during the day in this channel by comparing the TISIij in the daytime and the nighttime. Once the bidirectional reflectivity in an MIR channel is retrieved, the directional emissivity in that MIR channel can be estimated to be complementary to the hemispheric-directional reflectivity, which can be estimated from a bidirectional reflectivity data series. Finally, based on the concept of the TISI, the LSEs in the TIR channels can be obtained from the two-channel TISI and the emissivity in the MIR channel (Jiang et al., 2006; Z. Li et al., 2000)

Several requirements may limit the usage of this algorithm in LST retrieval from space. First of all, approximate atmospheric corrections and concurrence of both MIR and TIR data are required (Jiang et al., 2006) .Then, accurate image co-registration must be performed (Dash et al., 2005). Additionally, the surfaces must be observed under similar observation conditions, e.g., viewing angle, during both day and night (Dash et al., 2005)

Classification-based emissivity method (CBEM)

According to this methodology, land covers with similar classifications would have had fairly similar LSEs. Based on information on conventional land cover classification, the LSE can be determined using look-up tables. By taking into account seasonal and dynamic state changes, (Snyder et al., 1998) found that the LSE values of 70% of land cover could be predicted using this method with sufficient precision (around 0.01), theoretically fulfilling the target of 1 K accuracy of LST retrieval.

NDVI-based emissivity method (NBEM).

This method is based on a statistical relationship between the NDVI derived from the VNIR bands and the LSE in the TIR channels. This method makes the following assumptions: 1) that the surface is only made up of soil and vegetation; 2) that the surface reflectivity in the red channel can linearly represent the emissivity of the bare soil; and 3) that the LSE changes linearly with respect to the percentage of vegetation in a pixel. As a result, three linear functions that correspond to the situations when a pixel is composed of full vegetation, full soil, or a mixed soil/vegetation content can be used to estimate the LSE of TIR channel i.(Z. L. Li et al., 2013)

Two-temperature method (TTM)

The TTM is based on the principle of reducing unknowns through numerous observations. If the land surface is viewed by N channels at two separate times, there are two N measurements with N+ 2 unknowns (N channel LSEs and two LSTs), provided that precise atmospheric corrections in the TIR channels have been carried out and that the LSEs are time-invariant. Therefore, if N >2, the 2 N equations can be used to simultaneously determine the N LSEs and the two LSTs (Watson, 1992)

The 2 N equations are highly linked, which makes their solutions potentially unstable and extremely vulnerable to sensor noise and mistakes in the atmospheric corrections. As a result, the retrieval accuracy is not always guaranteed (Caselles et al., 1997; Gillespie et al., 1999; Watson, 1992)

Physics-based day/night operational method (D/N)

Wan and Li (1997) further developed a physics-based D/N approach to simultaneously obtain LST and LSEs from a combined usage of the day/night pairs of MIR and TIR data, which was inspired by the day/night TISI based method and TTM method. In order to lower the number of unknowns and increase the stability of the retrieval, this method makes the assumption that the LSEs do not considerably change from day to night and that the angular form factor only slightly varies (b2%) in the relevant MIR wavelength range. Two variables, the air temperature at the surface level (Ta) and the atmospheric WV, are introduced to adjust the initial atmospheric profiles in the retrieval in order to lessen the impact of the residual error of atmospheric corrections on the retrieval.

The number of unknowns with two measurements (day and night) in N channels is N+7 (N channel LSEs, 2 LSTs, 2 Ta, 2 WV, and 1 angular form factor in the MIR channels). N must therefore be equal to or bigger than seven for the equations to be deterministic.

However, the D/N technique still experiences the crucial issues of geometry mis-registration and variations in the VZA, just like the other multi-temporal methods.(Z. L. Li et al., 2013)

`

Methods	Assumptions	Advantages	Disadvantages and Limitations
Day/night temperature independent spectral indices (TISI) based methods	Emissivity ratios are the same or do not change significantly between two times. i.e., day and night	1) Approximate atmospheric corrections are sufficient 2) Physical basis and suitable for various surfaces	1) Require approximate atmospheric corrections 2) At least two channels, one in MIR and another in TIR atmospheric windows, are available 3) Require accurate geometric registration 4) Observations must be conducted at similar
Classification-based emissivity method (CBEM)	Surface materials in the same class have the same emissivity	1) Simplicity 2) Accurate atmospheric correction is not required	1) Require a priori knowledge of the emissivity of each class, as well as the corresponding classification map 2) Seasonal and dynamic states of surfaces may degrade the accuracy 3) Less accurate at coarse resolutions and less reliable for classes with contrast emissivities.
NDVI-based emissivity method (NBEM).	1) Surface is composed of soil and vegetation 2) Variation of LSE is linearly dependent on the fraction of vegetation in a pixel	1) Simplicity 2) Suitable for various sensors with red/near infrared bands and TIR band 3) Accurate atmospheric correction is not required	1) Uncertainty of the soil and the vegetation emissivities, of the NDVI thresholds for soil and vegetation, of the vegetation fraction, and of cavity effects may degrade the accuracy 2) Less accurate for surfaces covered only by soil 3) Inapplicable on surfaces such as water, ice, snow, and rocks and fails for surfaces containing sense recent vegetation
Two-temperature method (TTM)	Emissivity is invariant at two times	1) More suitable for geostationary satellite data 2) Simultaneously retrieve LST and LSEs	1) Require accurate atmospheric corrections at different times 2) Requires multi-temporal TIR data and large temperature difference between different times 3) Require accurate geometric registration

`

			4) Solution more sensitive to instrument noise and errors in atmospheric corrections 5) Observations must be conducted under similar viewing angles
Physics-based day/night operational methods (D/N)	1) LSEs do not change significantly at day and night times 2) Angular form factor has very small variation in MIR channels	1) Does not require a prior accurate atmospheric profiles 2) Solutions become more stable and accurate by introducing the MIR channels 3) Accuracy of the LSTs and LSEs is greatly improved by modifying the atmospheric profiles in the retrieval 4) Accurately retrieve both LSTs and LSEs on a physical basis	1) Require multi-temporal data in several channels in the MIR and TIR atmospheric windows 2) Require accurate geometric registration 3) Approximate shapes of the atmospheric profiles need to be given a priori 4) Retrieval process is complicated, and initial guess values are required 5) Observations must be conducted at similar viewing angles

Table 2.3 Land Surface Emissivity Methods, Assumptions, Advantages and Disadvantages

2.9 Land cover spectral indices

A spectral index is a formula used in science that is applied to various spectral bands of an image per pixel to produce significant evidence. Spectral indices support surface process modeling, prediction, or inference. Spectral indices help in modeling, predicting, or infer surface processes. Indices are derived for many different combinations of satellite spectral bands. There are various applications of the satellite indices that are explored in the past studies includes agriculture, water resources, urban development, forest ecology, geology, soil sciences, vegetation, and other applications.(Prasad et al., 2022)

Normalized difference vegetation index (NDVI)

NDVI is a dimensionless index that describes the difference between visible and nearinfrared reflectance of vegetation cover and can be used to estimate the density of green on an area of land (Weier & Herring, 2000). NDVI values vary from -1 to 1, regardless of whether radiance, reflectance, or DN are used as input. In general, its values are near to zero for rocks, sand, or concrete surfaces, negative for bodies of water, and positive for vegetation, such as crops, shrubs, grasses, and woods.(Jones & Vaughan, 2011)

Normalized difference Built-up index (NDBI)

Furthermore, (Zha et al., 2003) made a contribution in this field by creating the well-known Normalized Difference Built-up Area Index to aid in urban built-up area extraction (NDBI). The creation of NDBI on the basis of previously developed NDVI allowed for the monitoring and mapping of urban built-up areas. This widely used algorithm has been developed as an automatic built-up area recognition technique using Landsat TM data satellite pictures of medium spatial and spectral resolution without the usage of training samples. Additionally, this built-up area index is capable of identifying built-up surfaces by using the reflecting wavelengths of near-infrared (NIR) and mid-infrared (MIR) (i.e., band 4 and band 5 of Landsat TM satellite). The NDBI was derived based on the fact that built-up surfaces reflect more light in the MIR than the NIR. Additionally, this index is widely used because of how quickly it processes data and how simple calculations are. The NDBI values typically range from -1 to +1. The developed area is thought to be represented by the NDBI's favorable result.(Zha et al., 2003)

`

Normalized difference Water Index (NDWI)

The normalized difference water index (NDWI) was created in 1996. It resembles the NDVI, or normalized difference vegetation index (Goward et al., 1991; McFeeters, 1996). Solar radiation interacts with liquid molecules in vegetation canopies as measured by NDWI. It uses the green band and near infrared band of Landsat TM to create two-band spectral water indices. Water absorbs heavily in the NIR band and is significantly reflected in the green band. As a result, NDWI took advantage of this, and the following equation is used to calculate NDWI (McFeeters, 1996)

Normalized Difference Bareness Index (NDBAI)

Using Landsat data, (Chen et al., 2006) suggested a normalized difference bareness index (NDBAI) to identify bare land from other land use groups. This index is based on the fact that bare soil radiates more heat on the thermal band. The value of NDBAI ranges between 1 and +1, and it can be used to monitor bare soil, land conversion, impervious surface, and its relationship to surface temperature (Zhao & Chen, 2005) NDBAI's positive number typically denotes bare land. With an increase in the positive NDBAI, the bareness increases.

2.10 EMPERICAL REVIEW

Currently, more than 50% of the world's population lives in cities, and by 2050, that percentage is projected to rise to 66%. (*2014 | UN DESA | United Nations Department of Economic and Social Affairs*, n.d.) This number shows a fluctuating rise in the number of urban residents. African and Asian developing nations, in particular, are more responsible for this rapid rise in urbanization ((UN-HABITAT, 2010, 2013)). As a result the urban and rural landscapes are both changed by the rapid growth of the urban population. Extreme LULC change will result in the replacement of natural vegetation and greenery areas with impermeable surfaces which in turn primarily influences surface temperature of the urban and surrounding area. (Balew & Korme, 2020; Feyisa et al., 2016; Pham & Yamaguchi, 2011; Renee et al., 2006; Sisay & Korme, 2019; Zhao et al., 2016; Zheng et al., 2014).

2.10.1 Global Perspective

Studies that sought to comprehend how changes in land use and cover affected the land surface temperature in rural and urban areas (Urban Heat Island) used urban-rural gradient analysis to establishing several buffer zones surrounding study areas, (Estoque & Murayama, 2017) found in general, the pattern of mean LST throughout urban-rural gradients represents a typical profile of the UHI Phenomena, with LST steadily dropping along the urban-rural gradient with some spikes, valleys, plateaus, and basins. (Ranagalage et al., 2019) found that URZ1 near the city center has the highest mean LST value. The mean LST of URZ1 was 19.8 C in 1996, 18.9 C in 2006, and 24.4 C in 2017. In 1996, the mean LST was 19.8 C. On the other hand, from 1996 to 2017, the mean LST of all other URZs grew. The findings showed that between 1996 and 2017, the mean LST of the other URZs ranged from 18.9 C to 21.2 C. The data also showed that URZ12 in 1996, URZ10 in 2006, and URZ19 in 2017 had the lowest recorded temperatures.

Regarding the impact of vegetation in lowering land surface temperature (An et al., 2022) examined how UGS affected LST in various urban blocks. The findings revealed that UGS acts as chilly islands between different urban blocks. The findings also indicate that both the composition and arrangement of UGS can influence LST among various urban blocks, and that a logical distribution of UGS would be useful for reducing the effects of UHI. (Brown et al. 2015; Shiflett et al. 2017) showed that Vegetation, particularly trees, helps to cool the surface of hot and arid cities by providing shade, evapotranspiration, intercepting solar radiation, and establishing park cool islands.

Considering how water bodies acted as a cooling agent (Gupta et al., 2019) showed that the presence of surface water bodies in a region is what causes potential cooling through evaporation, which lessens the heating effect. The result showed that Land surface temperature of the surrounding increased as the distance from the surface water increased and vice versa. (Khan et al., 2019)) also showed that According to their findings, Surface water bodies decreased from 11,379 km2 in 2000 to 9657 km2 in 2015. According to the trend study, the country's LST rise was accelerated by changes in Surface Water bodies. According to the spatial study conducted throughout the relevant years, there is a correlation between a rise in LST and a fall in Surface water bodies showing the effect of water bodies on Land surface Temperature.

(Adeyeri et al., 2019) and (Hellman & Ramsey, 2004) also showed that surface reflectance from volcanic ash deposit on bare land and the presence of hot rocks located deeper in the crust are the major cause for the observed cold and hot islands in the current study area.

Considering the impact of spatial arrangement and its connection to land surface temperature (Estoque et al., 2017) found that size, shape complexity and aggregation of the patches of impervious surface and green space showed a noticeable relationship with Land surface Temperature, while aggregation had a very strong correlation with land surface Temperature. In this study Mean patch size and mean shape index of the patches of impervious showed positive relationship with Land surface temperature while green space showed negative relationship with Land surface Temperature. Aggregation of patches of impervious and green land use showed a very strong consistent relationship with Land surface temperature. (Maimaitiyiming et al., 2014) findings demonstrated that (1) both the composition and configuration of green space contribute to urban heat island, (2) joint effects of any two combinations of metrics were greater than the effect of a single metric, (3) ED and PD combined was the most deterministic factor of LST than the unique effects of a single variable or the joint effects PLAND and PD or PLAND and ED, and (4) optimizing the configuration of green space which increases the PD and ED should be prioritized in planning To lessen the consequences of urban heat islands, they must to be given priority in urban planning and development.

`

2.10.2 Local Perspective

Given the fact Land use Land cover plays a strong role in surface temperature it is important to understand the role of Land use Land cover on Land surface Temperature. (Balew & Korme, 2020) found that Land surface Temperature was higher for Agricultural Land and Paved surface while it was lower for Vegetation and Water body. similarly (Haylemariyam, 2018) found that Built up area and barren Land recorded Higher Land surface temperature while shrub land and Dry river exhibited lower Land Surface Temperature.This findings were constant with (Asfaw,2017) who also found that Urban, bare and cultivated land exhibited higher Land surface temperature and had a positive gain relationship with Land surface temperature whilst shrub and forest land showed Lower Land surface temperature and showed a negative gain relationship with Land surface temperature. However, these studies did not address the impact of newly added land use land cover classes such a built up on Land surface temperature.

Studies that attempted to understand Land use Land cover change and its effect on the LST on Urban and rural areas (Urban Heat Island) applied urban-rural gradient analysis by creating studies (Abel Balew &Fisha Semaw, 2022) found that SUHI was higher in the urban area and lower in the surrounding or rural area. (Balew & Korme, 2020) found that urban city has lower Land surface temperature due to the cool air because the urban area was near Lake Tana while the sub urban area had higher Land surface temperature. However, these studies did not show whether the landscape metrics of vegetation and built up played an important in the urban and rural surface temperature variation.

With respect to vegetation role in reducing Land surface temperature (Samson et al.,2018) found that public parks reach in vegetation in urban area compared to the surrounding area showed a difference up to 5oc difference showing the role urban vegetation played in reducing Land surface Temperature. (Amanuel, 2020) also found that the placement of Green infrastructure played a major role in reducing lad surface temperature. The results showed that distance from park was positively correlated with Land surface Temperature. As a distance increased by 500m the mean Land surface Temperature increased by 0.53oc. The study also found that increasing the Green infrastructure on hot spot area by 13 % the mean Land surface temperature drops approximately by 0.79oc cementing the importance role vegetation plays in reducing Land surface Temperature. Nega et al., (2019) also signified the impact of vegetation. In his study in recorded that mean annual Land surface rainfall decrease as vegetation decreased as a result of decreasing vegetation cover which in turn resulted in the increment of Land surface Temperature of the study area. However, these studies did not show whether the composition or pattern of vegetation had a stronger effect on reducing land surface temperature.

Taking into consideration how water bodies played a cooling role Balew & Korme, (2020) showed that the land surface temperature in urban city was lower when compare to sub urban land surface temperature because of the fact the urban area was near to Lake Tana. Dagnachew et al., (2019) also found that the minimum temperature was found in the lake and surrounding areas of wet land. However, these studies did not show to what extent the distance from water bodies affected the land surface temperature of the surrounding area and how land surface temperature of water bodies behaved on different seasons.

Dagnachew et al., (2019) also found that volcanic process in the city are one of the main caused for the high land surface temperature in the city. The study showed that hot rocks located deep in the crust transferred heat into the earth surface resulting in higher land surface temperature.

Taking into consideration the effect of spatial configuration and its relation with land surface temperature (Ezra, 2022) tried to analyze the relationship between vegetation cover spatial pattern and Land surface Temperature. Among the four vegetation land cover configuration used Edge Density, Patch Density and Fractional Dimension index related more closely than Land surface Temperature. It also found that 57% of variation in Land surface Temperature was jointly by the three configuration variables. The study showed that 10 % increase in Patch Density and Edge Density of vegetation land cover approximately resulted in 0.91 oc and 0.24oc decrease in Land surface Temperature and 0.1 increase in Fractional Dimension of vegetation configuration decreased Land surface Temperature by 2.58oc, therefore cementing the Geographical distribution and arrangement of vegetation and land cover had a recognizable effect on Land surface Temperature. However, these study did not the correlation of land use land cover classes density and land surface temperature and whether landscape pattern configuration or composition played a stronger role in land surface temperature.

`

2.10.3 Research and Knowledge Gap

The above studies effectively showed the importance of understanding effect of Land use and Land cover and its change on Land surface Temperature and how it affected our environment. However, given the existing urbanization-induced increase in land surface temperature and the possibility of a future increase due to urbanization and Land use Land cover change, they fall short and raise a number of significant issues.

Furthermore, existing Ethiopian studies concentrating on the above studies concluded their result in studies conducted for dry season. This gap left it unclear how the aforementioned data behaved over other seasons, as well as what the influence of land use and land cover change on land surface temperature will be seasonally in a given research area. Moreover the dry season and wet season will have different impact on the surface temperature of major land use and land cover classes such as built up, vegetation, water bodies, agricultural lands and bare lands and understanding how these classes' surface temperature will interact and affect the environment is relevant. For example water bodies may exhibit higher land surface temperature during winter and lower land surface temperature on dry season whilst other may exhibit vice versa .Therefore understanding how these phenomena affect the formation of urban heat island seasonally will enhances our understanding for future mitigation. More over the above researches focused on the effect of land use and land cover on land surface temperature on the current situation and did not predict or model what the future trend of land surface temperature will be with respect to land use land cover change in the future. Modelling and predicting future land use land cover changes along with land surface temperature will allow us how severe the increment of land surface temperature will be and take the necessary steps needed to counteract it.

It is evident that Adama city urbanization rate is increasing at a faster rate from time to time which has led to an increased urban heat island phenomena. As this increment is bound to increase it is important to have a deeper understanding of the effect of land use land cover change on land surface temperature in different scenarios and one of these scenarios being seasonal variation. It is evident Seasonal variation of land surface temperature as a result of change in land use land cover will have adverse effect in construction, planning, agriculture, climate and many more if not addressed.

`

CHAPTER 3. MATERIALS AND METHODS

3.1 Description of Study Area

3.1.1 Geographical Location

Adama is a city in Ethiopia's central Oromia Region (Figure 1), located in the east Shewa Zone 99 kilometers southeast of Addis Abeba. The city is situated between the base of an escarpment to the west and the Great Rift Valley to the east. Encompassing an area of roughly 313.04 km2 and falling within the latitude range of 8° 26'35" to 8° 38'46"N and the longitude range of 39° 9'20" to 39° 21'30"E. One of the railway urban centers, Adama city was established in 1916 as a depot along the Addis Ababa-Djibouti railway line. The development of the Addis Ababa-Djibouti railway line was a key component in the emergence.

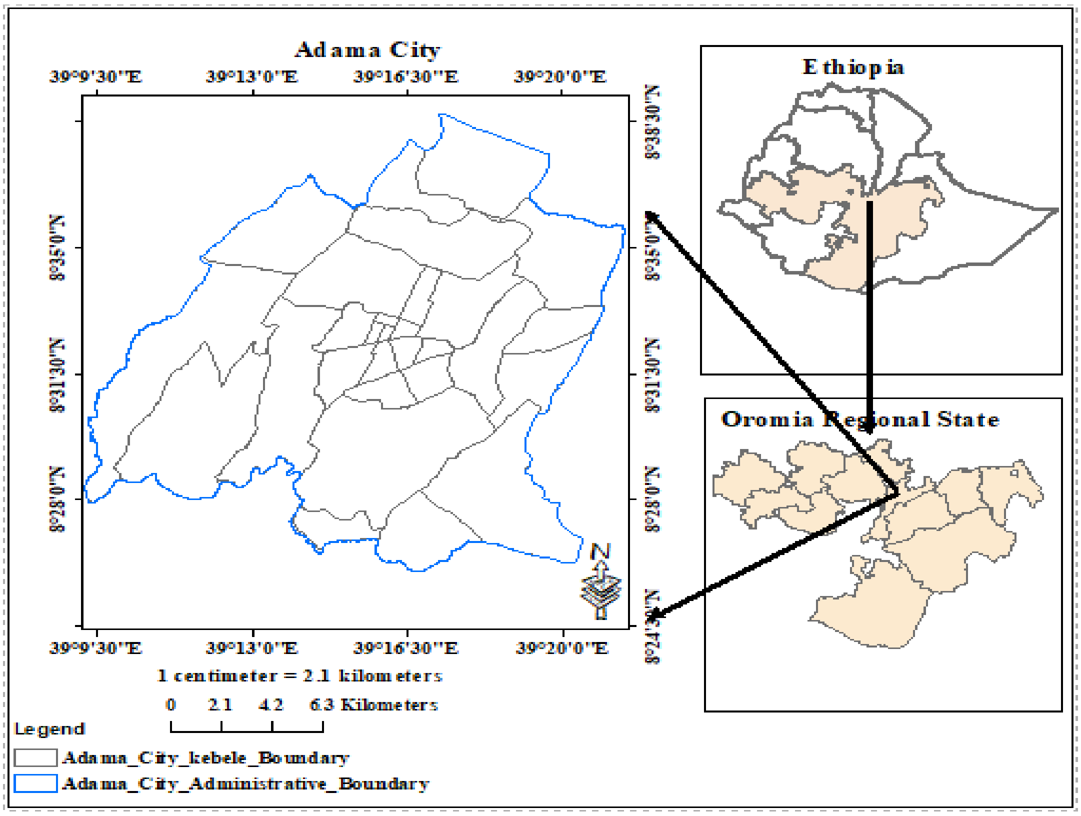

Figure 3.1 Location Map of study Area

`

3.1.2 Demographic

Adama city is Ethiopia's fourth largest urban center in terms of population size (Central Statistical Authority, 2021). Additionally, it is one of the few cities in the nation with a threshold population of over 300,000 and the largest urban hub in the Oromia Region. Since 1965 G.C., when the first baseline urban demographic survey was carried out in the nation, the city has experienced long-term population survey trends that have been documented by the majority of demographic and housing censuses and surveys (Socio Economic Profile of Adama, 2018). According to the country's past three successive censuses, Adama city showed a significant rise in population in the first Ethiopian population and housing census, which was held in May 1984. The population of Adama was 77,237. In the third base Ethiopian population and housing census, which was held in 2007 (the most recent year for which statistics are available), 220,212 people were inhabited in Adama. The following population and housing census, conducted in 1994, indicated that Adama had a total population of 127,842. According to the Oromia Urban Planning Institution (OUPI), the population of Adama City was 232,152 in 2007 due to the exclusion of four Gandas/kebeles, namely Daka Adi, Dabe Soloke, Boku Shenen, and Melka Adama, with a combined population of around 11,940. According to the revised structural plan, 11 new rural Gandas/kebeles are defined within the city administrative limit based on the projected population of 435,222 (Central Statistical Authority, 2021), with 212,991 men and 222,231 women.

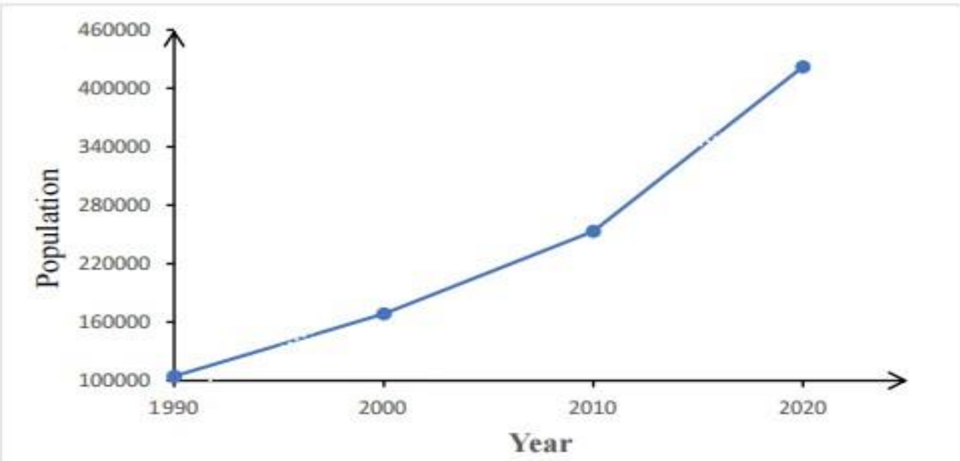

Figure 3.2 Population of Adama City from 1990 – 2021

`

3.1.3 Urban Growth

In terms of population, urban built-up area, and economic function, Adama is one of Ethiopia's fastest-growing cities. According to Tesema & Assefa (2019), the city's population increased by 9% between 2004 and 2016; by 2021, the overall population is expected to be close to 435,222. (Central Statistical Authority,2021). Both naturally occurring urbanization and rural-to-urban migration contribute to the growth of Adama city. In fact, migrants from nearby rural areas, rural areas in other regions, and other cities make up the majority of the city's population. According to the 1984 census, migrants made up 53.7% of the city's population, making Adama one of the regions and countries with a substantial intake of migrants each year. Similar to how the proportion of migrants peaked at 52.9% in the second census of 1994 after a decade, and was expected to have reached 59.2% in the 2007 census (CSA, 1984, 1994, 2007), As was already said, a significant section of the population of Adama city consists of migrants, who are primarily drew to the city in quest of job, demonstrating a city's capacity to pull citizens from other cities or rural regions.

Between 1984 and 2015, Adama City's built-up area increased by 293%. (Sinha et al., 2016) Similar to this, Dejene & Abebe (2019) claimed that from 1995 to 2019, the city's built-up area increased by 22% year, more than doubling. The city of Adama is growing and expanding, and it is making an ever-greater economic contribution to the area and the nation. The top three industries for employment in Adama City are wholesale trade, manufacturing, and construction, which account for 23.2%, 19.0%, and 9.4% of all jobs, respectively. However, the city's economy also greatly benefits from other sectors, such as transportation and storage, the service sector (real estate, hotels, food, and services), retail, and construction (Dube & Mulugeta, 2015). To summarize, Adama City's urban growth over the last few decades can be linked to geological as well as socio-demographic factors.

`

3.1.4 Climate condition

3.1.4.1 Temperature

The city's mean annual temperature is 22.87°C, according to data from the Ethiopian Meteorology Agency's Adama station (1990-2021). The climate is categorized as semi-humid to semi-arid. The hottest months of Adama are from March through June, with a maximum mean temperature of above 32°C in May. (Figure 3) November through December and January through February had the lowest monthly mean temperatures. Maximum temperatures range from 27.36 to 32.24 degrees Celsius, and the minimum monthly humidity ranges from 14.01 to 18.56 degrees Celsius.

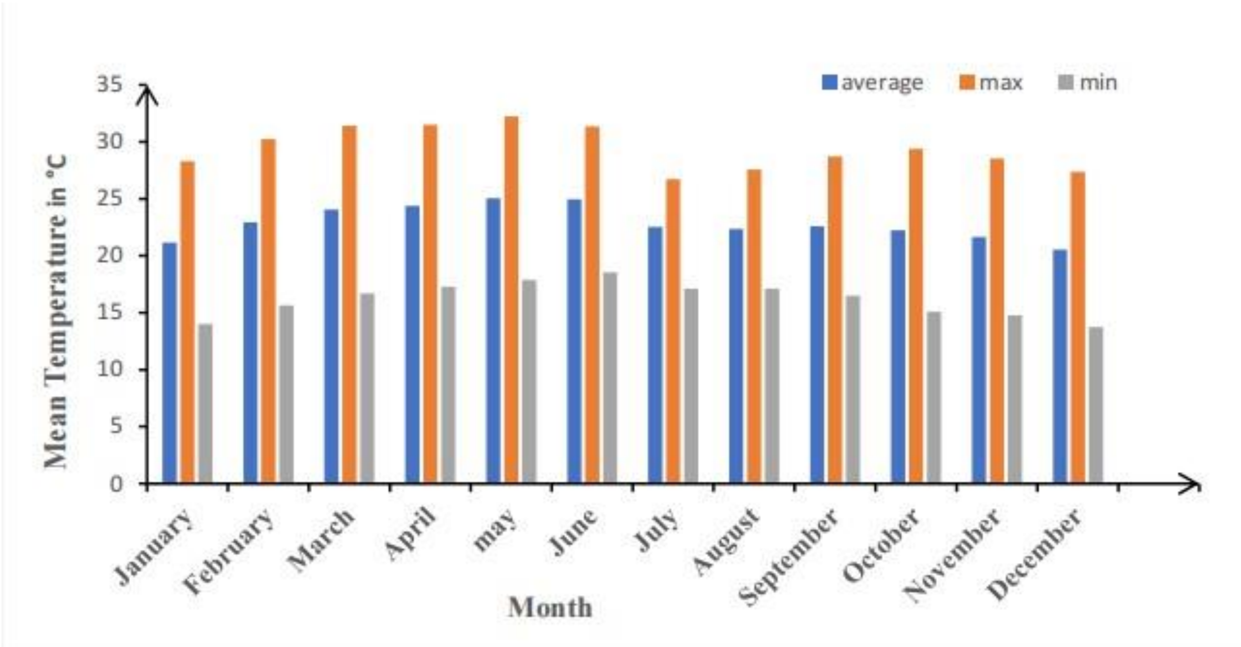

Figure 3.3 Adama city monthly Mean Max, Min and Average Temperature from 1990-2021

Due to its geographical location, Adama City has a hospitable climate. It is surrounded by plateaus with moderate temperatures and copious, heavy rainfall that is beneficial for life. Summer is the rainiest season of the year in Adama City, where there is just one meteorology station.

3.1.4.2 Rainfall

According to the Adama Meteorological Station's rainfall data from 2001 to 2021, Adama City is located in the country's region with the most summer rainfall. The maximum monthly average rainfall in Adama City was 240.227 mm in the month of July, with the mean annual rainfall of the city being 1035.217 mm (Figure 3.3). The two months that produce the most rainfall are July and August, whereas the minimum rainfall acquired was during December–February.

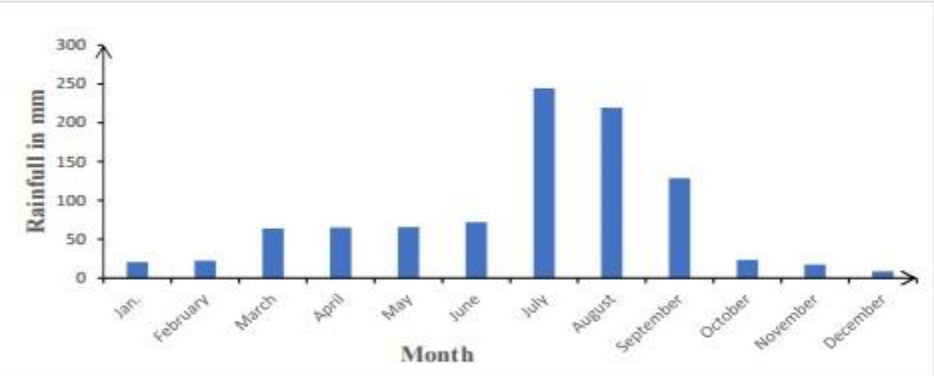

Figure 3.4 Adama City Monthly Average Rainfall from 2001-2020

3.1.5 Topography

The current built-up region of Adama city has a flat topography and is situated between the "Kechema" and "Boriticha" uplands. This topography typically rolls down from north (Dhaka Adi) to south high to the expressway that connects Addis Abeba to Adama. During the rainy season, flooding from the dissected uplands affects the western and eastern portions of the built-up areas that are close to the Kechema and Boriticha uplands. In the Great Ethiopian Rift Valley is the city of Adama. Plain and plateau landscapes can be found within this significant landform. There are also smaller, wider, shallower, and deeper gullies within these landscapes. The elevation varies between 1,452 and 2055 meters above sea level. The expansion zones' extreme east and northwest corners are where the lowest and highest points are found.

3.1.6 Land use land cover

Residential, commercial, business administrative, open spaces and environmentally sensitive regions with graveyards, sports and recreational, manufacturing, and storage are among the land use categories in Adama city.

`

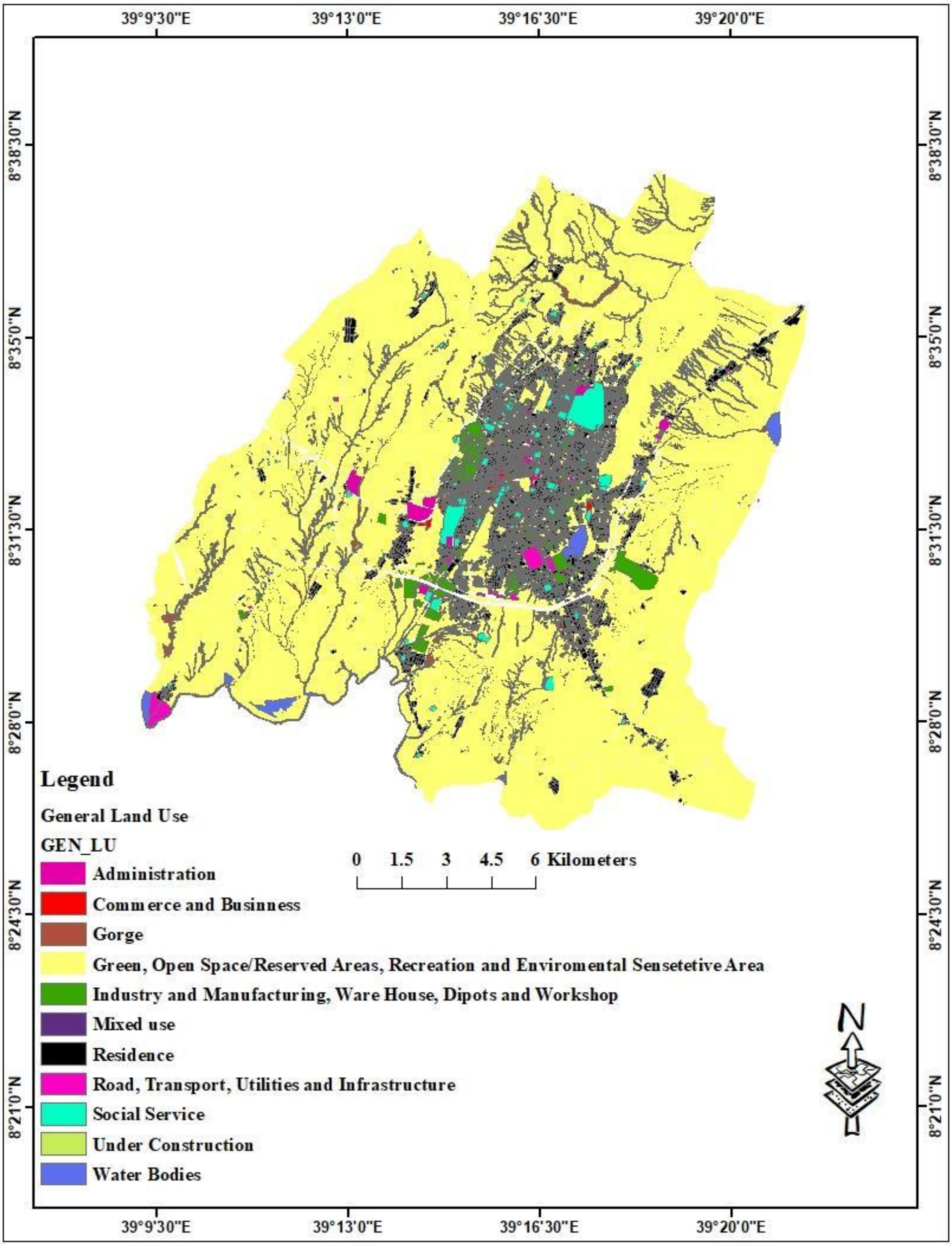

Figure 3.5 Land use category map of adama city

3.2 Data Source

This study utilizes Landsat and MODIS satellite data to analyze the land surface temperature (LST) patterns in Adama, Ethiopia, across different seasons (Bega, Belge, and Kiremete) and years (1991, 2000, 2010, and 2022). The Landsat data, obtained from the United States Geological Survey (USGS), includes Landsat 5 TM, Landsat 7 ETM+, and Landsat 8 OLI/TIRS imagery with a spatial resolution of 30 meters. The Landsat scenes were selected based on the season and year of interest, considering factors such as cloud coverage and data availability.

The MODIS data, specifically the MOD11A2 Version 6 product, was acquired from United States Geological Survey (USGS). The MOD11A2 product provides an 8-day composite of land surface temperature and emissivity data at a spatial resolution of 1000 meters (1 km). The MODIS data was selected to correspond with the seasons and years of the Landsat data, allowing for a multi-scale analysis of LST patterns.

Table 3.1 Data source used

Satellite/ Sensor	Season	Date	Scene Center time in GMT	Cloud Coverage	Spatial Resolution
Landsat 5 TM	Bega	1991-01-19	"07:00:45.8710690Z"	0.00	30
	Belge	1991-04-09	"07:02:12.1310630Z"	5.00	30
	Kiremete	1991-09-16	"07:04:18.7710130Z"	6.00	30
Landsat 7 ETM+	Bega	2000-12-05	"07:30:42.0892444Z"	0.00	30
	Belge	2000-05-27	"07:32:21.0346824Z"	10.00	30
	Kiremete	2000-09-16	"07:30:57.5111704Z"	24.00	30
	Bega	2010-01-15	"07:31:54.6902892Z"	0.00	30
	Belge	2010-04-05	"07:32:36.2731444Z"	15.00	30
	Kiremte	2010-09-28	"07:32:40.0353533Z"	12.00	30

Landsat 8 OLI/TIRS	Bega	2022-11-16	"07:40:52.1474710Z"	4.50	30
	Belge	2022-05-16	"07:40:19.8069910Z"	1.92	30
	Kiremte	2022-09-21	"07:41:02.6824319Z"	27.85	30

Table 3.2 Validation Data Used for Land Surface Temperature

Product	Date	Season	Temporal Resolution	Spatial Resolution
MOD11A2.061	2000-337 (2000-12-02	Bega	8 days	1000 m
MOD11A2.061	2000-137 (2000-05-16)	Belge	8 days	1000 m
MOD11A2.061	2000-257 (2000-09-13)	Kiremete	8 days	1000 m
MOD11A2.061	2010-017 (2010-01-17)	Bega	8 days	
MOD11A2.061	2010-097 (2010-04-07)	Belge	8 days	1000 m
MOD11A2.061	2010-265 (2010-09-22)	Kiremete	8 days	1000 m
MOD11A2.061	2022-313 (2022-11-09)	Bega	8 days	1000 m
MOD11A2.061	2022-129 (2022-05-09)	Belge	8 days	1000 m
MOD11A2.061	2022-257 (2022-09-14)	Kiremete	8 days	1000 m

Administrative border, road network, existing LULC, city structure plan, population, and meteorological data are obtained from their respective sources, as mentioned in the report

Table 3.3 Ancillary Data Source used

Data	Data Source
Administrative Boundary	Oromia Urban Planning Institute
Population Data	CSA and Oromia Urban Planning Institute
Climate Data	NMA Adama Station

Existing Land use	Adama City administration urban land sectors office
Validation Data Reference	Google Image

3.3 Software Used

The software that are utilized in this study are chosen based its ability to work on existing problems while meeting the set objectives. Different applications are employed to accomplish the study's goal. In order to process and classify satellite pictures, ENVI 5.3 is utilized. Additionally, Fragstats 4.2 is used to analyze spatial patterns, and Google Earth Pro is used to verify the accuracy of the land use/land cover class. Additionally, ArcGIS 10.8 is used for LST inversion, spatial analysis, and map creation and SPSS is utilized for statistical analysis.

Table 3.4 Software used

Software	Purpose
ENVI	Image preprocessing and classification
FRAGSTAT	Landscape dynamics analysis of Landscape pattern
ArcGIS	LST Retrieval ,Spatial Analysis And Mapping
SPSS	Statical analysis and graphical Representation
Google Earth Pro	Visual Image Interpretation and validation of the result

`

3.4 Data collection Method

Justification for the Selection of Seasons

According to the Ethiopian Meteorology Agency:

- Bega (October to January): Dry and cold weather conditions prevail over much of the nation.
- Belg (February to May): Short rainy season for northeast, east, central, and southern highlands; main rainy season for south and southeast portions. May is usually the hottest month in Adama.
- Kiremte (June to September): Main rainy season across much of Ethiopia. July is usually the coldest month in Adama

Justification for the Selection of Years

As part of this study, an interdecadal time frame from 1991 to 2022 was selected to analyze urbanization-induced land use and land cover (LULC) change in Adama city. This time frame can be attributed to two main factors. First, Ethiopia maintained a legacy of a centralist government structure until 1991 (Ferdissa, 2019), with cities and towns regarded as extensions of central authorities. This period illustrates the trend of urbanization in Adama city before and after the abolition of the centralized government structure. Second, Adama city's growth rate was moderate until 1991. The city had an area of 1.2 km² in 1937 and expanded slowly over 54 years to 34.20 km² in 1991. However, after 1991, the expansion intensified, with the city's size becoming roughly four times larger in 2004 and nine times larger in 2017 compared to its size in 1991. Furthermore, there is no ground truth available for the study area prior to 1990 in the decadal range.

Adama's population began to increase following decentralization, as the city became the capital of the Oromia region in 2000, attracting people from urban and rural areas seeking jobs and associated opportunities (Äthiopien, 2019). The incorporation of Kebeles under municipal management after the 2005 parliamentary election was another significant factor, with four rural kebeles managed as a city's district, comprising about 18% of the urban population (Äthiopien, 2019). The second wave of decentralization, also known as "Woreda or District level decentralization," has been in effect since 2002, transferring authority from the region to the Woreda, Kebele, and Zonal levels of government to improve service delivery, increase participation in governance, and foster local economic development (UN-HABITAT, 2002:89).

In August 2000, Adama received a new status as the capital of the National Regional State and the largest Regional State in Ethiopia, Oromia, significantly impacting the city's rapid development. The city's population grew from 127,842 in 2004 to 356,304 in 2016 ((Bulti & Sori, 2017)

Landsat Sensor

The Landsat Program is a collection of Earth-observing satellite missions managed cooperatively by NASA and the United States Geological Survey. In order to effectively track land use and document land change brought on by climate change, urbanization, drought, wildfire, biomass changes (carbon assessments), and a host of other natural and human-caused changes, Landsat satellites have the best ground resolution and spectral bands. For In this study Landsat 5 TM, Landsat 7 ETM+ and Landsat 8 OLI/TIRS are used for three seasons mainly Bega, Belge and Kiremete Seasons. These imageries are collected free of charge from the United States Geological Survey website (http://earthexplorer.usgs.gov).

Cloud Cover

It is apparent that an image free from cloud cover is an important criteria for accurate analysis. However since this study focuses on seasonal effects .Bega, Belge and Kiremete, a certain amount of cloud coverage is present. By observing some literatures it was found that the cloud coverage was more predominant in other area of the scene rather that the study area, images are acquired for the three seasons.

3.5 Method of Data Preprocessing

3.5.1 Pre-Processing

- **Radiometric calibration**

The capacity to translate digital numbers captured by satellite imaging systems into physical units is referred to as radiometric calibration. Either radiance (W/m2/sr/m) or apparent top-of-atmosphere reflectance are used as those units. This type of correction is important for reliable quantitative measurements of the imagery. This correction is made using ENVI software.

- **Atmospheric Correction**

Atmospheric image correction is critical for obtaining an accurate image since the radiation from the source always interacts with the atmosphere, which might affect the image brightness level. Therefore in order to increase the quality of the images atmospheric correction is used. ENVI software is used for the atmospheric correction

- **Gap filling method**

Landsat 7 ETM+ suffered a scan line corrector failure in May 2003, causing the imaged region to be duplicated and the scanning pattern to exhibit wedge-shaped scan-to-scan gaps that ranged from a single pixel at the center of the image to about 14 pixels along the east and west corners of each scene on average (Maxwell et al., 2007). This scan line error is corrected in ENVI using an additional module called Landsat gap fill.

- **Layer Stacking**

Layer stacking is the process of mixing numerous distinct bands to create a new multiband image. These multiband graphics are helpful for seeing and locating the various Land Use and Land Cover classes. The extent of numerous image bands must match in order to layer stack (no. of rows and columns). ENVI layer stacking tool is used to layer the various Bands into a multiple band.

`

- **Projection**

Every Landsat image needs to be projected to a local reference Datum. To Adindan in our case study. This is done using ENVI software.

- **Sub setting**

Because the study area is Adama city, the city's most recent structural plan is used as a boundary to subset the study area portion from the Image.

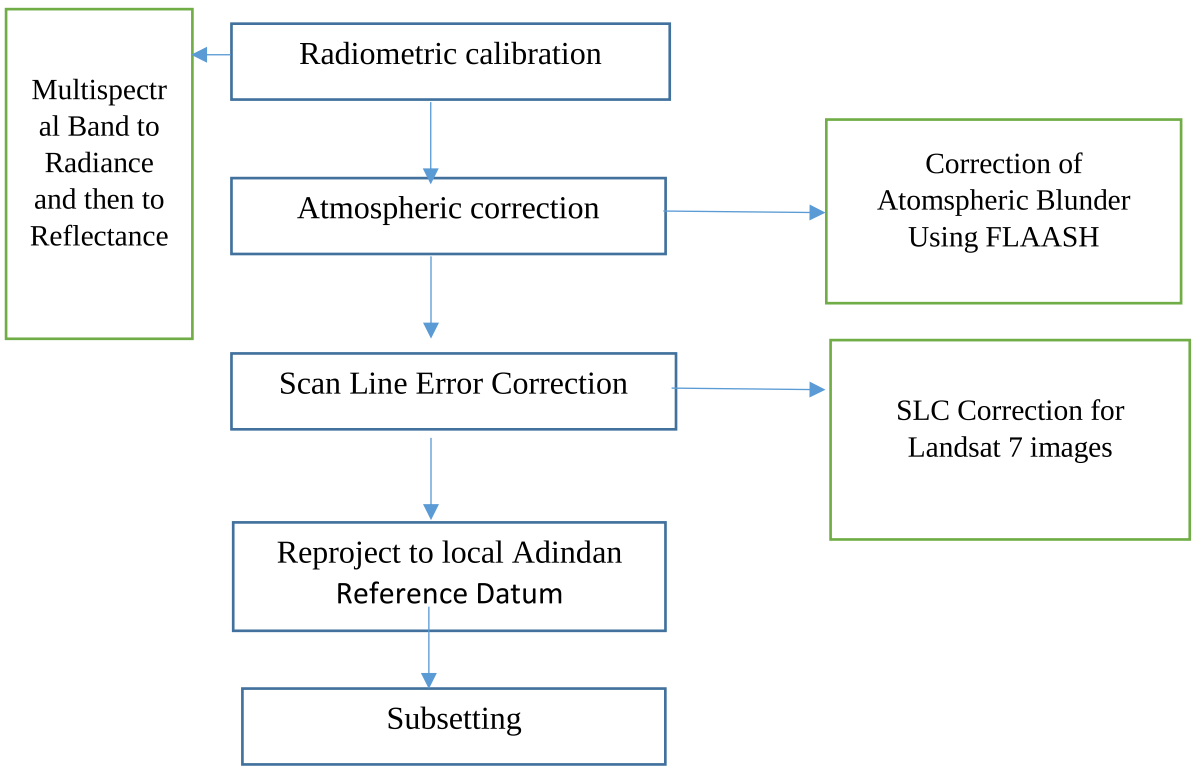

Figure 3.6 Image pre-Processing

3.6 Method of Data analysis

3.6.1 Land Use Land Cover Dynamics

3.6.1.1 Land use Land Cover extraction

Supervised Land Use Land cover Classification

Using supervised classification, the analyst finds representative samples of the various surface cover types (information classes) of relevance in the images. Training areas are the names given to these examples. Based on the analyst's familiarity with the region and understanding of the real surface cover types shown in the image, relevant training regions are chosen. The analyst is thus "supervising" the classification of a number of distinct classes. To "train" the computer to identify spectrally related areas for each class, numerical data in all spectral bands for the pixels making up these areas is employed. The computer determines the numerical "signatures" for each training class using a special program or algorithm (of which there are many variations). Each pixel in the image is compared to these signatures once the computer has identified the signatures for each class. The class that the pixel most closely "resembles" is then digitally labeled. To establish the spectral classes that represent them, we must first identify the information classes in a supervised classification.

SVM Classification

The Support Vector Machine classification (SVM) algorithm is used for this study since it is unaffected by training sample size and distribution, which is critical in supervised image classification. Additionally, it's critical for the mixed-pixel problem in metropolitan areas. Support Vector Machine (SVM) is a supervised classification technique that generally produces accurate classification results from complex and noisy data. It is derived on statistical learning theory. With a decision surface that optimizes the margin between the classes, it divides them. The closest data points to the hyperplane are known as support vectors, and the surface is frequently referred to as the ideal hyperplane. The crucial components of the training set are the support vectors.SVM draws a decision boundary which is a hyperplane between any two classes in order to separate them or classify them.

Accuracy assessment

The accuracy of information produced from remotely sensed data is determined by accuracy assessments. The objective is to quantitatively evaluate how well pixels in the study region were classified into the appropriate feature classes. The accuracy evaluation evaluates how effectively a categorization was made and how well one can interpret. Overall accuracy is the most typical estimate of inaccuracy, and Kappa coefficient (K) is a measure of accuracy agreement. It offers a measurement of the difference between the observed agreement between two maps and agreement that is just the result of chance.

In this study, ENVI is used for an accuracy assessment. To prevent bias in sampling, stratified random sampling type is utilized, which uses generated ground truth from ROIs. Using a Google image as a reference, ground truth ROIs are produced. After that, a confusion matrix between the ground truth ROIs and the categorized image is constructed.

Producer's Accuracy - quantifies the percentage of correctly identified pixels in a sample dataset or reveals errors of omission for a specific class. The total number of sample units from the reference data for a category will be divided by the number of correct sample units in that category (i.e., the column total).

$$\text{Producer's Accuracy} = (Ci) / (Ct) \times 100 \;\ldots\ldots\ldots\ldots\text{Equation 1}$$

Where Ct is the total number of sample sites in the column and Ci is the number of correctly identified sample locations in the reference data or column.

User's Accuracy - The total number of correct sample units in a category will be divided by the entire number of sample units on the map classified into that category (i.e., the row total). The commission error is measured by this outcome. The calculation is:

$$\text{User's Accuracy} = (Ri) / (Rt) \times 100 \ldots\ldots\ldots\ldots\text{Equation 2}$$

Where, Ri = correctly classified samples in the row and Rt = total number of samples in the row

Overall Accuracy - will be calculated by dividing the total number of correctly classified sample units by the total number of sample units in the error matrix. The accuracy evaluation statistic with the highest frequency of reporting is this one.

$$\text{Overall Accuracy} = (Sd) / (n) \times 100 \ldots\ldots\ldots\ldots\text{Equation 3}$$

`

Where, Sd = sum of values along diagonal and, n = total number of samples

Kappa statistics - was used to measure the agreement or accuracy between the remote sensing derived classification map and the reference data.

$$\textit{Kappa statistics} = \sum nii - \sum ni{+}n{+}I \;/\; N2 - \sum ni{-}n{-}i \text{..........} \textit{Equation 4}$$

Where K = number of rows in the error matrix; nii = number of observations in row i and Column i (on the major diagonal); ni+ = total of observations in row i (shown as marginal total to right of the matrix); n+i = total of observations in column i (shown as marginal total at bottom of the matrix) and N = total number of observations included in matrix

3.6.1.2 Land use Land cover Detection

In order to do a post classification change study, it is necessary to have two photos of the same scene that were shot under the same acquisition settings but at different times. The aforementioned method was determined to be the most effective at spotting changes in land use and land cover and will be used to reduce the potential impacts of atmospheric variables and sensor variances. By comparing the area values of one data set with the equivalent value of the second data set for each time, change statistics were calculated. According to Butt et al. (2015), the following equations will be used to determine change and percentages of change detection of LULCC.

$$\textit{Observed change } (\Delta) = A2 - A1 \text{..........} \textit{Equation 5}$$

$$\textit{Percentage of change } (\Delta\ \%) = A2 - A1 \;/\; A1 \times 100 \text{ ....} \textit{Equation 6}$$

`

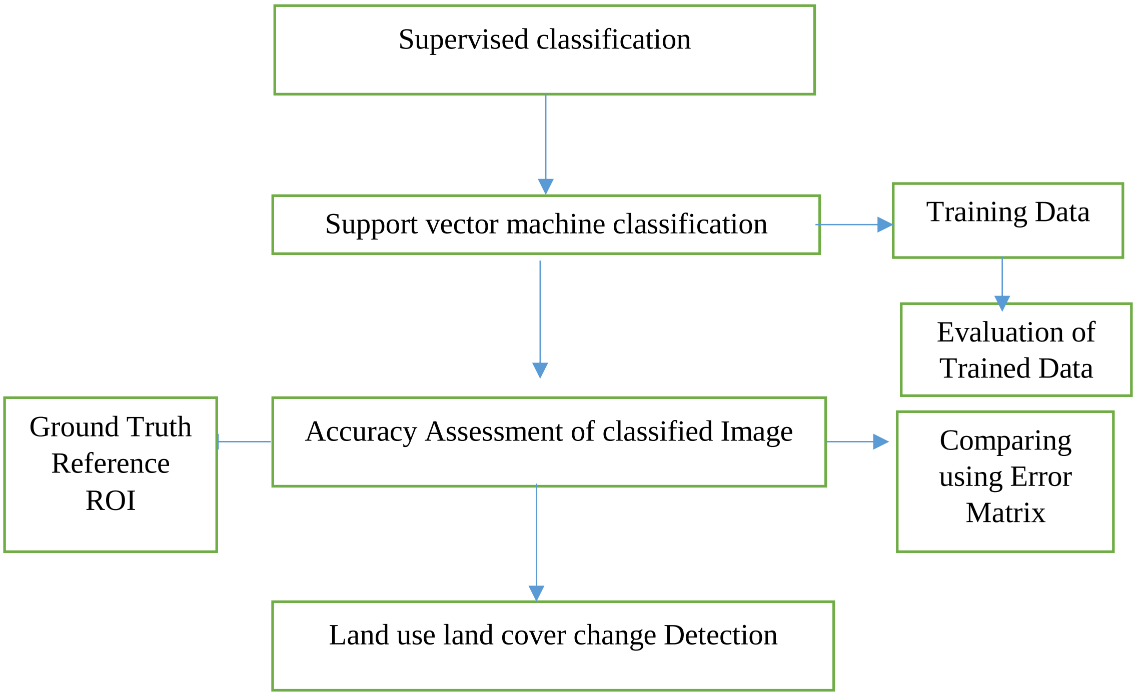

Figure 3.7 Land use Land cover change Detection

3.6.2 Retrieving Land Surface Temperature

To extract LST from Landsat pictures, raw data (digital numbers) from thermal bands (Band 6 in Landsat 5 TM and Landsat 7 ETM+, and Band 10 in Landsat 8 OLI/TIRS) are used transformed to spectral radiance using equation 7. (USGS, 2016).

$$L\lambda = M\lambda \times Qcal + AL \text{..........} \textit{Equation 7}$$

Where Lλ represents sensor spectrum radiance, Mλ represents radiance multiplicative scaling factor for the band from metadata, AL represents radiance additive scaling factor for the band from metadata, and Qcal represents quantized and calibrated pixel values in DN.

After converting raw data to spectral radiance, the brightness temperature is calculated using equation 8 (Balew & Korme, 2020; Sisay and Korme, 2019; Sultana & Sa

$$TB = K2 / ln(K1/L\lambda + 1) \text{..........} \textit{Equation 8}$$

where TB is the actual sensor brightness temperature, K2=Calibration constant 2 [K], 1260.56 for Landsat 5 TM, 1282.71 for Landsat 7 ETM+band 6, and Landsat 8 OLI/TIRS band 10=1321.0789; K1=Calibration constant 1 [K], 607.76 for Landsat 5, 666.09 for Landsat 7 band 6, and 774.8853 for Landsat 8 band; Lλ=Spectral radiance at the sensor's aperture [w/(m2 sr µm)] and ln = Natural Logarithm.

Equation 9 is used to calculate land surface emissivity (Avdan & Jovanovska, 2016).

$$E = mPv + n \text{..........} \textit{Equation 9}$$

Where m = (ev - es) (1- es)Fev, n = es + (1 - es)*Fev, eV = vegetation emissivity, es = soil emissivity, and F = 0.55 form parameters. Therefore, according to Sobrino et al. (2004), n = 0.986 and m = 0.004.

PV is calculated using soil and vegetation NDVI values (equation 10) (Balew & Korme, 2020; Sisay & Korme, 2019; Weng et al., 2004).

$$PV = (NDVI – NDVImin / NDVImax - NDVImin) \wedge 2 \text{..........} \textit{Equation 10}$$

Where, NDVImin is the lowest NDVI value derived from the raster NDVI and NDVImax is the highest NDVI value.

In accordance with equation 11 (Balew & Korme, 2020;Sisay & Korme, 2019), the NDVI is extracted from the red band and near-infrared band.

`

$$NDVI = NIRB – RedB / NIRB + RedB..........Equation\ 11$$

where NIRB is the near-infrared band reflectance (Band 4 in Landsat 5 and 7; Band 5 in Landsat 8); and RedB is the red band reflectance (Band 3 in Landsat 5 and 7; Band 4 in Landsat 8).

Finally, LST is recovered using equation 12 (; Balew & Korme, 2020; Dissanayake et al., 2019;Sisay & Korme, 2019).

$$ST = TB\ 1 + (\lambda \times TB/p)\ lne\ \lambda..........Equation\ 12$$

where λ is emitted radiance wavelength (11.435 μm and 11.335 μm for Landsat 5 and 7 band 6, respectively, and 10.9 μm for Landsat 8 band 10), p = 14380 which is calculated as = p = h C/a(1.438× 10−2 mK); σ is the Boltzmann constant (1.38× 10−23 J/K); h is Planck's constant (6.626× 10– 34 J/s), and C is the velocity of light (2.998× 108m/s)

Equation 13 is used to calculate LST values in degrees Celsius (°C).

$$ST(\circ C) = ST\ (K) - 273.15..........Equation\ 13$$

`

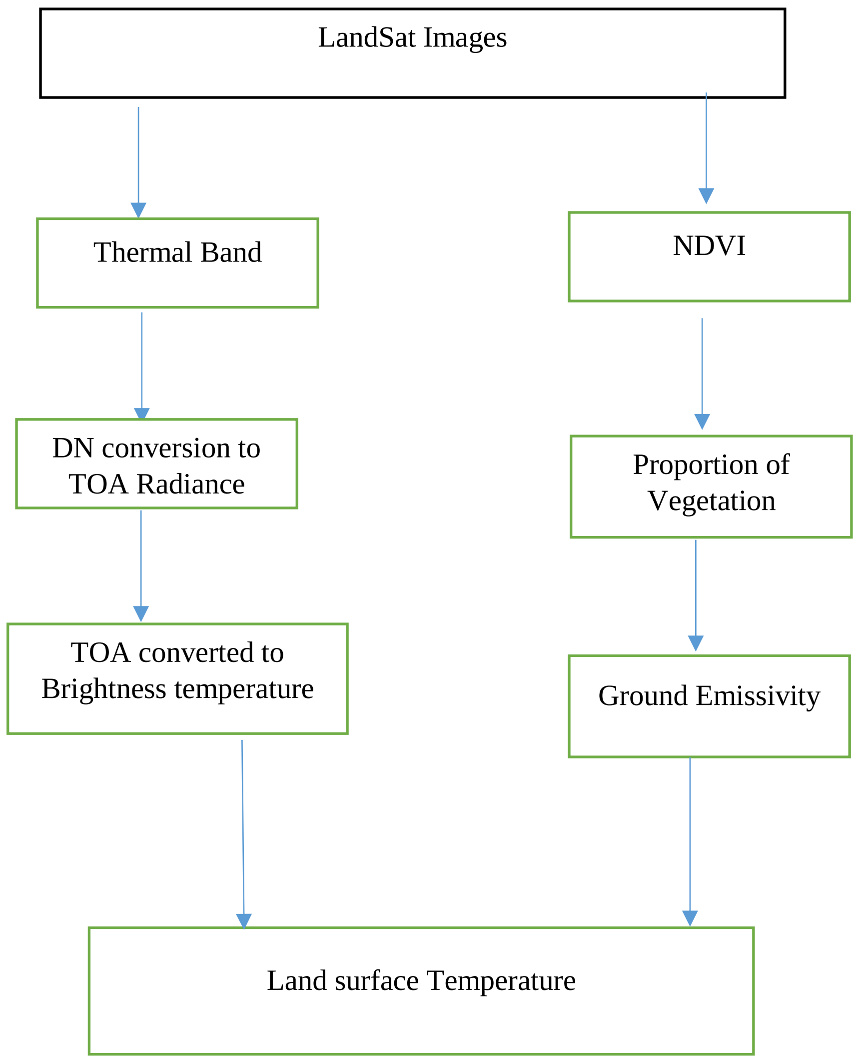

Figure 3.8 Land Surface Temperature Derivation

`

3.6.3 Urban–rural gradient analysis

The use of urban-rural gradient analysis to reveal the geographical distribution and variation of SUHI along urban-rural zones is a highly significant method. (Dissanayake et al., 2019a, b; Estoque et al., 2017; Ranagalage et al., 2017, 2018a; Rousta et al., 2018; Simwanda et al., 2019) are a few recent SUHI studies that have focused on it. Two methods can be used to analyze urban-rural gradients: (1) directional transects that extend from the city's center to its rural areas (Zhang et al., 2004; Zhou & Wang, 2011); and (2) concentric rings that surround the city's core and have standard distance intervals that extend to the city's rural areas (Balew & Korme, 2020; Estoque et al., 2017; Simwanda et al., However, for cities with a single-core urban growth pattern, the concentric ring urban-rural gradient analysis technique is more effective (Estoque et al., 2017; Ranagalage et al., 2017; Simwanda et al., 2019). Because of this, the study will employ the concentric ring urban-rural gradient analysis approach to illustrate the spatial pattern and intensity of SUHI in each LULC type and urban-rural zone (URZ). The city core will be identified by old structures, and various concentric zones with distance intervals of 210 m will be established around it. Following that, the densities of LULC types in each zone will be determined and plotted along the urban-rural gradient. The proportion ratio of IS from the city center will be utilized to distinguish between urban and rural areas. According to Estoque and Murayama (2017), the URZ is classified as an urban region when the IS fraction ratio is greater than 10% and as a rural area when it is less than 10%.

3.6.4 SUHI intensity analysis

The SUHI intensity (SUHII) is a well-established measure of the spatiotemporal variation of LST and SUHI effects across urban-rural boundaries (Ranagalage et al., 2019b; 2018a; Simwanda et al., 2019). A fundamental component of SUHI investigations has been examining SUHII patterns and their changes between urban and rural locations (Dissanayake et al., 2019a, b; Estoque et al., 2017; Ranagalage et al., 2017, 2018a; Rousta et al., 2018; Simwanda et al., 2019). In order to comprehend SUHII, zonal statistics will be used to extract the mean LST of each LULC class in each URZ and the mean LST of each URZ. Based on the approach presented by (Estoque & Murayama, 2017), the magnitude of SUHII in URZ will be determined based on the mean LST diference and mean LST diference of each LULC class (diference proportion of IS, CL, FL, VC, and GL). The mean LST-based magnitude of

SUHII for URZ1 is calculated by deducting the mean LST at the city center (zero kilometer) from the mean LST of URZ1, and the magnitude of SUHII for the other zones is calculated by deducting the mean LST values for each zone from the mean LST of URZ1, i.e., URZ1-URZ2, URZ1-URZ3, URZ1-URZ4...n.

The above is implemented using a python automation script which was written to make the process efficient and accurate.

Python script snippet of codes that are used are found in the appendix A section

3.6.5 Spatial Metric Based Analysis

Landscape metrics, which were developed in the late 1980s and combined measures from both information theory and fractal geometry based on a categorical, patch-based description of the landscape, are the origins of spatial metrics. Patches are homogeneous zones for a specific landscape property of importance, such as "industrial land", "park", or "high-density residential area". When measuring the spatial heterogeneity of individual patches, patches belonging to the same class, and the landscape as a whole, landscape metrics are used. The metrics can be used to examine and describe changes in the amount of spatial heterogeneity in multi-scale or multi-temporal datasets (Dunn et al, 1991; J. Wu et al., 2000) Herold et al. (2003) noted that the methods and presumptions could be more broadly referred to as "spatial metrics" in the application to the urban environment.

Generally speaking, pattern metrics need to meet the following requirements They should not be connected with other pattern metrics, be able to capture changes in landscape pattern across time and space, be unaffected by the number of land cover classes utilized or the spatial resolution of the underlying remote sensing data. (2017) Sinha et al. This metrics will be chosen (Table 3.10) based on their suitability for capturing changes in land cover's composition, configuration, and structure, as well as their effects on LST. -> check the type and number of spatial metrics to be used

Edge Density (ED) = is a landscape metric that measures the length of all edge segments in the landscape per unit area. Edge refers to the boundary between different patch types or land cover classes. ED is typically expressed as the length of edges per hectare or another unit of area. High edge density values indicate a landscape with many small patches and a large amount of edge habitat, while low values suggest fewer, larger patches with less edge habitat. This metric is crucial for understanding edge effects, which can influence various ecological processes, such as species interactions, microclimate, and habitat availability.

FRAC_AM (Area-Weighted Mean Fractal Dimension) = FRAC_AM stands for Area-Weighted Mean Fractal Dimension Index, a landscape metric used in spatial ecology to measure the complexity of patch shapes within a landscape. The fractal dimension is a statistical index of complexity that compares how the detail in a pattern changes with the scale at which it is measured. The FRAC_AM is calculated by weighting the fractal dimension of each patch by its area and then averaging these values across the landscape. This approach emphasizes the influence of larger patches. Higher FRAC_AM values indicate more complex and convoluted patch shapes, while lower values indicate simpler and more compact shapes. This metric provides insights into habitat fragmentation and edge effects.

PD (Patch Density) = PD, or Patch Density, is a measure of the number of patches per unit area within a landscape. It is one of the most fundamental landscape metrics, providing a basic measure of landscape fragmentation. PD is calculated by dividing the number of patches by the total landscape area and is typically expressed as the number of patches per 100 hectares. Higher patch density values indicate a more fragmented landscape with more patches of different land cover types, while lower values suggest fewer, larger patches and potentially less fragmentation. This metric is useful for understanding habitat fragmentation, landscape structure, and the spatial arrangement of patches.

IJI (Interspersion and Juxtaposition Index) = IJI stands for Interspersion and Juxtaposition Index, a metric used to measure the extent to which different patch types are interspersed with each other, providing an indication of the landscape's heterogeneity. IJI is calculated based on the proportional adjacency of different patch types and is usually expressed as a percentage. Higher values of IJI indicate a greater degree of interspersion, meaning that patch types are more evenly mixed throughout the landscape, while lower values suggest that certain patch types are more isolated or clustered. This metric is important for understanding landscape connectivity, edge effects, and habitat diversity.

These metrics are widely used in landscape ecology to describe the structure, function, and changes within landscapes. They help ecologists and land managers make informed decisions about conservation and land-use planning.

3.7 Statistical analysis

Correlation and regression analysis is used to observe the relation and cause effect of various Land use land cover classes with Land surface Temperature, Landscape metrics with Land surface temperature, Land surface temperature with Indices

`

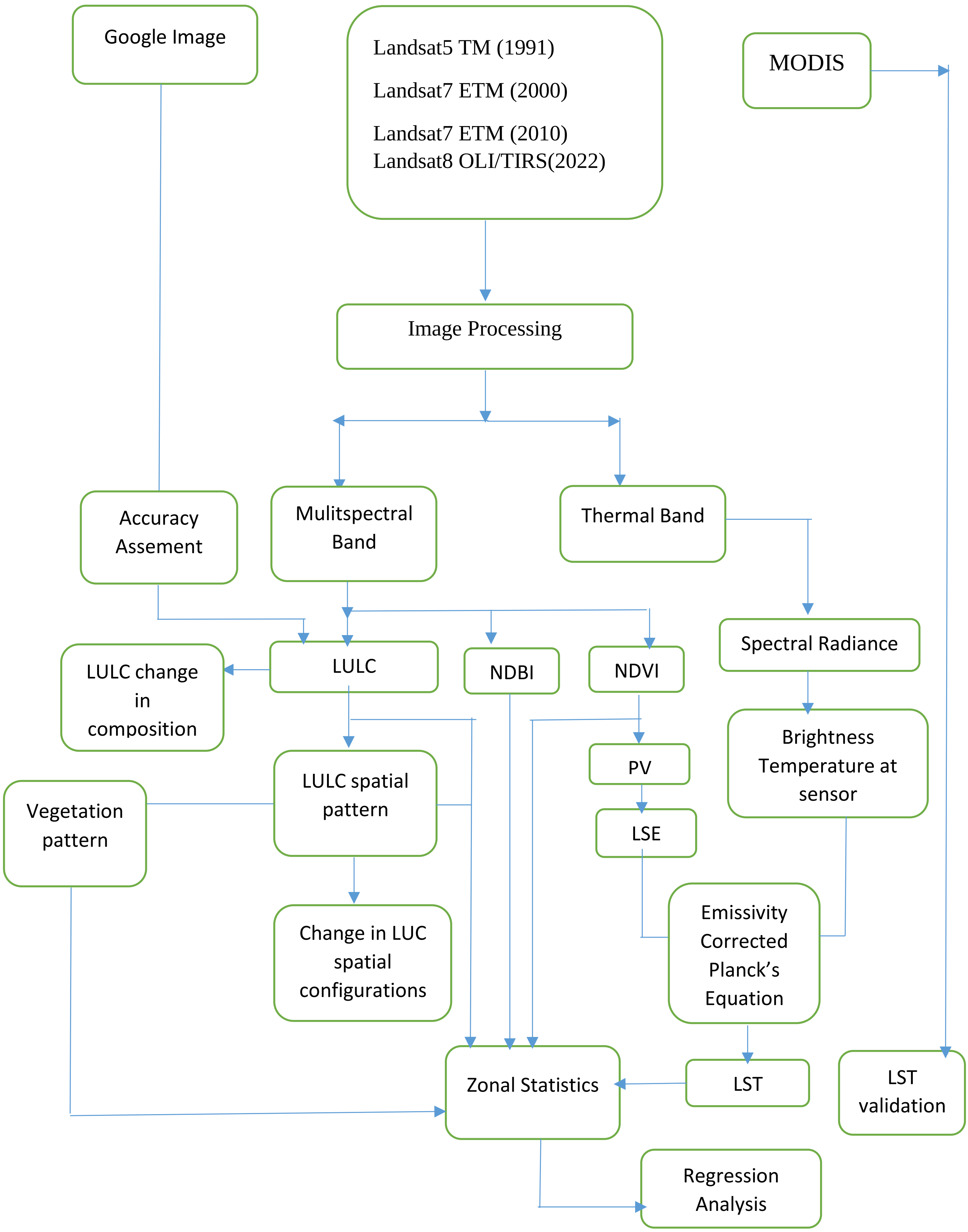

Figure 3.9 Schematic Methodology Flow chart of the Study

CHAPTER 4: RESULTS AND DISCUSSION

4.1 Dynamics of Land Use and Land Cover

4.1.1 Accuracy of Image Classification

Bega Season

Table 4.1 Error Matrix of classification 1991 – 2022 Bega Season

	1991		2000		2010		2022	
LULC	Producer Accuracy (%)	User Accuracy (%)	Producer Accuracy (%)	User Accuracy (%)	Producer Accuracy (%)	User Accuracy (%)	Producer Accuracy (%)	User Accuracy (%)
Built Up	67.38	95.73	93.09	100.0	92.15	99.35	94.39	98.18
Bare Land	64.87	77.51	97.14	90.18	98.74	97.52	85.98	82.06
Vegetation	85.75	87.60	92.24	97.70	96.42	86.92	81.54	90.88
Agriculture	93.97	87.10	95.75	93.68	94.46	97.31	92.96	87.39
Ovearll Accuracy (%)	86.1665%		94.7668%		95.3398%		89.7794%	
Kappa Coefficient	0.73		0.92		0.9308		0.8518	

Belge Season

Table 4.2 Error Matrix of classification 1991 – 2022 Belge Season

	1991		2000		2010		2022	
LULC	Producer Accuracy (%)	User Accuracy (%)	Producer Accuracy (%)	User Accuracy (%)	Producer Accuracy (%)	User Accuracy (%)	Producer Accuracy (%)	User Accuracy (%)
Built Up	87.79	87.79	88.83	98.78	93.70	97.48	95.97	97.75
Bare Land	76.10	81.25	93.06	96.53	86.74	95.34	87.00	89.05
Vegetation	92.96	83.16	84.38	95.74	86.76	97.27	83.62	91.18
Agriculture	86.95	87.26	95.97	82.88	96.33	78.24	91.18	85.02
Ovearll Accuracy (%)	85.2941%		90.9747%		90.5725%		89.7659%	
Kappa Coefficient	0.7588		0.8744		0.8726		0.8591	

Kiremete Season

Table 4.3 Error Matrix of classification 1991 – 2022 Kiremete Season

	1991		2000		2010		2022	
LULC	Producer Accuracy (%)	User Accuracy (%)	Producer Accuracy (%)	User Accuracy (%)	Producer Accuracy (%)	User Accuracy (%)	Producer Accuracy (%)	User Accuracy (%)
Built Up	79.73	98.67	96.53	97.42	97.34	98.77	100.00	94.64
Bare Land	97.18	91.88	95.88	98.67	98.71	98.17	91.43	100.00
Vegetation	64.36	83.38	85.16	86.10	90.95	97.11	91.46	96.09
Agriculture	97.90	93.65	90.20	87.99	96.51	89.41	94.81	90.44
Ovearll Accuracy (%)	92.5946%		91.1753%		95.3998%		94.3437%	
Kappa Coefficient	0.8362		0.8782		0.9378		0.9209	

`

4.1.2 Temporal Land Use and Land Cover Maps

Bega Season Temporal Land Use and Land cover Map

From 1991 to 2000 in Bega, the agriculture land use increased from 224.83 sq km to 235.9 sq km, which was a 5% increase by 11.07 sq km. The bare land decreased from 57.6 sq km to 41.33 sq km, which was a 28% decrease by 16.27 sq km. The built up area increased from 6.46 sq km to 12.88 sq km, which was a 99% increase by 6.42 sq km. The vegetation cover decreased from 22.31 sq km to 21.10 sq km, which was a 5% decrease by 1.21 sq km.

From 2000 to 2010 in Bega, the agriculture land use decreased from 235.9 sq km to 235.45 sq km, which was a 0.2% decrease by 0.45 sq km. The bare land decreased from 41.33 sq km to 35.04 sq km, which was a 15% decrease by 6.29 sq km. The built up area increased from 12.88 sq km to 20.42 sq km, which was a 59% increase by 7.54 sq km. The vegetation cover decreased from 21.10 sq km to 20.34 sq km, which was a 4% decrease by 0.76 sq km.

From 2010 to 2022 in Bega, the agriculture land use decreased from 235.45 sq km to 173.55 sq km, which was a 26% decrease by 61.9 sq km. The bare land increased from 35.04 sq km to 45.26 sq km, which was a 29% increase by 10.22 sq km. The built up area increased from 20.42 sq km to 58.98 sq km, which was a 189% increase by 38.56 sq km. The vegetation cover increased from 20.34 sq km to 33.15 sq km, which was a 63% increase by 12.81 sq km.

From 1991 to 2022 in Bega, the agriculture land use decreased from 224.83 sq km to 173.55 sq km, which was a 23% decrease by 51.28 sq km. The bare land decreased from 57.6 sq km to 45.26 sq km, which was a 21% decrease by 12.34 sq km. The built up area increased from 6.46 sq km to 58.98 sq km, which was an 813% increase by 52.52 sq km.The vegetation cover increased from 22.31 sq km to 33.15 sq km, which was a 49% increase by 10.84 sq km.

`

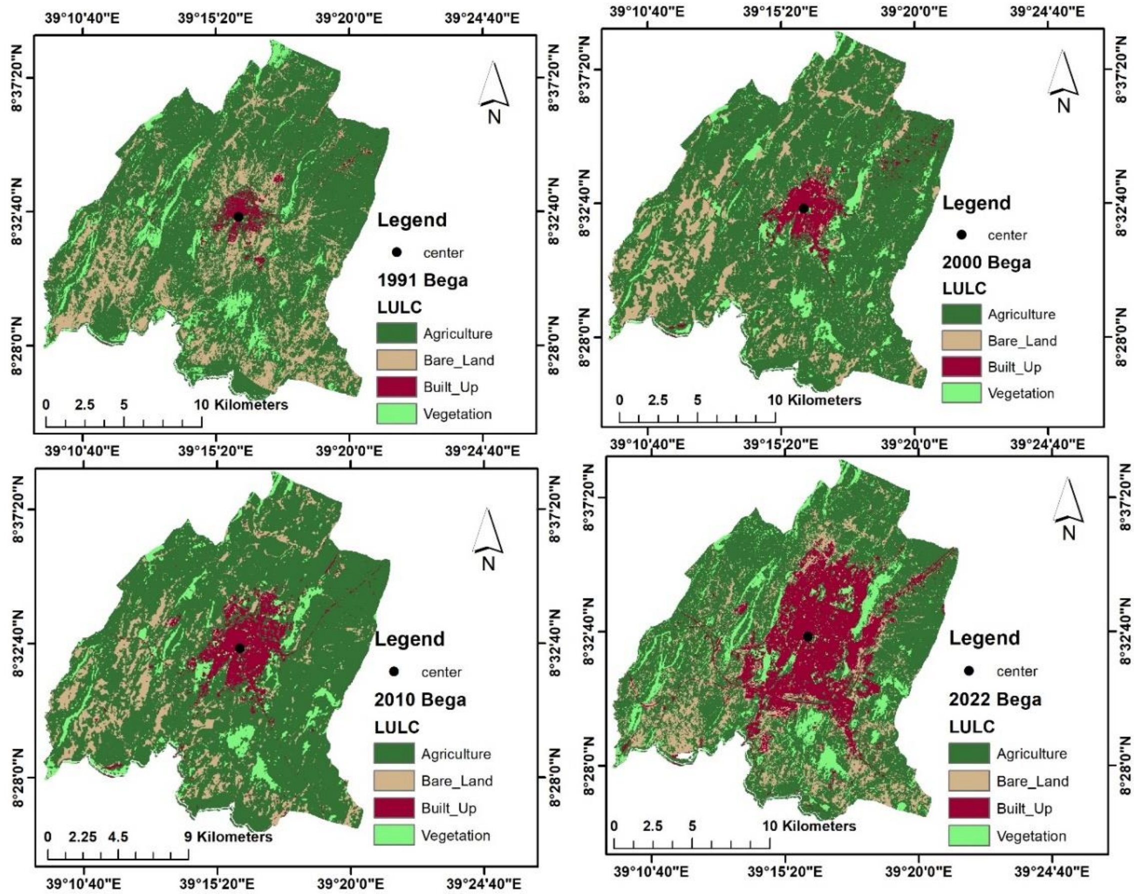

Figure 4.1 LULC Map of Adama City from 1991 – 2022 Bega Season

Table 4.4 Area and Percentage of LULC Classes of Adama City from 1991 – 2022 Bega Season

Bega LULC Types	1991 KM^2	%	2000 KM^2	%	2010 KM^2	%	2022 KM^2	%
Agriculture	224.83		235.9		235.45		173.55	
Bare Land	57.6		41.33		35.04		45.26	
Built Up	6.46		12.88		20.42		58.98	
Vegetation	22.31		21.10		20.34		33.15	

Table 4.5 Area and Percentage Change of LULC of Adama City from 1991 – 2022 Bega Season

LULC Bega	1991 - 2000		2000 - 2010		2010 - 2022		1991 - 2022	
Types	KM^2	%	KM^2	%	KM^2	%	KM^2	%
Agriculture	11.07	5%	-0.45	-0.2%	-61.9	-26%	-51.28	- 23%
Bare Land	-16.27	-28%	-6.29	-15%	10.22	29%	- 12.34	- 21%
Built Up	6.42	99%	7.54	59%	38.56	189%	52.52	813%
Vegetation	-1.21	-5%	-0.76	-4%	12.81	63%	10.84	49%

Belge Season Temporal Land Use and Land cover Map

From 1991 to 2000 in Belge, agricultural land use increased from 227.15 sq km to 235.29 sq km, a 4% increase by 8.14 sq km. Bare land decreased from 54.32 sq km to 39.05 sq km, a 28% decrease by 15.27 sq km. Built-up area increased from 6.34 sq km to 11.6 sq km, an 83% increase by 5.26 sq km. Vegetation cover increased from 20.57 sq km to 25.19 sq km, a 22% increase by 4.62 sq km.

From 2000 to 2010 in Belge, agricultural land use increased from 235.29 sq km to 237.21 sq km, a 1% increase by 1.92 sq km. Bare land decreased from 39.05 sq km to 30.07 sq km, a 23% decrease by 8.98 sq km. Built-up area increased from 11.6 sq km to 20.35 sq km, a 75% increase by 8.75 sq km. Vegetation cover decreased from 25.19 sq km to 23.75 sq km, a 6% decrease by 1.44 sq km.

From 2010 to 2022 in Belge, agricultural land use decreased from 237.21 sq km to 181.2 sq km, a 24% decrease by 56.01 sq km. Bare land increased from 30.07 sq km to 33.71 sq km, a 12% increase by 3.64 sq km. Built-up area increased from 20.35 sq km to 59.65 sq km, a 193% increase by 39.3 sq km. Vegetation cover increased from 23.75 sq km to 36.98 sq km, a 56% increase by 13.23 sq km.

From 1991 to 2022 in Belge, agricultural land use decreased from 227.15 sq km to 181.2 sq km, a 20% decrease by 45.95 sq km. Bare land decreased from 54.32 sq km to 33.71 sq km, a 38% decrease by 20.61 sq km. Built-up area increased from 6.34 sq km to 59.65 sq km, an 841% increase by 53.31 sq km. Vegetation cover increased from 20.57 sq km to 36.98 sq km, an 80% increase by 16.41 sq km.

`

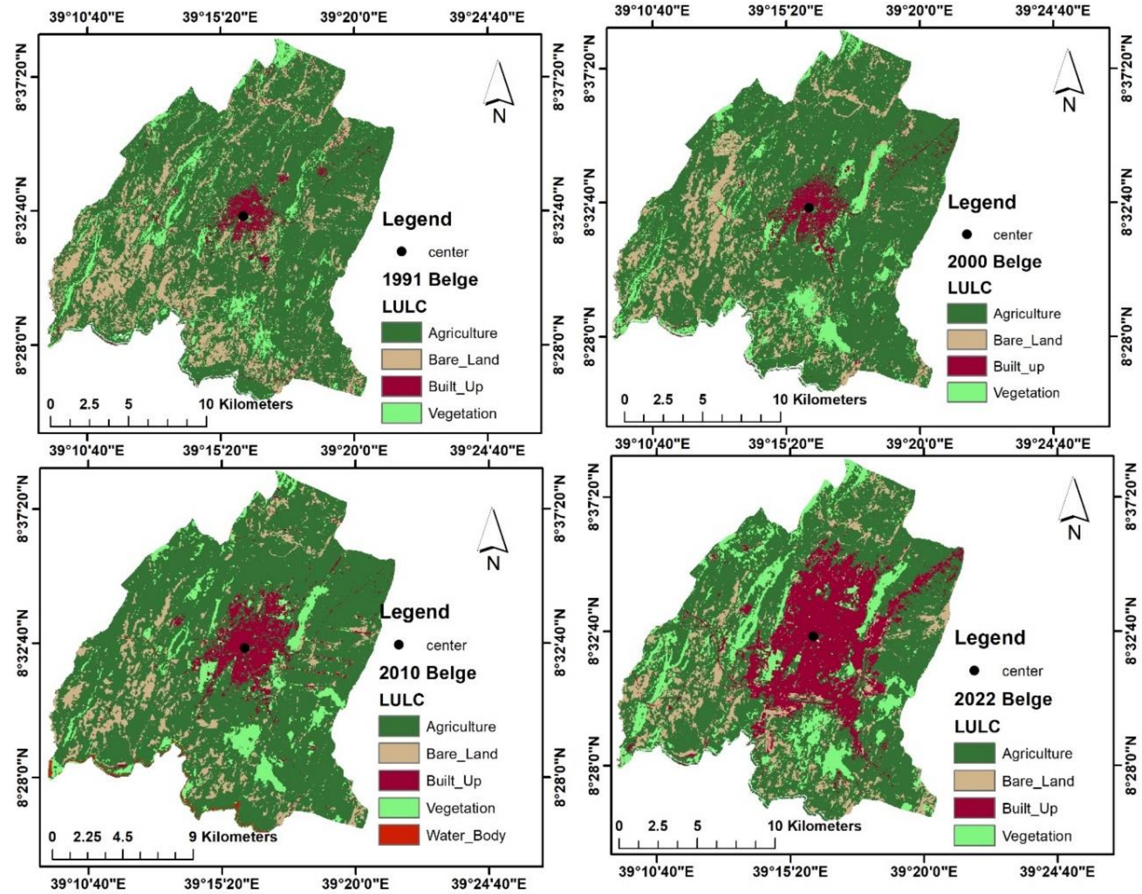

Figure 4.2 LULC Map of Adama City from 1991 – 2022 Belge Season

Table 4.6 Area and Percentage of LULC Classes of Adama City from 1991 – 2022 Belge Season

LULC Belge Types	1991		2000		2010		2022	
	KM^2	%	KM^2	%	KM^2	%	KM^2	%
Agriculture	227.15		235.29		237.21		181.2	
Bare Land	54.32		39.05		30.07		33.71	
Built Up	7.34		11.6		20.35		59.65	
Vegetation	20.57		25.19		23.75		36.98	

Table 4.7 Area and Percentage Change of LULC Classes of Adama City from 1991 – 2022 Belge Season

LULC Belge Types	1991 - 2000		2000 - 2010		2010 - 2022		1991 - 2022	%
	KM^2	%	KM^2	%	KM^2	%	KM^2	%
Agriculture	8.14	4%	1.92	1%	-56.01	- 24%	-45.95	20%
Bare Land	- 15.27	-28%	-8.98	-23%	3.64	12%	- 20.61	-38%
Built Up	5.26	83%	8.75	75%	39.3	193%	53.31	841%
Vegetation	4.62	22%	-1.44	-6%	13.23	56%	16.41	80%

`

Kiremete Season Temporal Land Use and Land cover Map

From 1991 to 2000 in Kiremete, the agriculture land use increased from 227 sq km to 240.98 sq km, which was a 6% increase by 13.98 sq km. The bare land decreased from 45.45 sq km to 34.34 sq km, which was a 24% decrease by 11.11 sq km. The built up area increased from 7 sq km to 11.5 sq km, which was a 64% increase by 4.5 sq km. The vegetation cover decreased from 30.01 sq km to 24.51 sq km, which was an 18% decrease by 5.5 sq km.

From 2000 to 2010 in Kiremete, the agriculture land use decreased from 240.98 sq km to 239.81 sq km, which was a 1% decrease by 1.17 sq km. The bare land decreased from 34.34 sq km to 28.18 sq km, which was an 18% decrease by 6.16 sq km. The built up area increased from 11.5 sq km to 19.82 sq km, which was a 72% increase by 8.32 sq km. The vegetation cover decreased from 24.51 sq km to 23.61 sq km, which was a 4% decrease by 0.9 sq km.

From 2010 to 2022 in Kiremete, the agriculture land use decreased from 239.81 sq km to 183.6 sq km, which was a 23% decrease by 56.21 sq km. The bare land increased from 28.18 sq km to 31.49 sq km, which was a 12% increase by 3.31 sq km. The built up area increased from 19.82 sq km to 58.78 sq km, which was a 197% increase by 38.96 sq km. The vegetation cover increased from 23.61 sq km to 39.35 sq km, which was a 67% increase by 15.74 sq km.

From 1991 to 2022 in Kiremete, the agriculture land use decreased from 227 sq km to 183.6 sq km, which was a 19% decrease by 43.4 sq km. The bare land decreased from 45.45 sq km to 31.49 sq km, which was a 31% decrease by 13.96 sq km. The built up area increased from 7 sq km to 58.78 sq km, which was a 740% increase by 51.78 sq km. The vegetation cover increased from 30.01 sq km to 39.35 sq km, which was a 31% increase by 9.34 sq km

`

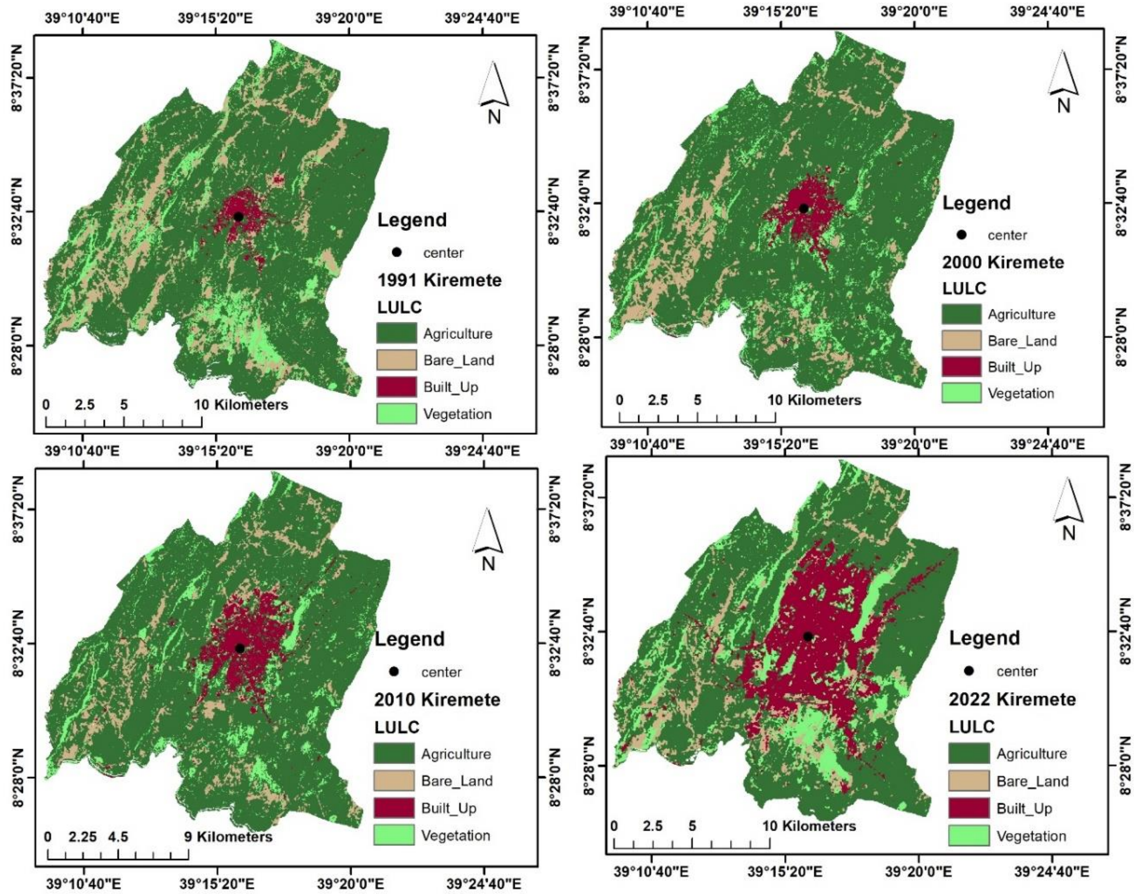

Figure 4.3 LULC Map of Adama City from 1991 – 2022 Kiremete Season

Table 4.8 Area and Percentage of LULC Classes of Adama City from 1991 – 2022 Kiremete Season

LULC Kiremete Types	1991		2000		2010		2022	
	KM^2	%	KM^2	%	KM^2	%	KM^2	%
Agriculture	227		240.98		239.81		183.60	
Bare Land	45.45		34.34		28.18		31.49	
Built Up	7.00		11.50		19.82		58.78473	
Vegetation	30.01		24.51		23.61		39.35	

Table 4.9 Area and Percentage Change of LULC Classes of Adama City from 1991 – 2022 Kiremte Season

LULC Kiremete Types	1991 - 2000		2000 - 2010		2010 - 2022		1991 - 2022	%
	KM^2	%	KM^2	%	KM^2	%	KM^2	%
Agriculture	13.98	6%	-1.17	-1%	- 56.21	-23%	- 43.4	- 19%
Bare Land	- 11.11	-24%	-6.16	-18%	3.31	12%	- 13.96	- 31%
Built Up	4.5	64%	8.32	72%	38.96	197%	51.78	740%
Vegetation	-5.5	-18%	-0.9	4%	15.74	67%	9.34	31%

`

4.2 Dynamics of Landscape Strucutre and its pattern

4.2.1 Kiremete Season

Patch Density Kiremete

Patch density (PD) analysis offers insights into landscape fragmentation in Kiremete over time. In 1991, vegetation exhibited the highest PD at 13.421, indicating significant habitat fragmentation. Bare land also showed considerable fragmentation with a PD of 6.512. By 2022, these figures had notably decreased, with vegetation PD dropping to 4.132 and bare land PD to 3.224, reflecting changes in vegetation growth and land use patterns. Agriculture PD remained stable around 3, indicating consistent fragmentation of farm plots. Conversely, built-up area PD increased from 1.147 in 1991 to 3.799 in 2022, reflecting the expansion of urban development.

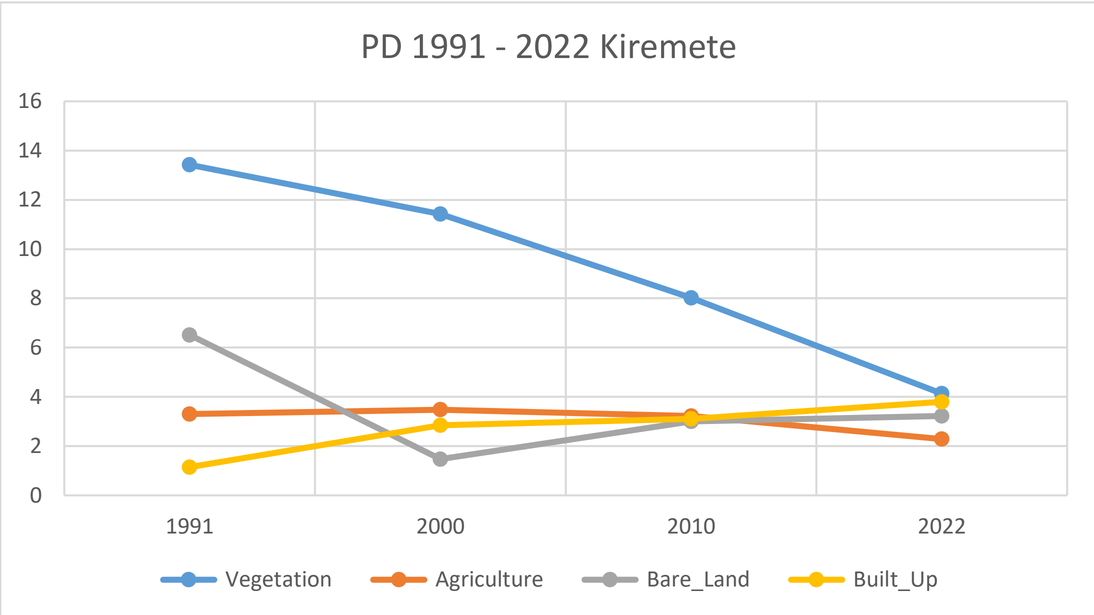

Figure 4.4 PD of LULC of Adama city 1991 - 2022 Kiremte

FRAC_AM Kiremete

The area-weighted mean fractal dimension (FRAC_AM) measures landscape complexity, with values typically ranging between 1 and 2. In 1991, agriculture had the highest FRAC_AM of 1.356 in Kiremete indicating intricate field shapes. By 2022, agriculture FRAC_AM declined to 1.292 suggesting a shift toward simpler farm geometries over time.

Built-up FRAC_AM changed little, from 1.253 in 1991 to 1.263 in 2022, reflecting consistently complex urban patch shapes. Bare land FRAC_AM dropped from 1.199 to 1.139, pointing to greater shape simplification. Vegetation FRAC_AM also decreased from 1.220 to 1.159, indicating a trajectory towards more regular habitat shapes.

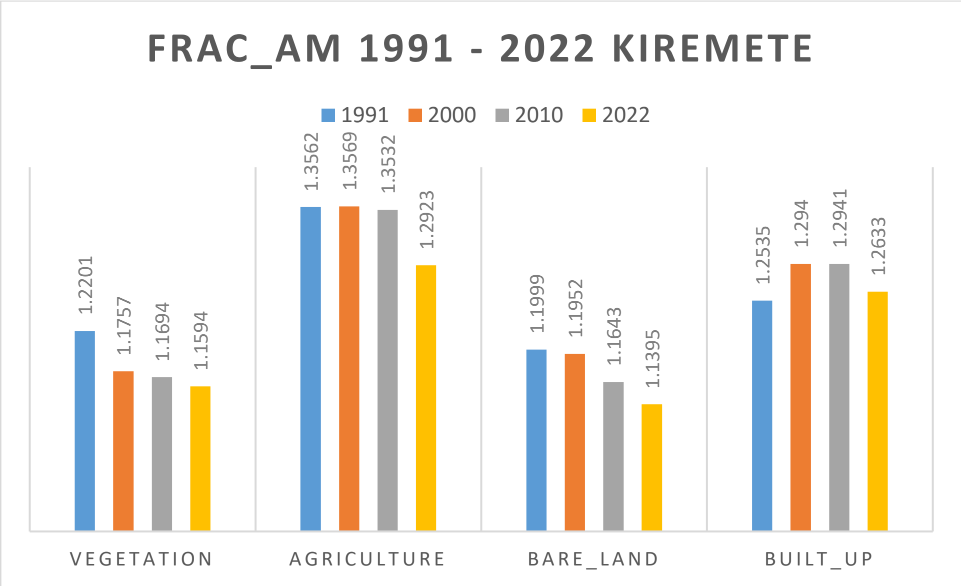

Figure 4.5 FRAC_AM of LULC of Adama city 1991 - 2022 Kiremte

`

IJI Kiremete

The interspersion and juxtaposition index (IJI) measures the intermixing of land cover types, on a scale from 0 (no interspersion) to 100 (complete interspersion). In 1991, agriculture had the highest IJI of 70.610 in Kiremete indicating substantial interspersion of farming patches with natural areas. Agriculture IJI remained high through 2022 at 78.512.

Built-up IJI rose from 61.802 in 1991 to 74.380 in 2022, reflecting greater land cover intermixing as urbanization expanded into other areas. Bare land IJI increased from 59.512 to 70.965, while vegetation IJI surged from 46.085 to 61.492, also indicating higher integration of these covers by 2022.

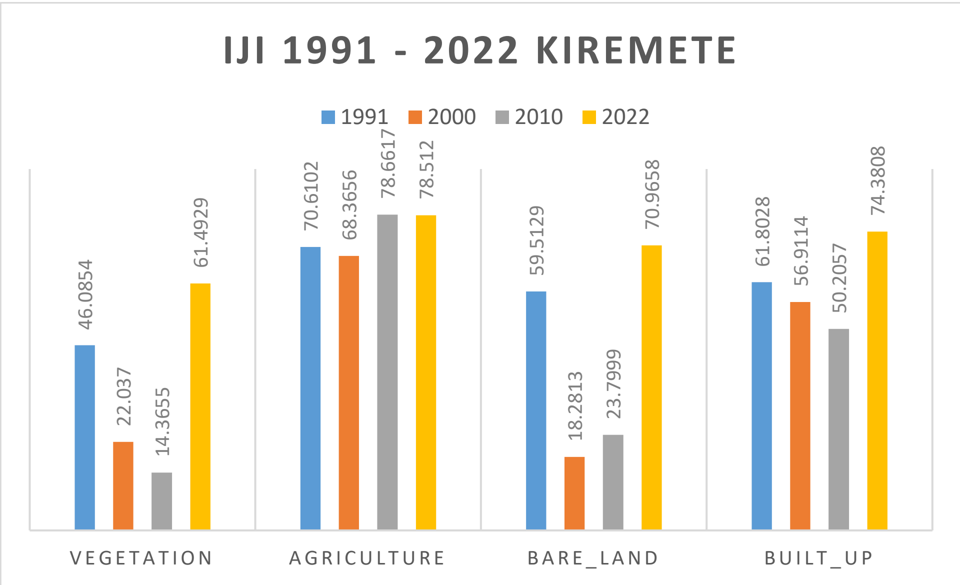

Figure 4.6 IJI LULC of Adama city 1991 - 2022 Kiremte

`

4.2.2 Belge Season

Patch Density Belge

Analysis of patch density (PD) provides additional perspective on landscape fragmentation in Belge over time. In 1991, bare land had the highest PD at 9.718, indicating a high degree of open area fragmentation. Agriculture followed with 2.94 PD, reflecting dispersed individual farm plots. By 2022, agriculture PD declined to 1.978 as farm areas became more consolidated.

In contrast, built-up PD increased from 1.829 in 1991 to 3.275 in 2022, signaling urban development expanding across the landscape. Bare land PD fluctuated, reaching 9.110 in 2022, indicating sustained fragmentation. Finally, vegetation PD declined from 6.736 in 1991 to 2.473 in 2022, pointing to restoration efforts.

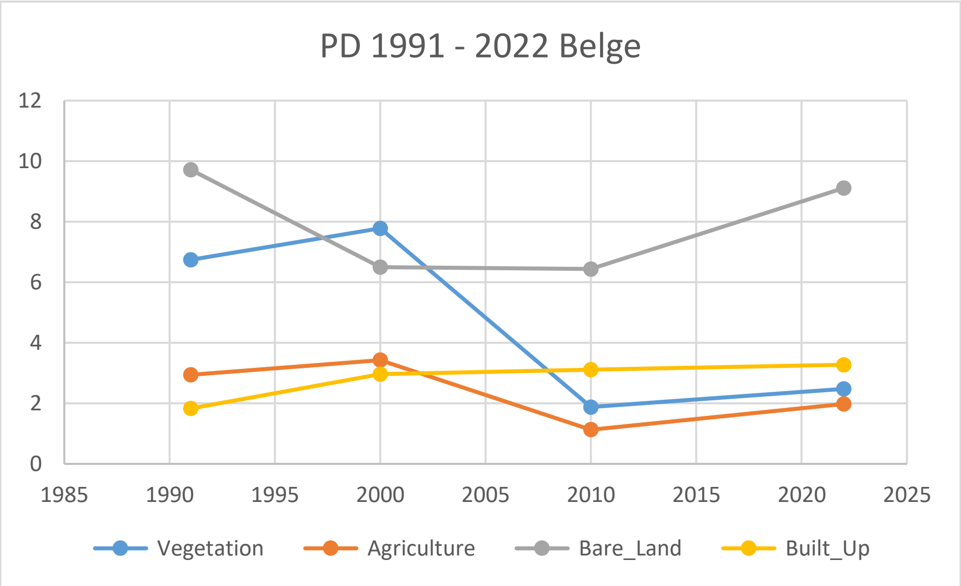

Figure 4.7 PD of LULC of Adama city 1991 - 2022 Belge

`

FRAC_AM Belge

The area-weighted mean fractal dimension (FRAC_AM) measures landscape complexity, with values typically ranging between 1 and 2. In Belge in 1991, agriculture had the highest FRAC_AM of 1.401 indicating complex field shapes. By 2022, agriculture FRAC_AM declined slightly to 1.371, suggesting a trajectory towards simpler farm geometries.

Built-up FRAC_AM increased marginally from 1.22 in 1991 to 1.302 in 2022, reflecting somewhat greater intricacy in urban patch shapes over time. Vegetation FRAC_AM fluctuated around 1.12-1.19, signaling consistently simple habitat shapes. Bare land FRAC_AM changed little, staying near 1.14-1.22 for moderate complexity.

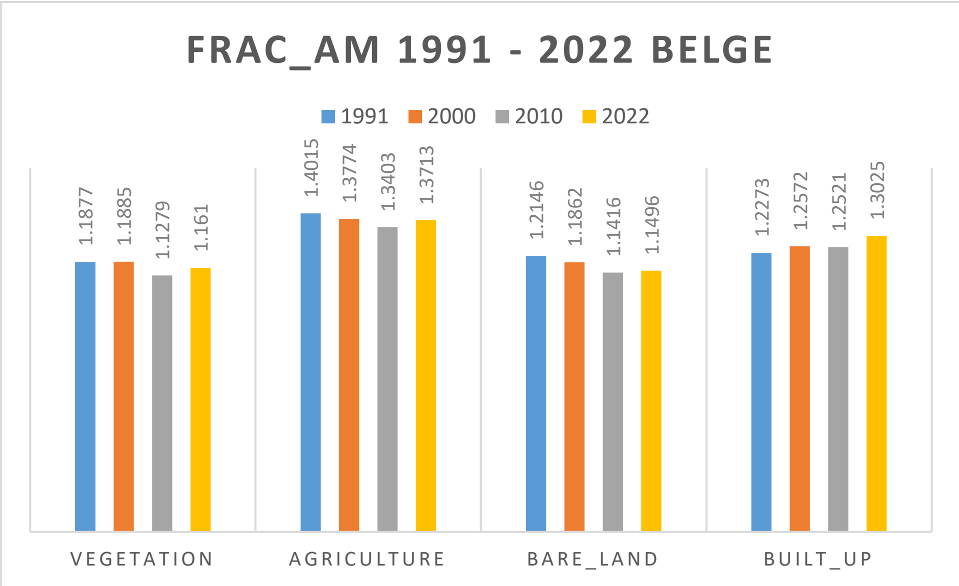

Figure 4.8 FRAC_AM of LULC of Adama city 1991 - 2022 Belge

`

IJI Belge

The interspersion and juxtaposition index (IJI) measures the intermixing of land cover types on a scale from 0 (no interspersion) to 100 (complete interspersion). In Belge, agriculture maintained the highest IJI throughout, ranging from 72.129 in 1991 to 82.324 in 2022, indicating consistently high farming patch interspersion with natural areas.

Built-up IJI increased from 50.603 in 1991 to 58.4056 in 2022, reflecting greater land cover intermixing as urbanization expanded. Bare land IJI rose from 20.648 to 39.113, and vegetation IJI from 14.83 to 28.115, signaling overall increasing integration of these covers.

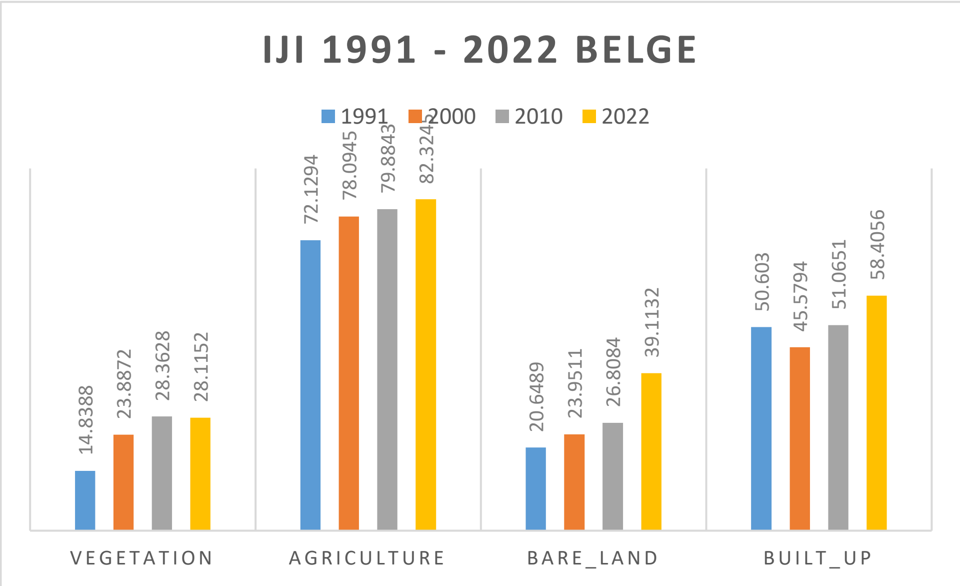

Figure 4.9 IJI LULC of Adama city 1991 - 2022 Kiremte

`

4.2.3 Bega Season

Patch Density Bega

Analysis of patch density (PD) provides additional perspective on landscape fragmentation in Bega over time. In 1991, bare land had the highest PD of 11.45, indicating a high degree of fragmentation. Agriculture followed with 4.22 PD, reflecting the dispersed pattern of individual farms. By 2022, bare land PD increased further to 12.19 as these areas became more divided. In contrast, agriculture PD declined to 2.28 in 2022, suggesting changes in the pattern of farmlands.

Built-up area PD surged from 2.51 in 1991 to 3.65 in 2022, a 46% increase. This signals the scattered expansion of urban development across the landscape. Finally, vegetation PD declined from 5.19 in 1991 to 2.17 in 2022, indicating efforts to connect fragmented habitats.

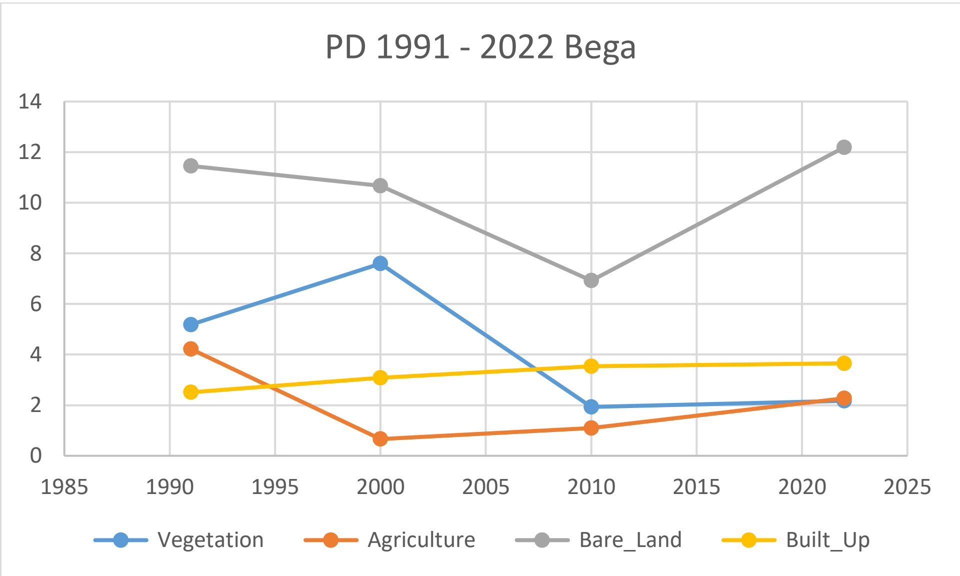

Figure 4.10 PD of LULC of Adama city 1991 - 2022 Bega

FRAC_AM Bega

The area-weighted mean fractal dimension (FRAC_AM) measures landscape complexity, with values typically ranging between 1 and 2. Values approaching 1 indicate simple, regular patches while values nearing 2 signal complex, irregular shapes. In Bega, vegetation had the highest FRAC_AM of 1.199 in 1991, reflecting intricate habitat shapes. By 2022, vegetation FRAC_AM declined slightly to 1.166, indicating a trend toward simpler, more rounded patches.

Built-up area FRAC_AM increased from 1.258 in 1991 to 1.313 in 2022, suggesting greater complexity and irregularity in urban patch shapes over time. Agriculture FRAC_AM fluctuated between 1.347 and 1.401, signaling consistently complex field geometries. Bare land FRAC_AM declined from 1.255 in 1991 to 1.177 in 2022, reflecting a shift toward simpler bare soil shapes

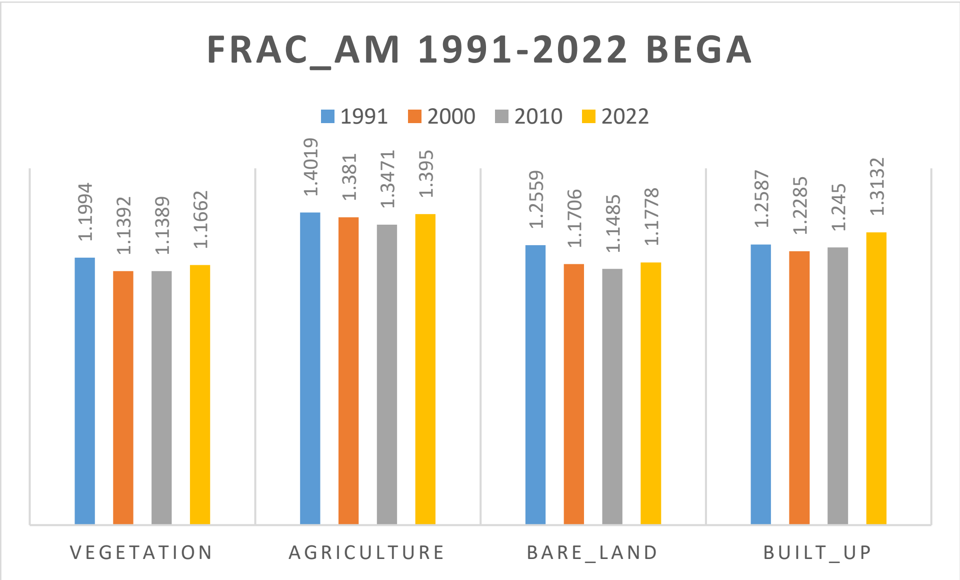

Figure 4.11 FRAC_AM of LULC of Adama city 1991 - 2022 Bega

`

IJI Bega

The interspersion and juxtaposition index (IJI) measures the intermixing of land cover types, with values ranging from 0 (no interspersion) to 100 (complete interspersion). In 1991, built-up area had the lowest IJI of 42.821 indicating segregated urban development. By 2022, built-up IJI rose to 76.043 reflecting increased land cover intermixing as urbanization expanded into other areas.

Agriculture maintained the highest IJI throughout, ranging from 63.534 in 1991 to 76.301 in 2010, signaling consistently high interspersion of farming patches with natural areas. Bare land IJI increased from 11.691 in 1991 to 38.299 in 2022, pointing to greater integration of bare soils amidst other covers. Vegetation IJI showed a similar upward trend

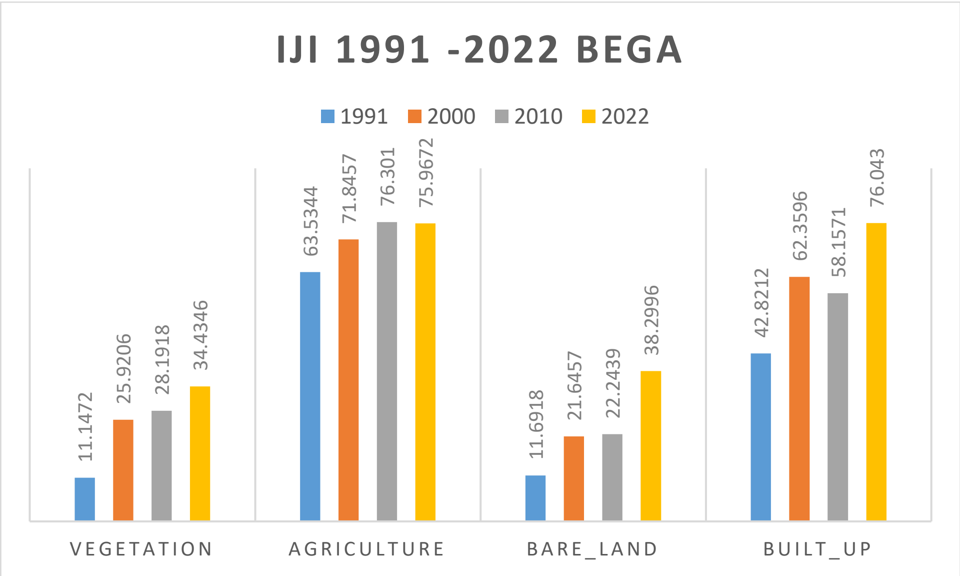

Figure 4.12 IJI of LULC of Adama city 1991 - 2022 Bega

4.3 Spatial distribution of Normalized differential vegetation index

Spatial distribution of NDVI Kiremete Season

Table 4.13 and Figure 4.33 outline the statistical summary of the Normalized Differential Vegetation Index (NDVI) for Kiremete across four selected years: 1991, 2000, 2010, and 2022. NDVI values, which range from -1 to 1, are used to assess vegetation health and coverage. The minimum NDVI values observed were -0.1504 in 1991, deteriorating to -0.544 in 2000, then improving slightly to -0.363 in 2010, and further to -0.177 in 2022, indicating variable vegetation stress levels. Maximum values showed a peak in 2010 at 0.724888, suggesting healthier vegetation compared to other years. The mean NDVI values, reflecting average vegetation health, were highest in 1991 (0.356) and 2022 (0.351), with a notable decline in 2000 (0.153). The standard deviation values provide insights into the spatial variability of NDVI, with the year 2000 showing the highest variability (0.1416) and 2022 the lowest (0.109), suggesting a more uniform vegetation cover in the latter year.

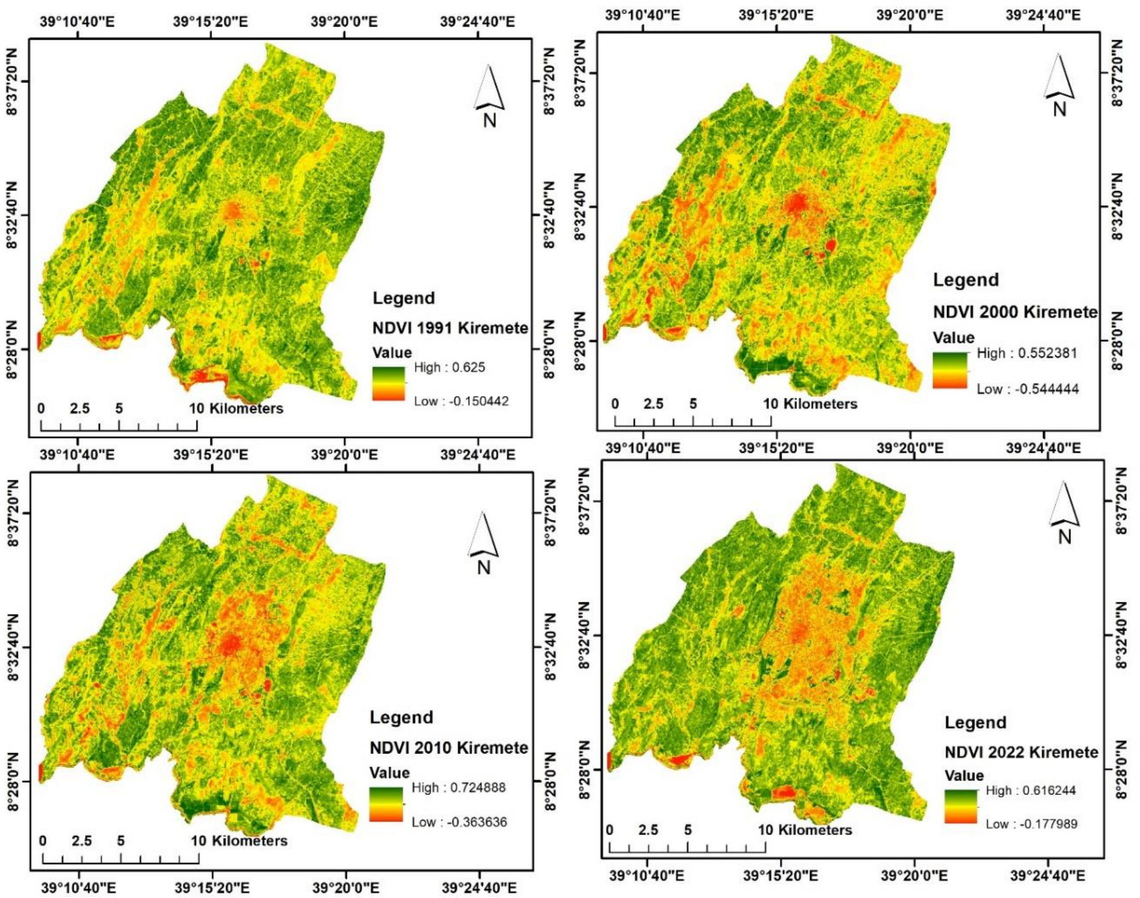

Figure 4.13 NDVI Map of Adama City from 1991 – 2022 Kiremete

Table 4.10 Normalized difference vegetation index results from 1991 – 2022 Kiremete

Year	1991	2000	2010	2022
Min	-0.150	-0.544	-0.363	-0.177
Max	0.625	0.552	0.724	0.616
Mean	0.3566	0.153	0.281	0.351
St_Div	0.0931	0.141	0.125	0.109

`

Spatial distribution of NDVI Belge Season

Table 4.11 and Figure 4.14 presents the statistical analysis of the Normalized Differential Vegetation Index (NDVI) for Kiremete during the Belg season across four distinct years: 1991, 2000, 2010, and 2022. NDVI values, which help gauge the health and density of vegetation, range from -1 to 1. In 1991, the minimum NDVI recorded was notably low at -0.968, indicating significant vegetation stress. This value improved over the subsequent years, with -0.555 in 2000, -0.406 in 2010, and significantly in 2022 to -0.076, suggesting a recovery in vegetation health.

The maximum NDVI values also reflect changes in the healthiest vegetation, peaking at 0.868 in 1991 and then showing a decline in the following years with values of 0.395 in 2000 and 0.625 in 2010, before decreasing again to 0.474 in 2022.

The mean NDVI values, which provide an average measure of vegetation health, were highest in 1991 at 0.168 but dipped into the negative in 2000 (-0.218), indicating poor vegetation conditions. This value rose slightly above zero in 2010 (0.032) and improved further in 2022 (0.133).

Standard deviation values across the years show the variability of NDVI, with 1991 having the highest variability (0.099) and 2022 showing the least variability (0.033), suggesting a more consistent vegetation cover during the latter year.

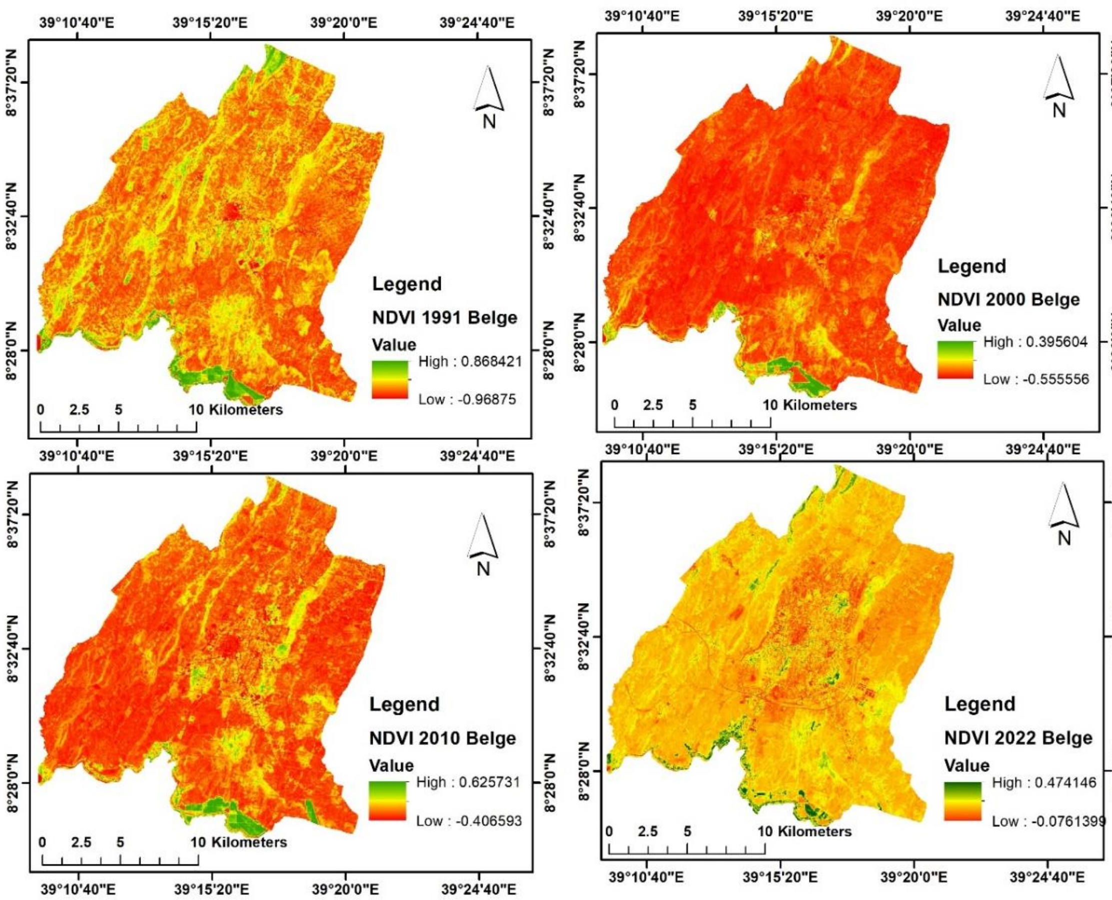

Figure 4.14 NDVI Map of Adama City from 1991 – 2022 Belge

Table 4.11 Normalized difference vegetation index results from 1991 – 2022 Belge

Year	1991	2000	2010	2022
Min	-0.96	-0.555	-0.406	-0.0761
Max	0.868	0.395	0.625	0.474
Mean	0.168	-0.218	0.0329	0.133
St_Div	0.099	0.0614	0.098	0.0334

Spatial distribution of Normalized differential vegetation index Bega Season

Table 4.12 and Figure 4.15 displays the NDVI statistics for the Bega season across the years 1991, 2000, 2010, and 2022, illustrating variations in vegetation health and coverage. NDVI values, which measure vegetation greenness from -1 to 1, varied notably across the years. The minimum NDVI values observed were -0.254 in 1991, -0.6027 in 2000, -0.431 in 2010, and -0.1835 in 2022, showing an improvement in the least vegetative conditions over the years. The maximum values remained relatively stable, with 1991 recording 0.513, increasing slightly in 2000 to 0.546, and showing little variation in 2010 and 2022. The mean NDVI values highlight contrasting vegetation conditions: a modest positive value in 1991 (0.0682), a dip into negative territory in 2000 (-0.099) and 2010 (-0.0147), and a notable improvement in 2022 (0.1850). The standard deviation values, reflecting the spatial spread of NDVI, were lowest in 1991 (0.0460) and highest in 2000 (0.106), indicating variable vegetation distribution across the analyzed years.

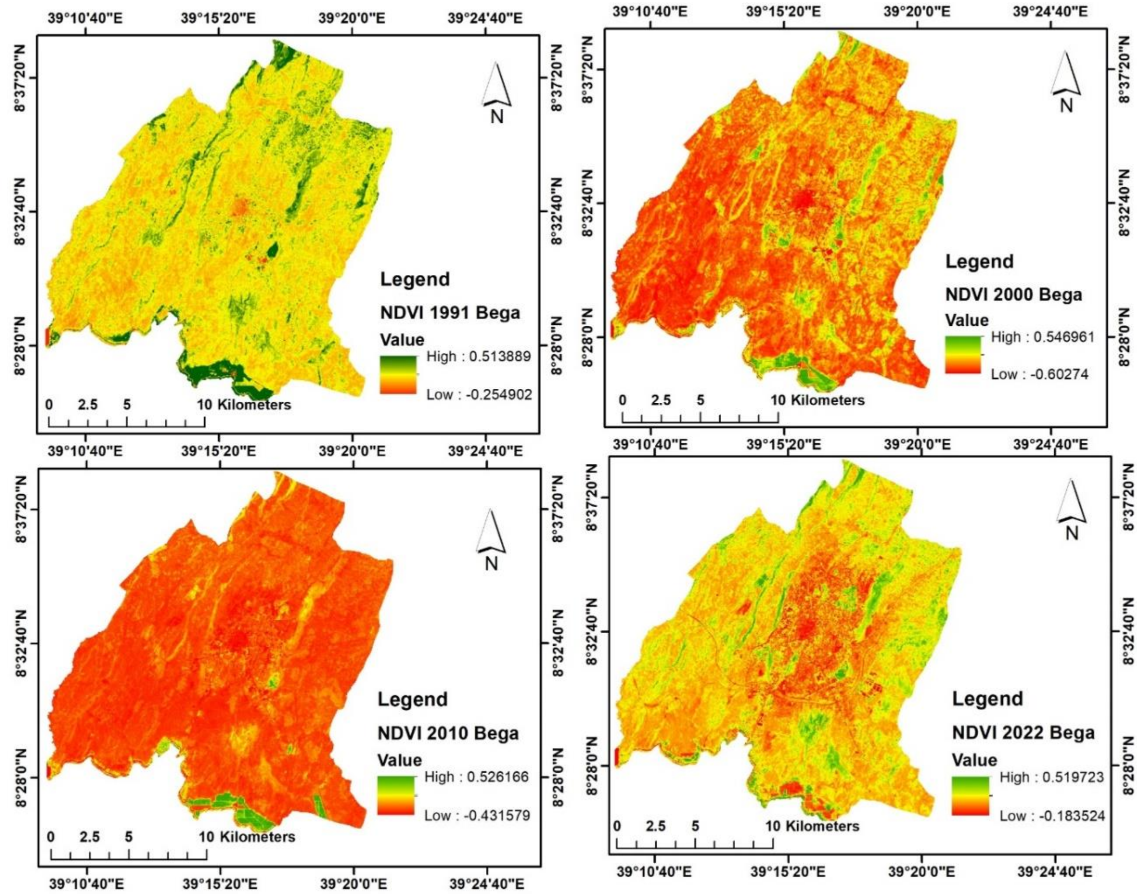

Figure 4.15 NDVI Map of Adama City from 1991 – 2022 Bega

Table 4.12 Normalized difference vegetation index results from 1991 – 2022 Bega

Year	1991	2000	2010	2022
Min	-0.254	-0.602	-0.431	-0.183
Max	0.513	0.546	0.526	0.519
Mean	0.068	-0.099	-0.014	0.185
St_Div	0.046	0.106	0.068	0.0566

`

4.4 Spatial distribution of Normalized differential built up index

Spatial distribution of Normalized differential built up index Kiremete Season

Table 4.13 and Figure 4.16 provides an analysis of the NDBI values for the Kiremet season across the years 1991, 2000, 2010, and 2022, offering insights into changes in built-up areas. The NDBI, an indicator used to assess urbanization, spans values from -1 to 1, with positive values suggesting greater built-up density. The minimum NDBI values have shown significant variability over the decades, starting from -0.507 in 1991, dropping to -0.831 in 2000, and -0.789 in 2010, before improving to -0.418 in 2022. The maximum values suggest a consistent presence of built-up areas, albeit with some fluctuation, peaking at 0.423 in 1991 and slightly decreasing thereafter, with a moderate recovery to 0.419 in 2022. The mean values reflect predominantly negative averages, indicating a general scarcity of built-up areas across the years, with the least negative mean in 1991 (-0.0143) and the most negative in 2000 (-0.229). Standard deviation values, indicating the variability of NDBI, were highest in 2000 (0.1233) and lowest in 2022 (0.0923), suggesting a stabilizing trend in the spatial distribution of built-up areas by the latest year.

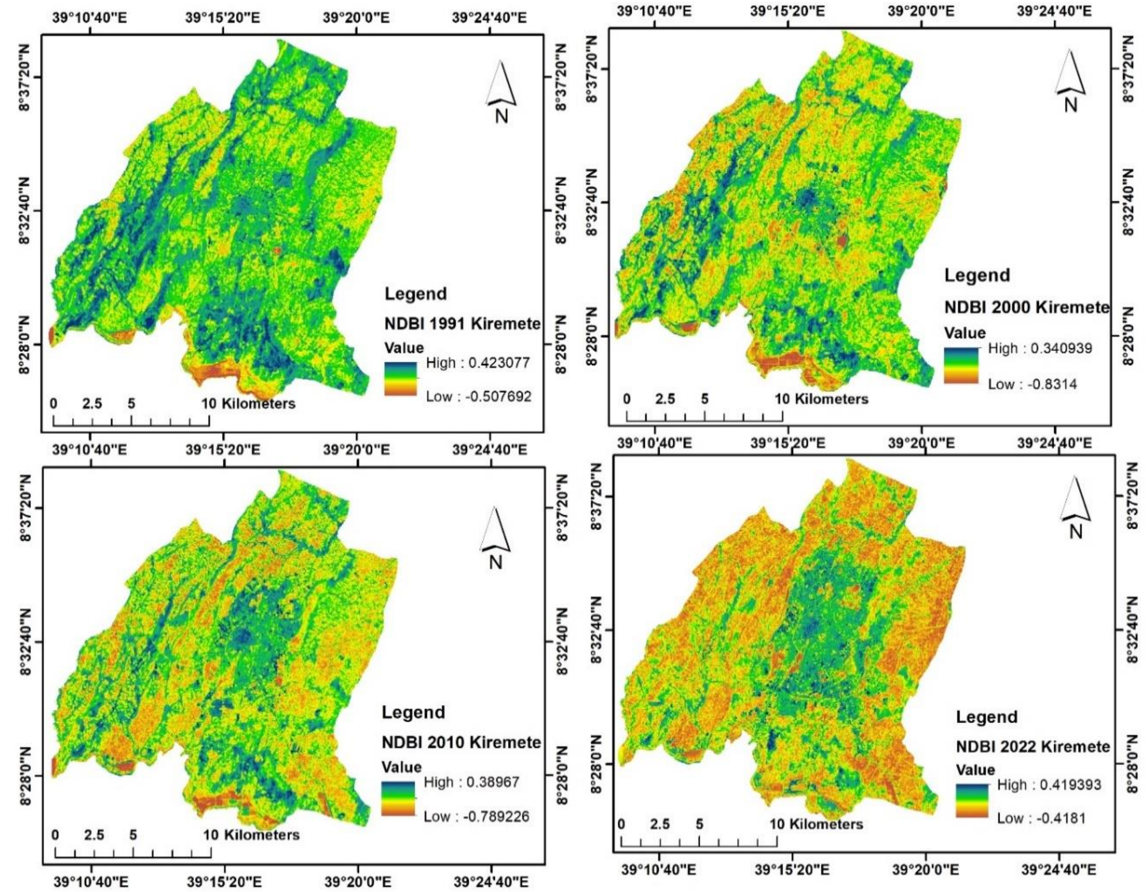

Figure 4.16 NDBI Map of Adama City from 1991 – 2022 Kiremete

Table 4.13 Normalized difference Built Up index results from 1991 – 2022 Kiremete

Year	1991	2000	2010	2022
Min	-0.507	-0.831	-0.789	-0.418
Max	0.423	0.340	0.389	0.419
Mean	-0.0143	-0.229	-0.198	-0.178
St_Div	0.102	0.123	0.119	0.0923

Spatial distribution of Normalized differential built up index Belge Season

Table 4.14 and Figure 4.17 presents the NDBI values for the Belge season across the years 1991, 2000, 2010, and 2022, providing insights into urban expansion and built-up area dynamics. NDBI, an index used to assess built-up land areas, ranges from -1 to 1, where positive values indicate higher concentrations of built-up materials. The minimum NDBI values show a decline from -0.437 in 1991 to -0.506 in 2000, improving slightly in 2010 to -0.392, but deteriorating again to -0.486 in 2022. The maximum values, reflecting the peak extent of built-up areas, were highest in 2022 at 0.499, indicating increased urban development compared to previous years. The mean NDBI values have varied, with 1991 recording a relatively high average of 0.2378, which dropped significantly by 2000 to 0.0813 and remained relatively low in subsequent years. The standard deviation values, which indicate the spread of NDBI, were relatively consistent, with the lowest variability observed in 2022 (0.0551), suggesting a more homogeneous distribution of built-up areas in the most recent year.

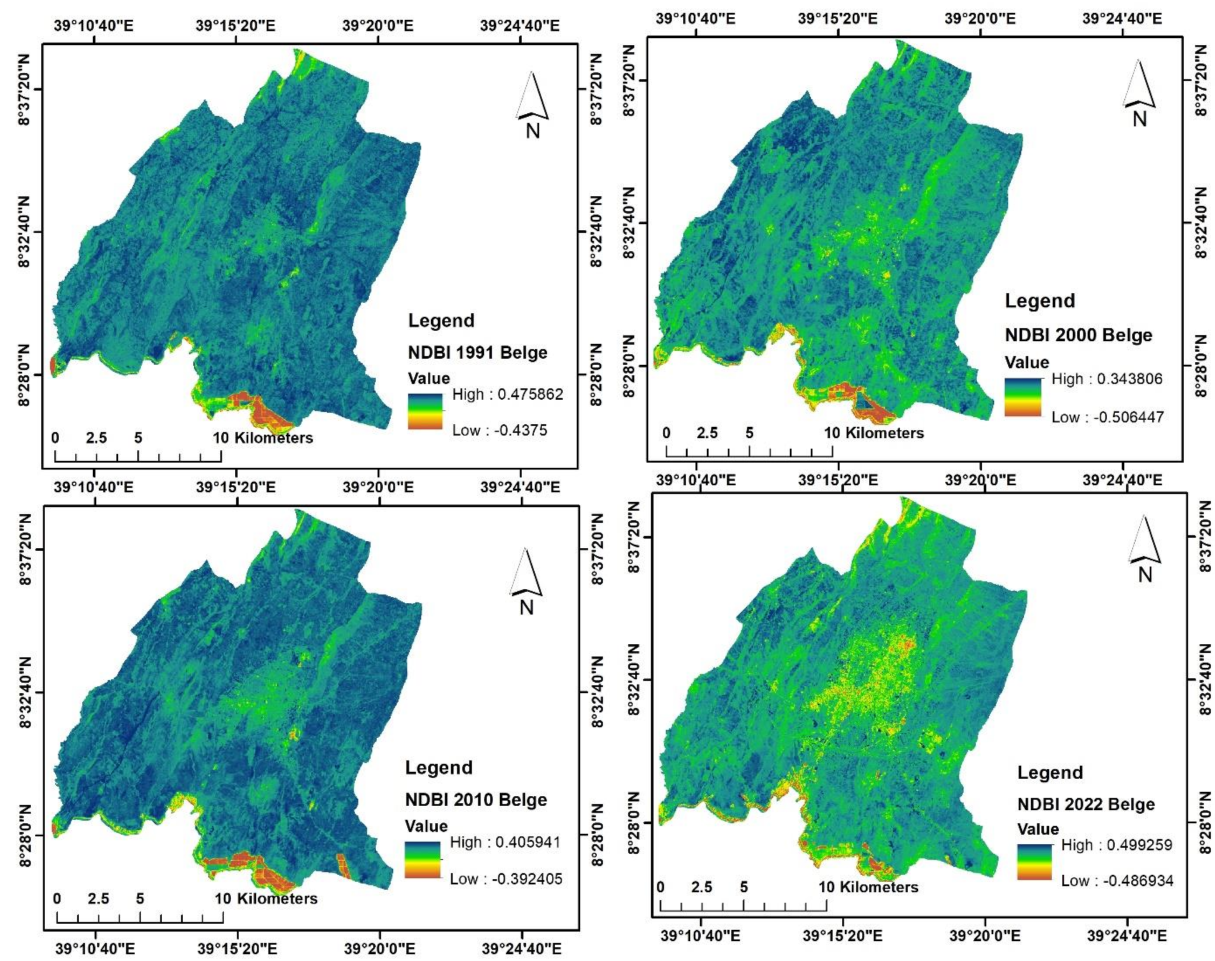

Figure 4.17 NDBI Map of Adama City from 1991 – 2022 Belge

Table 4.14 Normalized difference Built Up index results from 1991 – 2022 Belge

Year	1991	2000	2010	2022
Min	-0.437	-0.506	-0.392	-0.486
Max	0.475	0.343	0.405	0.499
Mean	0.237	0.0813	0.112	0.061
St_Div	0.066	0.0718	0.0679	0.055

Spatial distribution of Normalized differential built up index Bega Season

Table 4.15 and Figure 4.18 analyzes the NDBI values for the Bega season spanning the years 1991, 2000, 2010, and 2022, providing a detailed view of the urbanization dynamics over time. NDBI is crucial for evaluating the extent of built-up areas, with its values ranging from -1 to 1, where higher positive values indicate greater urban density. The minimum NDBI values reveal an improvement in reducing the least amount of built-up areas, from -0.428 in 1991 to -0.370 in 2022, though the lowest dip occurred in 2000 at -0.555. The maximum values indicate the extent of built-up presence, reaching the highest in 2000 at 0.561, with a subsequent decrease in later years, reflecting a reduction in maximum urban expansion by 2022 to 0.337. The mean NDBI values show varying trends, with a peak in 2000 (0.234) and a notable decrease by 2022 (-0.021), suggesting fluctuations in average built-up density over the decades. The standard deviation values, reflecting spatial variability, were highest in 2000 (0.087) and lowest in 2022 (0.049), indicating a more uniform spread of built-up areas in the most recent year.

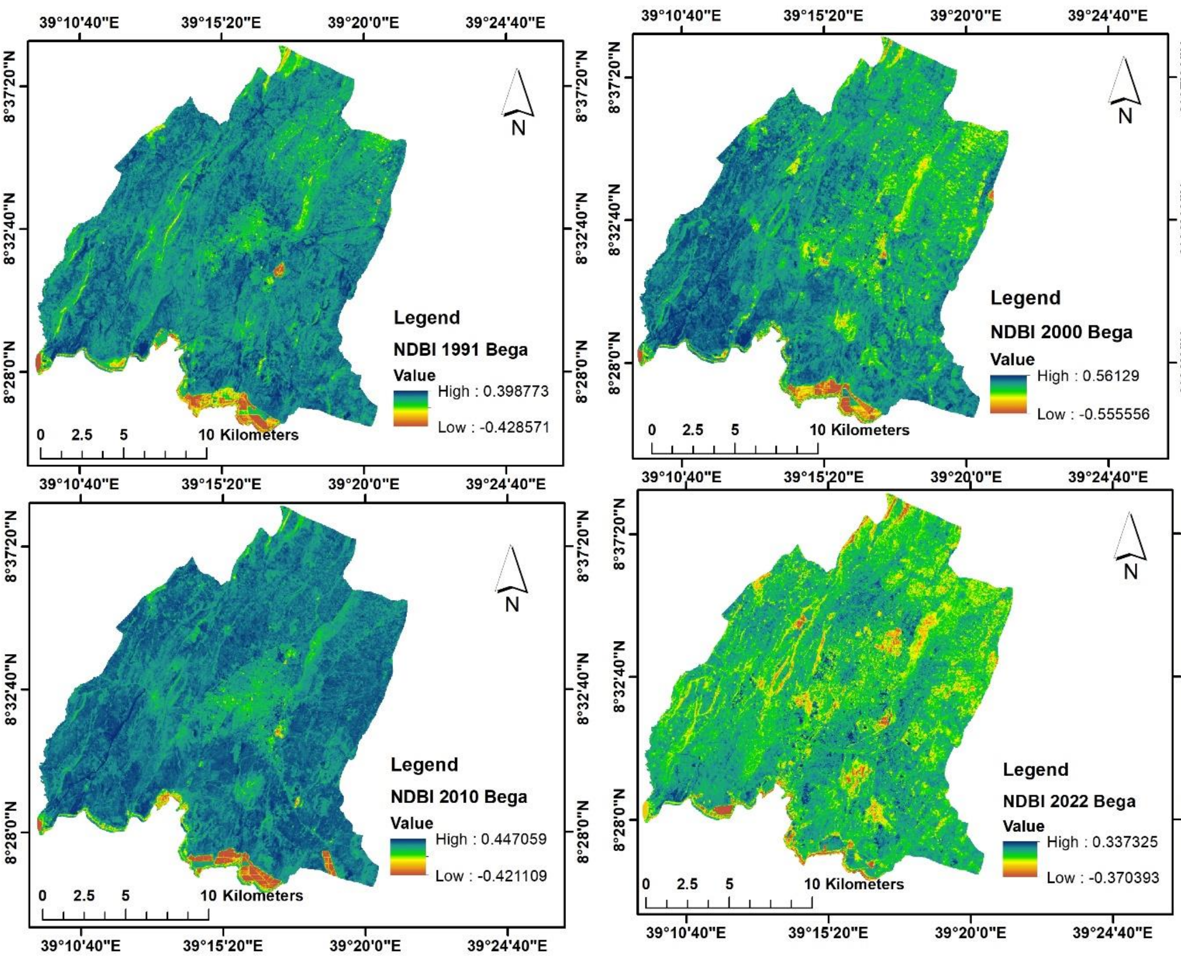

Figure 4.18 NDBI Map of Adama City from 1991 – 2022 Bega

Table 4.15 Normalized difference Built Up index results from 1991 – 2022 Bega

Year	1991	2000	2010	2022
Min	-0.428	-0.555	-0.421	-0.370
Max	0.398	0.561	0.447	0.337
Mean	0.207	0.234	0.111	-0.021
St_Div	0.061	0.087	0.073	0.049

4.5 Spatiotemporal variation of LST of Adama City

Accuracy of Retrieved Land Surface Temperature

The accuracy assessment of land surface temperature (LST) derived from MODIS and Landsat data was conducted for three different regions - Bega, Belge, and Kirmeete - across three years: 2000, 2010, and 2022. Landsat 7 data was used for the years 2000 and 2010, while Landsat 8 data was used for 2022. The root mean square error (RMSE) and standard deviation (STD) were calculated to quantify the differences between the MODIS LST and the derived LST from Landsat data.

For the year 2000, the RMSE values ranged from 3.40°C to 9.04°C, with Belge showing the highest RMSE of 9.04°C and Bega having the lowest RMSE of 3.40°C. The STD values for 2000 varied from 1.39°C to 2.25°C.

In 2010, the RMSE values ranged from 2.65°C to 5.56°C, with Belge exhibiting the highest RMSE of 5.56°C and Kirmeete having the lowest RMSE of 2.65°C. The STD values for 2010 ranged from 1.87°C to 2.46°C.

For the year 2022, the RMSE values ranged from 2.65°C to 5.82°C, with Belge showing the highest RMSE of 5.82°C and Kirmete having the lowest RMSE of 2.65°C. The STD values for 2022 varied from 1.42°C to 2.07°C.

It is important to note that the spatial resolution of the MODIS LST (1km by 1km) is significantly coarser than the derived LST from Landsat data (30m by 30m). This resolution discrepancy can contribute to the observed differences between the two datasets. The process of resampling the MODIS LST to match the higher resolution of the Landsat-derived LST introduces uncertainties and may not capture the finer-scale temperature variations. Additionally, the cropping process in ArcMap may have excluded some relatively cool areas, potentially affecting the accuracy assessment.

Despite these limitations, the derived LST from Landsat data shows reasonable agreement with the MODIS LST, considering the resolution difference

Spatiotemporal variation of LST of Kiremete Season

Table 4.16 and Figure 4.19 present an analysis of land surface temperature (LST) variations during the Kiremet season across four distinct years: 1991, 2000, 2010, and 2022. Land surface temperature is a critical environmental indicator that reflects the condition of the Earth's surface and is pivotal for studying climatic changes and environmental dynamics.

The data reveals that the minimum LST recorded during the Kiremet season shows notable fluctuations over the selected years. It decreased from 19.30°C in 1991 to a low of 15.83°C in 2010, then slightly increased to 18.65°C by 2022. The maximum LST values indicate significant annual variability, peaking at 38.31°C in 2010, which contrasts sharply with the lower peak of 31.53°C in 2000. The mean LST throughout these periods also varies, with the highest average of 27.68°C in 2010, suggesting a particularly warm year, compared to the lowest average of 23.20°C in 2000.

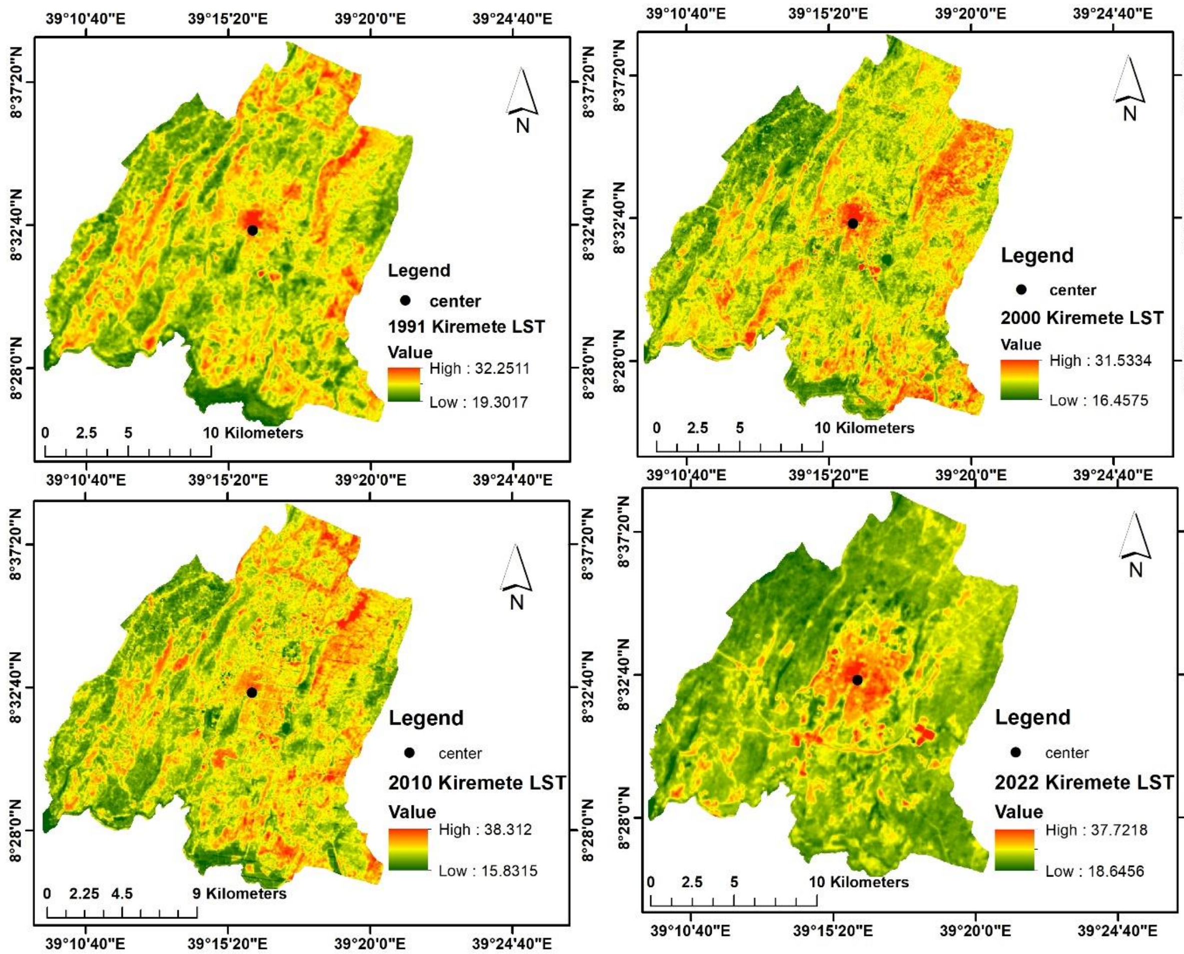

Figure 4.19 LandSat LST Map of Adama City 1991 – 2022 Kiremete

Table 4.16 Min, Max and Mean LST of Adama 1991 – 2022 Kiremete

Year	1991	2000	2010	2022
Min	19.30	16.46	15.83	18.64
Max	32.25	31.53	38.31	37.72
Mean	24.65	23.20	27.67	23.23

Spatiotemporal variation of LST of Belge Season

Table 4.17 and Figure 4.20 present an analysis of land surface temperature (LST) variations in Adama City during the Belge season for the years 1991, 2000, 2010, and 2022. LST serves as an essential indicator of the urban heat island effect and is crucial for assessing climatic and environmental changes over time.

The data indicates that the minimum LST recorded during the Belge season exhibits significant fluctuations across the years. It starts at a higher 20.66°C in 1991, drops to 14.31°C in 2000, shows a moderate recovery to 16.14°C in 2010, and stabilizes around 17.45°C in 2022. The maximum temperatures also reveal a trend of increasing heat, with the highest peak of 43.10°C in 2022, up from 41.31°C in 1991 and 40.09°C in 2000, indicating a progressive warming trend. The mean LST data align with this observation, showing an upward trajectory from 29.79°C in 1991 to a peak of 36.60°C in 2022, with a notable dip to 32.76°C in 2000 and a slight increase in 2010 to 31.58°C.

`

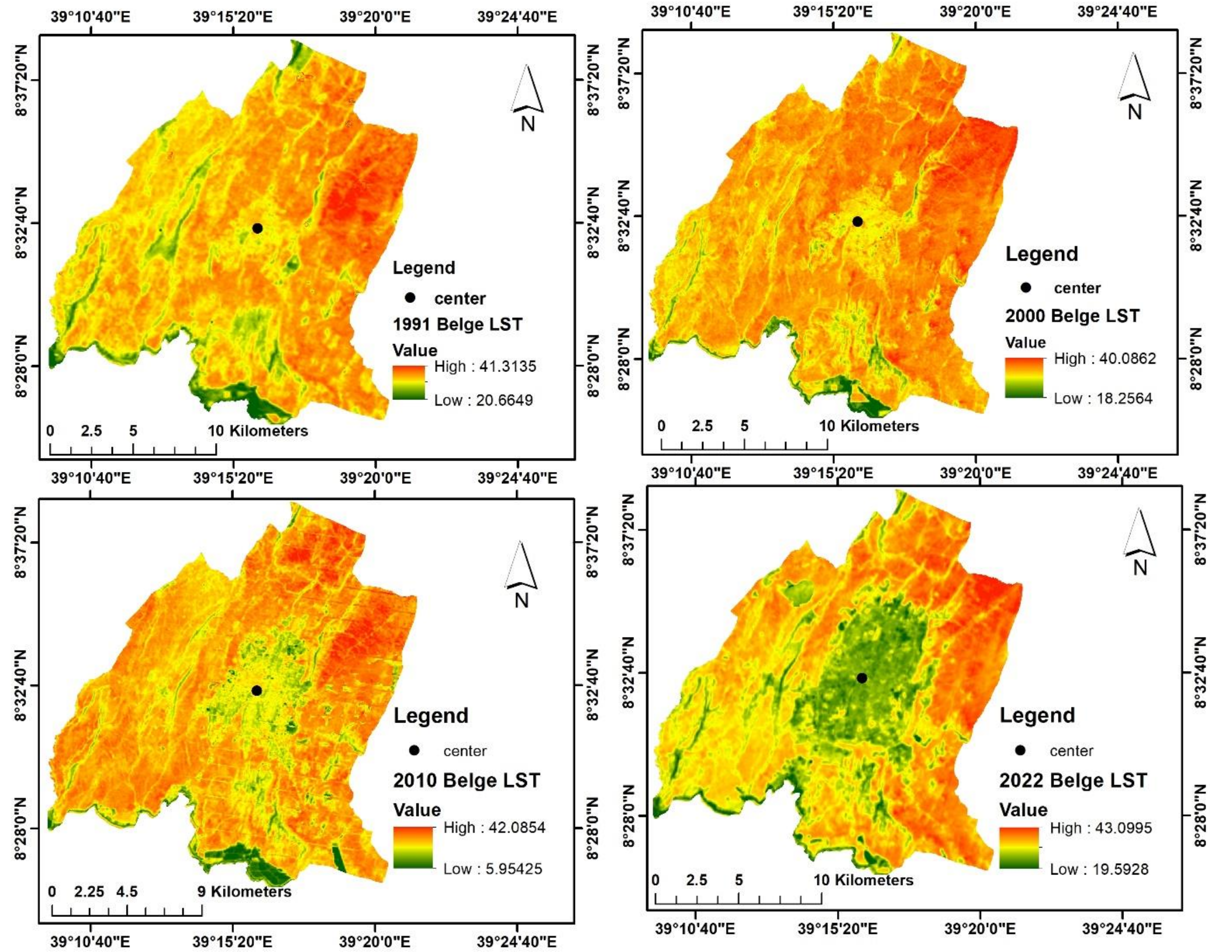

Figure 4.20 LandSat LST Map of Adama City 1991 – 2022 Belge

Table 4.18 Min, Max and Mean LST of Adama 1991 – 2022 Belge

Year	1991	2000	2010	2022
Min	20.66	18.25	5.95	19.59
Max	41.31	40.086	42.08	43.099
Mean	34.51	33.94	35.039	36.60

Spatiotemporal variation of LST of Bega Season

Table 4.19 and Figure 4.21 illustrate the analysis of land surface temperature (LST) variations in Adama City during the Bega season across the years 1991, 2000, 2010, and 2022. LST is a vital environmental indicator that provides insights into urban heating effects and broader climatic conditions.

The dataset reveals variable minimum LST readings throughout the selected years. It began at 17.51°C in 1991, dropped to a lower 14.31°C in 2000, rebounded slightly to 16.14°C in 2010, and then slightly increased to 17.45°C in 2022. In contrast, the maximum LST values peaked at 42.31°C in 2000, showcasing an extreme high compared to 37.44°C in 1991, 38.81°C in 2010, and a decrease to 34.57°C in 2022. The mean LST has also shown fluctuations: starting at 29.79°C in 1991, peaking at 32.76°C in 2000, then decreasing to 31.58°C in 2010, and further to 29.21°C in 2022.

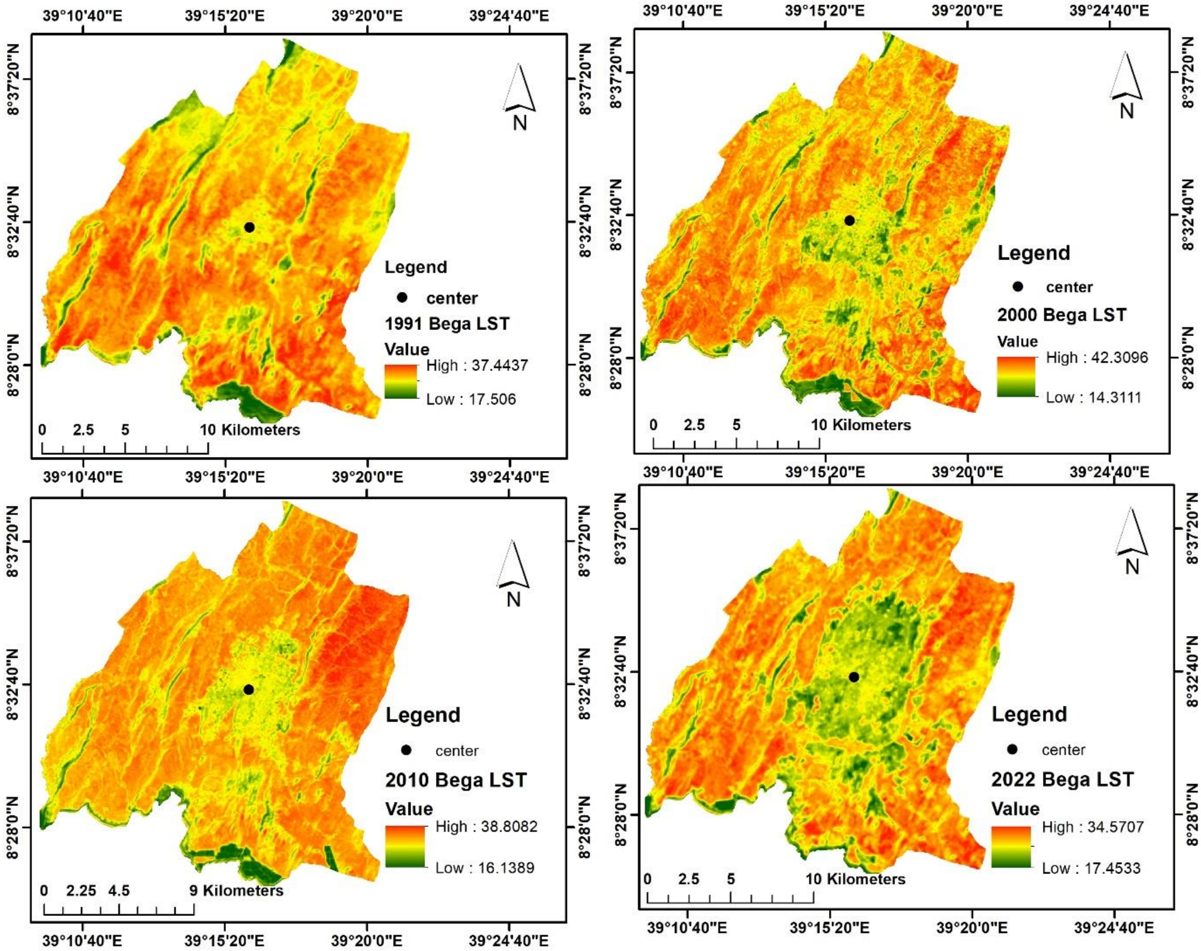

Figure 4.21 LandSat LST Map of Adama City 1991 – 2022 Bega

Table 4.19 Min, Max and Mean LST of Adama 1991 – 2022 Bega

Year	1991	2000	2010	2022
Min	17.51	14.311	16.14	17.45
Max	37.44	42.31	38.81	34.57
Mean	29.78	32.75	31.58	29.21

4.6 The behavior of LST pattern and SUHI effects

4.6.1 SUHII across LULC types Kiremete Season

In 1991, the agricultural areas in Kiremete exhibited a minimum LST of 19.30°C, indicating the presence of cooler cropland zones. The maximum LST reached 30.14°C, showing the distribution of hotter farms. The mean LST across agricultural pixels was 24.064°C, representing the average temperature of farmlands.

For bare land, the minimum LST was 21.92°C and the maximum LST was 31.84°C, revealing a relatively narrow range. The mean bare land LST was 26.75°C, slightly warmer than agriculture on average.

In the built-up urban pixels, the minimum LST was 20.64°C and the maximum LST was 32.25°C. The mean LST for developed areas was 27.073°C, warmer than vegetation and agriculture.

Vegetation cover demonstrated the lowest minimum LST of 19.67°C across cooler habitat areas. The maximum LST was 30.543°C in the hottest forest patches. The mean vegetation LST was 25.26°C

Agriculture had a mean land surface temperature (LST) 1.2°C lower than vegetation, indicating croplands were considerably cooler than natural habitat areas likely due to evapotranspiration on farms to provide cooling effects like those in wooded regions. Bare land showed a mean LST 2.69°C higher than agriculture as bare exposed soils were slightly warmer than croplands, potentially due to the complete lack of vegetation and moisture in bare areas to mitigate temperatures through shading and evaporation. In contrast, built-up areas had a mean LST 3.01°C higher than agriculture with urban developed areas markedly hotter than agricultural croplands; the structures, impervious surfaces, and lack of moisture in cities contributed to higher surface temperatures compared to irrigated, vegetation-covered farms. Additionally, bare land demonstrated a mean LST 1.49°C higher than vegetation, highlighting the substantial warming effect of bare uncovered ground versus the cooling provided by tree shading and evapotranspiration in wooded areas. However, bare land had a mean LST just 0.322°C lower than built-up areas. Finally, vegetation showed a mean LST 1.81°C lower than built-up areas, underscoring the mitigating effect of natural habitat in reducing surface warmth relative to the heat-retaining effects of concrete and asphalt in urban settings.

`

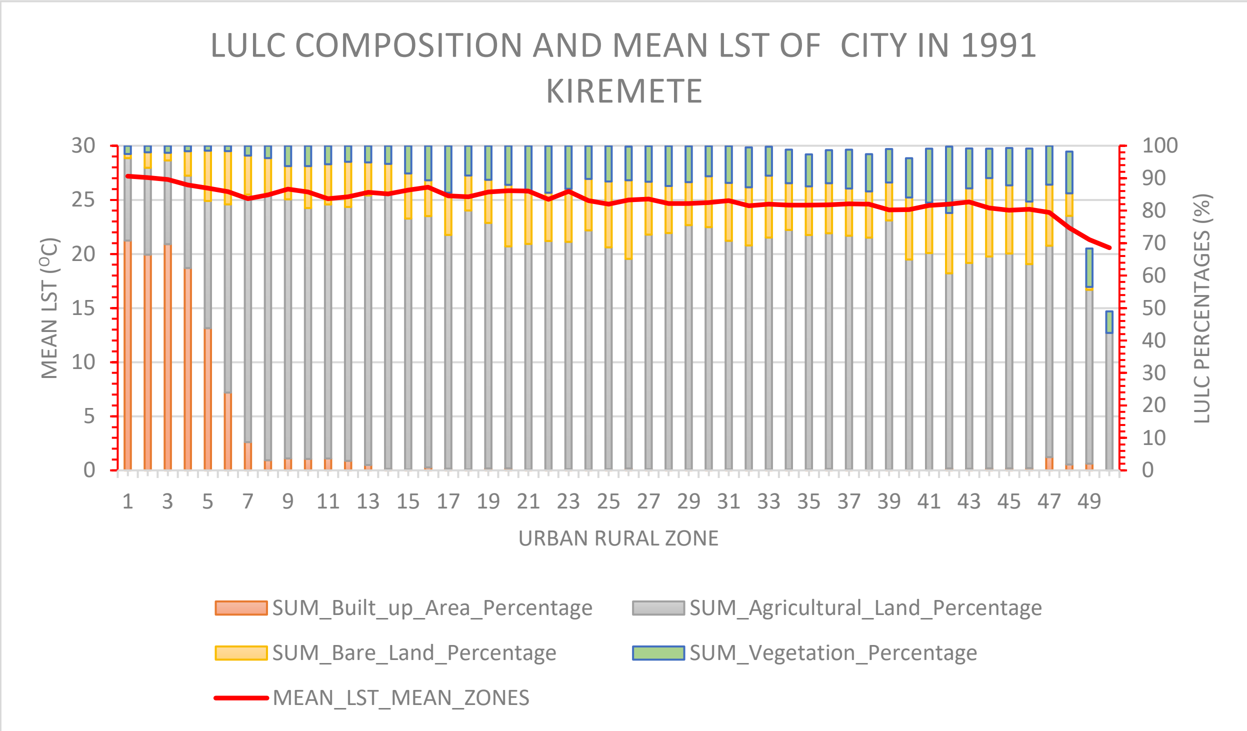

Figure 4.22 LULC Composition and Mean LST Urban-Rural Zone 1991 Kiremete

In 2000, the agricultural pixels exhibited a minimum LST of 17.75°C, indicating expansion of cooler farmland areas. The maximum LST was 29.35°C in the hottest croplands. The mean agriculture LST was 23.054°C, showing overall cooling compared to 1991.

Bare land demonstrated a minimum LST of 18.551°C and a maximum of 29.31°C, also representing a shift to a cooler range. The mean bare land LST was 24.48°C, nearly 2°C lower than in 1991.

For built-up urban areas, the minimum LST was 16.46°C and the maximum was 31.53°C. The mean urban LST was 24.95°C, over 2°C cooler than 1991 levels.

In vegetation cover, the minimum LST was 18.15°C and the maximum was 28.79°C, indicating a cooling shift. The mean vegetation LST lowered to 22.24°C from 25.26°C in 1991.

`

In 2000, agriculture showed a mean land surface temperature (LST) just 0.81°C higher than vegetation, indicating croplands were warming only moderately more than habitat areas, unlike the substantial gap in 1991. However, agriculture had a mean LST 1.42°C lower than bare land as bare exposed soils became markedly hotter than croplands, potentially due to the continuing lack of any vegetation or moisture to mitigate temperatures in bare areas. Built-up areas still demonstrated a higher mean LST than agriculture by 1.89°C with urban zones remaining hotter than croplands. Bare land had a mean LST 2.23°C higher than vegetation, underscoring the considerable warming effect of uncovered ground versus wooded areas, though this large margin also declined from 1991. Additionally, bare land showed a small mean LST decrement of 0.48°C relative to built-up areas, indicating exposed soils were slightly cooler than urban development by 2000. Finally, built-up areas maintained a markedly lower mean LST of 2.71°C compared to vegetation, highlighting the consistent mitigating effect of natural habitat in reducing warmth versus developed areas.

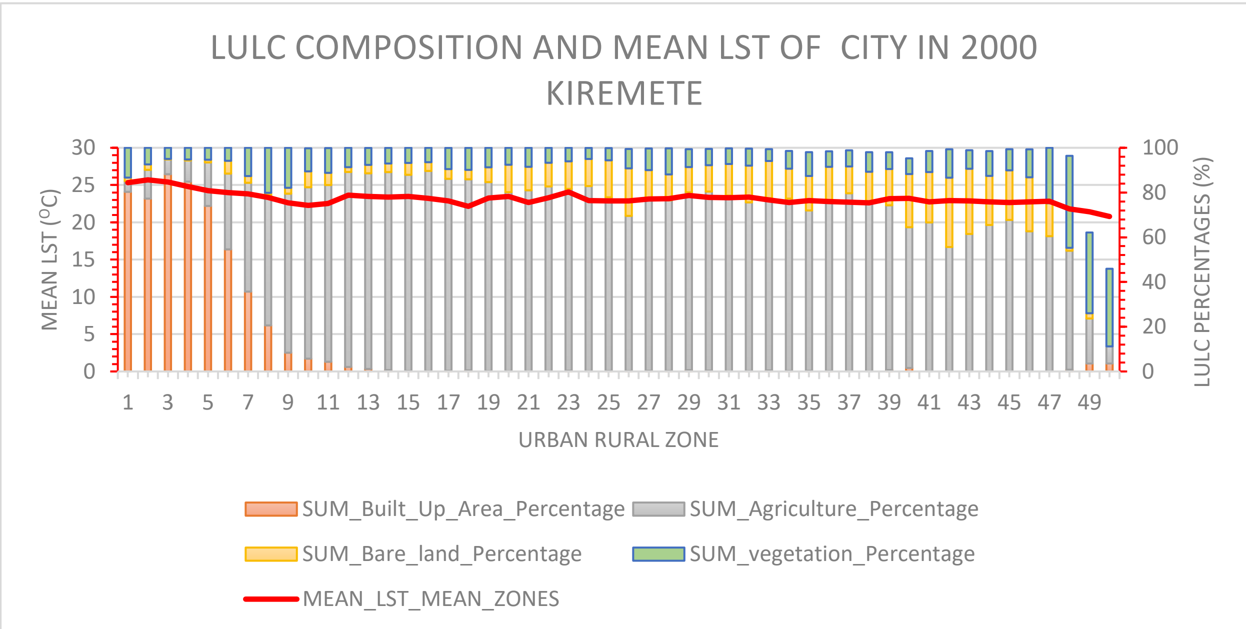

Figure 4.23 LULC Composition and Mean LST Urban-Rural Zone 2000 Kiremete

In 2010, the agricultural pixels exhibited a minimum LST of 17.76°C, showing the presence of cooler farmlands. However, the maximum LST reached 38.31°C, indicating the emergence of very hot croplands. The mean LST was 27.37°C, over 4°C warmer than 2000.

`

Bare land demonstrated a minimum LST of 22.77°C and a maximum of 38.31°C, representing a hotter range. The mean bare land LST increased to 30.75°.

For built-up urban areas, the minimum LST was 15.831°C, but the maximum was 38.05°C, revealing greater extremes. The mean urban LST was 29.14°C, over 4°C warmer than 2000.

In vegetation cover, the minimum LST was 18.145°C and the maximum was 38.30°C, also showing expanded extremes. The mean vegetation LST was 26.15°C, nearly 4°C higher than 2000.

In 2010, the mean LST gap between agriculture and vegetation narrowed to 1.21°C, with croplands just moderately warmer than habitat areas unlike the more extreme difference in 1991. Agriculture showed a mean LST 3.38°C lower than bare land as exposed soils remained substantially hotter than croplands, likely due to the ongoing lack of vegetation or moisture in bare areas to mitigate temperatures. The agriculture vs built-up difference was 1.77°C as urban areas became markedly hotter than croplands by 2010. Bare land maintained a considerable mean LST margin of 4.6°C above vegetation. However, bare land demonstrated a smaller mean LST difference of just 1.10°C relative to built-up areas, indicating exposed soils were warming only slightly more than urban development by 2010. Finally, built-up areas continued showing a substantially higher mean LST of 2.99°C compared to vegetation, highlighting the persisting cooling impact of natural habitat versus developed land.

`

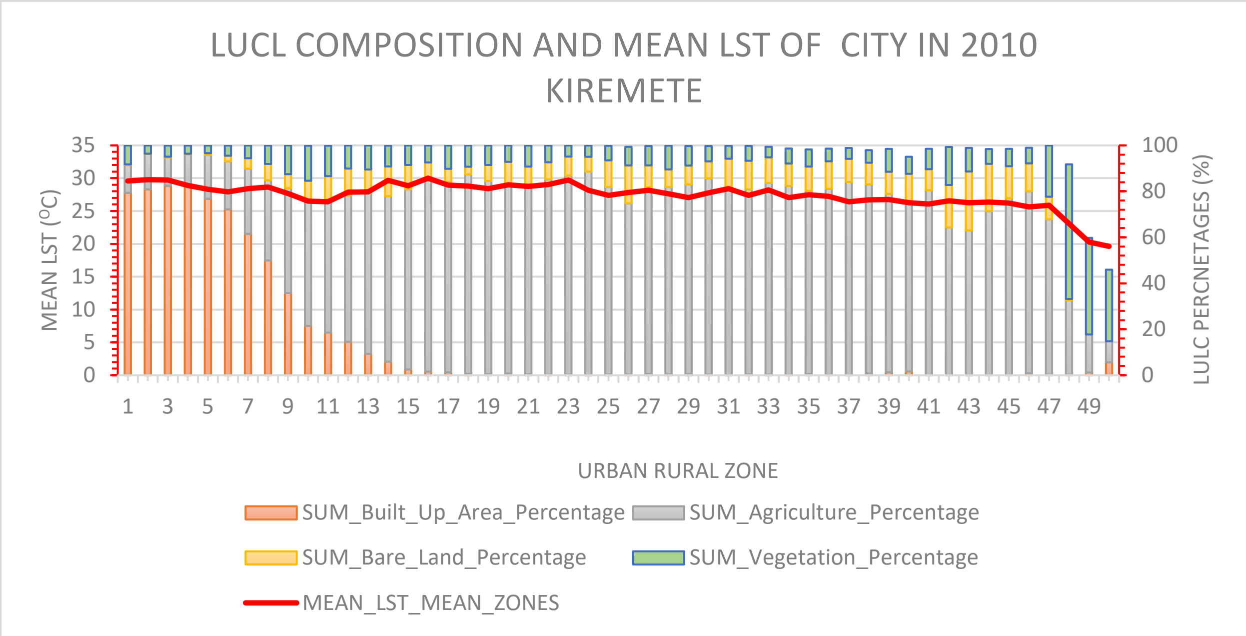

Figure 4.24 LULC Composition and Mean LST Urban-Rural Zone 2010 Kiremete

In 2022, the agricultural pixels exhibited a minimum LST of 18.85°C, indicating the presence of cooler farmland areas again. The maximum reached 29.32°C in the hotter croplands. The mean agricultural LST was 22.57°C, nearly 5°C cooler than 2010, suggesting a reversal of warming.

Bare land showed a minimum LST of 20.50°C and a maximum of 31.71°C, also representing a cooler range compared to 2010. The mean bare land LST was 24.53°C, over 6°C lower than 2010.

For built-up urban areas, the minimum LST was 18.64°C and the maximum was 37.72°C. While a wide range, the mean LST was 25.06°C, around 4°C cooler than 2010.

Vegetation cover demonstrated a minimum LST of 18.01°C and a maximum of 28.98°C. The mean vegetation LST was 22.64°C, indicating cooling from 2010.

By 2022, agriculture showed an almost negligible mean LST difference of just 0.07°C relative to vegetation, indicating cropland and habitat area temperatures was smaller than vegetation by small amount. Agriculture maintained a lower mean LST than bare land by 1.96°C as exposed soils continued exhibiting higher warmth without vegetation or moisture mitigation. The agriculture vs built-up difference remained considerable at

`

2.49°C with urban zones much hotter than croplands. Bare land still had a higher mean LST than vegetation by 1.89°C. The bare land vs built-up gap also declined to just 0.52°C, indicating built up was hotter. Finally, built-up areas persisted in showing a substantially higher mean LST of 2.42°C relative to vegetation, underscoring the lasting cooling effect of natural habitat versus developed land covers.

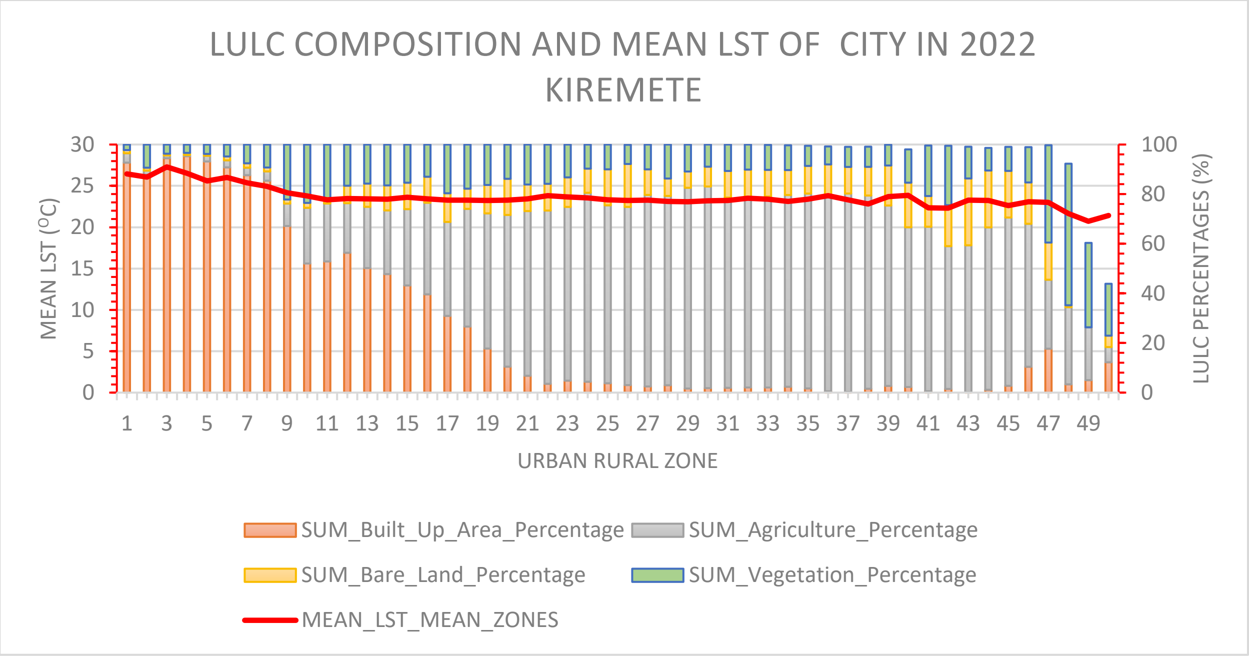

Figure 4.25 LULC Composition and Mean LST Urban-Rural Zone 2022 Kiremete

Table 4.20 Mean LST and Mean LST Changes from 1991-2022 Kiremete

LULC Types	Mean LST (°C) Kiremte							
	1991	2000	2010	2022	1991 - 2000	2000 - 2010	2010 - 2022	1991 - 2022
Agriculture	24.06	23.05	27.37	22.57	- 1.01°C	4.31°C	-4.79°C	- 1.49°C
Bare Land	26.75	24.47	30.75	24.53	- 2.27°C	6.27°C	- 6.21°C	- 2.21°C
Built Up	27.07	24.95	29.14	25.06	-2.12°C	4.18°C	-4.07°C	- 2.01°C
Vegetation	25.26	22.24	26.15	22.64	-3.02°C	3.91°C	- 3.51°	- 2.62°C

Table 4.21 LULC Types LST cross comparisons from 1991 – 2022 Kiremete

LULC Types cross comparisons	Magnitude of mean LST (°C)			
	1991	2000	2010	2022
Agriculture - Vegetation	-1.2°C	0.81°C	1.22°C	-0.07°C
Agriculture – Bare Land	-2.69C	-1.42°C	-3.38°C	-1.96°C
Agriculture – Built up	-3.01°C	-1.89°C	-1.77°C	-2.49°C
Bare Land - Vegetation	1.49°C	2.23°C	4.6°C	1.89°C
Bare Land – Built Up	-0.32°C	-0.48°C	1.61°C	-0.53°C
Built Up - Vegtation	1.81°C	2.71°C	2.99°C	2.42°C

`

In summary, there was an overall cooling from 1991 to 2000, then warming from 2000 to 2010, followed again by cooling from 2010 to 2022. The 1991 to 2022 change shows a slight cooling trend across all land cover classes in Kiremete over the past few decades.

4.6.2 SUHII across LULC types Belge Season

In 1991, the agricultural areas in Belge exhibited a minimum LST of 20.99°C, indicating the presence of cooler farmlands. The maximum LST reached 41.314°C in the hottest cropland zones. The mean agricultural LST was 34.94°C, representing the average temperature across all farm pixels.

For bare land, the minimum LST was 21.50°C and the maximum was 41.30°C, showing that bare soils maintained relatively high temperatures. The mean bare land LST was 34.54°C, slightly cooler than agriculture on average.

In the built-up urban pixels, the minimum LST was 23.15°C and the maximum was 40.53°C. The mean urban LST was 33.60°C, warmer than vegetation but cooler than agriculture and bare land.

The vegetation cover demonstrated the lowest minimum LST of 20.96°C in the coolest habitat zones. The maximum vegetation LST was 41.27°C in the hottest areas. The mean was 30.89°C across all forested pixels.

The 1991 Belge season reveals several distinct dynamics in the relationships between land cover and surface temperature in Adama. Agriculture land surface temperature (LST) was found to be 4.05°C warmer than vegetation LST, 0.40°C hotter than bare land LST, and notably 1.34°C hotter than built up LST. The cooler bare land relative to agriculture land LST potentially results from lower soil moisture content on farms during the belge. Bare land LST was 3.65°C warmer than vegetation LST, due to lack of evapotranspiration over bare ground. However, bare land LST was only 0.94°C warmer than built up, indicating built up materials may elevate temperatures to near bare land levels during belge. Built up LST was 2.71°C warmer than vegetation, affirming urban heat island effects during Belge.

`

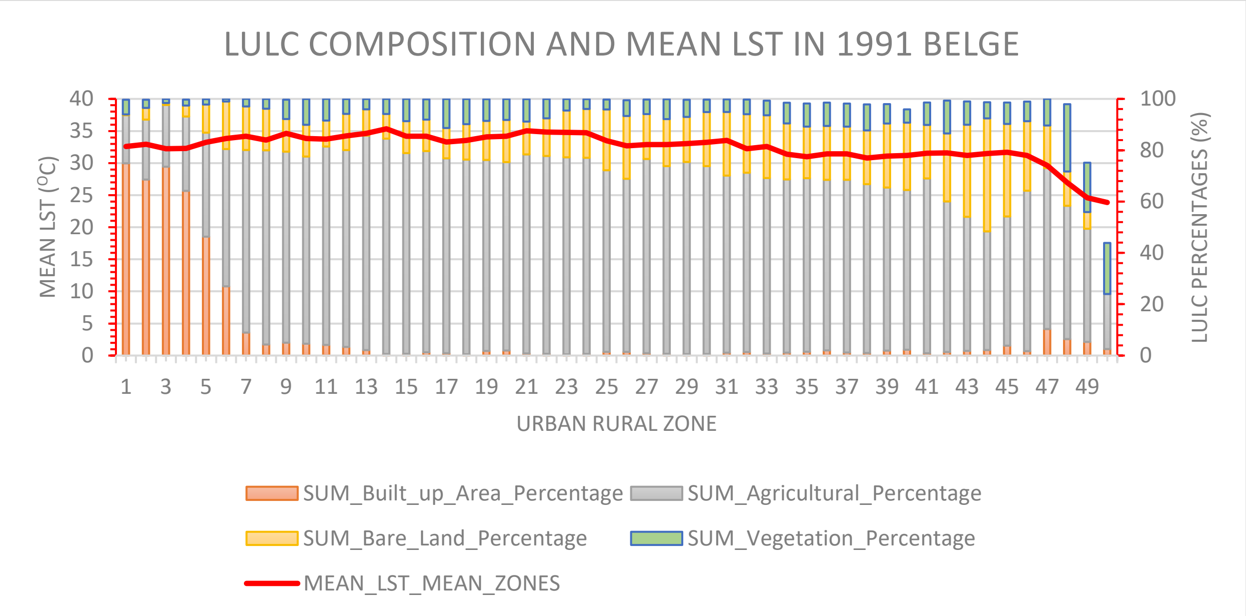

Figure 4.26 LULC Composition and Mean LST Urban-Rural Zone 1991 Belge

In 2000, the agricultural pixels exhibited a minimum LST of 22.26°C, indicating expansion of cooler farmlands compared to 1991. The maximum agriculture LST was 40.08°C in the hottest zones. The mean LST dropped to 34.38°C, showing slight cooling from 1991.

Bare land had a minimum LST of 25.21°C and a maximum of 38.31°C, representing a warmer range than 1991. However, the mean bare land LST decreased to 33.61°C.

For built-up urban areas, the minimum LST was 18.25°C, and the maximum was 38.57°C. The mean urban LST cooled to 32.475°C from 33.603°C in 1991.

In vegetation cover, the minimum LST was 23.71°C, and the maximum was 38.816°C. The mean vegetation LST was 31.74°C, also lower than 1991.

The 2000 Belge season reveals a distinct shift in the relationships between land cover and land surface temperature (LST) compared to 1991. In 2000, agriculture LST was 2.64°C warmer than vegetation LST, 0.77°C warmer than bare land LST, and 1.91°C hotter than built up LST. Agriculture LST was slightly warmer than bare land, also differing from 1991, potentially signaling lower soil moisture. Agriculture remained hotter than built up areas, by 1.91°C. Bare land LST was 1.86°C warmer than vegetation LST, though less than 1991, and 1.13°C hotter than built up LST.

`

Finally, built up LST was 0.72°C warmer than vegetation, a lower gap than 1991. Overall, the changing magnitudes showcase evolving seasonal influences of land cover on LST.

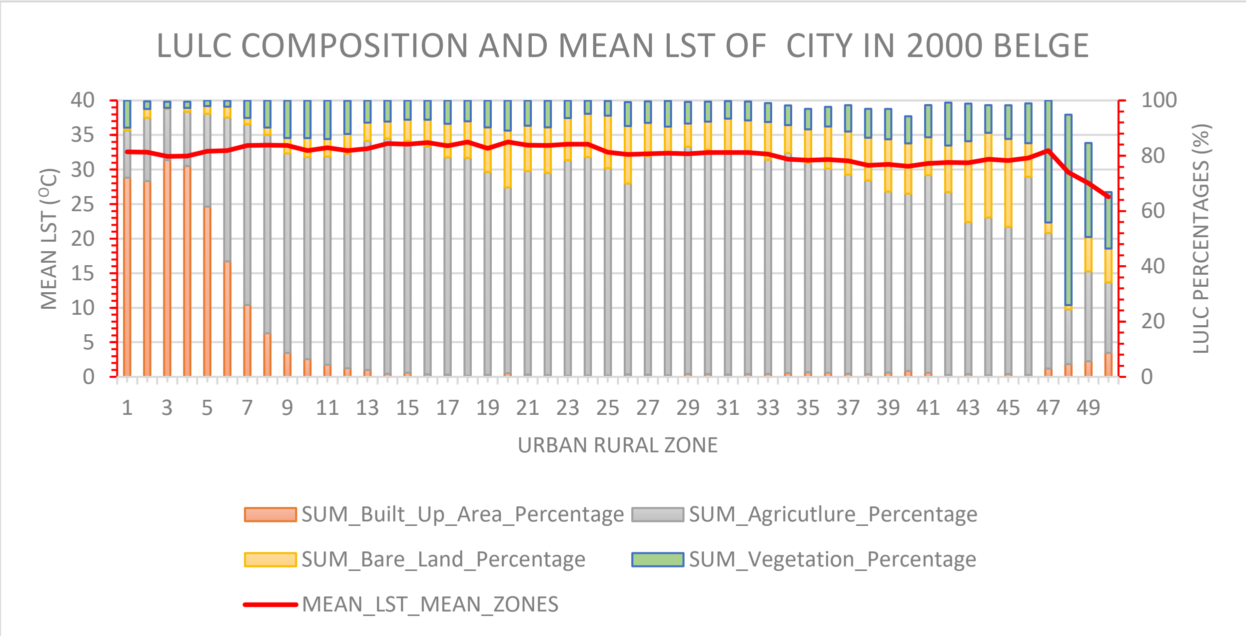

Figure 4.27 LULC Composition and Mean LST Urban-Rural Zone 2000 Belge

In 2010, the agricultural pixels exhibited a minimum LST of 14.41°C, indicating the emergence of cooler farmland areas. However, the maximum LST reached 42.08°C in extremely hot zones. The mean agricultural LST rose to 35.55°C, over 1°C warmer than 2000.

Bare land demonstrated a low minimum LST of 7.61°C but a high maximum of 40.58°C, representing a wide range. The mean bare land LST increased to 35.32°C, showing heating from 2000.

For built-up urban areas, the minimum LST was 5.95°C, and the maximum was 40.34°C, also a very wide spread. The mean urban LST warmed to 32.25°C compared to 2000.

In vegetation cover, the minimum LST was 24.55°C, and the maximum was 39.81°C. The mean vegetation LST was 32.01°C, nearly 1°C above 2000.

The 2010 Belge season marks another shift in the land cover and land surface temperature (LST) relationships. Agriculture LST was 3.07°C warmer than vegetation,

`

0.22°C warmer than bare land, and 3.27°C warmer than built up in 2010. The substantial agriculture-vegetation gap indicates considerably lower evapotranspiration of croplands. However, agriculture LST remained slightly warmer than bare land, similar to 2000. Most notably, agriculture was markedly warmer than built up areas. Bare land LST was 2.85°C warmer than vegetation, and 3.07°C hotter than built up, aligning with the expectation of hotter bare ground. Finally, built up LST was just 0.24°C warmer than vegetation, the smallest gap among years, and potentially signaling expansion of urban greener

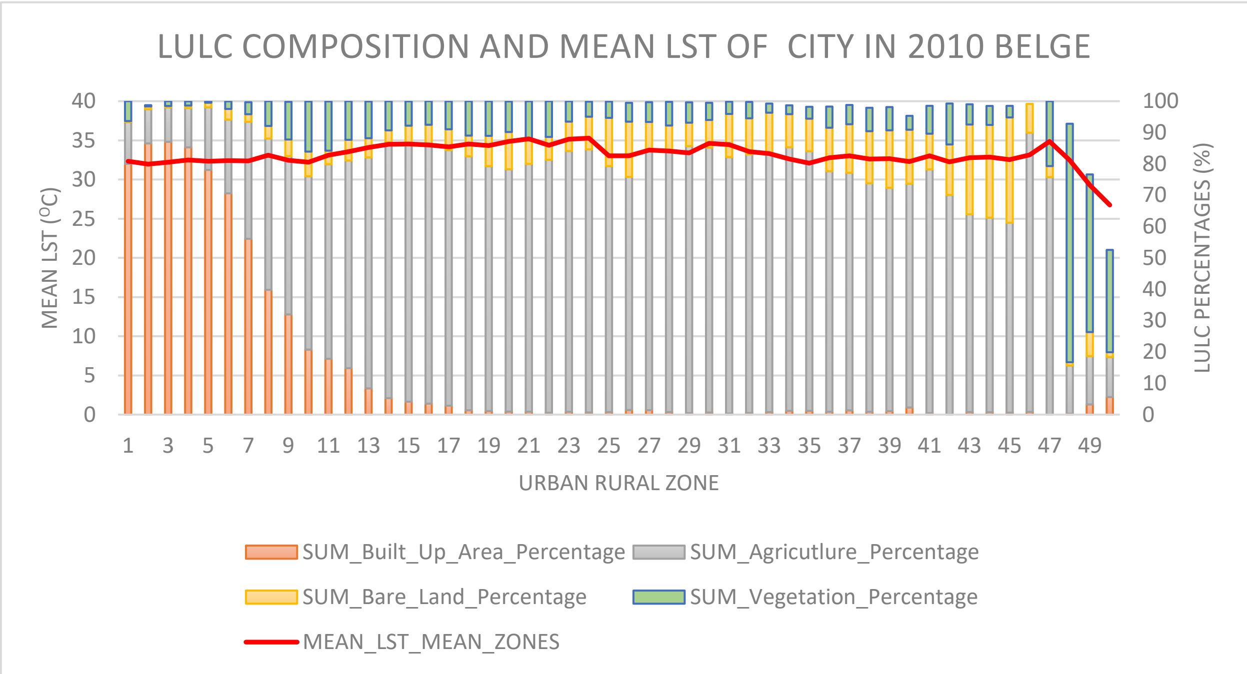

Figure 4.28 LULC Composition and Mean LST Urban-Rural Zone 2010 Belge

In 2022, the agricultural pixels exhibited a minimum LST of 25.77°C, indicating a lack of very cool farmlands unlike 2010. However, the maximum LST reached 43.10°C in extremely hot zones. The mean agricultural LST was 37.80°C, around 2°C warmer than 2010.

Bare land demonstrated a minimum LST of 27.51°C and a maximum of 42.29°C, representing a cooler and narrower range compared to 2010. However, the mean bare land LST was 37.11°C, nearly 2°C above 2010.

`

For built-up urban areas, the minimum LST was 19.59°C, and the maximum was 42.56°C. The mean urban LST increased to 33.73°C compared to 2010

In vegetation cover, the minimum LST was 24.74°C, and the maximum was 42.20°C. The mean vegetation LST was 32.09°C, around 3°C warmer than 2010.

The 2022 season reveals several notable relationships between land cover types and land surface temperatures (LST). Agriculture LST was markedly warmer than other covers, being 5.70°C warmer than vegetation, indicating lower evapotranspiration over croplands. Agriculture LST was also slightly warmer at 0.69°C compared to bare land, and substantially warmer at 4.07°C compared to built up areas. As expected, bare land LST was 5.01°C warmer than vegetation. However, bare land was 3.38°C hotter than built up areas, aligning with the expectation of hotter bare ground compared to urban development. Finally, built up LST was 1.64°C warmer than vegetation, representing a small gap between these covers.

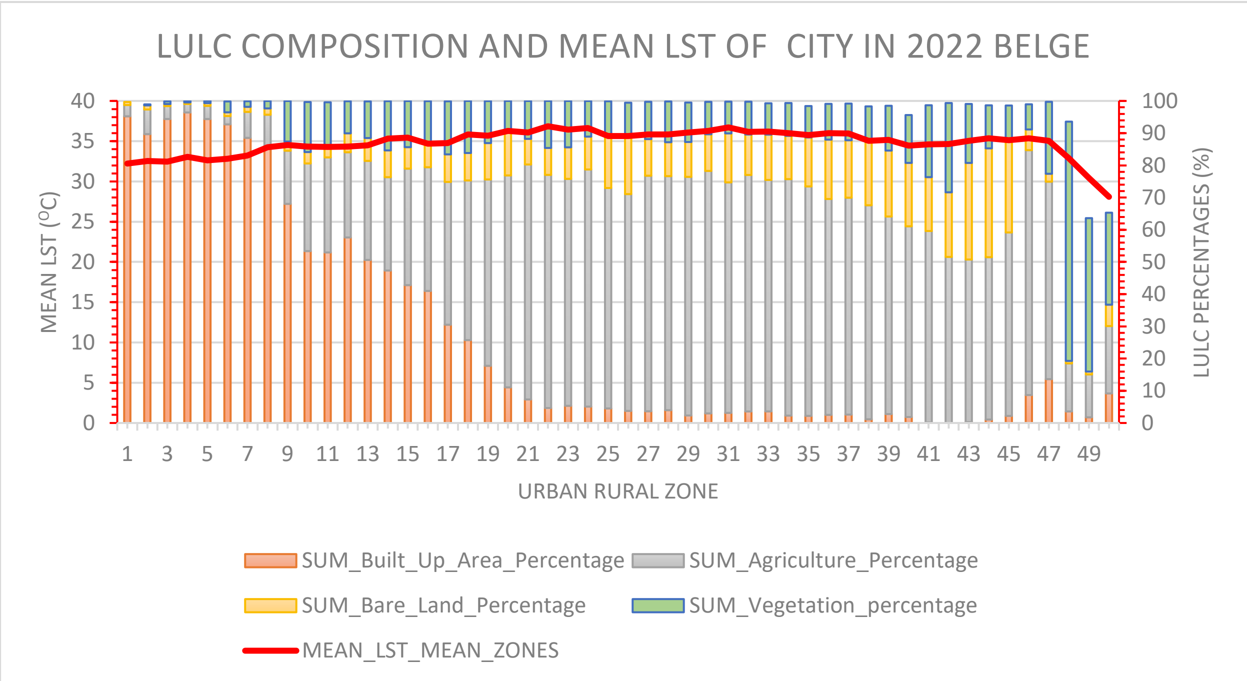

Figure 4.29 LULC Composition and Mean LST Urban-Rural Zone 2022 Belge

`

Table 4.22 Mean LST and Mean LST Changes from 1991-2022 Belge

LULC Types	Mean LST (℃)							
	1991	2000	2010	2022	1991 - 2000	2000 - 2010	2010 - 2022	1991 - 2022
Agriculture	34.94	34.38	35.55	37.80	-0.56°C	1.16°C	2.25°C	2.85°C
Bare Land	34.54	33.61	35.32	37.11	-0.92°C	1.70°C	1.79°C	2.57°C
Built Up	33.60	32.47	32.25	33.73	-1.12°C	0.22°C	1.48°C	0.13°C
Vegetation	30.89	31.74	32.01	32.09	0.85°C	0.72°C	2.62°C	1.20°C

Table 4.23 LULC Types LST cross comparisons from 1991 – 2022 Belge

LULC Types cross comparisons	Magnitude of mean LST (°C)			
	1991	2000	2010	2022
Agriculture - Vegetation	4.0550°C	2.6409°C	3.0784°C	5.7072°C
Agriculture – Bare Land	0.40°C	0.77°C	0.22°C	0.69°C
Agriculture – Built up	1.34°C	1.91°C	3.27°C	4.07°C
Bare Land - Vegetation	3.65°C	1.86°C	2.85°C	5.01°C
Bare Land – Built Up	0.94°C	1.13°C	3.07°C	3.38°C
Built Up - Vegtation	2.71°C	0.72°C	0.24°C	1.64°C

4.6.3 SUHII across LULC types Bega Season

The agricultural land areas in Bega exhibited a minimum LST value of 20.08°C, indicating the presence of cooler agricultural zones. The maximum LST reached 37.44°C, reflecting hotter cropland areas. The mean LST for agriculture was 29.72°C, signifying the average temperature across all agricultural pixels.

For bare land, the minimum LST was 24.60°C, suggesting even the coolest bare soil patches remained relatively warm. Bare land had a maximum temperature of 37.43°C, with hotter open ground present. The mean LST was 31.43°C, indicating bare land was warmer on average compared to other cover types.

In the built-up urban areas, the minimum LST was 21.99°C, and the maximum was 35.07°C, showing a smaller temperature range across developed zones. The mean LST for urban pixels was 28.63°C, demonstrating the central tendency of temperature across the city's infrastructure.

In Bega during 1991, agriculture showed a mean LST of 2.81°C higher than vegetation, indicating croplands were substantially warmer than habitat areas. However, agriculture had a lower mean LST than bare land by 1.71°C, as exposed soils were even hotter without any vegetation or moisture for cooling. Agriculture demonstrated a moderately higher mean LST than built-up areas by 1.09°C. Bare land maintained a considerable mean LST margin of 4.52°C above vegetation, underscoring the extreme warming effect of uncovered ground. The bare land vs built-up difference was 2.81°C, with exposed soils substantially warmer than urban areas. Finally, built-up areas had a slightly higher mean LST of 1.72°C relative to vegetation, unlike other seasons where developed areas were markedly cooler than habitat.

`

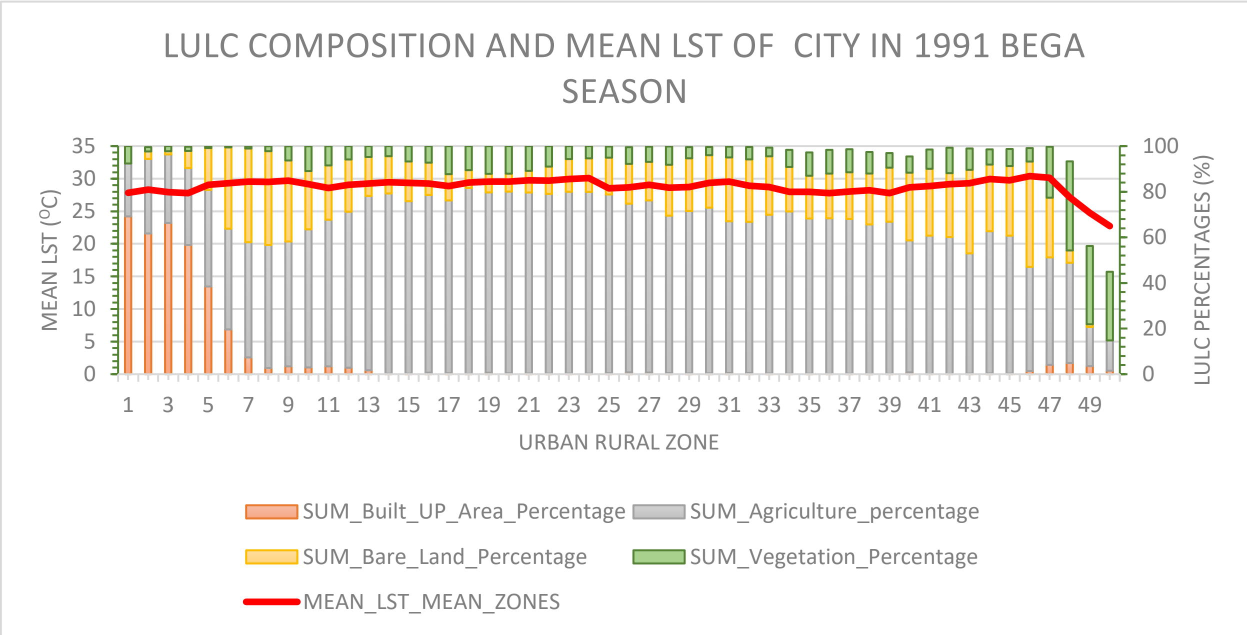

Figure 4.30 LULC Composition and Mean LST Urban-Rural Zone 1991 Bega

In 2000, the agricultural areas in Bega exhibited a minimum LST of 21.94°C, indicating the presence of some slightly cooler farmland, though still warmer than 1991. The maximum LST reached 42.31°C, reflecting substantially hotter croplands compared to just 37.44°C in 1991. The mean LST was 32.98°C across all agricultural pixels, showing average farm temperatures had increased nearly 3°C from 1991.

For bare land, the minimum LST was 23.33°C, and the maximum was 42.06°C, representing a similar but shifted range compared to 1991. The mean bare land LST was 34.66°C, an over 1°C increase from 1991, indicating heating of exposed soil surfaces.

In the built-up urban areas, the minimum LST had dropped to 14.31°C, suggesting some cooler developed zones. However, the maximum LST increased to 39.32°C, and the mean was 30.75°C, both higher than 1991, reflecting the growing urban heat island.

Vegetation cover showed a minimum LST of 21.13°C and a maximum of 38.30°C. The mean LST was 28.41°C, only slightly warmer than the 1991 mean of 26.90°C for forested areas.

`

In 2000, the gap between agriculture and vegetation mean LST increased substantially to 4.57°C, with croplands much warmer than habitat areas. However, agriculture was cooler than bare land by 1.67°C as exposed soils remained hotter without any moderating vegetation or moisture. The agriculture vs built-up margin grew to 2.23°C with croplands warmer than urban areas. Bare land maintained a considerable 6.24°C higher mean LST over vegetation, highlighting the extreme warming of uncovered ground. The bare land vs built-up gap increased to 3.90°C, indicating exposed soils were significantly hotter than urban development. Finally, built-up areas showed a mean LST of 2.33°C above vegetation, unlike other seasons where built-up areas were cooler than habitat due to mitigating effects of development.

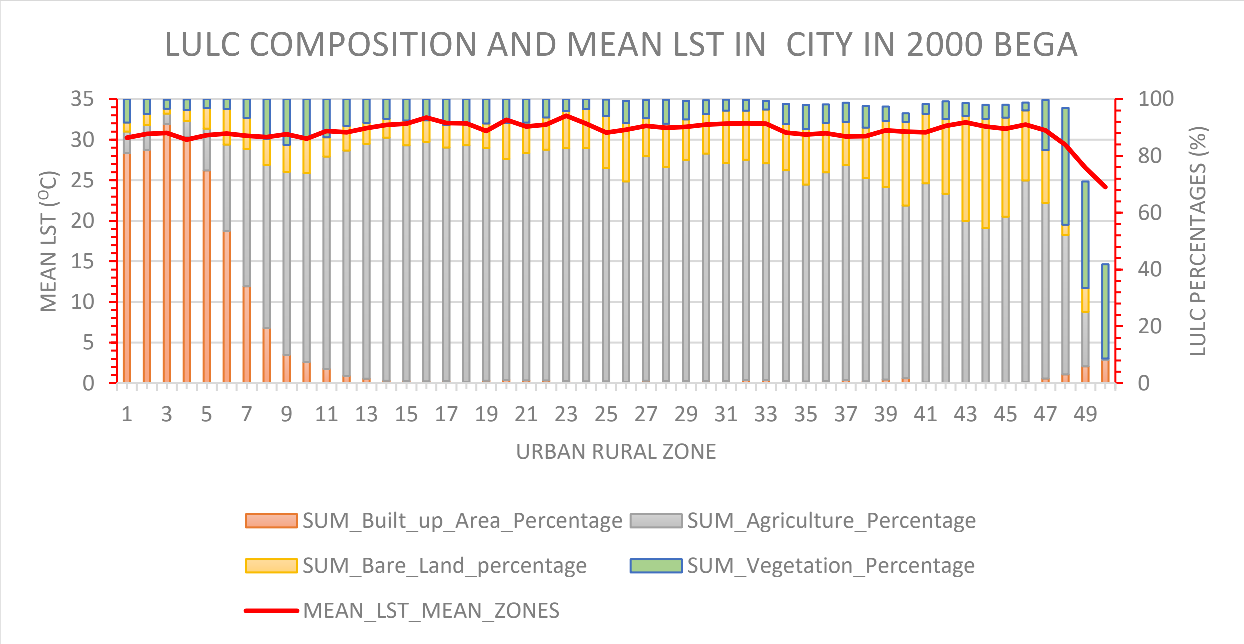

Figure 4.31 LULC Composition and Mean LST Urban-Rural Zone 2000 Bega

In 2010, the agricultural pixels in Bega showed a minimum LST of 19.20°C, indicating the presence of cooler farmland areas compared to 2000. However, the maximum reached 38.55°C, showing agricultural hotspots had further increased. The mean LST was 32.18°C, slightly lower than 2000 but still warmer than 1991.

Bare land exhibited a minimum LST of 22.34°C and a maximum of 38.30°C, representing a cooler range than 2000. Yet the mean LST remained high at 32.14°C, reflecting sustained heating of bare ground.

`

For built-up urban areas, the minimum LST was 16.13°C, the lowest among land cover classes, suggesting the city had some cooler developed microclimates. But the maximum LST was 38.80°C, and the mean was 28.30°C, showing the urban heat island effect persisted.

In vegetation pixels, the minimum LST was 18.51°C, and the maximum was 34.940°C, indicating a cooling shift back towards the 1991 range. The mean LST was 27.75°C, slightly lower than 2000.

In 2010, agriculture had a mean LST 4.42°C higher than vegetation, indicating a substantial warming gap between croplands and habitat. However, agriculture showed an almost negligible 0.04°C difference from bare land, suggesting comparable temperatures between these covers. The agriculture vs built-up margin remained high at 3.87°C with croplands substantially warmer than urban areas. Bare land maintained a 4.39°C higher mean LST over vegetation, continuing to highlight the extreme warming of bare ground. The bare land vs built-up difference declined slightly to 3.83°C but was still considerable, with exposed soils markedly hotter than development. Finally, built-up areas had a small 0.55°C higher mean LST than vegetation, unlike other seasons where urban areas were cooler than habitat.

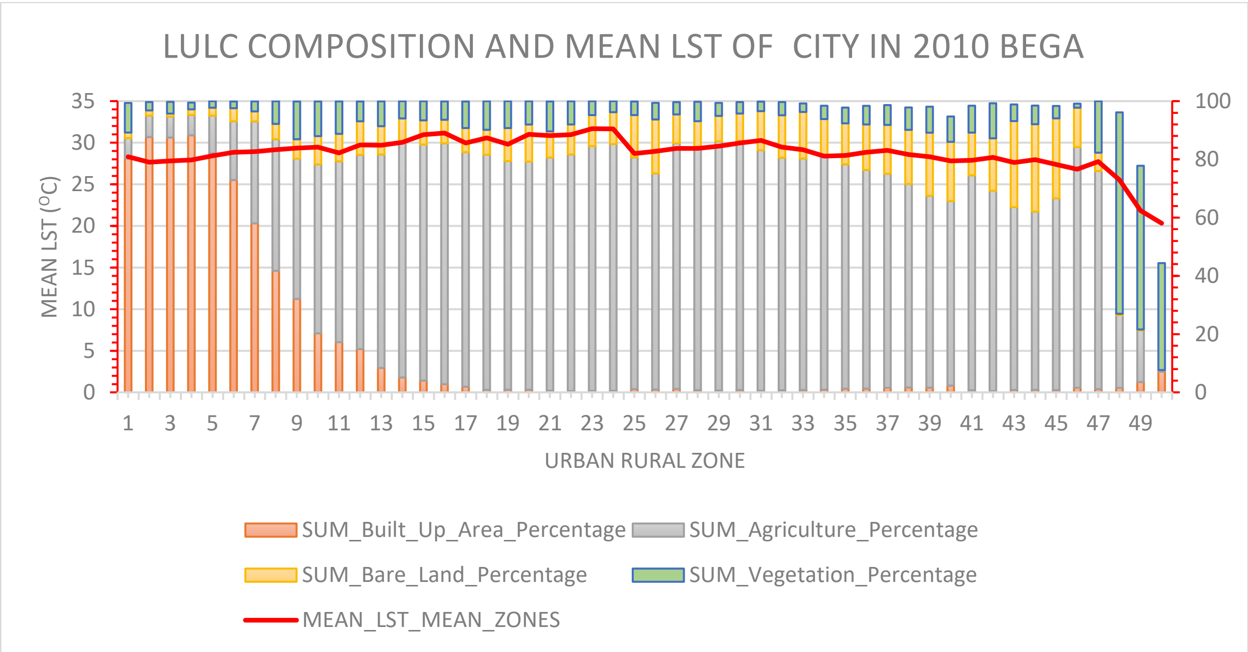

Figure 4.32 LULC Composition and Mean LST Urban-Rural Zone 2010 Bega

`

In 2022, the agricultural areas in Bega exhibited a minimum LST of 19.56°C, showing the presence of cooler farmland zones. The maximum LST was 34.57°C, indicating agricultural hotspots had eased compared to 2010. The mean LST dropped to 30.98°C, suggesting an overall cooling trend.

Bare land demonstrated a minimum LST of 23.20°C and a maximum of 34.41°C, representing a tighter range with lower extremes than 2010. The mean LST was 30.91°C, also reflecting cooling bare soil surfaces compared to prior years.

For built-up urban pixels, the minimum LST had decreased further to 17.96°C, showing the spread of cooler microclimates. The maximum was 34.29°C, and the mean was 26.94°C, revealing a slight mitigation of the urban heat island effect.

In vegetation cover, the minimum LST was 20.43°C, and the maximum was 33.92°C, representing a slightly warmer range than 2010. However, the mean LST remained similar at 26.90°C.

By 2022, the agriculture vs vegetation gap decreased to 4.09°C but was still substantial, with croplands considerably warmer than habitat. Agriculture became hotter than bare land by 0.07°C. The agriculture vs built-up difference grew to 4.04°C, with croplands again markedly warmer than urban zones. Bare land persisted in showing a sizeable 4.01°C higher mean LST over vegetation, reflecting the sustained extreme warmth of bare ground. The bare land vs built-up margin remained high at 3.97°C, with exposed soils considerably hotter than developed areas. Finally, built-up areas showed an almost negligible 0.05°C difference from vegetation, indicating comparable temperatures between these covers.

`

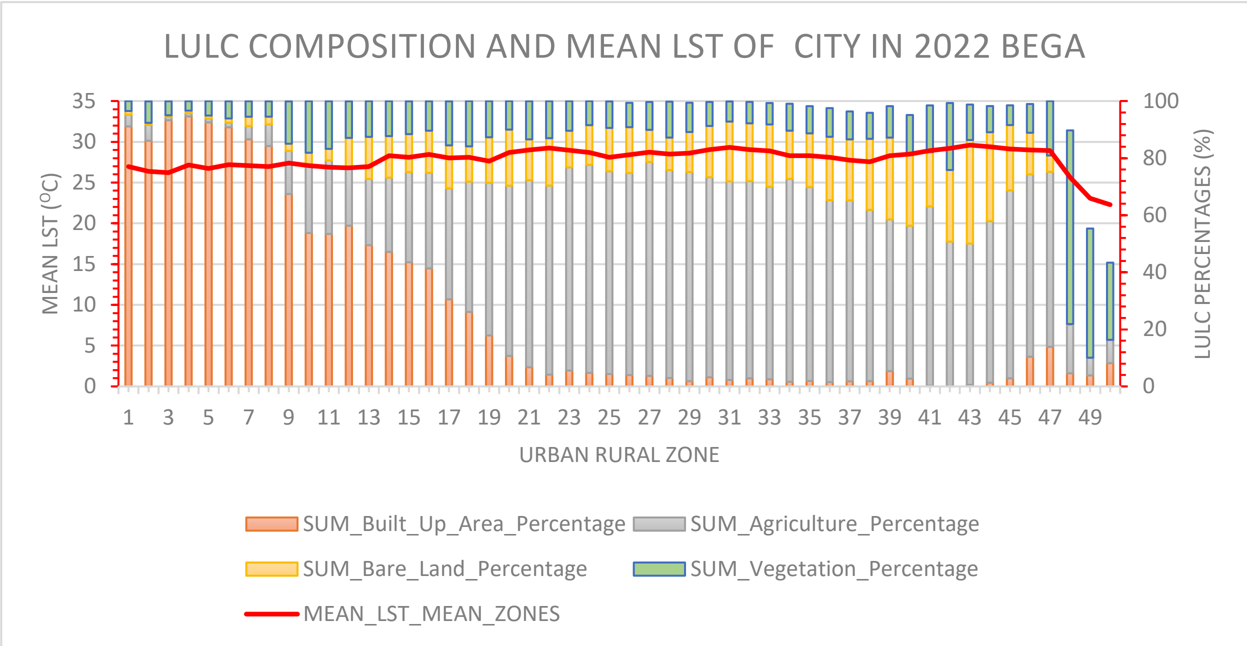

Figure 4.33 LULC Composition and Mean LST Urban-Rural Zone 2022 Belge

`

Table 4.24 Mean LST and Mean LST Changes from 1991-2022 Bega

LULC Types	Mean LST (°C)							
	1991	2000	2010	2022	1991 - 2000	2000 - 2010	2010 - 2022	1991 - 2022
Agriculture	29.72°C	32.98°C	32.18°C	30.98°C	3.25°C	-0.80°C	-2.20°C	0.24°C
Bare Land	31.43°C	34.66°C	32.14°C	30.91°C	3.22°C	- 2.51°C	-1.23°C	- 0.51°C
Built Up	28.63°C	30.75°C	28.30°C	26.94°C	2.12°C	-2.44°C	-1.36°C	- 1.68°C
Vegetation	26.90°C	28.41°C	27.75°C	26.89°C	1.51°C	- 0.66°C	-0.85°C	- 0.006°C

Table 4.25 LULC Types LST cross comparisons from 1991 – 2022 Bega

LULC Types cross comparisons	Magnitude of mean LST (°C)			
	1991	2000	2010	2022
Agriculture - Vegetation	2.81°C	4.57°C	4.42°C	4.09°C
Agriculture – Bare Land	-1.71°C	-1.67°C	0.04°C	0.07°C
Agriculture – Built up	1.09°C	2.23°C	3.87°C	4.04°C
Bare Land - Vegetation	4.52°C	6.24°C	4.39°C	4.01°C
Bare Land – Built Up	2.81°C	3.90°C	3.83°C	3.97°C
Built Up - Vegtation	1.72°C	2.33°C	0.55°C	0.05°C

4.7 Impact of land use land cover Change on land surface temperature in each season for 1991

Analysis of land surface temperatures (LSTs) by land cover type in 1991 reveals several key differences between the Kiremete, Bega, and Belge landscapes. For agricultural areas, Kiremete saw the coolest temperatures with a minimum of 19.30°C, maximum of 30.13°C, and mean of 24.06°C. Bega exhibited warmer agriculture LSTs ranging from 20.08°C to 37.44°C, averaging 29.72°C. Belge was the hottest region for agriculture, with extremes of 21.02°C and 41.31°C and a mean of 34.94°C.

Vegetation cover followed a similar pattern, with Kiremete the coolest (19.673°C min, 30.54°C max, 25.26°C mean), Bega moderate (18.72°C min, 35.05°C max, 26.90°C mean), and Belge the warmest (20.96°C min, 41.27°C max, 30.89°C mean).

For bare land, Kiremete again had the lowest temperatures, ranging from 21.922°C to 31.83°C, averaging 26.75°C. Bega saw higher bare land LSTs of 24.49°C to 37.434°C, mean 31.43°C. Belge was hottest with extremes of 21.50°C and 41.30°C, and a mean of 34.54°C.

A similar pattern emerged for built-up areas. Kiremete had the coolest built-up LSTs from 20.64°C to 32.25°C, averaging 27.07°C. Bega and Belge were warmer, with respective ranges of 21.92°C to 35.07°C (mean 28.63°C) and 23.15°C to 40.53°C (mean 33.603°C).

In summary, LST analysis showed Kiremete was generally the coolest landscape across all land cover types.

`

4.8 Impact of land use land cover Change on land surface temperature in each season for 2000

Analysis of 2000 land surface temperatures (LSTs) by land cover type shows several key variations between the Kiremete, Bega, and Belge landscapes. For agricultural areas, Kiremete exhibited the coolest LST range from 17.75°C to 29.35°C, averaging 23.05°C. Bega saw warmer agriculture temperatures spanning 22.04°C to 42.30°C, with a mean of 32.98°C. Belge was the hottest region for agriculture, with minimum and maximum LSTs of 22.26°C and 40.08°C respectively, averaging 34.38°C.

Vegetation cover followed a similar pattern, with Kiremete having the lowest vegetation LSTs ranging from 18.15°C to 28.78°C, mean of 22.24°C. Bega exhibited moderately higher vegetation temperatures from 21.13°C to 38.30°C, averaging 28.41°C. Belge was again the warmest landscape for vegetation, with extremes of 23.71°C and 38.81°C, mean of 31.74°C.

For bare land, Kiremete had the coolest LSTs varying between 18.55°C and 29.27°C, with a mean of 24.479°C. Bega saw substantially hotter bare land temperatures spanning 23.362°C to 41.99°C, averaging 34.64°C. Belge bare lands exhibited a range of 25.21°C to 38.30°C, mean of 33.60°C.

Built-up areas displayed the greatest variability. Kiremete had the lowest built-up LSTs from 16.457°C to 31.568°C, mean of 24.985°C. Bega showed the hottest built-up maximum of 39.325°C, ranging 14.31°C to 39.32°C, averaging 30.75°C. Belge built-up LSTs spanned 18.261°C to 38.57°C, with a mean of 32.47°C.

In summary, the year 2000 LST analysis revealed the coolest temperatures consistently occurred in Kiremete, while Belge and Bega were usually the hottest landscape across land cover types. However, some maximum LST variation occurred between Bega and Belge.

4.9 Impact of land use land cover Change on land surface temperature in each season for 2010

Analysis of 2010 land surface temperatures (LSTs) by land cover type reveals several key variations between the Kiremete, Bega, and Belge landscapes. For agriculture areas, Kiremete saw the coolest temperature range from 17.75°C to 38.31°C, with a mean of 27.371°C. Bega exhibited moderately higher agriculture LSTs spanning 19.2°C to 38.559°C and averaging 32.183°C. Belge was the hottest region for agriculture, with minimum and maximum temps of 14.417°C and 42.087°C respectively, mean of 35.55°C.

Vegetation followed a similar pattern, with Kiremete having the lowest vegetation LSTs from 18.146°C to 38.305°C, averaging 26.15°C. Bega showed slightly warmer vegetation temperatures ranging from 18.51°C to 34.93°C, mean of 27.75°C. Belge was again the warmest landscape for vegetation, with extremes of 24.55°C and 39.81°C, averaging 32.01°C.

For bare land, Kiremete had the coolest temperature span from 22.76°C to 38.31°C, with a mean of 30.75°C. Bega exhibited a range of 22.34°C to 38.30°C, averaging 32.04°C. Belge saw the hottest bare land LSTs from 7.61°C to 40.58°C, with a mean of 35.32°C.

Built-up areas showed the greatest differences. Kiremete had the lowest built-up LSTs varying from 15.83°C to 38.05°C, averaging 29.14°C. Bega spanned 16.18°C to 38.80°C for built-up, mean of 28.30°C. Belge built-ups reached extremes of 6.004°C and 40.33°C, averaging 32.25°C.

In summary, 2010 LST analysis revealed Kiremete as generally the coolest landscape while Belge and Bega was typically the hottest across land cover types. However, some variability occurred between regions in maximum temperatures

4.10 Impact of land use land cover Change on land surface temperature in each season for 2022

Analysis of 2022 land surface temperatures (LSTs) by land cover type shows clear differences between Kiremete, Bega, and Belge. For agriculture, Kiremete had the coolest temps ranging from 18.85°C to 29.32°C, averaging 22.57°C. Bega exhibited moderately higher agriculture LSTs from 19.56°C to 34.5°C, mean of 29.98°C. Belge saw the hottest agriculture temperatures spanning 25.77°C to 43.09°C, averaging 37.80°C.

Vegetation followed a similar trend, with Kiremete having the lowest LSTs from 18.96°C to 28.98°C, mean of 22.64°C. Bega showed slightly warmer vegetation temps from 20.432°C to 33.92°C, averaging 26.89°C. Belge was again hottest for vegetation, ranging 24.74°C to 42.20°C, mean of 32.09°C.

For bare land, Kiremete had the coolest span from 20.49°C to 31.71°C, averaging 24.53°C. Bega exhibited a range of 23.003°C to 34.20°C, mean of 30.91°C. Belge saw the highest bare land LSTs from 27.51°C to 42.22°C, averaging 37.11°C.

Built-up areas followed a similar pattern. Kiremete had the lowest built-up LSTs from 18.64°C to 37.72°C, averaging 25.056°C. Bega spanned 18.26°C to 34.29°C, averaging 26.943°C. Belge built-ups reached 19.48°C to 42.56°C, mean of 33.73°C.

In summary, 2022 LST analysis showed Kiremete consistently exhibited the coolest temperatures while Belge and Bega were typically hottest across land cover types.

`

4.11 SUHII along gradient

4.11.1 SUHII along gradient for the year 1991 Kiremete Season

Examination of the 1991 land surface temperature (LST) statistics for Kiremete reveals Zone 0 has the highest mean zonal LST of 27.18°C. This aligns with Zone 0 having the greatest built-up area presence at 70.80%. The specific built-up LST in Zone 0 is 28.78°C. In contrast, Zone 49 has the lowest mean zonal LST of 20.57°C and contains no built-up area. Zone 49 is characterized by agricultural land cover with an LST of 20.84°C and vegetation with an LST of 20.77°C . Comparing Zone 0 and Zone 49 indicates increased built-up area presence corresponds to elevated zonal mean LST. This relationship is further evidenced in zones 1-5, categorized as urban areas.

The regression analysis for the 1991 Kiremete season indicates differing relationships between land cover percentages and mean land surface temperature (LST) across urban, rural, and other land cover categories.

Within urban areas (built-up >10%), increased built-up percentage correlated positively ($y = 0.0285x + 24.949$, $R^2 = 0.8555$) with mean LST, demonstrating the urban heat island effect where higher built-up area leads to increased surface temperatures.

However, in rural areas (built-up <10%) the positive relationship was much weaker ($y = 0.0739x + 24.498$, $R^2 = 0.0234$), indicating built-up area has less influence on LST in rural contexts during Kiremete.

For agricultural land, increased area correlated negatively ($y = -0.0295x + 27.104$, $R^2 = 0.2323$) with mean LST, likely due to the cooling effects of vegetation and irrigation associated with farmland.

Similarly, higher vegetation cover also correlated negatively ($y = -0.1133x + 26.232$, $R^2 = 0.3806$) with LST, as anticipated given the cooling effects of evapotranspiration.

Bare land also demonstrated a negative relationship ($y = -0.0942x + 26.471$, $R^2 = 0.2723$) with LST, which may indicate soil moisture is an important factor during Kiremete and bare ground retains more moisture than built-up areas

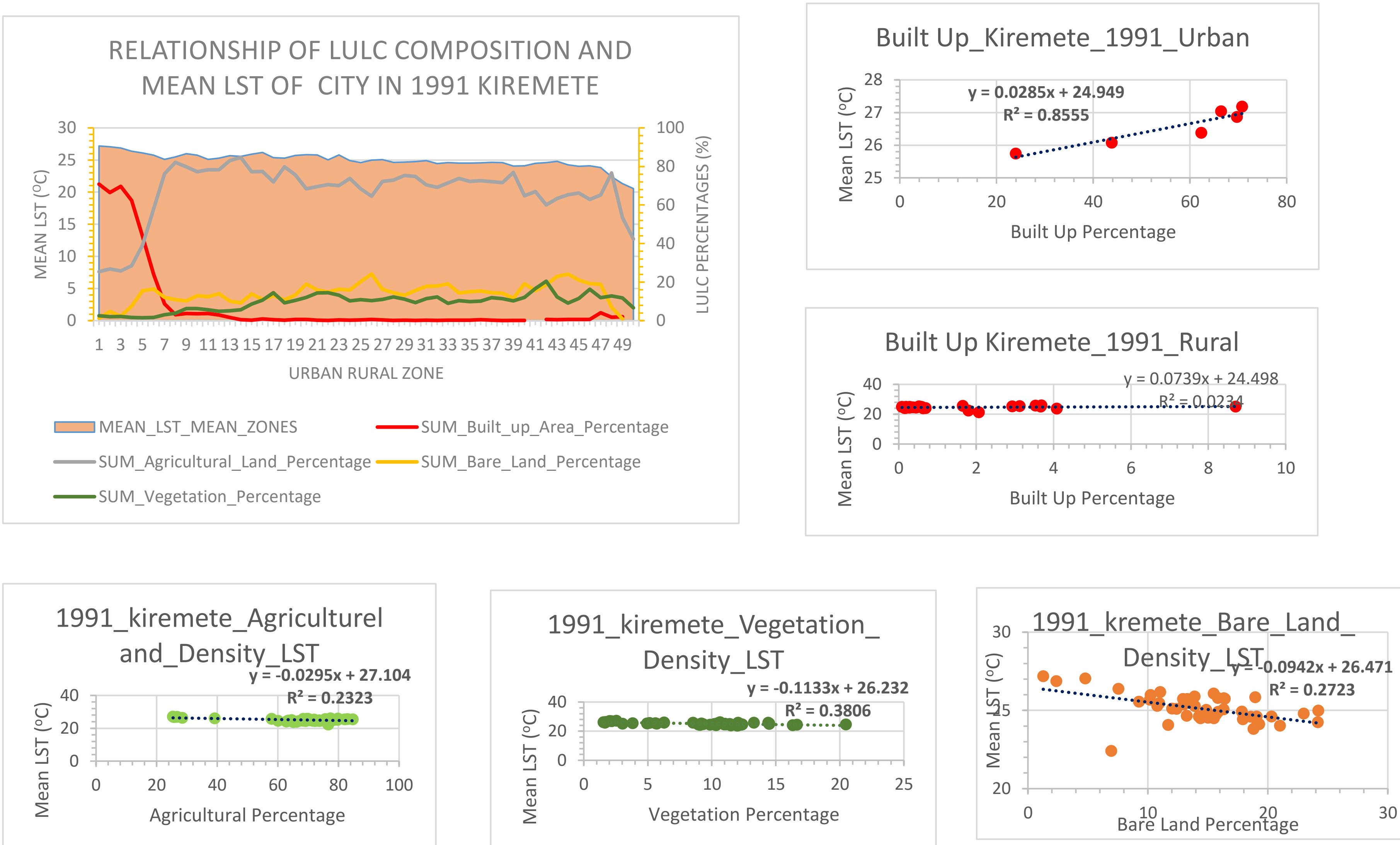

Figure 4.34 SUHII along Gradient 1991 Kiremete

`

4.11.2 SUHII along gradient for the year 2000 Kiremete Season

Analysis of the 2000 zonal statistics for Kiremete indicates Zone 1 exhibited the highest mean LST at 25.70°C, which corresponded with its high built-up percentage of 77.28%. Notably, the built-up class in Zone 1 also showed the maximum LST across zones at 27.17°C. In contrast, Zone 49 displayed the lowest mean zonal LST at 20.79°C and was dominated by vegetation cover at 34% with an LST of 20.81°C. Agricultural land in Zone 49 had an LST of 21.12°C. Comparing Zone 1 and Zone 49 reveals increased built-up presence is associated with elevated zonal mean LST. This trend was further evidenced in categorized urban Zones 0-7.

The regression analysis for the 2000 Kiremete season reveals some changes in the relationship between land cover types and mean land surface temperature (LST) compared to 1991.

Within urban regions (built-up >10%), built-up area continues to correlate positively ($y = 0.0301x + 22.639$, $R^2 = 0.7583$) with mean LST, further demonstrating the urban heat island effect in Adama.

However, in rural areas (built-up <10%), the relationship flipped to negatively correlate ($y = -0.1567x + 23.112$, $R^2 = 0.202$) with LST which may suggest the rural area had cooling effect on the LST

For agricultural land, the negative correlation ($y = -0.0192x + 24.487$, $R^2 = 0.2943$) with LST strengthened compared to 1991, underscoring the cooling impacts of farmland.

Vegetation cover also demonstrated increased negative correlation ($y = -0.0646x + 23.89$, $R^2 = 0.3145$) with LST compared to 1991, likely due to expansion of green spaces.

Bare land changed minimally ($y = -0.0466x + 23.81$, $R^2 = 0.2324$), retaining a negative relationship with LST pointing to the importance of soil moisture

`

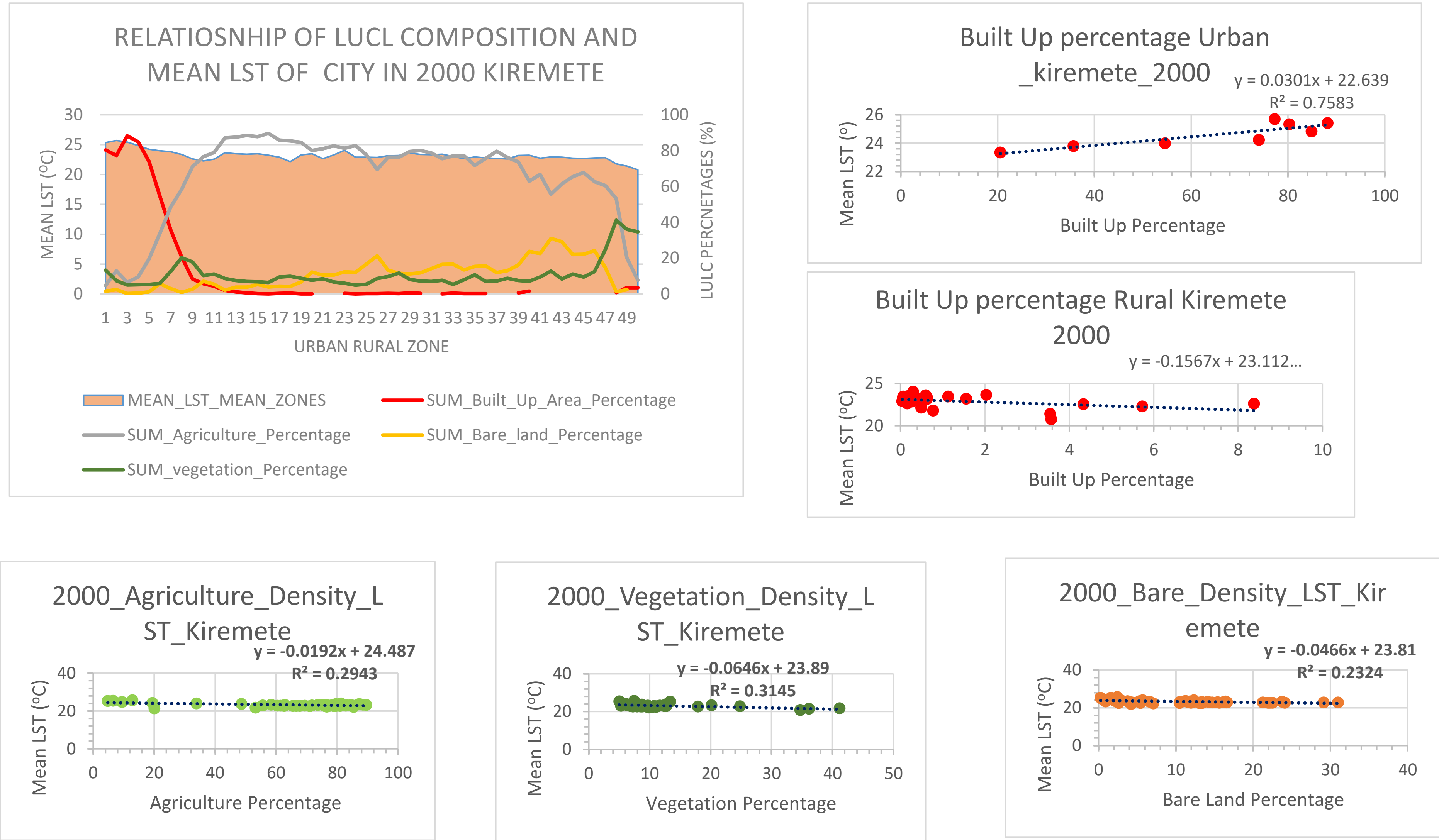

Figure 4.35 SUHII along Gradient 2000 Kiremete

`

4.11.3 SUHII along gradient for the year 2010 Kiremete Season

Examination of the 2010 Kiremete zonal data reveals Zone 15 had the highest mean LST at 30.00°C, characterized by a high agricultural land percentage of 83% with an LST of 27.65°C. Zone 1 ranked next highest in mean zonal LST at 29.77°C corresponding to its predominant built-up cover of 80.9% and associated high built-up LST of 30.82°C. Zone 2 followed with a mean LST of 29.75°C and 82.45% built-up presence exhibiting an LST of 30.51°C. In contrast, Zone 49 displayed the lowest mean zonal LST at 19.90°C with 31.12% vegetation cover and an LST of 19.90°C. Comparing Zone 15, Zone 1, and Zone 2 against Zone 49 indicates increased built-up area correlates with elevated zonal mean LSTs. This trend aligned with the urban heat island effect was further evidenced in categorized urban Zones 0-11.

The 2010 Kiremete season regression analysis shows urban built-up area continues to positively correlate ($y = 0.0343x + 26.39$, $R^2 = 0.6859$) with mean land surface temperature (LST), demonstrating intensification of the urban heat island effect over time in Adama.

In rural areas (built-up <10%), the relationship remains negative ($y = -0.149x + 27.404$, $R^2 = 0.0164$) but is weaker

For agriculture, the relationship flipped to positively correlate ($y = 0.0184x + 26.234$, $R^2 = 0.0543$) with LST, contrasting the negative correlations in 1991 and 2000. This may reflect changes in agricultural practices or reductions in soil moisture content.

However, vegetation cover continues to negatively relate ($y = -0.1558x + 29.015$, $R^2 = 0.5458$) to LST, and this relationship strengthened the most out of all land cover classes since 1991. This highlights the growing importance of urban greenery in mitigating the heat island effect.

Bare land retained a negative correlation ($y = -0.0925x + 28.557$, $R^2 = 0.1233$) with LST but weakened compared to 2000, further signaling diminishing moisture levels

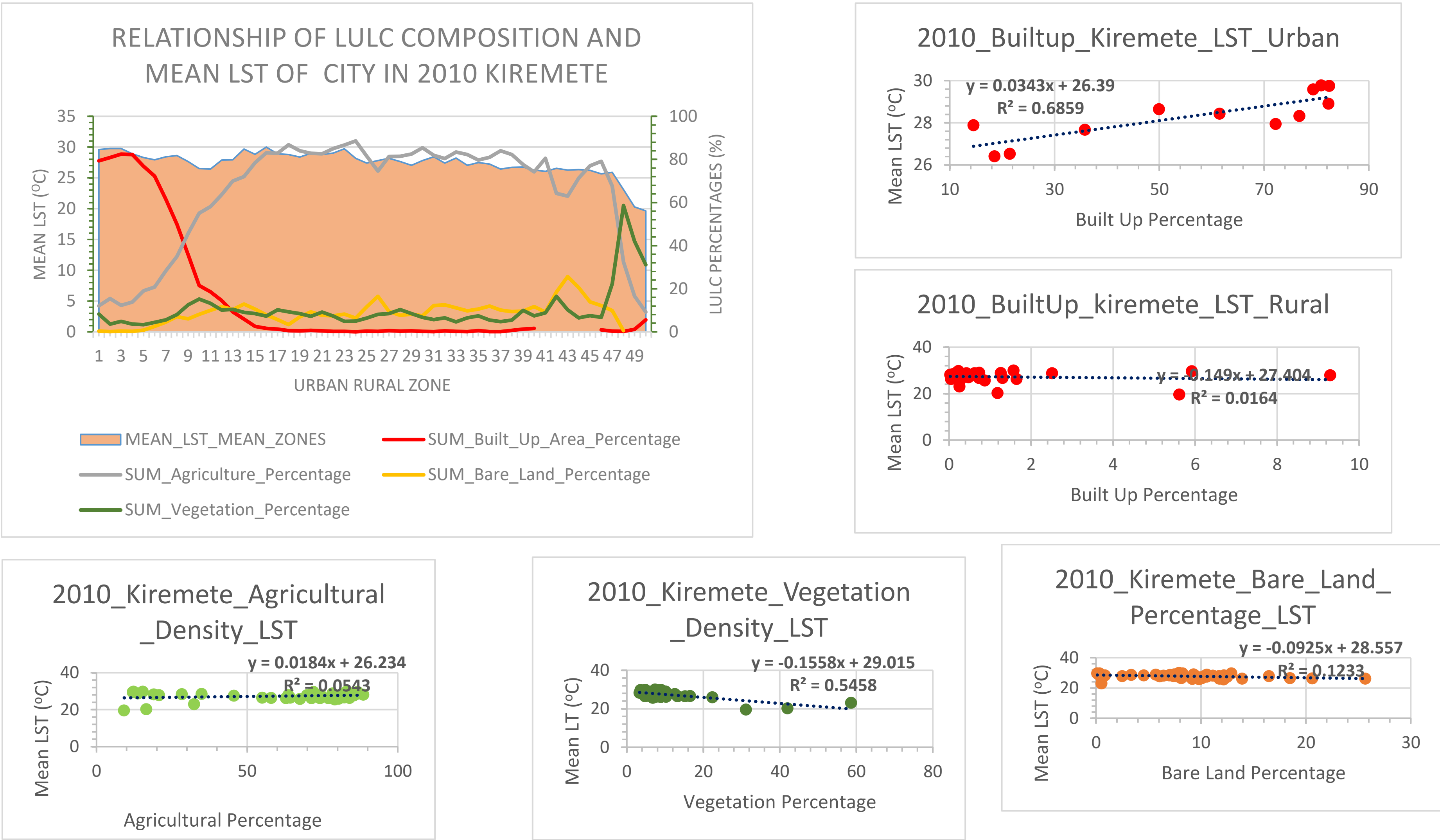

Figure 4.36 SUHII along Gradient 2010 Kiremete

`

4.11.4 SUHII along gradient for the year 2022 Kiremete Season

Examination of the 2022 Kiremete zonal data indicates Zone 2 exhibited the highest mean LST at 27.30°C, aligning with its predominant built-up percentage of 94.51% which also showed a peak LST of 28.18°C .In contrast, Zone 48 displayed the lowest mean zonal LST at 20.72°C characterized by 34.02% vegetation cover with an associated LST of 21.39°C. Comparing Zone 2 and Zone 48 reveals increased built-up presence correlates with elevated zonal mean LSTs. Additionally, Zones 0-18 were categorized as urban areas.

The 2022 Kiremete season regression analysis demonstrates continued strengthening of the positive relationship ($y = 0.0439x + 21.81$, $R^2 = 0.8036$) between urban built-up (>10%) and mean land surface temperature (LST). This reflects intensification of the urban heat island effect in Adama over the study period.

In rural areas (built-up <10%), the negative correlation ($y = -0.0485x + 23.224$, $R^2 = 0.0641$) with LST persists but is a very weak correlation.

For agriculture, the negative relationship ($y = -0.0212x + 24.635$, $R^2 = 0.2437$) with LST strengthens compared to 2010 but remains weaker than early years, potentially indicating agricultural land use changes.

Vegetation cover retains the strongest negative correlation ($y = -0.0777x + 24.73$, $R^2 = 0.3491$) with LST out of all land classes, highlighting the increasing importance of vegetation in mitigating urban heat.

Bare land also shows strengthened negative correlation ($y = -0.0995x + 24.649$, $R^2 = 0.2676$) compared to 2010, suggesting moisture levels may be rebounding.

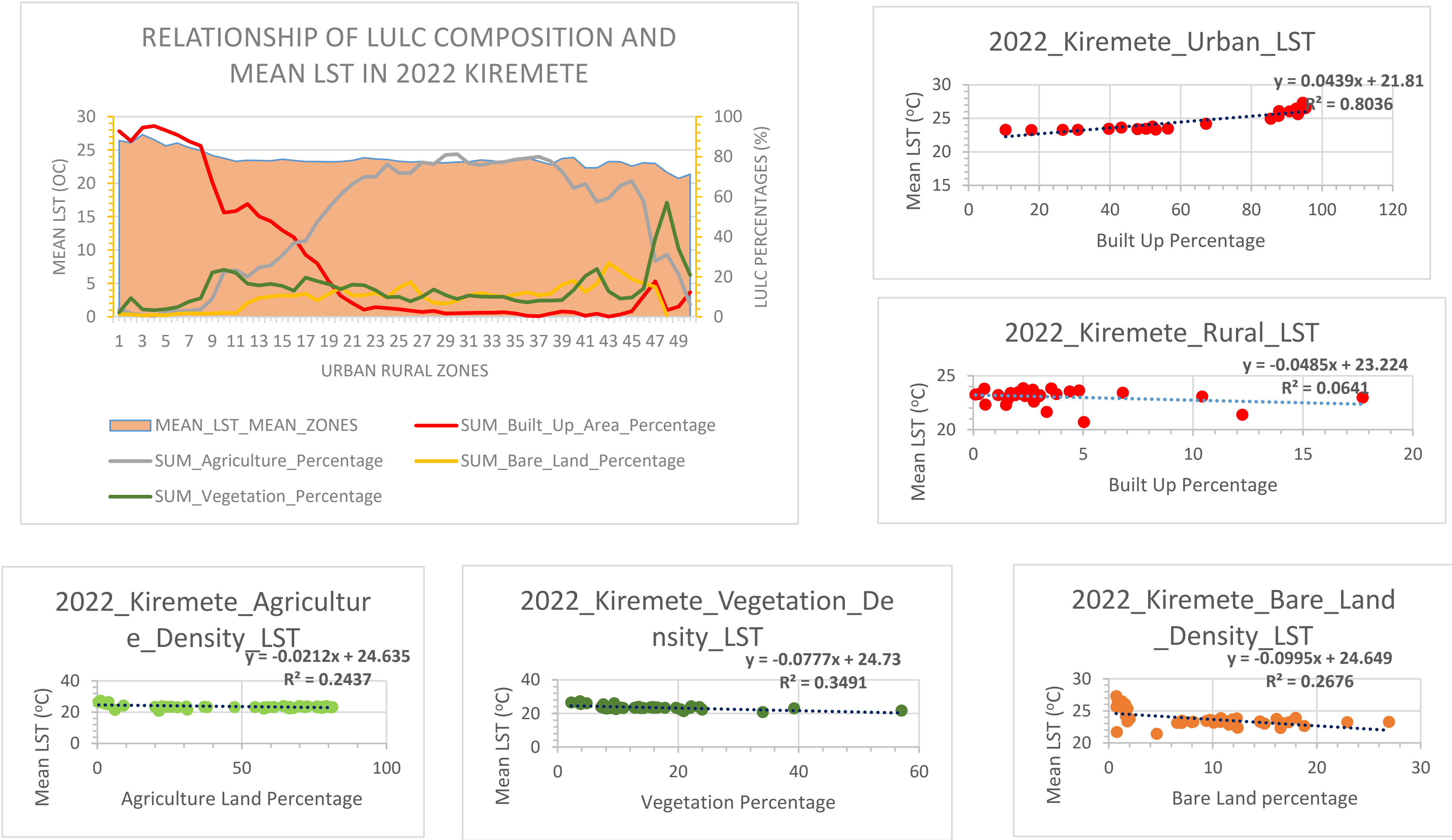

Figure 4.37 SUHII along Gradient 2022 Kiremete

`

4.11.5 SUHII along gradient for the year 1991 Belge Season

Examination of the 1991 Belge zonal data indicates Zone 13 exhibited the highest mean LST at 35.34°C. Zone 13 contained 83.9% agriculture cover with an associated LST of 35.51°C, along with 9.6% bare land and 5.84% vegetation exhibiting LSTs of 35.55°C and 32.00°C respectively. In contrast, Zone 49 displayed the lowest mean zonal LST at 23.86°C and was characterized by lower agricultural and vegetation percentages of 21.4% and 20% with corresponding LSTs of 24.56°C and 23.70°C.

Compared to Kiremete in 1991, increased built-up presence correlated with higher zonal LSTs rather than agriculture. Kiremete's most built-up Zone 0 had the peak LST, while rural Zone 49 with no built-up showed the minimum. However, both sites exhibited connections between specific land covers and zonal LST distributions.

In summary, the 1991 zonal statistics reveal relationships between land cover type and LSTs in Belge and Kiremete. Similar to the kiremete Season Zone 0 – 5 are urban areas while the rest are Rural Areas.

The 1991 Belge season regression analysis reveals some notable differences compared to the 1991 Kiremete season.

Within urban areas (built-up >10%), increased built-up was negatively correlated ($y = -0.0297x + 34.526$, $R^2 = 0.8023$) with mean land surface temperature (LST), contrasting the positive urban heat island effect seen in Kiremete. This may result from higher moisture levels during Belge.

In rural areas (built-up <10%), built-up change did not demonstrate any significant relationship ($y = 0.0339x + 32.584$, $R^2 = 0.0007$) with LST, similar to Kiremete.

For agriculture, increased area was positively correlated ($y = 0.075x + 27.666$, $R^2 = 0.297$) with LST, again contrasting the negative Kiremete relationship. Higher evapotranspiration may drive this difference during Belge.

However, like Kiremete, vegetation cover was strongly negatively correlated ($y = -0.3697x + 35.27$, $R^2 = 0.5216$) with LST, affirming the cooling effects of greenery during both seasons. Bare land also showed a negative correlation ($y = -0.0741x + 34.252$, $R^2 = 0.2077$) with LST, pointing to the sustained role of soil moisture.

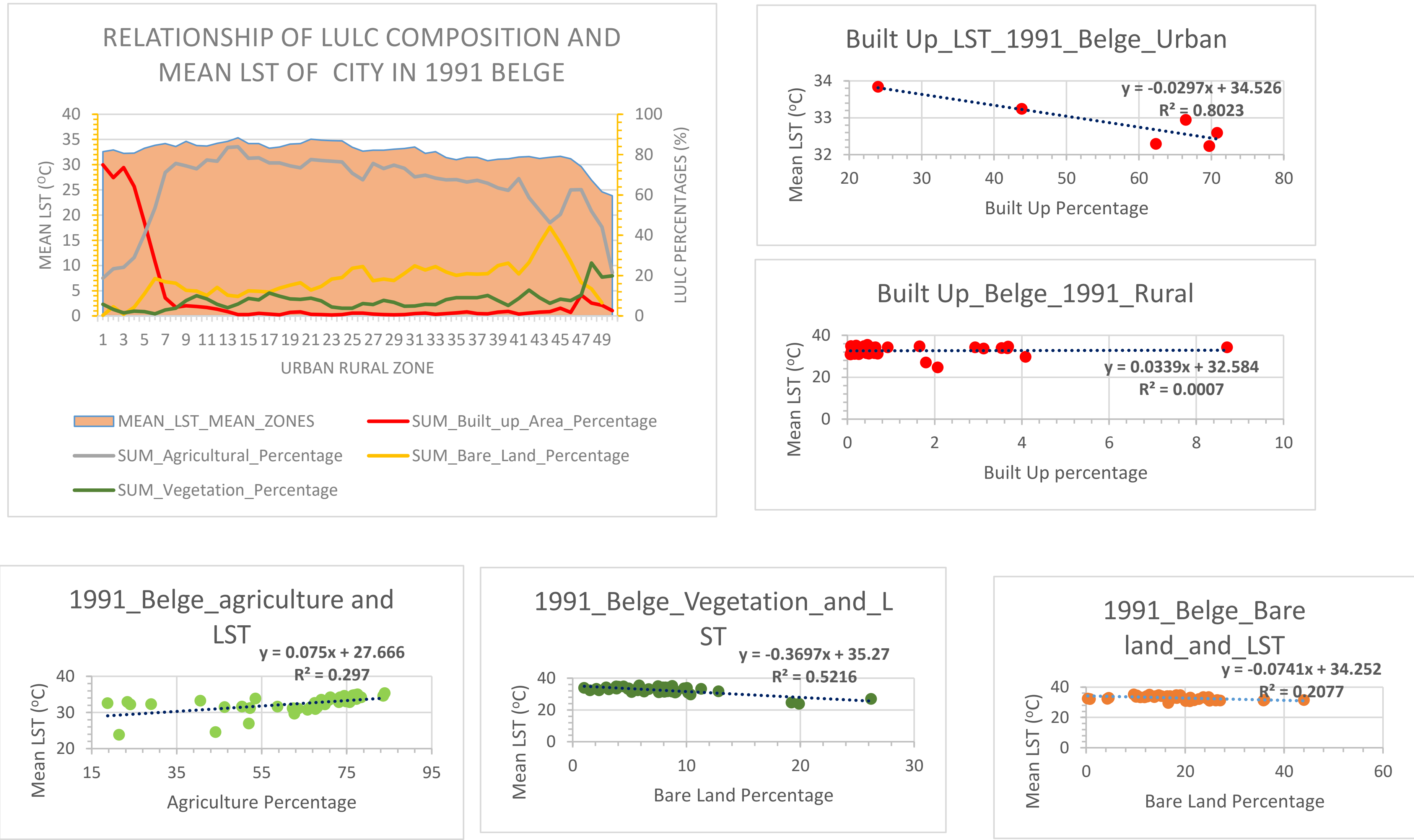

Figure 4.38 SUHII along Gradient 1991 Belge

`

4.11.6 SUHII along gradient for the year 2000 Belge Season

Examination of Belge's 2000 zonal data indicates Zone 17 exhibited the highest mean LST at 34.00°C. Zone 17 contained predominantly agricultural land cover at 78.84% with a corresponding LST of 34.74°C. The zone also had lower percentages of bare land and vegetation at 13.23% and 13% with respective LSTs of 33.68°C and 33.02°C. In contrast, rural Zone 49 displayed the lowest mean zonal LST at 26.05°C and had lower agricultural and vegetation percentages of 26% and 21%.

Unlike Belge, Kiremete's 2000 zonal statistics revealed built-up presence linked increased LSTs. Kiremete's most built-up Zone 1 showed the maximum LST, while rural Zone 49 with predominant vegetation exhibited the minimum. However, both sites demonstrated connections between specific land classes and zonal LST distributions.

In summary, the 2000 zonal data exhibits definitive relationships between land cover and LSTs in Belge and Kiremete's landscapesThis trend was further evidenced in categorized urban Zones 0-7.

Within urban areas (built-up >10%), increased built-up continued to negatively correlate (y = -0.0227x + 34.136, R2 = 0.8801) with mean LST. This further indicates an urban cool island effect during Belge seasons, contrasting Kiremete.

In rural areas (built-up <10%), built-up change became negatively correlated (y = -0.1715x + 32.416, R^2 = 0.0355) with LST, but still it was weak.

For agriculture, the relationship flipped to positively correlate (y = 0.0362x + 29.832, R^2 = 0.2321) with LST, aligning with the 1991 Kiremete season and contrasting the 1991 Belge outcomes.

However, vegetation cover retained a strong negative correlation (y = -0.0629x + 32.927, R^2 = 0.1937) with LST, though slightly weaker than 1991 Belge. This highlights the sustained cooling effects of greenery.

Bare land also continued to negatively relate (y = -0.0586x + 33.194, R^2 = 0.172) to LST, further demonstrating the key role of moisture availability in modulating surface heat across seasons.

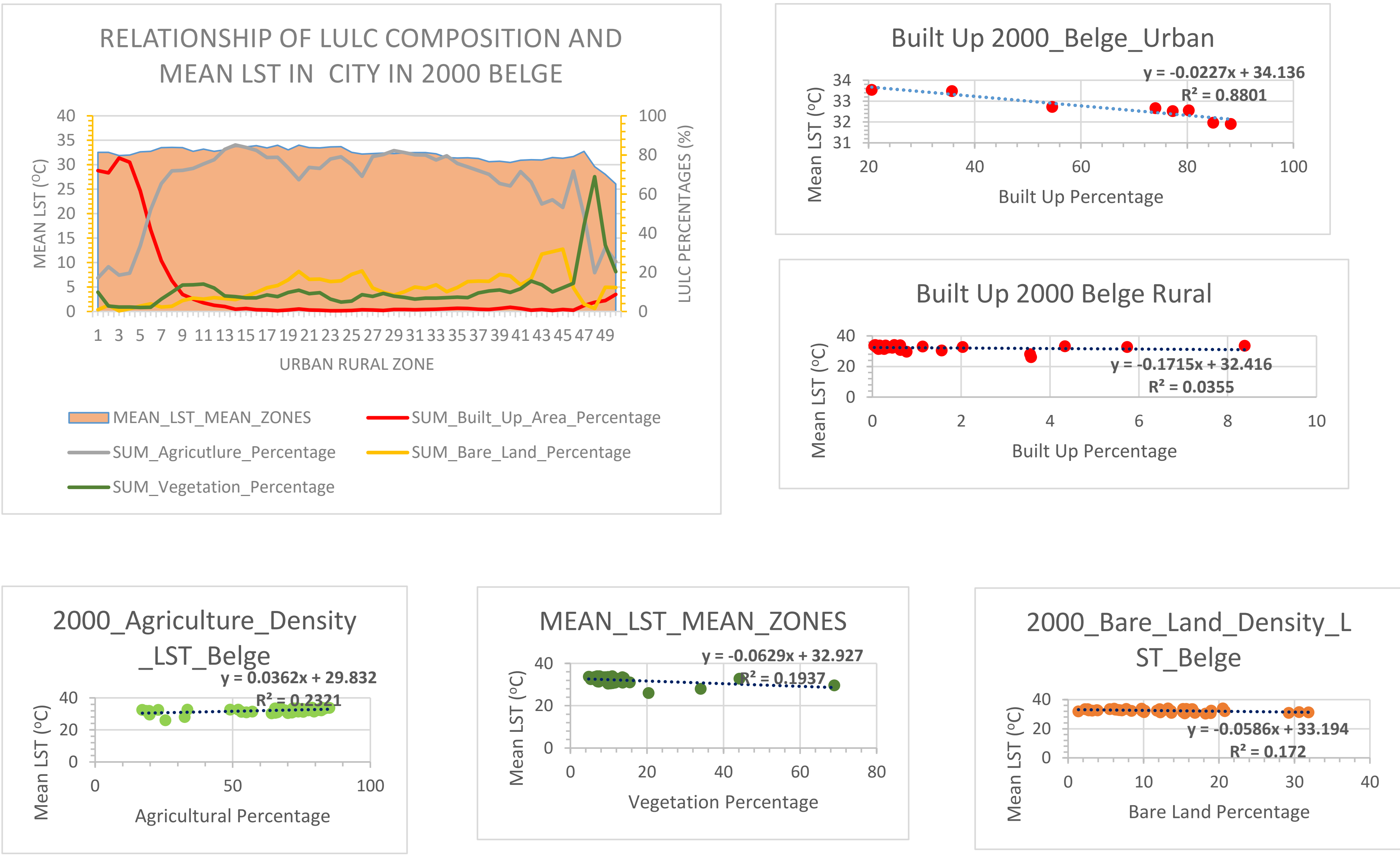

Figure 4.39 SUHII along Gradient 2000 Belge

`

4.11.7 SUHII along gradient for the year 2010 Belge Season

Analysis of the 2010 Belge data reveals Zone 23 exhibited the highest mean zonal LST at 35.28°C, corresponding to its agricultural dominance of 83% with a peak LST of 36.00°C. In contrast, Zone 49 showed the lowest mean LST at 25.74°C with 32.65% vegetation cover. As with previous years, increased agriculture presence in Belge correlated with higher zonal LSTs.

Conversely in Kiremete, built-up zones displayed elevated LSTs, with agricultural Zone 15 having the maximum zonal LST despite its lower built-up percentage. However, urban Zones 1 and 2 ranked next highest in LST, aligning with over 80% built-up cover. Both sites revealed connections between specific land classes and zonal LST distributions.

In summary, the 2010 zonal statistics continue to exhibit land cover's relationship with LSTs for Belge and Kiremete. Agriculture presence linked highest temperatures in Belge, while built-up presence associated with peak LSTs in Kiremete's landscape.

Within urban areas (built-up >10%), the negative correlation ($y = -0.0112x + 33.181$, $R^2 = 0.4252$) persists but is considerably weaker than 2000, potentially signaling attenuation of the urban cool island effect during Belge seasons.

In rural areas (built-up <10%), the negative relationship ($y = -0.1871x + 33.611$, $R^2 = 0.0485$) with LST even though it is weak.

For agriculture, positive correlation ($y = 0.0377x + 30.732$, $R^2 = 0.4348$) with LST continues to strengthen over time, aligning with Kiremete season patterns and contrasting earlier Belge years.

Vegetation cover retains a negative correlation ($y = -0.0616x + 34.28$, $R^2 = 0.2725$) with LST, though dampened compared to 2000, highlighting its sustained cooling utility despite potential moisture declines.

Bare land similarly persists with a negative LST relationship ($y = -0.0526x + 34.12$, $R^2 = 0.151$), though also dampened, reflecting complex moisture and temperature dynamics.

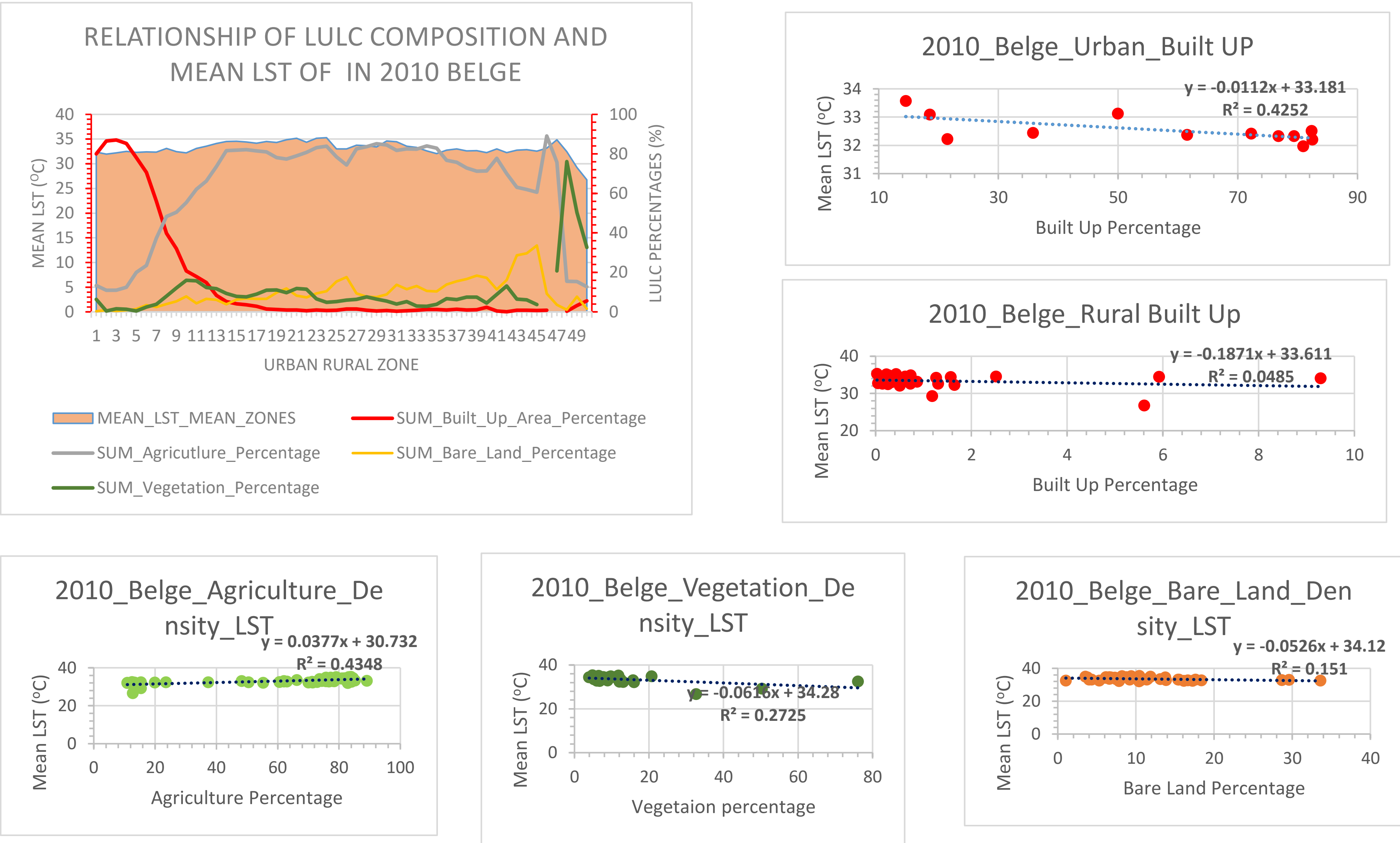

Figure 4.40 SUHII along Gradient 2010 Belge

`

4.11.8 SUHII along gradient for the year 2022 Belge Season

Examination of Belge's 2022 zonal statistics indicates Zone 21 exhibited the highest mean zonal LST at 36.86°C. Zone 21 contained 72.37% agriculture cover with associated LST of 38.20°C, 8.36% bare land cover at LST of 37.91°C , and 14.59% vegetation cover with LST of 35.33°C. In contrast, rural Belge Zone 49 displayed the lowest mean zonal LST at 28.10°C with 28.57% vegetation cover exhibiting LST of 29.77°C. For Kiremete, the most built-up Zone 2 showed the maximum zonal LST of 27.30°C with 94.51% built-up presence, while rural Zone 48 had the minimum zonal LST of 293.86°C (20.72°C adjusted) with 34.02% vegetation. In summary, the detailed 2022 zonal statistics continue to exhibit clear relationships between specific land cover percentages and associated LST values within zones for both Belge and Kiremete. Tracking these localized zonal LST-land cover correlations provides insights into the urban heat island effect's spatial dynamics.

The 2022 Belge season regression analysis shows the negative correlation between urban built-up and mean land surface temperature has strengthened again compared to 2010.

Within urban areas (built-up >10%), increased built-up relates negatively ($y = -0.0409x + 36.66$, $R^2 = 0.8648$) with LST, indicating potential resurgence of an urban cool island effect during Belge seasons.

In rural areas (built-up <10%), the negative correlation ($y = -0.2245x + 35.934$, $R^2 = 0.0494$) with LST is weak even though it is negatively correlated.

For agriculture, positive correlation ($y = 0.0517x + 32.337$, $R^2 = 0.6272$) with LST reaches the highest level seen, aligning with Kiremete seasons and contrasting earlier Belge years. This merits further investigation.

Vegetation cover retains a negative LST relationship ($y = -0.0835x + 36.453$, $R^2 = 0.3719$), though weakened compared to 2010, highlighting moisture availability may be declining.

However, bare land flips to positively correlate ($y = 0.0983x + 33.743$, $R^2 = 0.2204$) with LST for the first time, providing further evidence of potential moisture reductions.

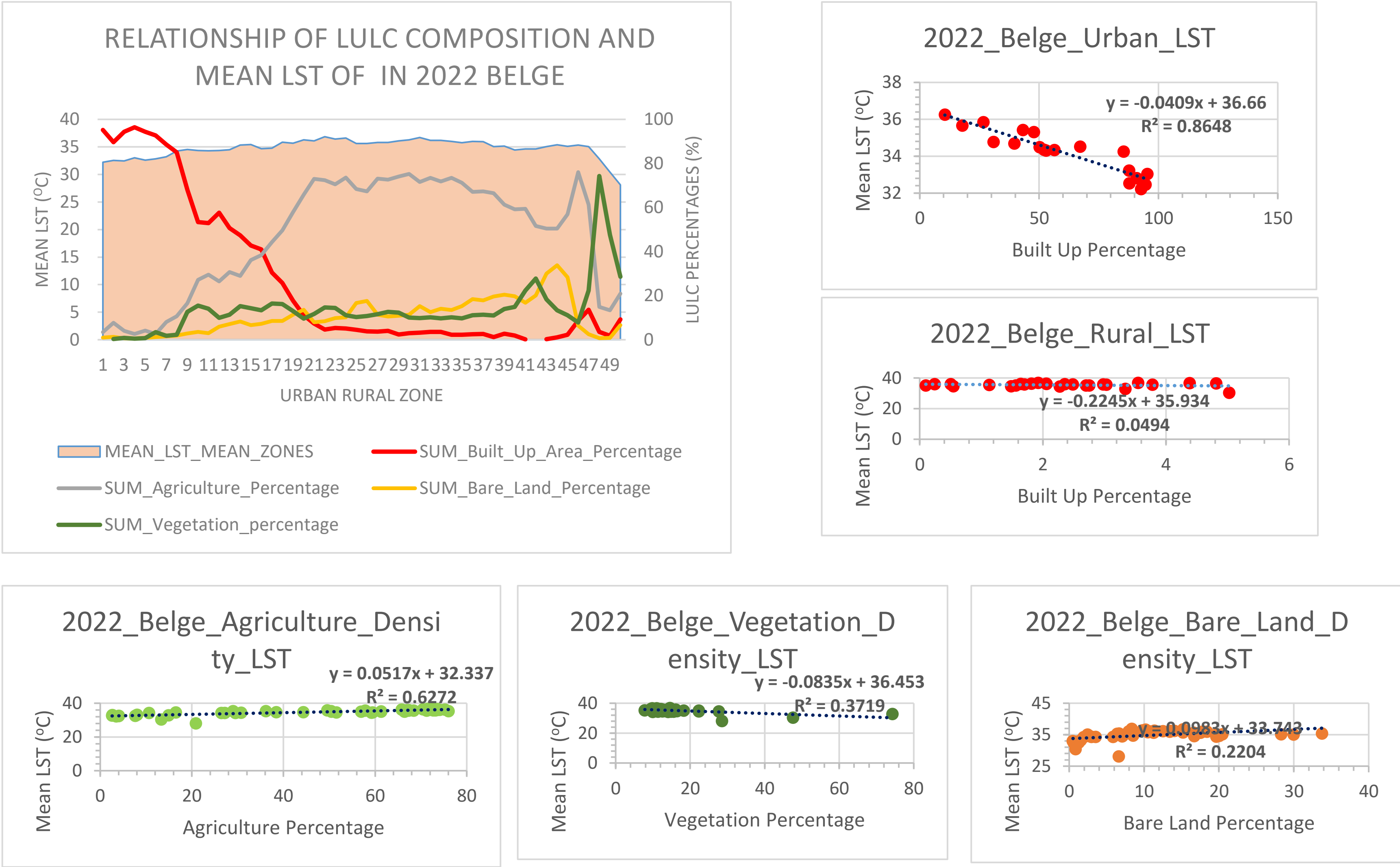

Figure 4.41 SUHII along Gradient 2022 Belge

4.11.9 SUHII along gradient for the year 1991 Bega Season

Examination of Bega's 1991 zonal data indicates Zone 45 exhibited the highest mean LST at 30.39°C with lower built-up cover (<1%) but higher agricultural and bare land percentages of 45.66% and 46.2% respectively. In contrast, rural Zone 49 displayed the lowest mean zonal LST at 22.72°C with increased vegetation presence (30.1%) and lower agriculture (13%).

Unlike Bega, Belge's 1991 peak zonal LST occurred in agricultural Zone 13 rather than bare land Zone 45. However, both zones had reduced built-up and vegetation. Kiremete differed with built-up Zone 0 having the maximum LST, contrasting vegetation-dominated Zone 49's minimum.

Despite different land covers linked to peak LSTs, all 3 sites demonstrated connections between specific classes and zonal LST distributions. Bega and Belge both exhibited higher LSTs correlated with increased agriculture and bare land fractions. Kiremete revealed increased built-up presence associated with higher zonal LSTs.

Within urban areas (built-up >10%), increased built-up correlated negatively (y = -0.0322x + 30.178, R^2 = 0.8516) with LST. This indicates an urban cool island effect specific to the Bega season, contrasting the other seasons.

In rural areas (built-up <10%), built-up change showed little relationship (y = 0.0391x + 28.93, R^2 = 0.0044) with LST, similar to other seasons.

For agriculture, increased area positively correlated (y = 0.0435x + 26.099, R^2 = 0.3492) with LST. The reasons for this differing seasonal response merits exploration.

As expected, vegetation cover correlated negatively (y = -0.0998x + 29.644, R^2 = 0.351) with LST, aligning with other seasons and pointing to consistent cooling effects.

However, bare land positively correlated (y = 0.0397x + 28.099, R^2 = 0.1926) with LST, contrasting other seasons where negative relationships prevailed.

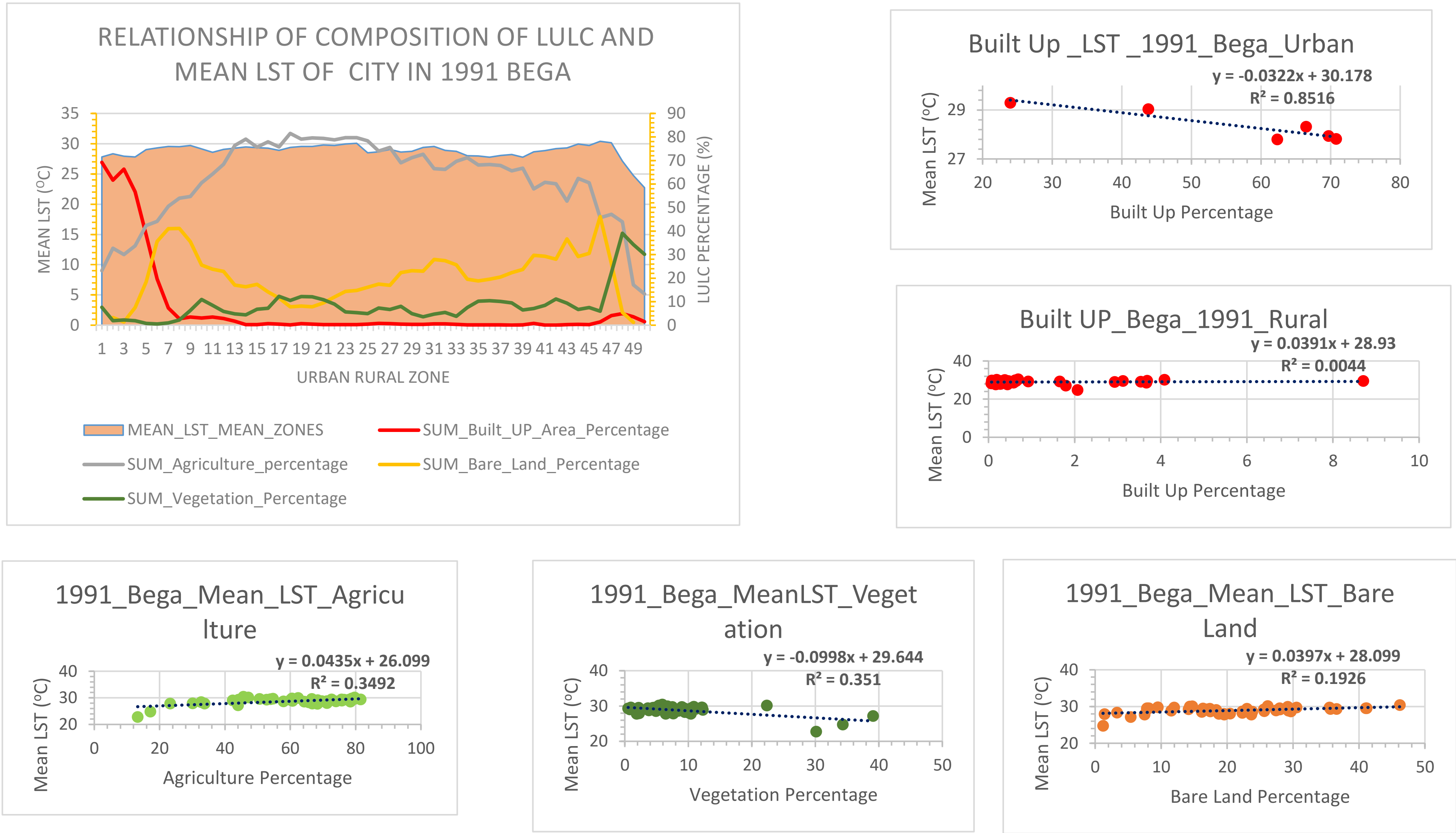

Figure 4.42 SUHII along Gradient 1991 Bega

`

4.11.10 SUHII along gradient for the year 2000 Bega Season

Examination of Bega's 2000 zonal data indicates Zone 45 exhibited the highest mean LST at 30.39°C with lower built-up cover (<1%) but higher agricultural and bare land percentages of 45.66% and 46.2% respectively. In contrast, rural Zone 49 displayed the lowest mean zonal LST at 22.72°C with increased vegetation presence (30.1%) and lower agriculture (13%).

Unlike Bega, Belge's 1991 peak zonal LST occurred in agricultural Zone 13 rather than bare land Zone 45. However, both zones had reduced built-up and vegetation. Kiremete differed with built-up Zone 0 having the maximum LST, contrasting vegetation-dominated Zone 49's minimum.

Despite different land covers linked to peak LSTs, all 3 sites demonstrated connections between specific classes and zonal LST distributions. Bega and Belge both exhibited higher LSTs correlated with increased agriculture and bare land fractions. Kiremete revealed increased built-up presence associated with higher zonal LSTs.

Within urban areas (built-up >10%), the negative correlation with LST (y = -0.0029x + 30.788, R^2 = 0.1531) weakens considerably compared to 1991. This indicates attenuation of the distinct urban cool island effect seen in 1991 Bega seasons.

However, in rural areas (built-up <10%), the relationship flipped to strongly negatively correlate (y = -0.4024x + 31.507, R^2 = 0.2082) with LST.

For agriculture, the positive LST relationship (y = 0.0367x + 28.725, R^2 = 0.4163) persisted and aligned with other seasons. The reasons for this seasonal difference from Kiremete and Belge warrant further exploration.

As expected, vegetation cover demonstrated increased negative correlation (y = -0.1262x + 32.139, R^2 = 0.5231) with LST, pointing to its consistent cooling utility.

Bare land changed minimally (y = 0.0317x + 30.656, R^2 = 0.1685), retaining a positive relationship with LST that differentiates Bega from other seasons.

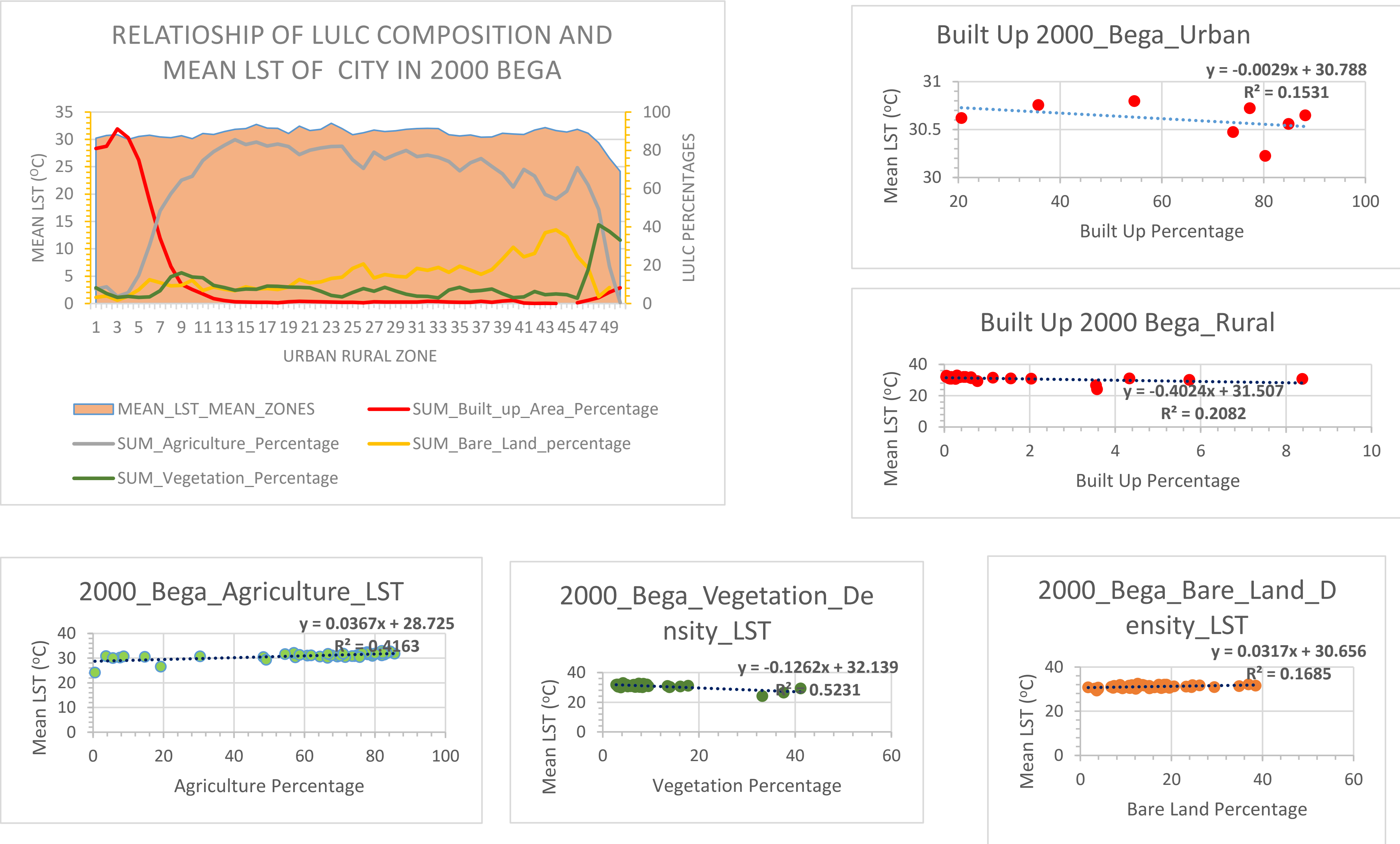

Figure 4.43 SUHII along Gradient 2000 Bega

4.11.11 SUHII along gradient for the year 2010 Bega Season

Examination of Bega's 2010 zonal data indicates Zone 22 exhibited the highest mean LST at 31.68°C. It contained 84.08% agriculture with an LST of 32.77°C , 11% bare land at 32.46°C, and 4.80% vegetation at 28.45°C . In contrast, rural Zone 49 displayed the lowest mean zonal LST at 20.32°C with increased vegetation presence (36.73%) at an LST of 21.29°C.

For Belge in 2010, agricultural Zone 23 similarly showed the peak zonal LST over bare Zone 22. However, Kiremete differed with agricultural Zone 15 having the maximum LST despite lower built-up percentage than urban Zones 1 and 2. Nonetheless, all sites revealed connections between specific land classes and zonal LSTs.

The 2010 Bega season regression analysis shows the distinct urban cool island effect has strengthened again compared to 2000, while other relationships remain relatively consistent.

Within urban areas (built-up >10%), increased built-up negatively correlated ($y = -0.021x + 29.893$, $R^2 = 0.7039$) with mean land surface temperature (LST). This relationship strengthened the most over time, highlighting the unique Bega urban cooling effect.

In rural areas (built-up <10%), built-up change continued to negatively relate ($y = -0.2486x + 29.183$, $R^2 = 0.0413$) to LST, though the correlation weakened slightly from 2000.

For agriculture, increased agricultural land kept a positive LST correlation ($y = 0.0472x + 25.829$, $R^2 = 0.3764$) on par with 2000. The reasons for this sustained seasonal difference from other seasons requires further investigation.

As seen over time, vegetation cover showed a negative relationship ($y = -0.1072x + 29.792$, $R^2 = 0.4197$) with LST, reflecting its consistent cooling effects.

Bare land demonstrated negligible correlation ($y = 0.0117x + 28.811$, $R^2 = 0.0025$) with LST, with the relationship continuing to contrast other seasons.

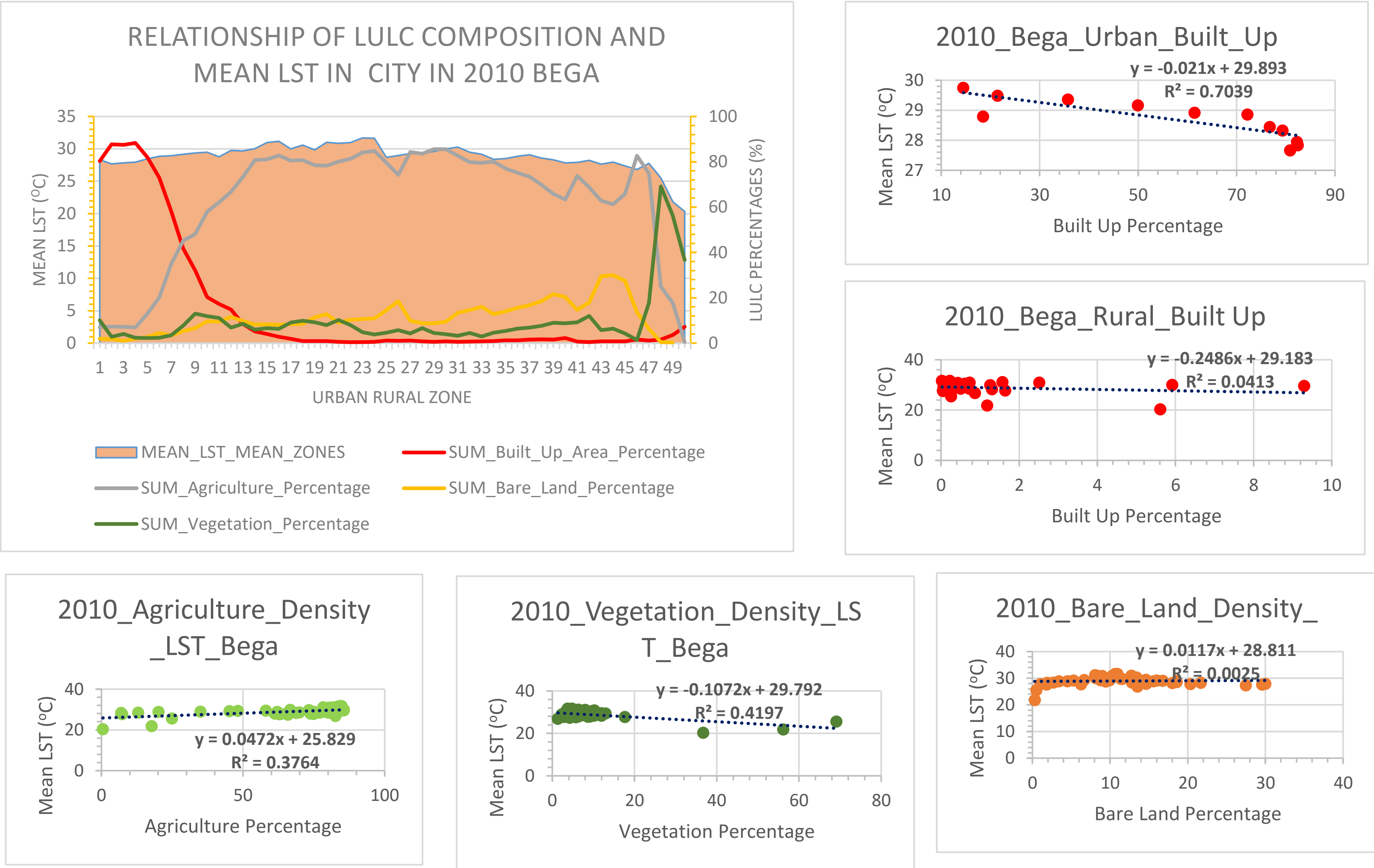

Figure 4.44 SUHII along Gradient 2010 Bega

`

4.11.12 SUHII along gradient for the year 2022 Bega Season

Examination of Bega's 2022 zonal data indicates Zone 42 exhibited the highest mean LST at 29.59°C. It contained 50% agriculture with LST of 30.58°C, 36% bare land at 32.32°C, and 12% vegetation at 28.07°C. In contrast, rural Zone 49 displayed the lowest mean zonal LST at 22.28°C with increased vegetation presence (27.04%) at an LST of 23.34°C.

For Belge in 2022, agricultural Zone 21 similarly showed the peak zonal LST over bare Zone 42. However, built-up Zone 2 had Kiremete's maximum zonal LST, differing from vegetation-dominated Zone 48's minimum. Still, all sites revealed localized LST-land cover relationships.

The relationship between land surface temperature (LST) and land cover was analyzed for the Bega region. In urban areas with over 10% built up land cover, there was a significant negative correlation between built up percentage and mean LST of zones ($y = -0.0222x + 28.765$, $R^2 = 0.6721$). This indicates that increased urbanization is associated with decreased LST in highly built up areas. In rural regions with under 10% built up land, the correlation was also negative but weaker ($y = -0.4185x + 29.322$, $R^2 = 0.1728$). For agricultural land, there was a positive correlation between mean LST and agricultural percentage ($y = 0.0396x + 26.115$, R2 = 0.529). Increases in agriculture were associated with higher LST. Vegetation cover exhibited a negative correlation with LST ($y = -0.0875x + 29.315$, $R^2 = 0.4094$), suggesting vegetation lowers surface temperature. Bare land percentage had a positive relationship with LST ($y = 0.0797x + 26.967$, $R^2 = 0.547$), indicating bare ground is linked to warmer temperatures. In summary, built up and vegetated areas in Bega showed an inverse relationship with LST, while agriculture and bare land demonstrated a direct positive association with temperature.

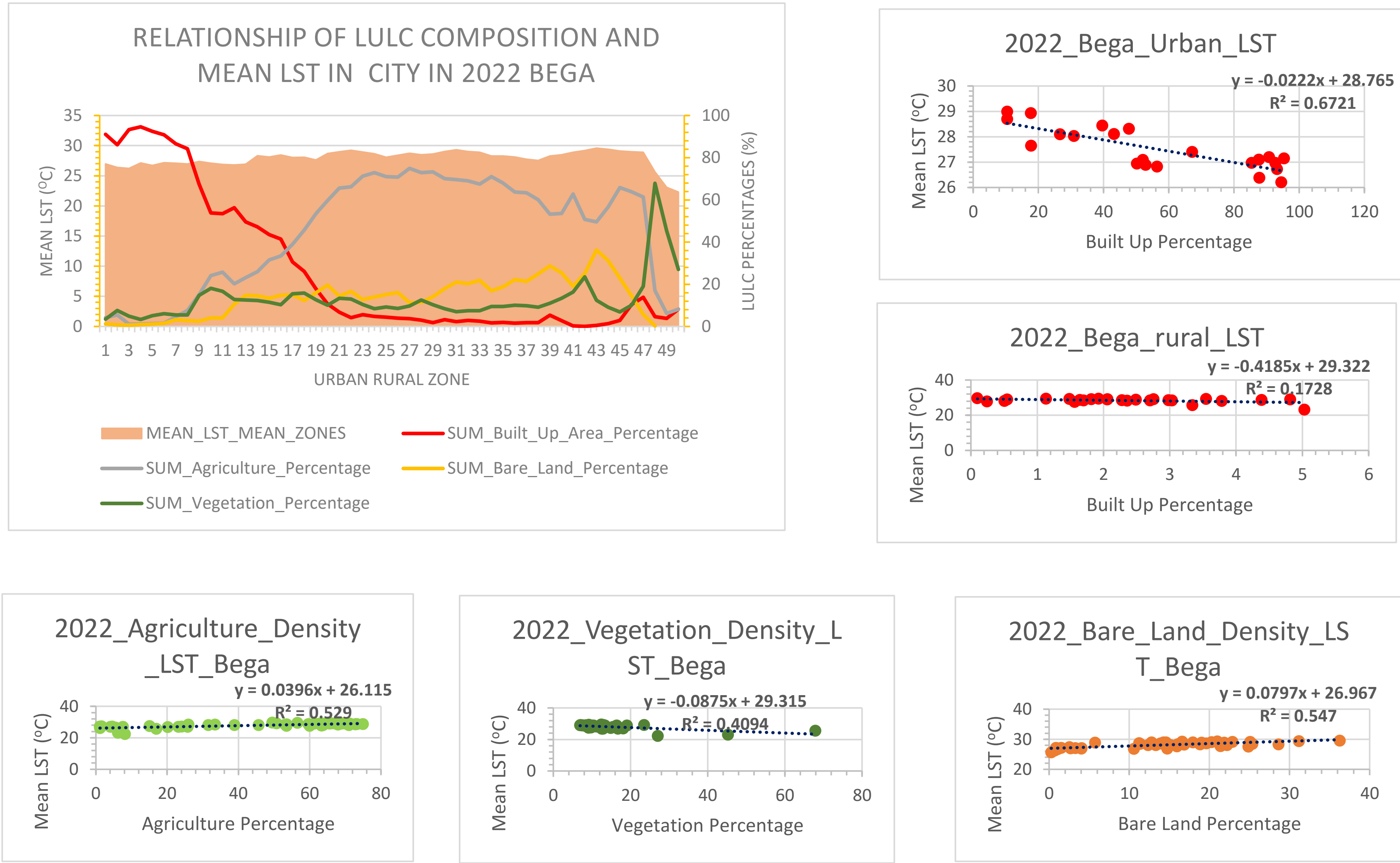

Figure 4.45 SUHII along Gradient 2022 Bega

4.12 Relation between Spectral Indices and LST Seasonally

4.12.1 Relation between NDVI and LST Kiremete Season

Analysis of the correlation equations for Kiremete in 1991, 2000, 2010, and 2022 reveals a consistent moderately strong negative relationship between the x and y variables. In 1991, the equation y = -14.081x + 29.747 with an R_2 value of 0.4129 indicates a negative correlation where y decreases as x increases. The R^2 of 0.4129 signifies a reasonably strong relationship between the variables for that year. Similarly, the 2000 equation shows a negative correlation with a slightly higher R^2 of 0.4307. The relationship peaks in strength in 2010 with an R2 of 0.465 based on the equation y = -14.301x + 31.733. However, by 2022 the strength declines somewhat to an R^2 of 0.3808 per the equation y = -11.43x + 27.328, though still demonstrating a moderately high negative correlation. Overall, examination of the R^2 values reveals the connection between the variables was strongest in 2010 and weakest in 2022, while remaining a reasonably strong negative correlation across all years for Kiremete.

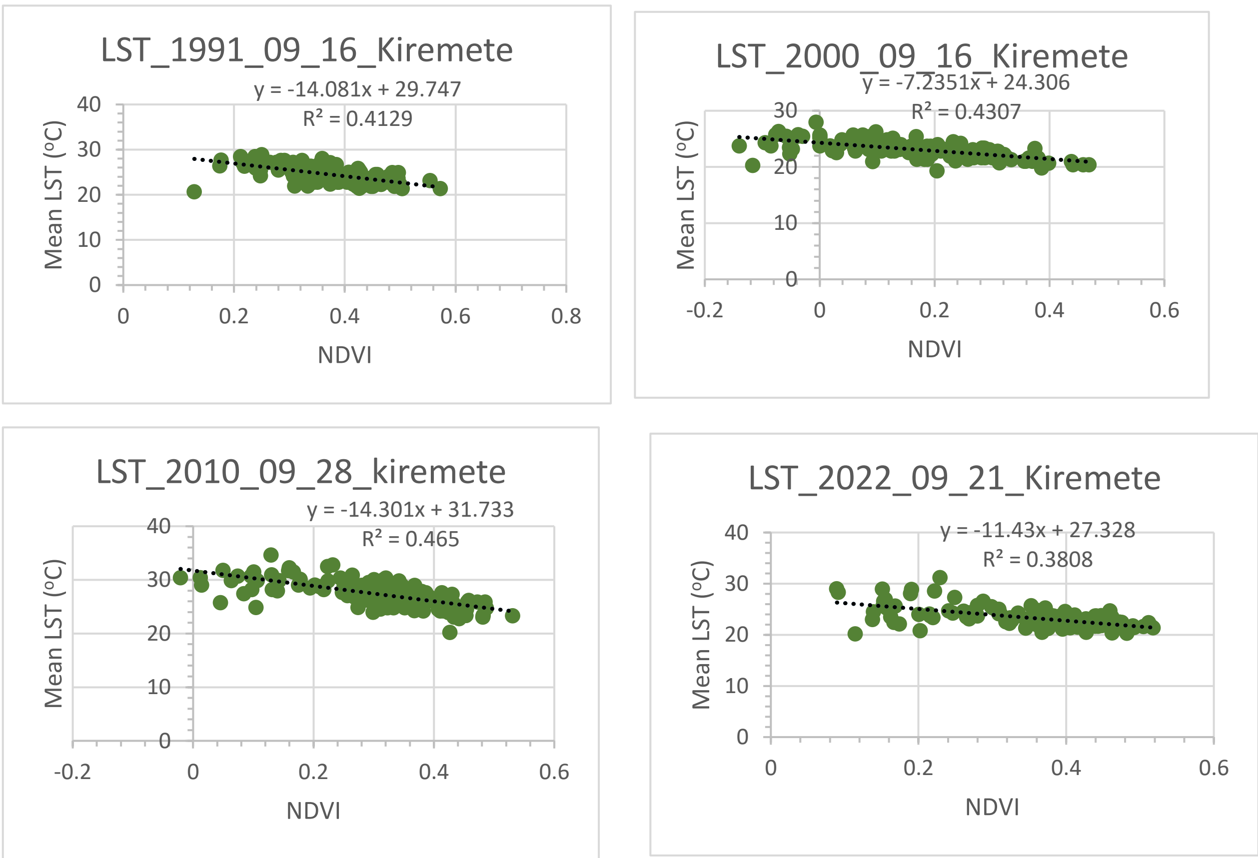

Figure 4.46 NDVI and LST relation for Kiremete Season

4.12.2 Relation between NDVI and LST Belge Season

Analysis of the correlation equations for Belge in 1991, 2000, 2010, and 2022 reveals a moderately strong negative relationship between the x and y variables across time. In 1991, the equation y = -19.948x + 37.948 with an R^2 of 0.426 indicates a negative correlation where y decreases as x increases. The R^2 value signifies a reasonably high correlation strength for 1991. The relationship remains negative per the 2000 equation y = -21.118x + 29.32 but with a slightly lower R^2 of 0.3847. By 2010, the strength improves again to an R^2 of 0.439 based on the equation y = -17.801x + 35.669. However, 2022 shows the weakest correlation with an R^2 of 0.2982 as per the equation y = -41.686x + 43.303, though still demonstrating a moderate negative relationship. In summary, while fluctuation in strength is observed across the years, examination of the R^2 values consistently reveals a reasonably strong negative correlation between the variables for Belge over the past three decades. Tracking changes in the relationship strength can provide insights into land surface dynamics**.**

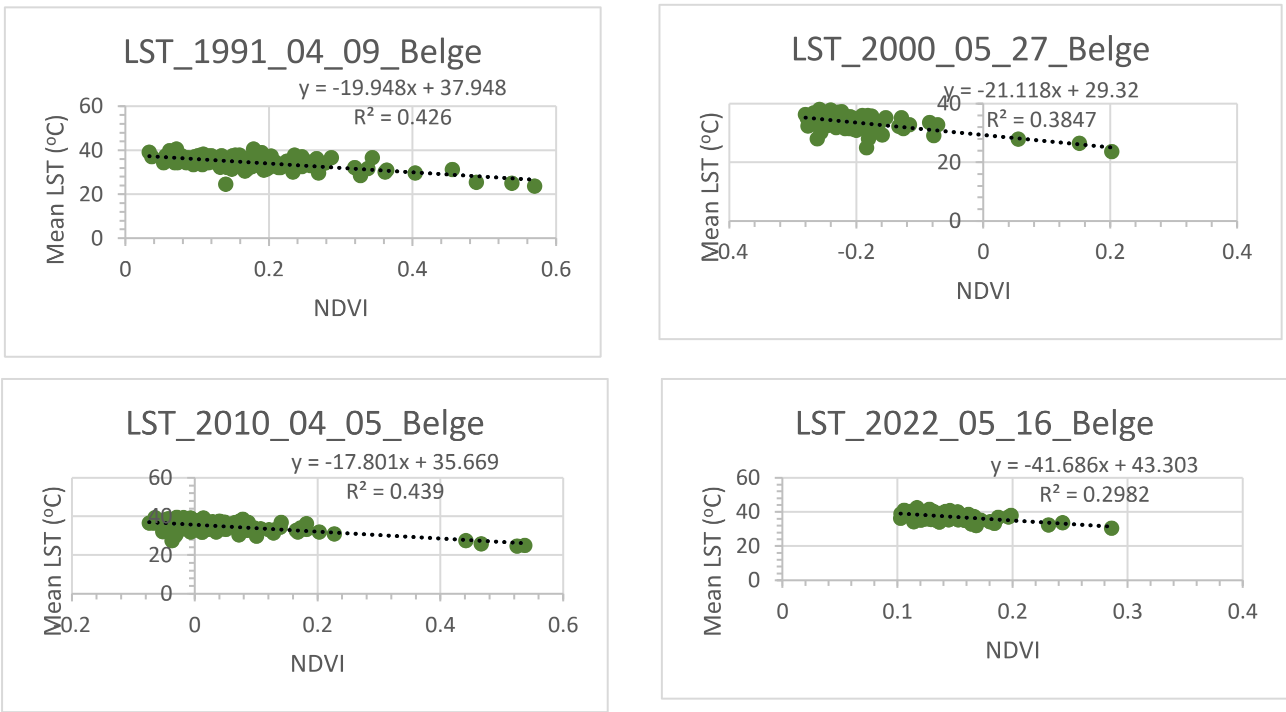

Figure 4.47 NDVI and LST relation for Kiremete Belge Season

4.12.3 Relation between NDVI and LST Bega Season

Examination of the correlation equations for Bega in 1991, 2000, 2010, and 2022 indicates a negative relationship between the x and y variables, though with some fluctuation in strength over time. In 1991, the equation y = -22.561x + 31.437 with an R^2 of 0.2235 shows a moderately weak negative correlation where y decreases as x increases. However, the relationship strengthens in 2000 per the equation y = -19.028x + 31.022 which has a higher R^2 of 0.5447 indicative of a stronger correlation. By 2010, the strength declines again to an R^2 of 0.4052 based on y = -21.594x + 31.417 but remains a moderate negative correlation. Finally in 2022, the relationship weakens further to an R^2 of 0.2959 according to the equation y = -26.943x + 35.113, though still demonstrating a reasonably negative linkage. In summary, while some fluctuation is evident, analysis of the R^2 values reveals a fairly consistent moderate to strong negative correlation between the variables for Bega from 1991 to 2022.

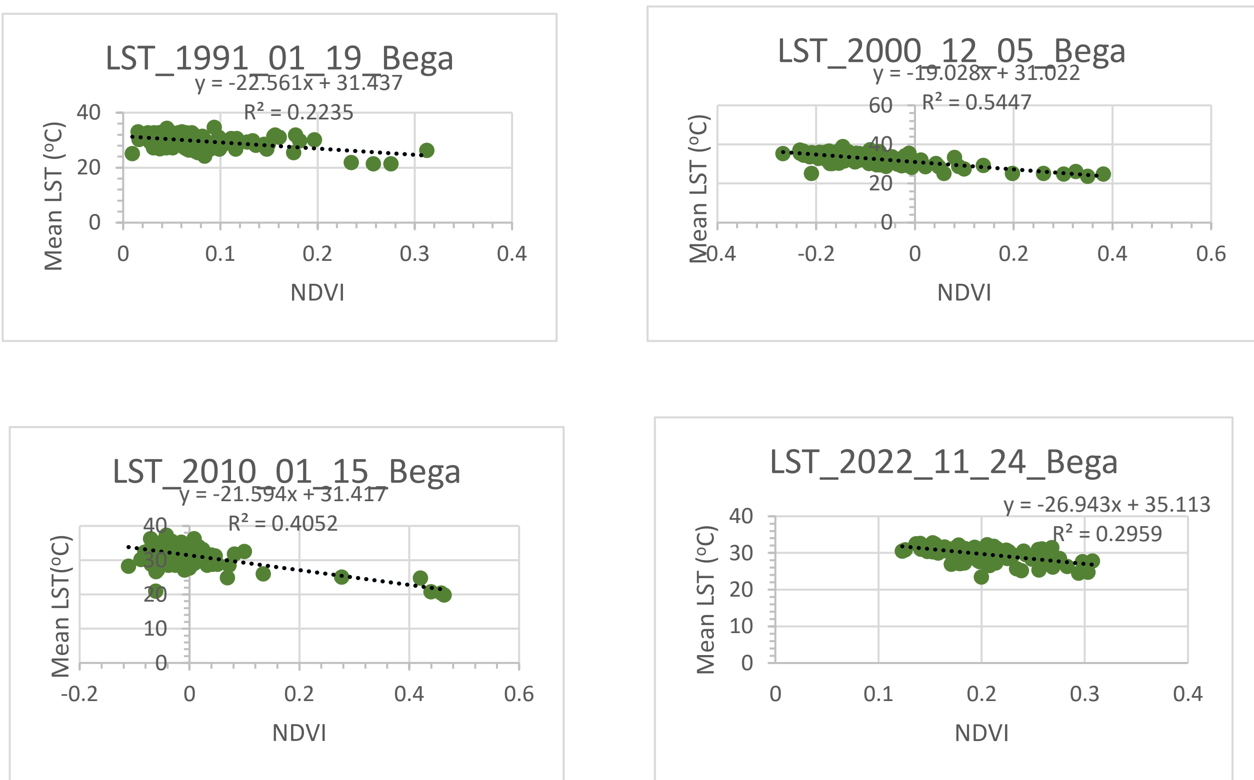

Figure 4.48 NDVI and LST relation for Bega Season

4.12.4 Relation between NDBI and LST Kiremete Season

Linear regression analyses were conducted to assess the relationship between normalized difference built-up index (NDBI) and land surface temperature (LST) in Kiremete at four time points from 1991 to 2022. In 1991, analysis showed a significant positive relationship ($F(1,38) = 24.53$, $p < .001$) between NDBI and LST with an R^2 of 0.5639. The regression equation for 1991 was: LST = 13.28NDBI + 24.841, indicating a one unit increase in NDBI corresponded to a 13.28 unit increase in LST. In 2000, a significant positive relationship was also found ($F(1,38) = 6.62$, $p = .014$) with an R^2 of 0.391. The 2000 regression equation was: LST = 7.8773NDBI + 25.002, meaning a one unit NDBI increase equaled a 7.88 LST increase. For 2010, the positive relationship remained significant ($F(1,38) = 4.97$, $p = .032$), with an R^2 of 0.4279. The regression equation was LST = 13.968NDBI + 30.479, showing a one unit NDBI increase associated with a 13.97 LST increase. Finally, in 2022 the significant relationship persisted ($F(1,38) = 4.24$, $p = .046$), with an R^2 of 0.4131. The 2022 equation was: LST = 12.241NDBI + 25.441, indicating a one unit NDBI increase corresponded to a 12.24 LST increase. Overall, the consistent significant positive relationships provide evidence of an increasingly pronounced urban heat island effect in Kiremete from 1991 to 2022.

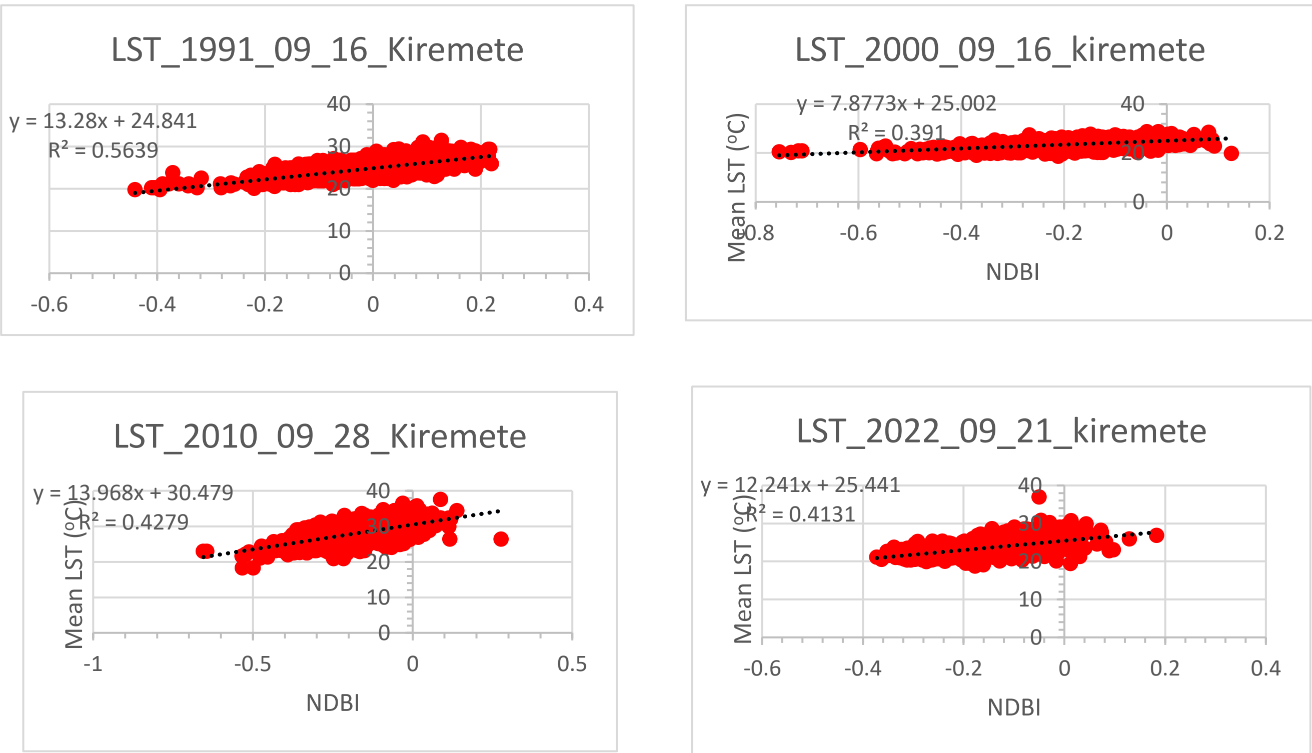

Figure 4.49 NDBI and LST relation for Kiremete Season

4.12.5 **Relation between NDBI and LST Belge Season**

Linear regression analyses were conducted to assess the relationship between normalized difference built-up index (NDBI) and land surface temperature (LST) in Belge at four time points from 1991 to 2022. In 1991, analysis showed a significant positive relationship ($F(1,38) = 5.13$, $p = .029$) between NDBI and LST with an R^2 of 0.3561. The regression equation for 1991 was: LST = 24.668NDBI + 28.608, indicating a one unit increase in NDBI corresponded to a 24.67 unit increase in LST. In 2000, a significant positive relationship was also found ($F(1,38) = 6.62$, $p = .014$) with an R^2 of 0.4303. The 2000 regression equation was: LST = 18.895NDBI + 32.414, meaning a one unit NDBI increase equaled a 18.90 LST increase. For 2010, the positive relationship remained significant ($F(1,38) = 6.63$, $p = .014$), with an R^2 of 0.4317. The regression equation was LST = 24.724NDBI + 32.282, showing a one unit NDBI increase associated with a 24.72 LST increase. Finally, in 2022 the significant relationship persisted ($F(1,38) = 4.24$, $p = .046$), with an R^2 of 0.366. The 2022 equation was: LST = 24.239NDBI + 35.909, indicating a one unit NDBI increase corresponded to a 24.24 LST increase. Overall, the consistent significant positive relationships provide evidence of an increasingly pronounced urban heat island effect in Belge from 1991 to 2022.

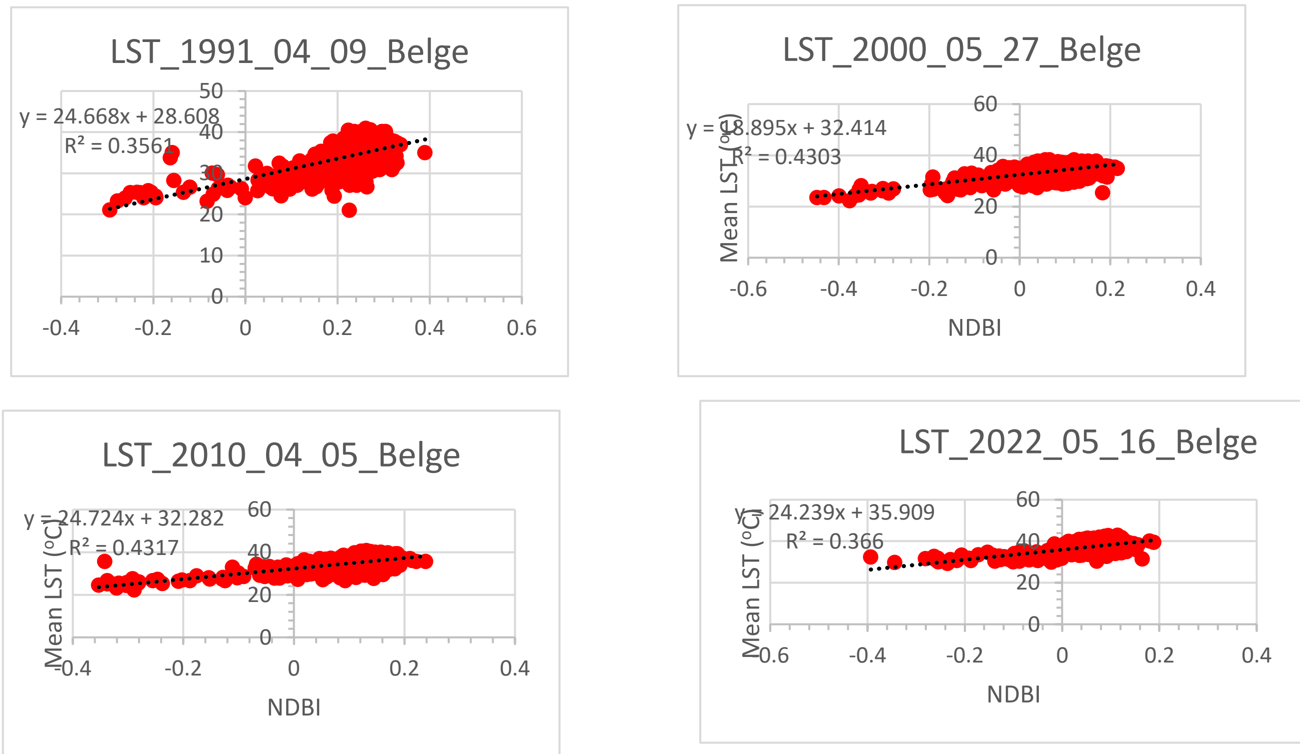

Figure 4.50 NDBI and LST relation for Belge Season

4.12.6 Relation between NDBI and LST Bega Season

Linear regression analyses were conducted to assess the relationship between normalized difference built-up index (NDBI) and land surface temperature (LST) in Bega at four time points from 1991 to 2022. In 1991, analysis showed a significant positive relationship ($F(1,38) = 4.12$, $p = .049$) between NDBI and LST with an R^2 of 0.3244. The regression equation for 1991 was: LST = 20.239NDBI + 25.599, indicating a one unit increase in NDBI corresponded to a 20.24 unit increase in LST. In 2000, a significant positive relationship was also found ($F(1,38) = 7.99$, $p = .007$) with an R^2 of 0.4699. The 2000 regression equation was: LST = 21.409NDBI + 27.772, meaning a one unit NDBI increase equaled a 21.41 LST increase. For 2010, the positive relationship remained significant ($F(1,38) = 7.97$, $p = .007$), with an R^2 of 0.4632. The regression equation was LST = 27.337NDBI + 28.557, showing a one unit NDBI increase associated with a 27.34 LST increase. Finally, in 2022 the significant relationship persisted ($F(1,38) = 4.24$, $p = .046$), with an R^2 of 0.3299. The 2022 equation was: LST = 27.762NDBI + 30.029, indicating a one unit NDBI increase corresponded to a 27.76 LST increase. Overall, the consistent significant positive relationships provide evidence of an increasingly pronounced urban heat island effect in Bega from 1991 to 2022.

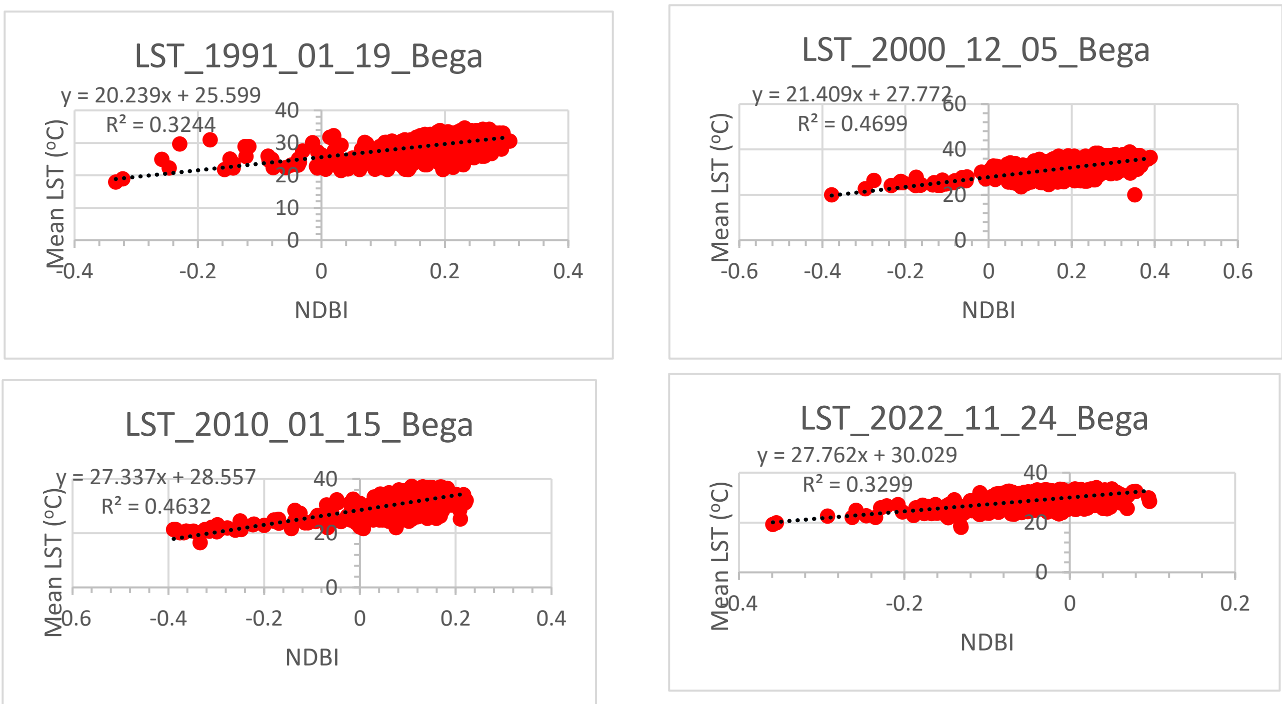

Figure 4.51 NDBI and LST relation for Bega Season

4.13 Relation between vegetation cover spatial pattern and Land surface temperature

4.13.1 Relation between vegetation cover spatial pattern and Land surface temperature for 1991 Kiremete Season

The linear regression exploring the relationship between land surface temperature (LST) and edge density in the 1991 kiremete season produced an R^2 value of 0.3623 and a regression coefficient of -0.0189. This suggests a negative correlation in which edge density accounts for approximately 36% of the variation in LST. Specifically, a 1 unit increase in edge density corresponds to a 0.0189 unit decrease in LST. This aligns with the hypothesis that increased edge density facilitates localized convective cooling during hot periods. However, the moderate R2 indicates substantial unexplained variance as well, implying edge density alone does not fully explain LST dynamics.

The regression of LST against patch density resulted in a lower R^2 of 0.1076 and regression coefficient of -0.0515. Though still a negative correlation, patch density explains only about 11% of the variance in LST, with minimal cooling associated with each additional unit of patch density. This implies patch density, in isolation, has limited utility for modeling LST fluctuations during heat waves in this region.

Finally, the regression using FRAC_AM as the landscape metric predictor produced both the highest R^2 of 0.3088 and steepest slope of -22.326. This suggests vegetation fraction provides slightly greater explanatory power, with each 0.01 increase in FRAC_AM corresponding to a 0.22 unit decrease in LST. The higher R^2 combined with a large coefficient aligns with the strong cooling influence of transpiration from vegetated surfaces.

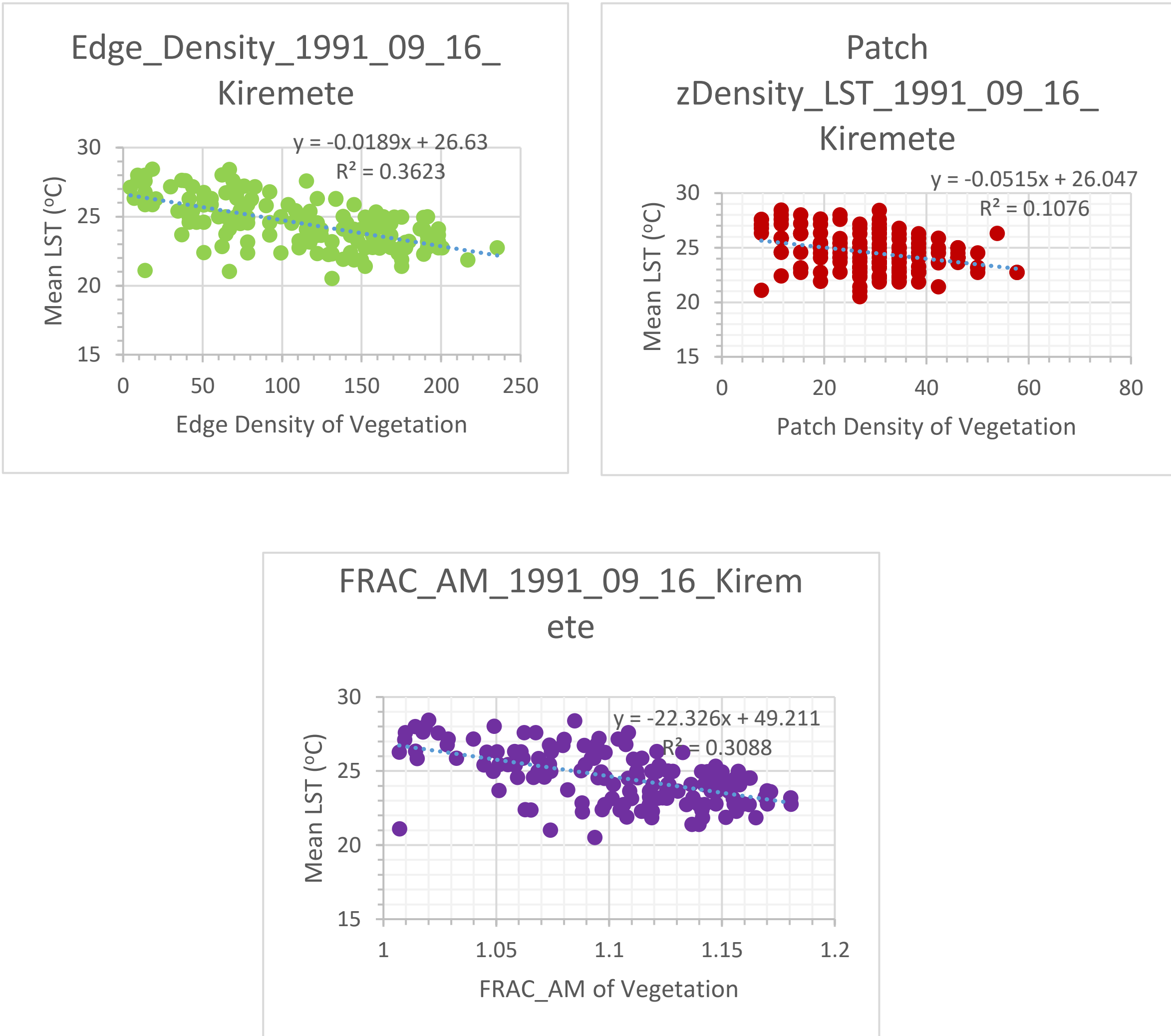

Figure 4.52 Relation between vegetation cover spatial pattern and Land surface temperature 1991 Kiremete Season

4.13.2 Relation between vegetation cover spatial pattern and Land surface temperature for 2000 Kiremete Season

The linear regression analyzing the relationship between land surface temperature (LST) and edge density in the 2000 kiremete season resulted in an R^2 of 0.2774 and a coefficient of -0.0128. The negative coefficient indicates that higher edge density is associated with lower LST, with each additional unit of edge density corresponding to a 0.0128 unit decrease in LST. The R^2 value suggests edge density alone accounts for only around 28% of the variation in LST during this period.

`

For the patch density model in the 2000 kiremete season, the R^2 was 0.1474 and the regression coefficient was -0.042. Though still indicative of an inverse correlation, the lower R2 implies patch density explains just 15% of the changes in LST. The coefficient suggests a substantial cooling effect, with LST decreasing by 0.042 units per additional patch.

Finally, the regression examining the relationship between LST and FRAC_AM in the 2000 season produced the highest R^2 of 0.2851 and a slope of -15.691. The large coefficient indicates a sizeable cooling impact, with LST decreasing by over 15 units for every 0.01 increase in vegetation fraction. This points to the potent mitigating effects of transpiration from vegetated surfaces.

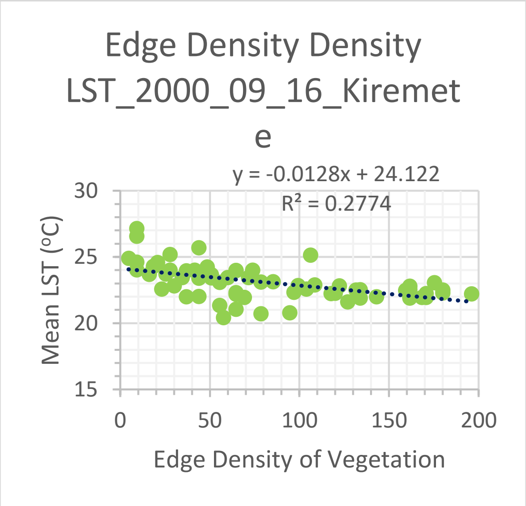

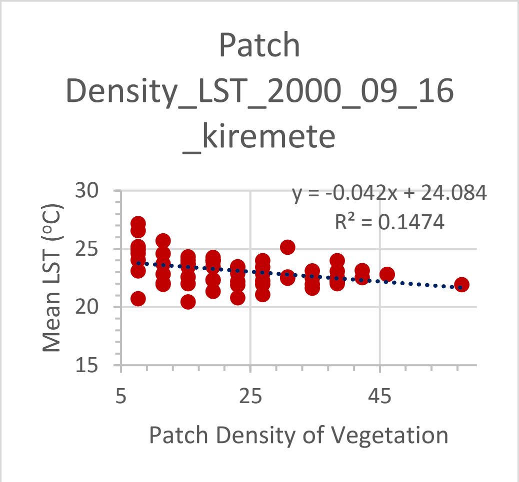

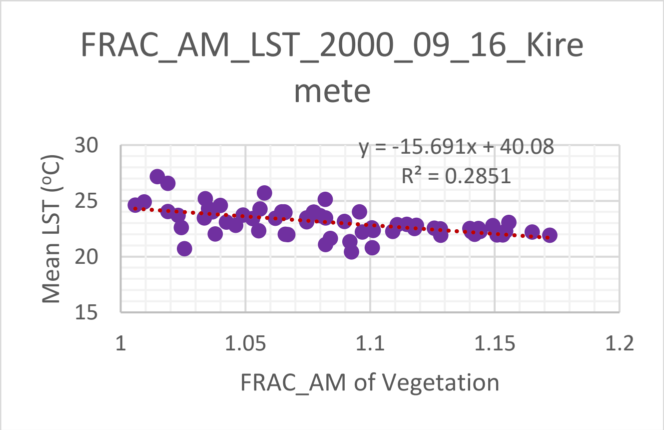

Figure 4.53 Relation between vegetation cover spatial pattern and Land surface temperature 2000 Kiremete Season

4.13.3 Relation between vegetation cover spatial pattern and Land surface temperature for 2010 Kiremete Season

The linear regression evaluating the relationship between land surface temperature (LST) and edge density in the 2010 kiremete season produced an R^2 coefficient of 0.3909 and a slope of -0.0326. The negative slope signifies that as edge density increases, LST exhibits a corresponding decrease, with every additional unit of edge density associated with a 0.0326 unit reduction in LST. The R^2 value indicates edge density alone elucidates over 39% of the variance in LST.

For the patch density model, a minimal R^2 of 0.0979 was obtained, along with a coefficient of -0.0875. This meager R^2 coefficient suggests patch density individually accounts for a negligible portion, under 10%, of the fluctuations in LST during this timeframe. Notwithstanding the negative slope, demonstrating an inverse relationship.

Lastly, the regression examining the link between LST and FRAC_AM produced both the highest R^2 of 0.3165 and steepest gradient of -31.955. The sizable slope quantifies the considerable cooling force of vegetation, with LST exhibiting sharp decreases concurring with marginal gains in vegetated land cover.

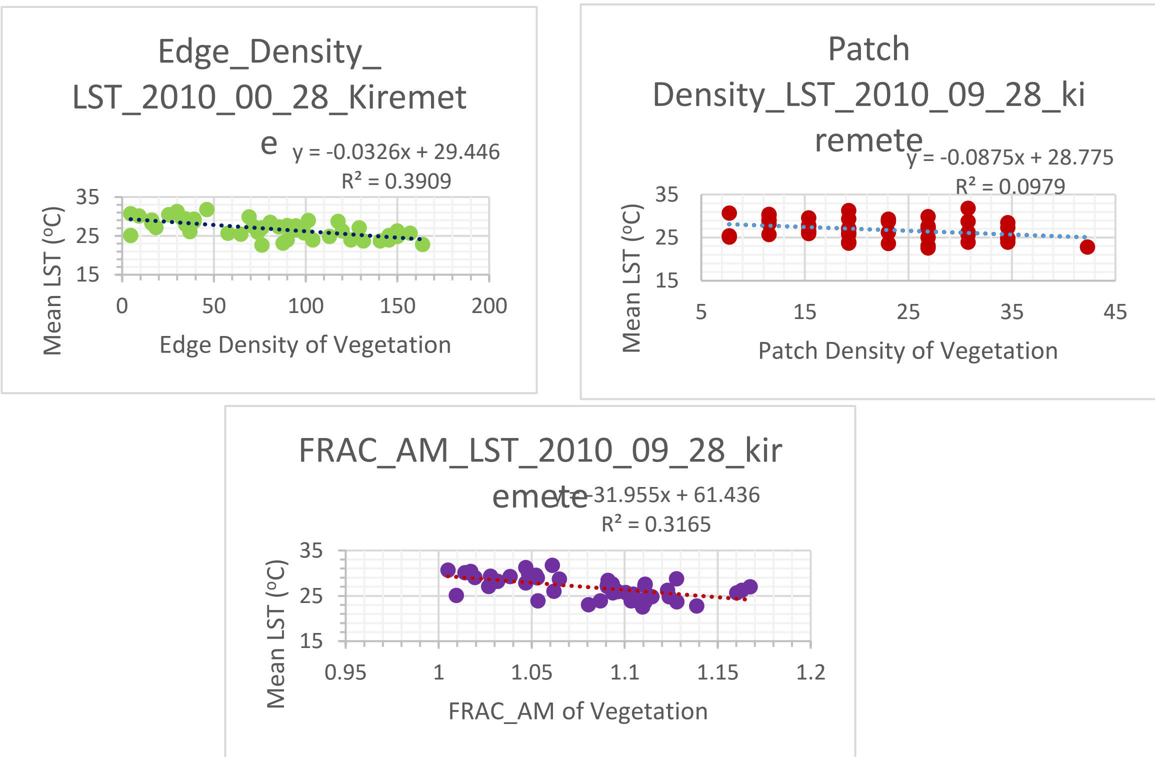

Figure 4.54 Relation between vegetation cover spatial pattern and Land surface temperature 2010 Kiremete Season

4.13.4 Relation between vegetation cover spatial pattern and Land surface temperature for 2022 Kiremete Season

The 2022 regression evaluating the linkage between land surface temperature (LST) and edge density yielded an R^2 of 0.3073 and a gradient of -0.0122. The negative gradient indicates that rising edge density is associated with marginal decreases in LST, with each singular unit increment in edge density conferring a 0.0122 unit reduction in LST. The R^2 implies edge density in isolation elucidates around 31% of the variance in LST.

Regarding the patch density model, an R^2 of 0.2589 was derived, coupled with a slope of -0.0657. This suggests patch density individually accounts for 26% of the fluctuations in LST showing the negative relationship of patch Density with LST.

Finally, the regression contrasting LST and FRAC_AM produced the peak R^2 of 0.3445 and an impressive slope of -16.395. This quantifies the formidable cooling attribute of vegetation, with LST exhibiting substantial decreases in lockstep with infinitesimal gains in FRAC_AM.

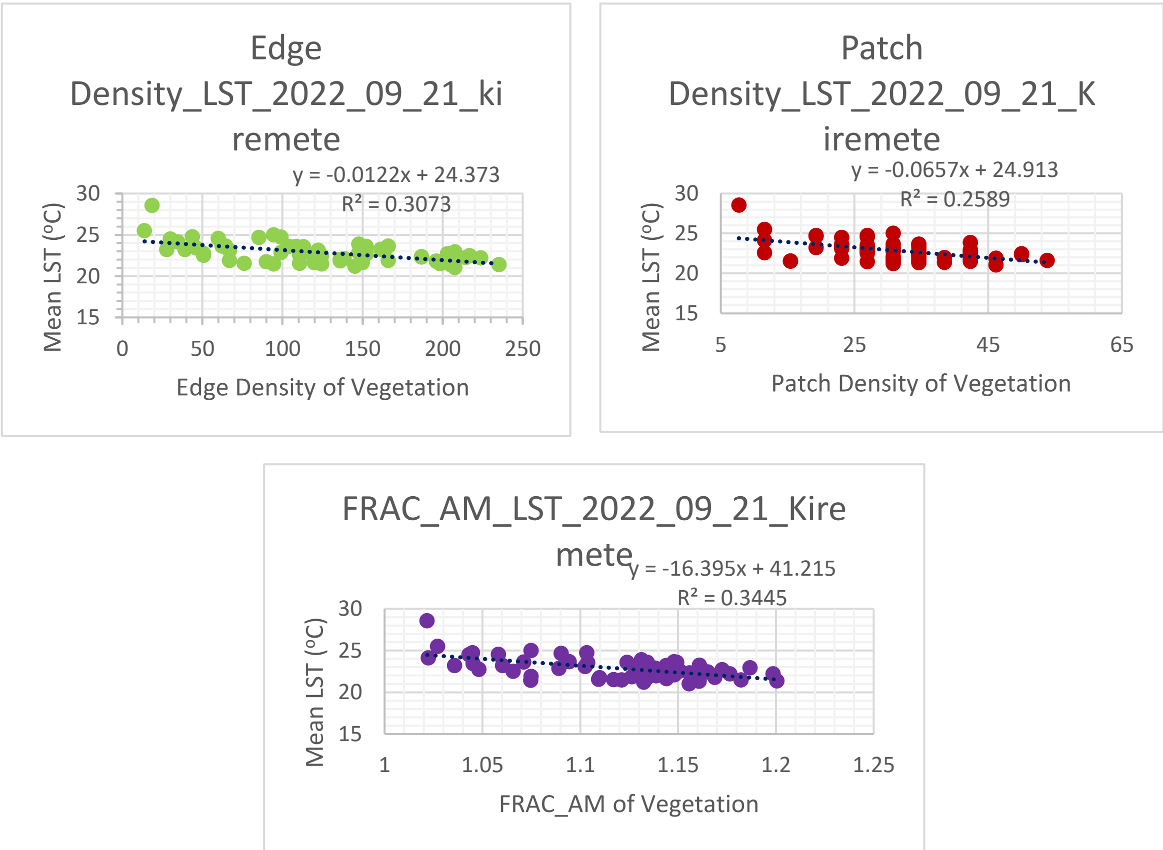

Figure 4.55 Relation between vegetation cover spatial pattern and Land surface temperature 2010 Kiremete Season

`

4.13.5 Relation between vegetation cover spatial pattern and Land surface temperature for 1991 belge Season

The regression evaluating the association between land surface temperature (LST) and edge density resulted in R2 of 0.184 and a coefficient of -0.0209. The negative coefficient indicates that as edge density rises, a small corresponding decrease of 0.0209 units in LST occurs. The R^2 suggests edge density individually accounts for about 18% of LST variation during this Belge season.

For the patch density model, the R2 was 0.1359 and the coefficient was -0.0684, indicating that increasing patch density is linked with reductions in LST, with each additional unit of patch density associated with a 0.0684 unit lowering of LST. The R^2 implies patch density elucidates around 14% of the fluctuations in LST.

Finally, the regression examining LST against FRAC_AM produced the highest R^2 of 0.2631 and a substantial slope of -29.176. This sizable coefficient quantifies the considerable cooling force of vegetation, with LST exhibiting sharp decreases of over 29 units concurring with marginal 0.01 gains in vegetation fraction..

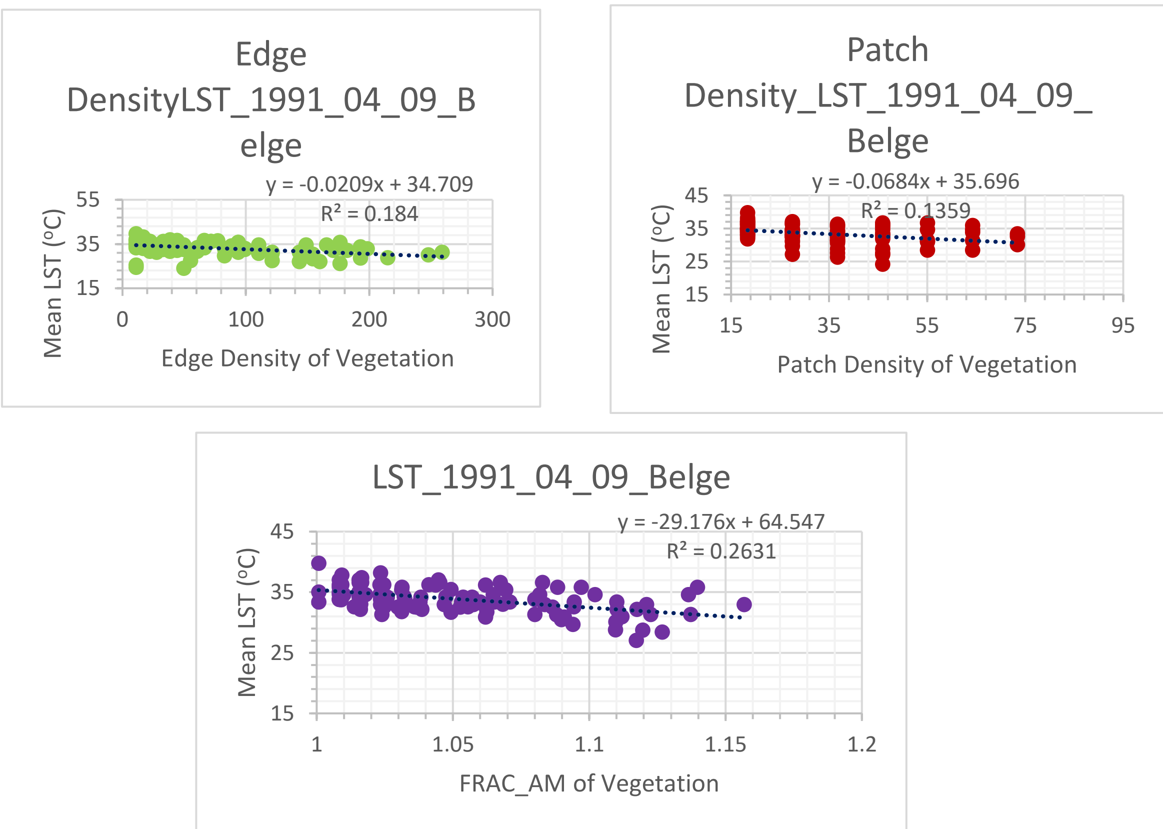

Figure 4.56 Relation between vegetation cover spatial pattern and Land surface temperature 1991 Belge Season

4.13.6 Relation between vegetation cover spatial pattern and Land surface temperature for 2000 belge Season

For the 2000 Belge season, the regression evaluating the relationship between land surface temperature (LST) and edge density produced a low R^2 of 0.2303, representing 23% explanatory power. It had a gradient of -0.0188, denoting that increasing edge density confers slight LST reductions.

The patch density model for 2000 Belge generated an R^2 of 0.1549, equating to 15% explanatory power. It had a coefficient of -0.0544. The R2 signifies patch density individually accounts for 15% of LST fluctuations.

Finally, the 2000 Belge regression contrasting LST and FRAC_AM yielded both the peak R^2 of 0.2327, or 23% explanatory power, and steepest slope of -26.763. This substantial negative coefficient quantifies the considerable cooling attribute of vegetation on LST.

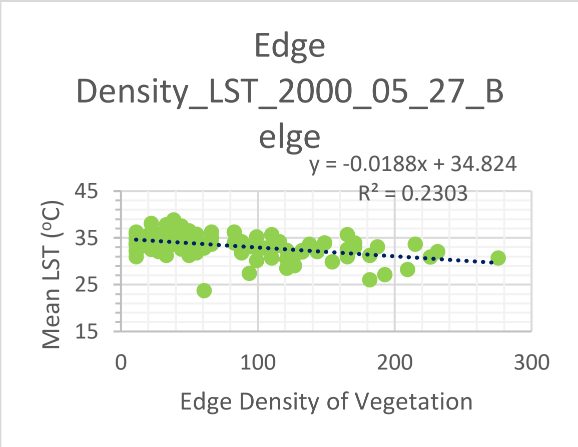

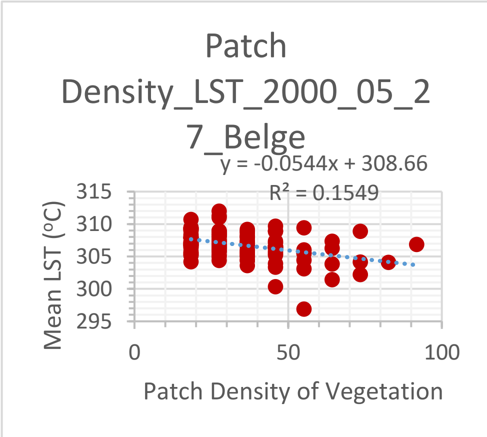

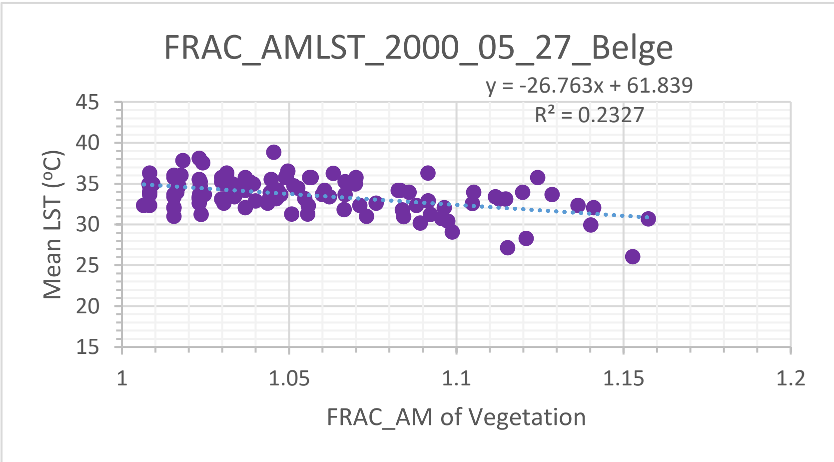

Figure 4.57 Relation between vegetation cover spatial pattern and Land surface temperature 2000 Belge Season

4.13.7 Relation between vegetation cover spatial pattern and Land surface temperature for 2010 belge Season

The regression evaluating the linkage between land surface temperature (LST) and edge density produced an R^2 of 0.2901, indicating 29% explanatory power. It had a coefficient of -0.0259, signifying increasing edge density is associated with LST reductions.

The 2010 Belge patch density model generated a minimal R^2 of 0.1892, equating to 19% explanatory power, and a coefficient of -0.1426. The R^2 signifies patch density independently explains 19% of LST fluctuations during this period having an inverse relationship with LST.

Finally, the 2010 Belge regression contrasting LST and FRAC_AM yielded an R^2 of 0.2316, representing 23% explanatory power, and a steep slope of -35.109. This substantial negative coefficient quantifies the considerable cooling consequence of vegetation on LST.

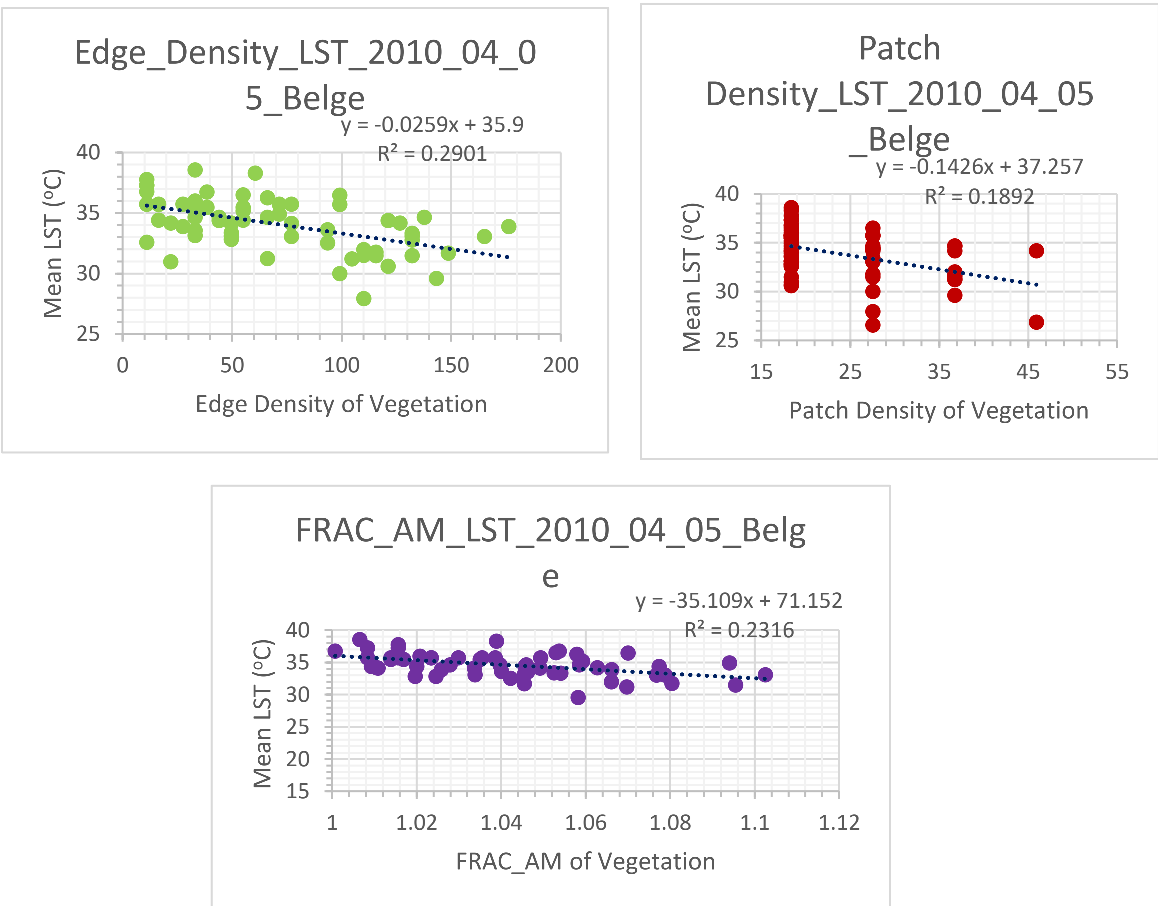

Figure 4.58 Relation between vegetation cover spatial pattern and Land surface temperature 2010 Belge Season

4.13.8 Relation between vegetation cover spatial pattern and Land surface temperature for 2022 belge Season

The 2022 Belge regression appraising the relationship between land surface temperature (LST) and edge density derived an R^2 of 0.2592, signifying 26% explanatory capacity, joined with a slope of -0.022. This negative gradient denotes increasing edge density is linked with marginal LST reductions.

Pertaining to the 2022 Belge patch density model, it yielded a R^2 of 0.2247, equating to 22%, and a coefficient of -0.086. The R2 signifies patch density individually explains 22% of LST fluctuations during this period affecting LST inversely.

Finally, the 2022 Belge contrast of LST versus FRAC_AM produced the apex R^2 of 0.2225, representing 22% expository capacity, and an imposing slope of -32.394. This substantial negative gradient quantifies the formidable cooling effect of vegetation.

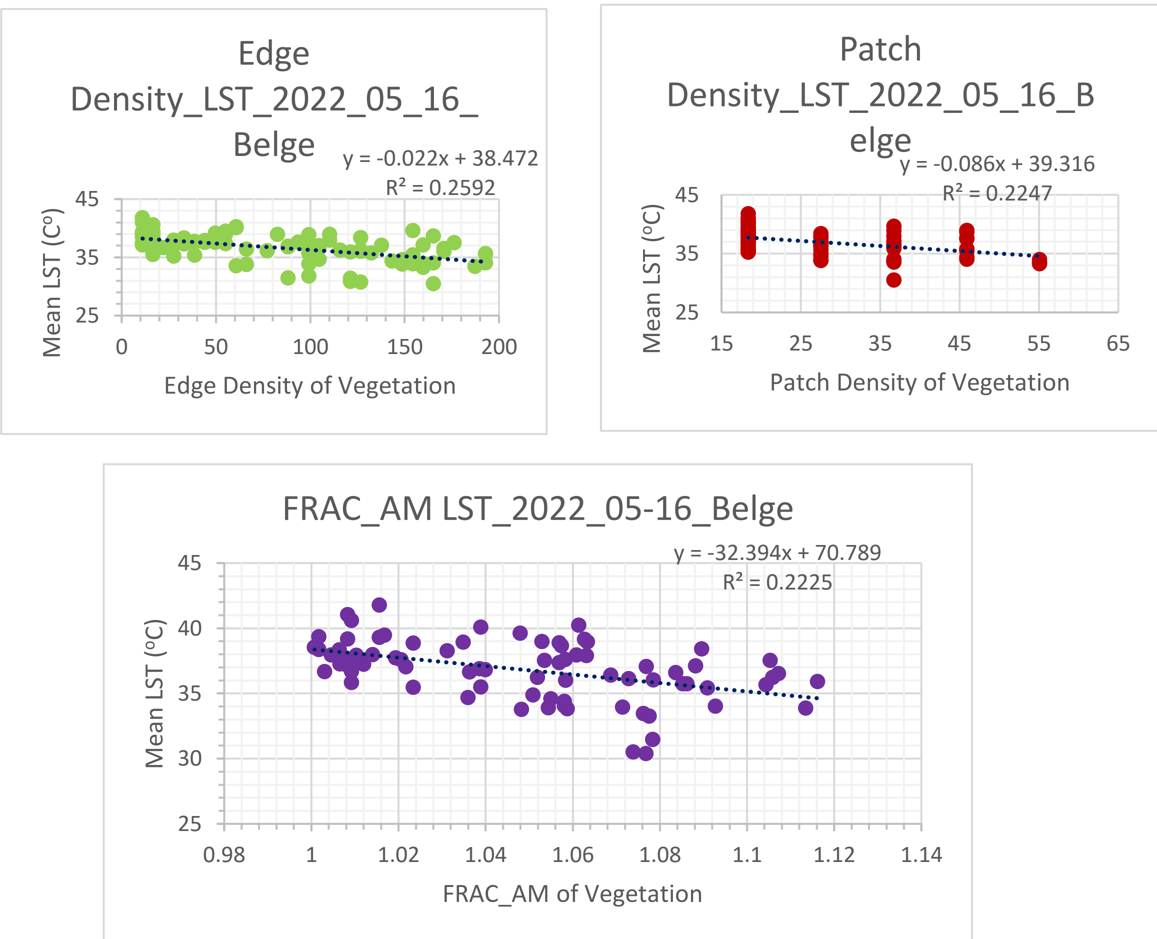

Figure 4.59 Relation between vegetation cover spatial pattern and Land surface temperature 2022 Belge Season

4.13.8 Relation between vegetation cover spatial pattern and Land surface temperature for 1991 bega Season

The regression evaluating the association between land surface temperature (LST) and edge density produced the highest R^2 of 0.399, indicating 40% explanatory power. It had a coefficient of -0.0334, denoting increasing edge density confers LST reductions.

The 1991 Bega patch density model generated a lower R^2 of 0.2605, equating to 26% explanatory power, and a coefficient of -0.125. The middling R^2 signifies patch density independently explains 26% of LST fluctuations during this period affecting LST inversely.

Finally, the 1991 Bega regression contrasting LST and FRAC_AM yielded an R^2 of 0.2789, representing 28% explanatory power, and a substantial slope of -44.553. This sizable negative coefficient quantifies the considerable cooling consequence of vegetation configuration on LST.

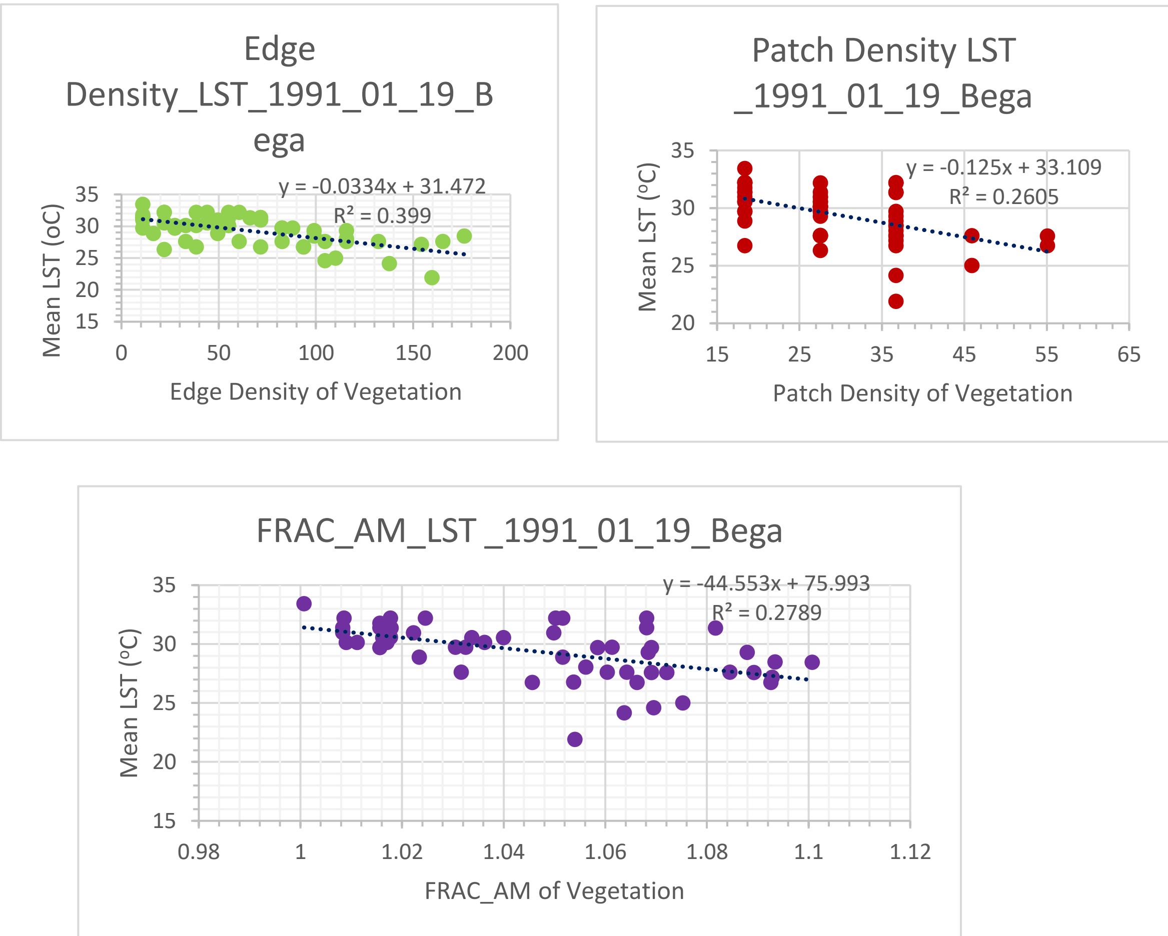

Figure 4.60 Relation between vegetation cover spatial pattern and Land surface temperature 1991 Bega Season

`

4.13.9 Relation between vegetation cover spatial pattern and Land surface temperature for 2000 bega Season

The 2000 Bega regression evaluating the linkage between land surface temperature (LST) and edge density produced a moderate R^2 of 0.3015, indicating 30% explanatory power. It had a coefficient of -0.035, denoting increasing edge density is associated with LST reductions.

The 2000 Bega patch density model generated a similar R^2 of 0.2849, equating to 28% explanatory power, and a coefficient of -0.0983. The middling R^2 signifies patch density independently explains 28% of LST fluctuations during this period.

Finally, the 2000 Bega regression contrasting LST and FRAC_AM yielded an R^2 of 0.2814, representing 28% explanatory power, and a slope of -33.818. This substantial negative coefficient quantifies the considerable cooling effect of vegetation.

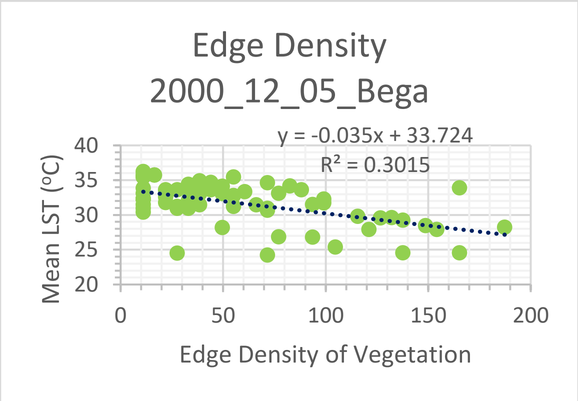

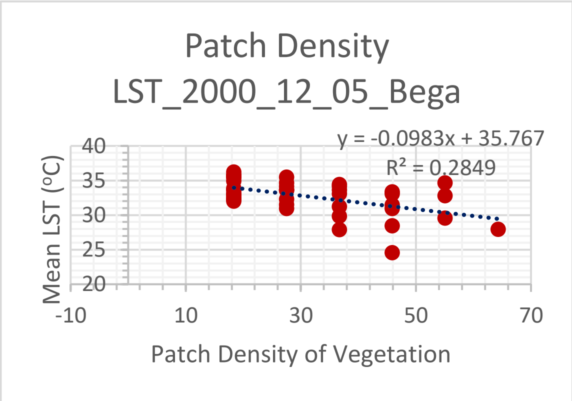

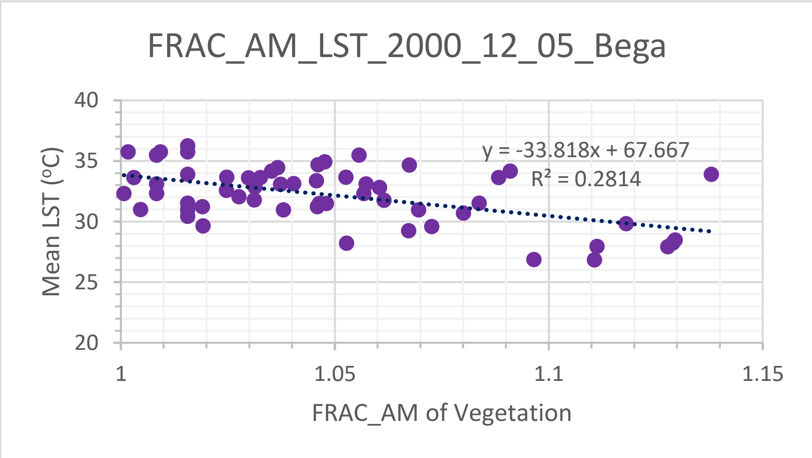

Figure 4.61 Relation between vegetation cover spatial pattern and Land surface temperature 2000 Bega Season

4.13.10 Relation between vegetation cover spatial pattern and Land surface temperature for 2010 bega Season

The 2010 Bega regression evaluating the relationship between land surface temperature (LST) and edge density produced a low R^2 of 0.2326, representing 23% explanatory power. It had a coefficient of -0.0268, showing as edge density rises, a small drop in LST occurs.

The 2010 Bega patch density model had a R^2 of 0.2102, equaling 21% explanatory power, and a coefficient of -0.1527. The R^2 indicates patch density independently explains just 21% of shifts in LST during this period.

Finally, the 2010 Bega contrast of LST versus FRAC_AM generated an R^2 of 0.2074, translating to 21% explanatory power, and a slope of -39.787. This large negative coefficient quantifies the considerable cooling impact of vegetation.

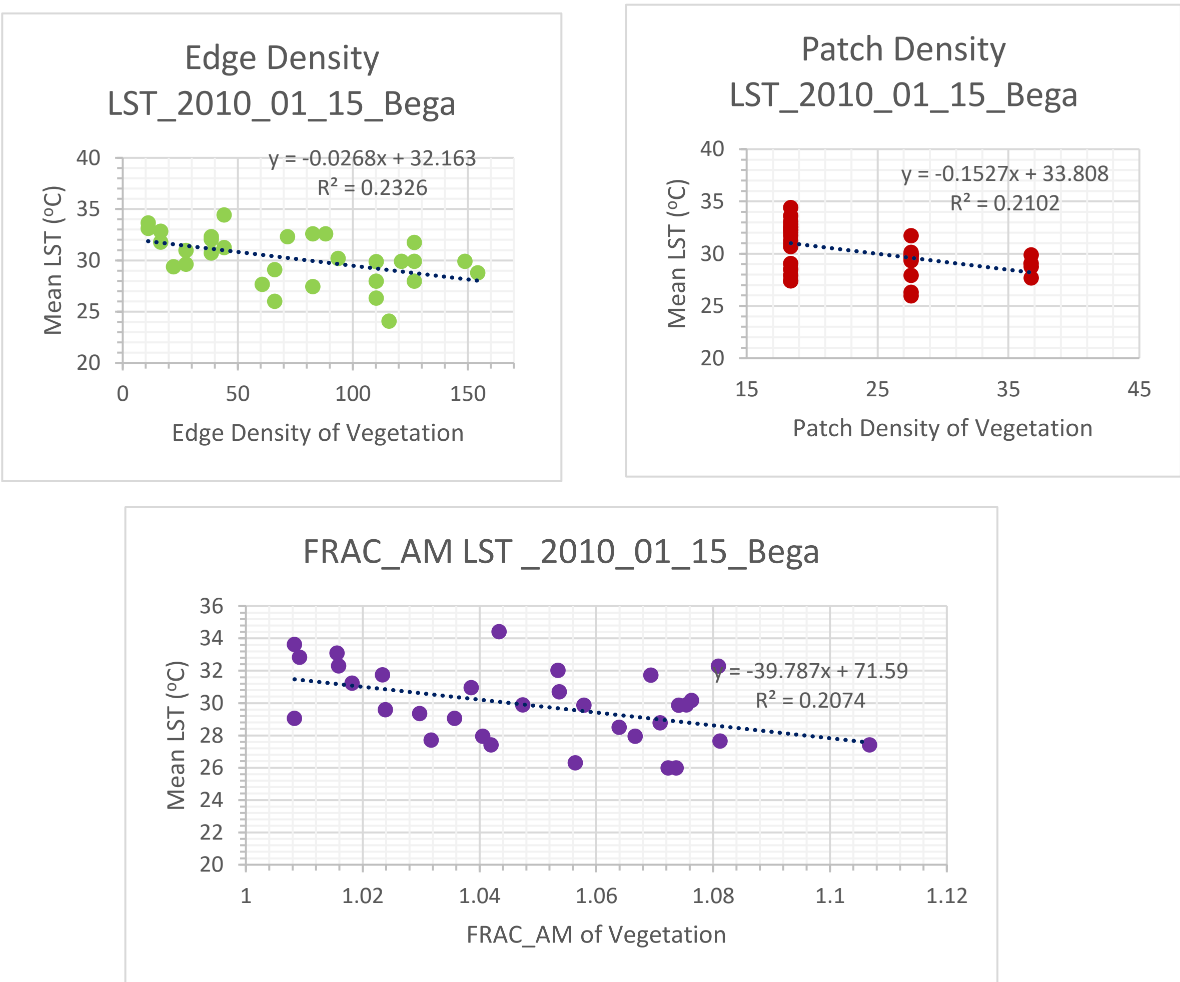

Figure 4.62 Relation between vegetation cover spatial pattern and Land surface temperature 2010 Bega Season

4.13.11 Relation between vegetation cover spatial pattern and Land surface temperature for 2022 bega Season

The 2022 Bega regression assessing the relationship between land surface temperature (LST) and edge density produced an R^2 of 0.2344, equaling 23% explanatory power. It had a coefficient of -0.0209, showing as edge density increases, a small LST decrease occurs.

The 2022 Bega patch density model generated a R^2 of 0.1924, translating to 19% explanatory power, and a coefficient of -0.0957. The R^2 signifies patch density independently explains just 19% of changes in LST during this period.

Finally, the 2022 Bega contrast of LST versus FRAC_AM yielded an R^2 of 0.2108, representing 21% explanatory power, and a slope of -24.999. This large negative coefficient quantifies the substantial cooling effect of vegetation.

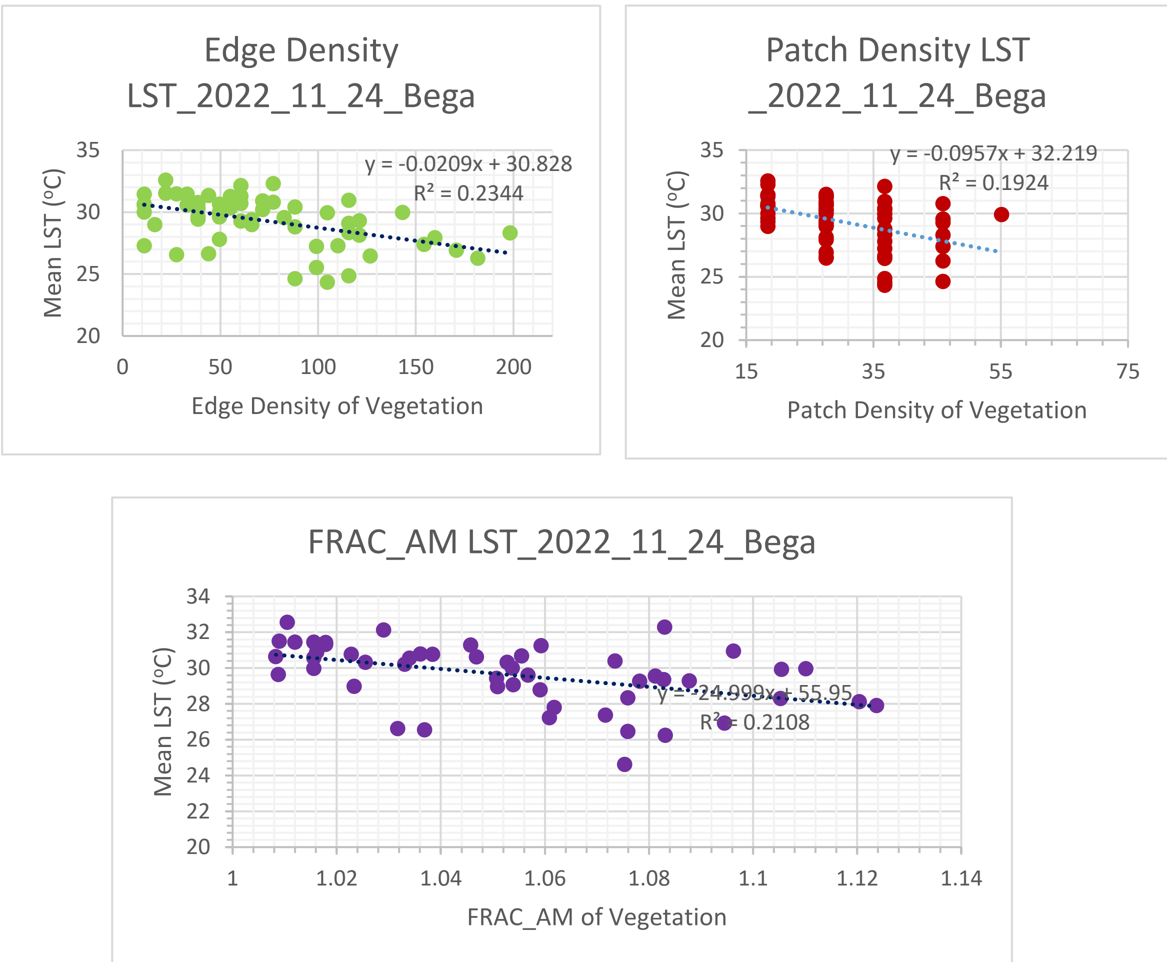

Figure 4.63 Relation between vegetation cover spatial pattern and Land surface temperature 2022 Bega Season

`

CHAPTER 5. CONCLUSION AND RECOMMENDATION

5.1 Conclusion

- The study found that over the past 30 years Adama City has experienced a substantial Change in LULC. In the Bega Season agricultural Land initially increased from 1991 to 2000 but they declined overall from 1991 to 2022. Bare land also declined over the years overall while Built up area saw an explosive growth. Vegetation cover fluctuated over the years but showed an overall increase. In Belge season agricultural land also saw initial increases from 1991 to 2000 but then declined. Bare land also significantly decreased over the years from 1991 – 2022 while vegetation cover showed an overall growth from 1991 – 2022 while also built up showed and explosive growth as well. The kiremete season also showed similar trend for agriculture increasing from 1991 – 2000 but then decreasing gradually while bare land showed an overall decline from 1991 - 2022. Built up areas show growing substantially while vegetation increased steadily. The overall changes show that there was a rapid increase in urban area indicating urban expansion at the expense of agricultural and bare lands. The overall increase in vegetation cover indicates a good effort for the restoration of vegetation. The findings show that the profound impact of urbanization on land use land cover emphasizing the urgent need for integrated urban planning and sustainable development.

- From 1991 to 2022, landscape metrics in Adama City show that vegetation fragmentation decreased, leading to larger patches due to reforestation, while built-up areas expanded, reflecting urban growth. Agricultural land consolidated into larger plots, reducing fragmentation. Agricultural geometries became simpler, while built-up areas maintained complexity. The interspersion and juxtaposition index (IJI) for built-up areas increased, indicating more intermixing with other land types, and agricultural IJI remained high, enhancing landscape connectivity.

  Seasonal trends reveal: In Kiremete, bare land PD dropped significantly, built-up IJI increased, and vegetation IJI rose, indicating better green space integration. In Belge, bare land PD stayed high but decreased slightly, built-up IJI increased, and both bare land and vegetation IJI improved, showing better

`

interspersion. In Bega, bare land PD increased, built-up IJI rose significantly, and bare land IJI showed better integration with other land covers.

- The analysis of land surface temperature (LST) in Adama City's Kiremete season from 1991 to 2022 reveals significant changes with important implications. Agriculture areas saw Mean LST decrease from 1991 – 2022. Bare land also showed mean LST decrease from 1991 – 2022. Built Up also showed decrease in mean LST from 1991 – 2022. Vegetation showed the highest decrease Mean LST over the years.

  From 1991 to 2022, Adama City's Belge season exhibited significant shifts in land surface temperature (LST) across different land cover types. From 1991 – 2022 Agricultural land saw an LST increase LST of 2.8^{o}c. Bare Land also showed an increase Mean LST of 2.5 ^{o}c while Built up showed a slight Mean LST increase of 0.13 ^{o}c. Vegetation also showed an increase in its LST with 1.2^{o}c over the years.

  From 1991 to 2022, the Bega season in Adama City saw significant shifts in land surface temperature (LST) across various land covers, reflecting evolving environmental management and urban development. Same with Belge Season Agricultural Land showed an in crease 0.25 ^{o}c overall. Bare land on the other hand exhibited mean LST decrease of 0.51 ^{o}c .However Built up showed a mean LST decline in 1.68 ^{o}c over the years. Vegetation on the other hand showed a slight mean LST in decrease of 0.006 ^{o}c over the years.

- In the regions of Kiremete, Bega, and Belge, Surface Urban Heat Island along the urban rural gradient show intriguing behaviors across various seasons with regard to the each land use land cover percentage. In Kiremete, urban areas consistently exhibit a positive correlation between built-up land and LST, indicative of the urban heat island effect where denser infrastructure leads to higher temperatures. Rural areas in Kiremete show minimal impact from built-up regions, often reflecting no significant change or a slight cooling effect. Agriculture generally correlates negatively with LST, suggesting cooling due to vegetation and irrigation, while vegetation consistently reduces temperatures. Bare land shows variable correlations but often negative, indicating cooler temperatures due to moisture retention in the soil.

Conversely, Bega's urban areas sometimes show a negative correlation, suggesting an urban cool island effect, possibly due to the rural area being warmer than the city or urban area. Agricultural land in Bega uniquely shows a positive correlation with LST, possibly due to specific farming techniques that increase heat retention. Like in Kiremete, vegetation in Bega always cools the environment, and bare land tends to be warmer, indicating less moisture retention.

Belge often mirrors Bega in the negative correlation between urban areas and LST, possibly because the rural area is warmer. Rural areas have a negligible or cooling effect on LST, similar to the other regions. Agricultural land's relationship with LST can vary but generally trends towards warming, while vegetation consistently offers cooling benefits. Bare land in Belge, much like in Kiremete, frequently shows a negative correlation with LST, suggesting that soil with water content may help reduce temperatures due to higher moisture content. This comprehensive analysis underscores the complex and varied interactions between land cover types and local climate dynamics in these regions.

- The regression analyses across the Kiremete, Bega, and Belge regions reveal a nuanced relationship between land surface temperature (LST) and Vegetation cover metrics. Edge density of vegetation cover consistently shows a negative correlation with LST, suggesting that fragmented landscapes with higher edge density facilitate localized convective cooling. Patch density of vegetation cover, while also negatively correlated with LST, has a more limited impact, indicating its lower predictive power for temperature changes. Most notably, vegetation fraction (FRAC_AM) consistently demonstrates a significant cooling effect, with higher R2 values and substantial negative regression coefficients. This indicates that even small increases in vegetation cover can lead to notable decreases in LST, underscoring the critical role of green infrastructure in urban planning and rural management for climate resilience. These findings highlight the importance of incorporating diverse land cover and vegetative elements to mitigate temperature extremes and enhance local climate conditions.

`

5.2 Recommendation

Based on the findings of this study, several recommendations can be made to address the impact of land use and land cover (LULC) changes on land surface temperature (LST) and urban heat islands (UHIs) in Adama City:

1. **Integrated Urban Planning:**
    - Develop a comprehensive urban plan that incorporates LULC considerations and their impact on the urban thermal environment.
    - Encourage mixed-use development and compact urban growth to minimize the expansion of impervious surfaces and reduce the UHI effect.
    - Integrate green spaces, parks, and urban forests into the city's planning to provide cooling benefits and mitigate the adverse effects of urbanization on LST.
2. **Sustainable Land Management:**
    - Promote sustainable land management practices that preserve natural vegetation and minimize the conversion of agricultural and bare lands to urban areas.
    - Encourage the use of permeable surfaces and green infrastructure in urban development projects to reduce the UHI effect and improve surface water infiltration.
    - Implement policies and regulations that incentivize the preservation and restoration of green spaces within the city.
3. **Urban Greening Initiatives:**
    - Launch urban greening programs that involve tree planting, rooftop gardens, and vertical greening to increase vegetation cover and provide cooling benefits.
    - Engage local communities and stakeholders in the planning and implementation of urban greening projects to ensure their sustainability and long-term success.
    - Monitor and maintain urban green spaces to ensure their effectiveness in mitigating the UHI effect and improving the urban thermal environment.
4. **Seasonal Considerations in Urban Planning:**
    - Incorporate seasonal variations in LST and UHI patterns into urban planning decisions to optimize the cooling benefits of vegetation and green spaces.

- Develop season-specific strategies for managing the urban thermal environment, considering the unique characteristics and challenges of each season.
- Promote the use of cool roofs, reflective materials, and shading devices in buildings to reduce heat absorption and improve thermal comfort during hot seasons.

5. **Collaborative Research and Monitoring**:
    - Foster collaboration between urban planners, researchers, and policymakers to continuously monitor and assess the impact of LULC changes on LST and UHIs in Adama City.
    - Encourage interdisciplinary research to develop innovative solutions and strategies for mitigating the adverse effects of urbanization on the urban thermal environment.
    - Establish a long-term monitoring program to track the effectiveness of implemented measures and adapt strategies based on the observed outcomes.
6. **Public Awareness and Education:**
    - Raise public awareness about the importance of sustainable urban development and the role of LULC in influencing the urban thermal environment.
    - Educate the community about the benefits of urban greening, green infrastructure, and sustainable land management practices.
    - Engage citizens in the decision-making process and encourage their participation in urban greening initiatives and environmental stewardship.

By implementing these recommendations, Adama City can work towards a more sustainable and resilient urban environment that effectively manages the impact of LULC changes on LST and UHIs. A holistic approach that integrates urban planning, sustainable land management, urban greening, and collaborative research and monitoring will be crucial in ensuring the long-term health and well-being of the city and its inhabitants.

`

References

Abdul Athick, A. S. M., & Shankar, K. (2019). Data on land use and land cover changes in Adama Wereda, Ethiopia, on ETM+, TM and OLI- TIRS landsat sensor using PCC and CDM techniques. *Data in Brief*, *24*, 103880. https://doi.org/10.1016/J.DIB.2019.103880.org/10.1007/s10668-021-01472-3

Adama Science and Technology University (ASTU) (2016).History of Adama City from its foundation to present (1919-2015)

Adeyeri, O. E., Lawin, A. E., Laux, P., Ishola, K. A., & Ige, S. O. (2019). Analysis of climate extreme indices over the Komadugu-Yobe basin, Lake Chad region: Past and future occurrences. *Weather and Climate Extremes*, *23*. https://doi.org/10.1016/J.WACE.2019.100194

Asfaw, M. (2017). *Modelling Land Surface Temperature from Satellite Data and Trigger by Land Use Land Cover Dynamics using Remote Sensing and GIS Technology, in Debra Tabor District, Ethiopia*. *7*(6). www.iiste.org

Äthiopien, V. (2019). Ethnic Decentralization and Negotiating Statehood in Urban Ethiopia: A Case Study of Adama and Hawassa Cities Dissertation zur Erlangung der Würde eines Doktors der Philosophie vorgelegt der Philosophisch-Historischen Fakultät der Universität Basel Von Demissie Ferdissa Bekele.

Balew, A., & Korme, T. (2020). Monitoring land surface temperature in Bahir Dar city and its surrounding using Landsat images. *Egyptian Journal of Remote Sensing and Space Science*, *23*(3), 371–386. https://doi.org/10.1016/j.ejrs.2020.02.001

Balew, A., & Semaw, F. (2022). Impacts of land-use and land-cover changes on surface urban heat islands in Addis Ababa city and its surrounding. *Environment, Development and Sustainability*, *24*(1), 832–866. https://doi.org/10.1007/s10668-021-01472-3

Becker, F., & Li, Z. L. (1990). Temperature-independent spectral indices in thermal infrared bands. *Remote Sensing of Environment*, *32*(1), 17–33. https://doi.org/10.1016/0034-4257(90)90095-4

Bouaziz, M., Eisold, S., & Guermazi, E. (2017). Semiautomatic approach for land cover classification: a remote sensing study for arid climate in southeastern Tunisia. *Euro-Mediterranean Journal for Environmental Integration*, *2*(1). https://doi.org/10.1007/S41207-017-0036-7

Bulti, D. T., & Sori, N. D. (2017). Evaluating land-use plan using conformance-based approach in Adama city, Ethiopia. Spatial Information Research, 25(4), 605–613. https://doi.org/10.1007/s41324-017-0125-3

Bulti, D. T. (n.d.). *Spatio-Temporal Analysis of Urban Expansion*.

Caselles, V., Coll, C., & Valor, E. (1997). Land surface emissivity and temperature determination in the whole HAPEX-Sahel area from AVHRR data. *International Journal of Remote Sensing*, *18*(5), 1009–1027. https://doi.org/10.1080/014311697218548

Chaka, D. S., & Oda, T. K. (2021). Understanding land surface temperature on rift areas to examine the spatial variation of urban heat island: the case of Hawassa, southern Ethiopia. *GeoJournal*, *86*(2), 993–1014. https://doi.org/10.1007/S10708-019-10110-5

Charney, J., Quirk, W.J., Chow, S.H. and Kornfield, J. (1977) A Comparative Study of the Effects of Albedo Change on Drought in Semi-Arid Regions. Journal of the Atmospheric Sciences, 34, 1366-1385. - References - Scientific Research Publishing. (n.d.). Retrieved December 23, 2022, from https://scirp.org/reference/ReferencesPapers.aspx?ReferenceID=1288947

Chen, X. L., Zhao, H. M., Li, P. X., & Yin, Z. Y. (2006). Remote sensing image-based analysis of the relationship between urban heat island and land use/cover changes. *Remote Sensing of Environment*, *104*(2), 133–146. https://doi.org/10.1016/J.RSE.2005.11.016

Dash, P., Göttsche, F. M., Olesen, F. S., & Fischer, H. (2005). Separating surface emissivity and temperature using two-channel spectral indices and emissivity composites and comparison with a vegetation fraction method. *Remote Sensing of Environment*, *96*(1), 1–17. https://doi.org/10.1016/J.RSE.2004.12.023

Dissanayake, D. M. S. L. B., Morimoto, T., Murayama, Y., & Ranagalage, M. (2019). Impact of landscape structure on the variation of land surface temperature in Sub-Saharan Region: A case study of Addis Ababa using Landsat Data (1986-2016). *Sustainability (Switzerland)*, *11*(8). https://doi.org/10.3390/su11082257

Ellis, E. C. (2011). Anthropogenic transformation of the terrestrial biosphere. *Philosophical Transactions of the Royal Society A: Mathematical, Physical and Engineering Sciences*, *369*(1938), 1010–1035. https://doi.org/10.1098/RSTA.2010.0331

Estoque, R. C., Murayama, Y., & Myint, S. W. (2017a). Effects of landscape composition and pattern on land surface temperature: An urban heat island study in the megacities of Southeast Asia. *Science of the Total Environment*, *577*, 349–359. https://doi.org/10.1016/J.SCITOTENV.2016.10.195

Estoque, R. C., Murayama, Y., & Myint, S. W. (2017b). Effects of landscape composition and pattern on land surface temperature: An urban heat island study in the megacities of Southeast Asia. *Science of the Total Environment*, *577*, 349–359. https://doi.org/10.1016/j.scitotenv.2016.10.195

FRAGSTATS HELP. (n.d.).

Feyisa, G. L., Meilby, H., Darrel Jenerette, G., & Pauliet, S. (2016). Locally optimized separability enhancement indices for urban land cover mapping: Exploring thermal environmental consequences of rapid urbanization in Addis Ababa, Ethiopia. *Remote Sensing of Environment*, *175*, 14–31. https://doi.org/10.1016/J.RSE.2015.12.026

Gala, T. S. (2020). *The Use of Remote Sensing and GIS for Monitoring Urban Growth: The Case of Addis Ababa, Ethiopia Hydrological Application of Remote Sensing View project Grand Ethiopian Renaissance Dam View project*. https://doi.org/10.13140/RG.2.2.15870.41280

Gillespie, A. R., Rokugawa, S., Hook, S. J., Matsunaga, T., & Kahle, A. B. (1999). *Temperature/Emissivity Separation Algorithm Theoretical Basis Document, Version 2.4*.

Gluch, R., Quattrochi, D. A., & Luvall, J. C. (2006). A multi-scale approach to urban thermal analysis. *Remote Sensing of Environment*, *104*(2), 123–132. https://doi.org/10.1016/J.RSE.2006.01.025

Goward, S. N., Markham, B., Dye, D. G., Dulaney, W., & Yang, J. (1991). Normalized difference vegetation index measurements from the advanced very high resolution radiometer. *Remote Sensing of Environment*, *35*(2–3), 257–277. https://doi.org/10.1016/0034-4257(91)90017-Z

Gupta, N., Mathew, A., & Khandelwal, S. (2019). Analysis of cooling effect of water bodies on land surface temperature in nearby region: A case study of Ahmedabad and Chandigarh cities in India. *The Egyptian Journal of Remote Sensing and Space Science*, *22*(1), 81–93. https://doi.org/10.1016/J.EJRS.2018.03.007

Gustafson, E. J. (1998). Quantifying landscape spatial pattern: What is the state of the art? *Ecosystems*, *1*(2), 143–156. https://doi.org/10.1007/S100219900011

Haylemariyam, M. B. (2018). Detection of Land Surface Temperature in Relation to Land Use Land Cover Change: Dire Dawa City, Ethiopia. *Journal of Remote Sensing & GIS*, *07*(03). https://doi.org/10.4172/2469-4134.1000245

Huang, C., Davis, L. S., & Townshend, J. R. G. (2002). An assessment of support vector machines for land cover classification. *International Journal of Remote Sensing*, *23*(4), 725–749. https://doi.org/10.1080/01431160110040323

Huang, S., Tang, L., Hupy, J. P., Wang, Y., & Shao, G. (2021). A commentary review on the use of normalized difference vegetation index (NDVI) in the era of popular remote sensing. In *Journal of Forestry Research* (Vol. 32, Issue 1). Northeast Forestry University. https://doi.org/10.1007/s11676-020-01155-1

Implementation of machine-learning classification in remote sensing: an applied review | Semantic Scholar. (n.d.). Retrieved January 23, 2023, from https://www.semanticscholar.org/paper/Implementation-of-machine-learning-classification-Maxwell-Warner/b3de1062d8a462dfdc2938558258f8884abe9f4e

Jiang, G. M., Li, Z. L., & Nerry, F. (2006). Land surface emissivity retrieval from combined mid-infrared and thermal infrared data of MSG-SEVIRI. *Remote Sensing of Environment*, *105*(4), 326–340. https://doi.org/10.1016/J.RSE.2006.07.015

Jones, H., & Vaughan, R. (2011). Remote sensing of vegetation: principles, techniques and applications. By Hamlyn G. Jones and Robin A Vaughan. *Journal of Vegetation Science*, *22*(6), 1151–1153. https://doi.org/10.1111/j.1654-1103.2011.01319.x

Khan, N., Shahid, S., Chung, E. S., Kim, S., & Ali, R. (2019). Influence of surface water bodies on the land surface temperature of Bangladesh. *Sustainability (Switzerland)*, *11*(23). https://doi.org/10.3390/SU11236754

Kaur, A., & Jyoti, Dr. K. (2014). Reproduction of Remote Sensing Image Using Supervised Mode of Learning Using Artificial Neural Network. *INTERNATIONAL JOURNAL OF COMPUTERS & TECHNOLOGY*, *13*(9), 4799–4808. https://doi.org/10.24297/IJCT.V13I9.2356

Latif, S. (2014). *Issue 4* |. *2*. www.ijedr.org

Li, Z. L., Tang, B. H., Wu, H., Ren, H., Yan, G., Wan, Z., Trigo, I. F., & Sobrino, J. A. (2013). Satellite-derived land surface temperature: Current status and perspectives. In *Remote Sensing of Environment* (Vol. 131, pp. 14–37). https://doi.org/10.1016/j.rse.2012.12.008

Li, Z., Petitcolin, F., & Zhang, R. (2000). A physically based algorithm for land surface emissivity retrieval from combined mid-infrared and thermal infrared data. *Science in China Series E: Technological Sciences*, *43*(SUPPL.), 32–33. https://doi.org/10.1007/BF02916575

Mahmon, N. A., & Ya'Acob, N. (2014). A review on classification of satellite image using Artificial Neural Network (ANN). *2014 IEEE 5th Control and System Graduate Research Colloquium*, 153–157. https://doi.org/10.1109/ICSGRC.2014.6908713

Maimaitiyiming, M., Ghulam, A., Tiyip, T., Pla, F., Latorre-Carmona, P., Halik, Ü., Sawut, M., & Caetano, M. (2014b). Effects of green space spatial pattern on land surface temperature: Implications for sustainable urban planning and climate change adaptation. *ISPRS Journal of Photogrammetry and Remote Sensing*, *89*, 59–66. https://doi.org/10.1016/j.isprsjprs.2013.12.010

Mallick, J., Bindajam, A. A., AlQadhi, S., Ahmed, M., Hang, H. T., & Thanh, N. V. (2020). A comparison of four land surface temperature retrieval method using TERRA-ASTER satellite images in the semi-arid region of Saudi Arabia. *Https://Doi.Org/10.1080/10106049.2020.1790675*, 1–25. https://doi.org/10.1080/10106049.2020.1790675

Maxwell, S. K., Schmidt, G. L., & Storey, J. C. (2007). A multi-scale segmentation approach to filling gaps in Landsat ETM+ SLC-off images. *International Journal of Remote Sensing*, *28*(23), 5339–5356. https://doi.org/10.1080/01431160601034902

McFeeters, S. K. (1996). The use of the Normalized Difference Water Index (NDWI) in the delineation of open water features. *Https://Doi.Org/10.1080/01431169608948714*, *17*(7), 1425–1432. https://doi.org/10.1080/01431169608948714

McGarigal, K., & Marks, B. J. (1995). FRAGSTATS: spatial pattern analysis program for quantifying landscape structure. *Gen. Tech. Rep. PNW-GTR-351. Portland, OR: U.S. Department of Agriculture, Forest Service, Pacific Northwest Research Station. 122 p, 351*. https://doi.org/10.2737/PNW-GTR-351

Mcgarigal, K. (2015) FRAGSTATS Help. - References - Scientific Research Publishing. (n.d.). Retrieved December 23, 2022, from https://www.scirp.org/(S(oyulxb452alnt1aej1nfow45))/reference/ReferencesPapers.aspx?ReferenceID=1903578

Mezgebo, T. G. (n.d.). *Urbanization and Development in Ethiopia: Policy Issues, Trends and Prospects*. https://www.researchgate.net/publication/348633575

Moisa, M. B., Dejene, I. N., Merga, B. B., & Gemeda, D. O. (2022). Impacts of land use/land cover dynamics on land surface temperature using geospatial techniques in Anger River Sub-basin, Western Ethiopia. *Environmental Earth Sciences*, *81*(3). https://doi.org/10.1007/s12665-022-10221-2

`

Ndossi, M. I., & Avdan, U. (2016). Inversion of land surface temperature (lst) using terra aster data: A comparison of three algorithms. *Remote Sensing*, *8*(12). https://doi.org/10.3390/rs8120993

Nega, W., Hailu, B. T., & Fetene, A. (2019). An assessment of the vegetation cover change impact on rainfall and land surface temperature using remote sensing in a subtropical climate, Ethiopia. *Remote Sensing Applications: Society and Environment*, *16*. https://doi.org/10.1016/j.rsase.2019.100266

Otterman, J. (1974). Baring High-Albedo Soils by Overgrazing: A Hypothesized Desertification Mechanism. *Science*, *186*(4163), 531–533. https://doi.org/10.1126/SCIENCE.186.4163.531

Otukei, J. R., & Blaschke, T. (2010). Land cover change assessment using decision trees, support vector machines and maximum likelihood classification algorithms. *International Journal of Applied Earth Observation and Geoinformation*, *12*(SUPPL. 1). https://doi.org/10.1016/J.JAG.2009.11.002

Patel, S. K., Verma, P., & Shankar Singh, G. (2019). Agricultural growth and land use land cover change in peri-urban India. *Environmental Monitoring and Assessment*, *191*(9). https://doi.org/10.1007/S10661-019-7736-1

Perumal, K., & Bhaskaran ----------, R. (2010). *SUPERVISED CLASSIFICATION PERFORMANCE OF MULTISPECTRAL IMAGES* (Vol. 2).

Pham, H. M., Yamaguchi, Y., & Bui, T. Q. (2011). A case study on the relation between city planning and urban growth using remote sensing and spatial metrics. *Landscape and Urban Planning*, *100*(3), 223–230. https://doi.org/10.1016/J.LANDURBPLAN.2010.12.009

Prasad, A. D., Ganasala, P., Hernández-Guzmán, R., & Fathian, F. (2022). Remote sensing satellite data and spectral indices: an initial evaluation for the sustainable development of an urban area. *Sustainable Water Resources Management*, *8*(1). https://doi.org/10.1007/s40899-022-00607-2

Priyankara, P., Ranagalage, M., Dissanayake, D. M. S. L. B., Morimoto, T., & Murayama, Y. (2019). Spatial process of surface urban heat island in rapidly growing seoul metropolitan area for sustainable urban planning using landsat data (1996-2017). *Climate*, *7*(9). https://doi.org/10.3390/cli7090110

Regasa, M. S., Nones, M., & Adeba, D. (2021). A review on land use and land cover change in ethiopian basins. *Land*, *10*(6). https://doi.org/10.3390/land10060585

Ranagalage, M., Dissanayake, D. M. S. L. B., Murayama, Y., Zhang, X., Estoque, R. C., Perera, E. N. C., & Morimoto, T. (2018). Quantifying surface urban heat island formation in the world heritage tropical mountain city of Sri Lanka. *Canadian Historical Review*, *7*(9). https://doi.org/10.3390/ijgi7090341

Remote sensing and radiative transfer – JAXA Earth-graphy / Space Technology Directorate I. (n.d.). Retrieved January 28, 2023, from https://earth.jaxa.jp/en/eo-knowledge/remote-sensing/index.html

Riebsame, W. E., Parton, W. J., Galvin, K. A., Burke, I. C., Bohren, L., Young, R., & Knop, E. (1994). Integrated modeling of land use and cover change. *BioScience*, *44*(5), 350–356. https://doi.org/10.2307/1312385/2/44-5-350.PDF.GIF

Sagan, C., Toon, O. B., & Pollack, J. B. (1979). Anthropogenic Albedo Changes and the Earth's Climate. *Science*, *206*(4425), 1363–1368. https://doi.org/10.1126/SCIENCE.206.4425.1363

Shih, H. chien, Stow, D. A., & Tsai, Y. H. (2019). Guidance on and comparison of machine learning classifiers for Landsat-based land cover and land use mapping. *International Journal of Remote Sensing*, *40*(4), 1248–1274. https://doi.org/10.1080/01431161.2018.1524179

Simwanda, M., Ranagalage, M., Estoque, R. C., & Murayama, Y. (2019). Spatial analysis of surface urban heat Islands in four rapidly growing african cities. *Remote Sensing*, *11*(14). https://doi.org/10.3390/rs11141645

Snyder, W. C., Wan, Z., Zhang, Y., & Feng, Y. Z. (1998). Classification-based emissivity for land surface temperature measurement from space. *International Journal of Remote Sensing*, *19*(14), 2753–2774. https://doi.org/10.1080/014311698214497

Tafesse, B., & Suryabhagavan, K. v. (2019). Systematic modeling of impacts of land-use and land-cover changes on land surface temperature in Adama Zuria District, Ethiopia. *Modeling Earth Systems and Environment*, *5*(3), 805–817. https://doi.org/10.1007/s40808-018-0567-1

Terfa, B. K., Chen, N., Zhang, X., & Niyogi, D. (2020). Spatial configuration and extent explains the urban heat mitigation potential due to green spaces: Analysis over Addis Ababa, Ethiopia. *Remote Sensing*, *12*(18). https://doi.org/10.3390/RS12182876

UN-HABITAT (2002). Local democracy and decentralization in East and Southern Africa. A publication of Global Campaign on Urban Governance.

UN DESA | United Nations Department of Economic and Social Affairs. (n.d.). Retrieved December 23, 2022, from https://www.un.org/en/development/desa/news/2014.html

Vitousek, P. M., Mooney, H. A., Lubchenco, J., & Melillo, J. M. (1997). Human Domination of Earth's Ecosystems. *Science*, *277*(5325), 494–499. https://doi.org/10.1126/SCIENCE.277.5325.494

Warkaye, S., Suryabhagavan, K. v, & Satishkumar, B. (2018). Urban Green Areas to Mitigate Urban Heat Island Effect: The Case of Addis Ababa, Ethiopia. *International Journal of Ecology and Environmental Sciences*, *44*(4), 353–367.

Watson, K. (1992). Two-temperature method for measuring emissivity. *Remote Sensing of Environment*, *42*(2), 117–121. https://doi.org/10.1016/0034-4257(92)90095-2

Weier, J., & Herring, D. (2000). Measuring Vegetation (NDVI & EVI). *Measuring Vegetation (NDVI & EVI). NASA Earth Observatory, Washington DC*.

Zhao, H., & Chen, X. (2005). Use of normalized difference bareness index in quickly mapping bare areas from TM/ETM+. *Proceedings. 2005 IEEE International Geoscience and Remote Sensing Symposium, 2005. IGARSS '05.*, *3*, 1666–1668. https://doi.org/10.1109/IGARSS.2005.1526319

Zhao, M., Cai, H., Qiao, Z., & Xu, X. (2016). Influence of urban expansion on the urban heat island effect in Shanghai. *International Journal of Geographical Information Science*, *30*(12), 2421–2441. https://doi.org/10.1080/13658816.2016.1178389

Zha, Y., Gao, J., & Ni, S. (2003). Use of normalized difference built-up index in automatically mapping urban areas from TM imagery. *International Journal of Remote Sensing*, *24*(3), 583– 594. https://doi.org/10.1080/01431160304987

Zhang, H., Wang, T., Zhang, Y., Dai, Y., Jia, J., Yu, C., Li, G., Lin, Y., Lin, H., & Cao, Y. (2018). Quantifying short-term urban land cover change with time series Landsat data: A comparison of four different cities. Sensors (Switzerland), 18(12). https://doi.org/10.3390/s18124319

Appendix

Python library for automating GIS tasks with ArcGIS software. This script is specifically designed to calculate the mean Land Surface Temperature (LST) for different zones within a geographical dataset and update these values in the same dataset.

```
import arcpy
...
... # Set the workspace
... arcpy.env.workspace = "D:/DataBase/Data_Base/LULC_LST.mdb"
...
... # Set the input table
... input_table = "Zonal_Statistics_1991_Bega_Merged"
...
... # Set the output field name
... output_field = "LST_MEAN_ZONES"
...
... # Create a dictionary to store the zone IDs and their corresponding LST values
... zone_dict = {}
...
... # Loop through the input table and populate the dictionary
... with arcpy.da.SearchCursor(input_table, ["zone_", "MEAN"]) as cursor:
...     for row in cursor:
...         if row[0] not in zone_dict:
...             zone_dict[row[0]] = [row[1]]
...         else:
...             zone_dict[row[0]].append(row[1])
...
... # Loop through the dictionary and calculate the mean LST for each zone
... with arcpy.da.UpdateCursor(input_table, ["zone_", output_field]) as cursor:
...     for row in cursor:
...         if row[0] in zone_dict:
...             mean_lst = sum(zone_dict[row[0]]) / len(zone_dict[row[0]])
```

`

```
...            row[1] = mean_lst
...            cursor.updateRow(row)
...
>>>
```

Python script that utilizes the ArcPy library to automate the calculation and updating of total land use and land cover (LULC) areas by zone in a geographic database table.

```
import arcpy


def calc_zone_area(table, zone_field, lulc_field, area_field):
    # Create a dictionary to store the total area of each zone
    zone_areas = {}
    # Use a SearchCursor to iterate over the rows in the table
    with arcpy.da.SearchCursor(table, [zone_field, lulc_field, area_field]) as cursor:
        for row in cursor:
            # Get the values of the zone_field, lulc_field, and area_field for this row
            zone = row[0]
            lulc_class = row[1]
            lulc_class_area = row[2]
            # If this is the first time we've encountered this zone, initialize its total area to 0
            if zone not in zone_areas:
                zone_areas[zone] = 0
            # Add the area of this LULC class to the total area of this zone
            zone_areas[zone] += lulc_class_area
    return zone_areas


# Replace 'Zonal_Statistics_2022_Kiremete_Merged' with the name of your table
# Replace 'zone_', 'LULC', and 'AREA' with the names of your zone field, LULC field, and area field
zone_areas = calc_zone_area('Zonal_Statistics_2022_Kiremete_Merged', 'zone_', 'LULC', 'AREA')


# Replace 'Zonal_Statistics_2022_Kiremete_Merged' with the name of your table
# Replace 'zone_' with the name of your zone field
```

```
# Replace 'Zone_AREA' with the name of your new field that will store the total area of each zone
with arcpy.da.UpdateCursor('Zonal_Statistics_2022_Kiremete_Merged', ['zone_', 'Zone_AREA']) as cursor:
    for row in cursor:
        # Get the value of the zone_ field for this row
        zone = row[0]
        # Update the value of the Zone_AREA field for this row with the total area of this zone
        row[1] = zone_areas[zone]
        cursor.updateRow(row)
```

Python script to calculate the total Area each of Zone

```
>>> import arcpy

def calc_zone_area(table, zone_field, lulc_field, area_field):
    # Create a dictionary to store the total area of each zone
    zone_areas = {}
    # Use a SearchCursor to iterate over the rows in the table
    with arcpy.da.SearchCursor(table, [zone_field, lulc_field, area_field]) as cursor:
        for row in cursor:
            # Get the values of the zone_field, lulc_field, and area_field for this row
            zone = row[0]
            lulc_class = row[1]
            lulc_class_area = row[2]
            # If this is the first time we've encountered this zone, initialize its total area to 0
            if zone not in zone_areas:
                zone_areas[zone] = 0
            # Add the area of this LULC class to the total area of this zone
            zone_areas[zone] += lulc_class_area
    return zone_areas

# Replace 'Zonal_Statistics_2022_Kiremete_Merged' with the name of your table
```

```
# Replace 'zone_', 'LULC', and 'AREA' with the names of your zone field, LULC field, and area field
zone_areas = calc_zone_area('Zonal_Statistics_2022_Kiremete_Merged', 'zone_', 'LULC', 'AREA')


# Replace 'Zonal_Statistics_2022_Kiremete_Merged' with the name of your table
# Replace 'Zone_Area' with the name of your new field that will store the total area of each zone
arcpy.AddField_management('Zonal_Statistics_2022_Kiremete_Merged', 'Zone_Area', 'DOUBLE')


# Replace 'Zonal_Statistics_2022_Kiremete_Merged' with the name of your table
# Replace 'zone_' with the name of your zone field
# Replace 'Zone_Area' with the name of your new field that will store the total area of each zone
with arcpy.da.UpdateCursor('Zonal_Statistics_2022_Kiremete_Merged', ['zone_', 'Zone_Area']) as cursor:
    for row in cursor:
        # Get the value of the zone_ field for this row
        zone = row[0]
        # Update the value of the Zone_Area field for this row with the total area of this zone
        row[1] = zone_areas[zone]
        cursor.updateRow(row)
>>> import arcpy
...
... def calc_zone_area(table, zone_field, lulc_field, area_field):
...     # Create a dictionary to store the total area of each zone
...     zone_areas = {}
...     # Use a SearchCursor to iterate over the rows in the table
...     with arcpy.da.SearchCursor(table, [zone_field, lulc_field, area_field]) as cursor:
...         for row in cursor:
...             # Get the values of the zone_field, lulc_field, and area_field for this row
...             zone = row[0]
...             lulc_class = row[1]
```

`

```
...             lulc_class_area = row[2]
...             # If this is the first time we've encountered this zone, initialize its total area to 0
...             if zone not in zone_areas:
...                 zone_areas[zone] = 0
...             # Add the area of this LULC class to the total area of this zone
...             zone_areas[zone] += lulc_class_area
...     return zone_areas
...
... # Replace 'Zonal_Statistics_2022_Kiremete_Merged' with the name of your table
... # Replace 'zone_', 'LULC', and 'AREA' with the names of your zone field, LULC field, and area field
... zone_areas = calc_zone_area('Zonal_Statistics_2022_Belge_Merged', 'zone_', 'LULC', 'AREA')
...
... # Replace 'Zonal_Statistics_2022_Kiremete_Merged' with the name of your table
... # Replace 'zone_' with the name of your zone field
... # Replace 'zone_area' with the name of your new field that will store the total area of each zone
... with arcpy.da.UpdateCursor('Zonal_Statistics_2022_Belge_Merged', ['zone_', 'zone_AREA']) as cursor:
...     for row in cursor:
...         # Get the value of the zone_ field for this row
...         zone = row[0]
...         # Update the value of the zone_area field for this row with the total area of this zone
...         row[1] = zone_areas[zone]
...         cursor.updateRow(row)
...
```